Mechanisms of Leak and Cotransport Modes of Renal Phosphate Transporters

Dissertation

zur

Erlangung der naturwissenschaftlichen Doktorwürde

(Dr. sc. nat.)

Vorgelegt der

Mathematisch-naturwissenschftlichen Fakultät

der

Universität Zürich

von

Andrini Olga

aus Italien

Promotionskomitee:

PD Dr. Ian Cameron Forster

Prof. Dr. Heini Murer

Prof. Dr. Jürg Biber

PD Dr. Stephan Kellenberger

Zürich 2011

Contents

1. SUMMARY:

Secondary-active membrane transporters drive ions and solutes across the plasma membrane using the energy of electrochemical gradients. Their function can be experimentally investigated by means of expression cloning in heterologous expression systems (*e.g. X. laevis* oocytes).

In this work, functional studies on the electrogenic isoforms of sodium-coupled phosphate cotransporters (NaPi-IIa/b) have been performed to gain new insights into the *cotransport mode* and the *leak mode*. The *cotransport* mode involves recognition of both co-substrate (Na^+) and substrate (P_i) and the translocation of each species according to a defined stoichiometry. $3Na^+$ ions together with $1HPO_4^{2-}$ are transported inside the cell, this results in a translocation of one net charge *per* transport cycle *per* transporter. The *leak* mode describes the action of uncoupled currents. These currents give rise to deviations from the tightly coupled electrogenicity and strict stoichiometry between co-substrates and substrates expected for ideal secondary-active cotransporters.

The first study focused on the leak mode of NaPi-IIa/b. The leak current is characterized by having a negative reversal potential (E_r ~ -20 mV), which is not consistent with Na^+ ions being the only cation spieces translocated. It was hypothesized that Cl^- ions participate in the leak, thereby giving the negative E_r. The Cl^- replacement by several different anions also had an effect on non-injected oocytes. We found that the leak current was masked by an endogenous anionic component that was sensitive to phosphonoformic acid used to quantify the NaPi-II-dependent leak. This result could therefore explain (i) the negative E_r of the leak and (ii) the variability of the E_r, which depends on the donor frog.

The second study focused on the characterisation of the interaction between lithium (Li^+) and NaPi-IIa/b. Previous structure-function studies on NaPi-II proteins had indicated a possible interaction of Li^+ ions, however the underlying mechanism was unclear. A detailed functional study on P_i-induced current and on the presteady-state currents was performed to determine (i) how many Li^+ ions interact with the transporter, (ii) if Li^+ could substitute for Na^+ in the transport cycle and (iii) if Li^+ had the same interaction properties of Na^+. It was observed that Li^+ could strongly affect the cotransport voltage-dependence suggesting (i) an interaction with NaPi-IIa/b and (ii) a modulation of voltage dependent partial reactions. From simultaneous electrophysiology and uptake experiments, we found that at least one Li^+ ion could substitute for one Na^+ in the transport cycle. The analysis of the presteady-state kinetics established that one Li^+ can substitute for Na^+ before the binding of P_i.

During my doctoral period, I also contributed to the development of the Cut-Open Voltage-Clamp (COVC). This technique allows a very fast voltage clamp (for resolution of fast presteady-state relaxations) and it also allows access to the cytoplasmic medium (to study intracellular solute interactions). The major improvements concerned the redesign of the hardware to ease the external and the internal perfusions and to provide a stable system. The new design allowed a precise control of the internal perfusion system by micromanipulators and high flow rates for fluid exchange in both internal and external perfusions.

ZUSAMMENFASSUNG:

Sekundäraktive Membrantransporter treiben Ionen und gelöste Substanzen durch die Plasmamembran, indem sie die Energie von elektrochemischen Gradienten nutzen. Deren Funktion kann mittels Klonierung in heterologen Expressionssystemen (z.B. in Oozyten von *X. laevis*) experimentell untersucht werden.

In dieser Arbeit wurden funktionelle Studien an den elektrogenen Isoformen von natriumgekoppelten Phosphat-Kotransportern (NaPi-IIa/b) durchgeführt, um neue Erkenntnisse über die Kotransport-Mechanismus und Sogenannte Leckprozess zu gewinnen. Der Prozess des Kotransports umfasst die Erkennung des Kosubstrats (Na^+) und Substrats (P_i) und die Translokation jeder Spezies gemäss einer definierten Stöchiometrie. Drei Na^+-Ionen zusammen mit einem HPO_4^{2}-Ion werden in die Zelle transportiert, was in einer Verschiebung einer Nettoladung pro Transportzyklus pro Transporter resultiert. Der Leckprozess umfasst die Präsenz ungekoppelter Ströme. Diese bilden Abweichungen von der eng gekoppelten Elektrogenität und strikten Stöchiometrie zwischen den erwarteten Kosubstraten und Substraten für die idealen sekundäraktiven Kotransporter.

Die erste Studie konzentrierte sich auf den Leckmodus von NaPi-Iia/b. Der Leckstrom ist durch ein negatives Umkehrpotential charakterisiert (E_r ~ -20 mV), was nicht mit der Translokation von Na^+-Ionen als einzige Spezies konsistent ist. Es wurde die Hypothese aufgestellt, dass Cl^--Ionen zum Leckstrom beitragen, was ein negatives E_r erklären würde. Das Ersetzen von Cl^--Ionen durch diverse andere Anionen zeigte auch beim nicht-injizierten Oozyten einen Effekt. Wir fanden heraus, dass der Leckstrom von einer endogenen anionischen Komponente überlagert wurde, welche auf phosphonoformische Säure, verwendet um den NaPi-II-abhängigen Strom zu isolieren, reagiert. Diese Erkenntnis könnte demnach (i) das negative E_r des Lecks und (ii) dessen Variabilität erklären, welche vom Donorfrosch abhängen.

Die zweite Studie konzentrierte sich auf die Charakterisierung der Interaktion zwischen Lithium (Li^+) und NaPi-IIa/b. Bisherige Struktur-Funktionsstudien an NaPi-II-Proteinen hatten eine mögliche Interaktion mit Li^+-Ionen angedeutet, wenngleich die darunterliegenden Mechanismen unklar waren. Eine detaillierte funktionelle Studie an P_i-induziertem Strom und an den sogenannten „Presteady-State" Strömen wurde durchgeführt, um zu verstehen (i) wieviele Li^+-Ionen mit dem Transporter reagieren, (ii) ob Li^+ ein Substituent für

Na^+ im Transportzyklus ist und ob Li^+ dieselben Interaktionseigenschaften wie Na^+ hat. Es wurde festgestellt, dass Li^+ die Spannungsabhängigkeit des Kotransports stark beeinflussen konnte, was (i) eine Interaktion mit NaPi-IIa/b und (ii) eine Modulation der spannungsabhängigen partiellen Reaktionen suggeriert. Mittels simultanen Elektrophysiologie- und Auf nahme experimenten fanden wir heraus, dass im Transportzyklus mindestens ein Li^+-Ion für ein Na^+-Ion substituiert werden kann. Die Analyse der „Presteady-State“ Kinetik etablierte die Hypothese, dass vor dem binden des P_i ein Li^+ für ein Na^+ substituiert werden kann.

Während meiner doktoralen Tätigkeit habe ich auch zur Entwicklung des Cut-Open Voltage-Clamp (COVC) beigetragen. Diese Technik erlaubt eine sehr schnelle Spannungsklemme (mit einer sich den schnellen Presteady-state-Relaxationen annähernden Auflösung) und Zugang zum cytoplasmischen Medium (um intrazelluläre Interaktionen von gelösten Stoffen zu untersuchen). Die hauptsächlichen Verbesserungen betraffen die Neukonzeptionierung der Hardware, um die externe und interne Perfusion zu vereinfachen und die Systemstabilität zu gewährleisten. Das neue Konzept erlaubt eine präzise Kontrolle des internen Perfusionssystems mittels Mikromanipulatoren und hohe Flussraten des internen und externen Flüssigkeitsaustausches.

2. INTRODUCTION

Phospholipid membranes create a hydrophobic barrier between the cell interior and its external environment, as well as between the interior of the cell (the cytosol) and the internal milieu of cellular organelles. However, these membranes alone can neither establish nor maintain life. A means of selective transmembrane transport of ions as well as inorganic and organic molecules is essential to regulate the constituents of the external and internal environment. Membrane transport systems are necessary to fulfill a multitude of essential functions such as uptake of nutrients in the intestine, excretion of metabolic products in the kidney, nerve signaling in the central nervous system, as well as homeostatic roles such as osmoregulation and maintenance of the membrane potential. Furthermore, from a thermodynamic point of view, membrane transport proteins establish a way of overcoming the otherwise high energetic costs of moving solutes between the two aqueous environments separated by the cell membrane.

2.1 MEMBRANE TRANSPORT PROTEINS

The presence of "pores" in biological membranes has been a topic of debate since the nineteenth century. Already in the 1800, "diffusion" through bladder membranes was studied (Brücke 1843). The diffusion phenomenon was explained by the presence of microscopic fluid filled spaces that could assemble to form tubes in the membrane to allow water molecules to pass from one compartment to another. The pore-theory was at the center of discussion and many scientists contributed to develop the theory until Widdas in 1952, studying glucose transport in the placenta, observed that experimental data obtained by direct and precise control over glucose concentration, were not in accord with the diffusion theory through pores (164). Over the next 50 years, the introduction of many new techniques, such as the use of radioactive tracer assays applied to native tissue, vesicle preparations, DNA cloning, heterologous expression and advanced electrophysiology (*e.g.* voltage clamp) techniques, have finally allowed physiologists and biophysicists to divide transport mechanisms into two classes: *carriers* and *channels*. The characteristics of the transport process such as substrate selectivity, as well as stoichiometry of transported molecules have been used to distinguish between these two classes of membrane transport proteins (71).

2.1.1 Channels

An *ion channel* can be thought of as a pore that spans the membrane and contains a water-filled cavity through which the solutes (*e.g.* ions) can freely diffuse and cross the membrane. The passive permeation of ions through their pore is driven by the free energy gradients (*e.g.* electrical and chemical) present across the membrane. The ion movement is defined as "downhill" and leads to the dissipation of the potential energy gradient for that species.

In general terms, the family of channels also includes pores, which allow polar solutes (*e.g.* water and glycerol) to cross the lipid bilayer from outside to inside and *vice versa*, only depending on the osmotic and concentration gradient. Most channels (Fig. 2.1) are characterized by a relative high transmembrane transport rate (*e.g.* > 10^8 ions/s in the case of high conductance K^+ channels or 10^9 H_2O molecules/s in the case of AQP1) as compared to most carriers (typically in the range of 10^2 -10^4/s, for details see next section). Another important property of channels is their high selectivity for a particular ion or a polar solute. The selectivity of the channels is achieved in the pore region by a specialized structure called a "selectivity filter" (71).

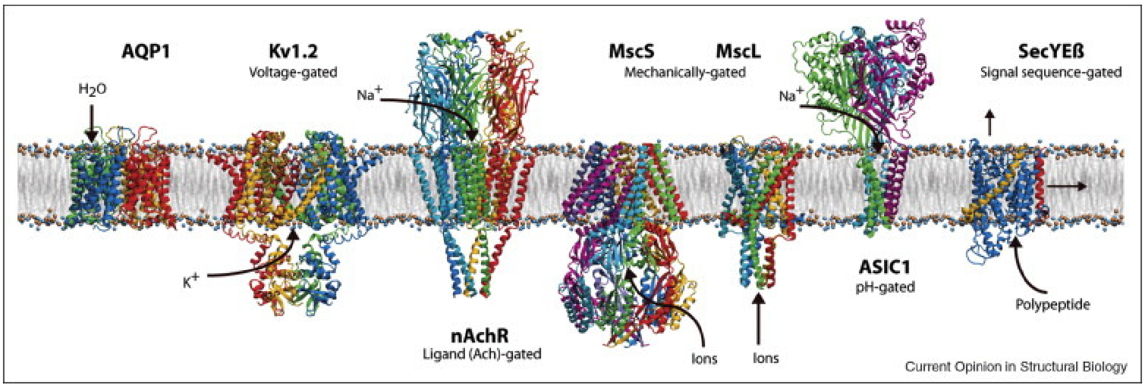

Figure 2.1 Channels are integral membrane proteins.
Crystallized bacterial channels are shown to illustrate the different types of intracellular and extracellular domains. Channels are characterized by transmembrane α-helices that constitute the permeation pathway or pore. Arrows represent the direction of ion movement through the pore. From (86).

Kinetics of ion channels describe the switching between two conformational states, namely open and closed. Some ion channels can also reach a so-called inactivated closed state (*e.g.* voltage-gated Na^+ channels) or a desensitized closed state (*e.g.* ligand-gated channels) after first opening. The occupancy of these closed states depends on the past activation events determined by changes in membrane voltage or ligand binding, respectively. Structurally, the opening and closing of the channels are provided by "gates" that act simultaneously. The gating process can be triggered by different factors such as changes in the membrane potential (*e.g.* voltage-dependent Na^+-channels, Na_v family), mechanical forces (*e.g.* Transient Potential Channels, TRPV), osmotic tension and pH (*e.g.* water channels, AQPs) (71).

2.1.2 Carriers

Carriers are integral membrane proteins that can be considered to function like enzymes (82, 87, 117, 165). The cloning of many mammalian and bacterial carriers and more recently, the crystallization of bacterial carriers, has revealed detailed 3-D structures and the mechanism by which these membrane proteins catalyse the transport of substrates across membranes.

In contrast to channels, carriers (Fig. 2.2) are able to accumulate solutes (*e.g.* ions, nutrients, amino acids, oligopeptides and monosaccharides) against their gradient. The transport process can be primary active, secondary active or facilitative, depending on the energy used (19). Two common features of the carriers are (i) the presence of specific substrate binding sites and (ii) the ordered binding of the substrates. Furthermore, as indicated above, carriers are generally characterized by a lower turnover rate compared to the ions flux through channels (*e.g.* 36 cycles/s for the Na^+-coupled iodide cotransporter (42)). This low turnover can be understood in terms of a so-called transport cycle, where a sequence of conformational changes is necessary to successively expose the substrate binding sites to the extracellular medium, then to the intracellular medium and allow the dissociation of the substrates on the opposite side of the membrane (150). The analogy with enzyme kinetic properties has been used to describe the transport cycle: *e.g.* how the carrier transfers its substrates from one side of the membrane to the other can be discriminated by pseudo-first order kinetics and by assigning values to backward and forward rate constants (146).

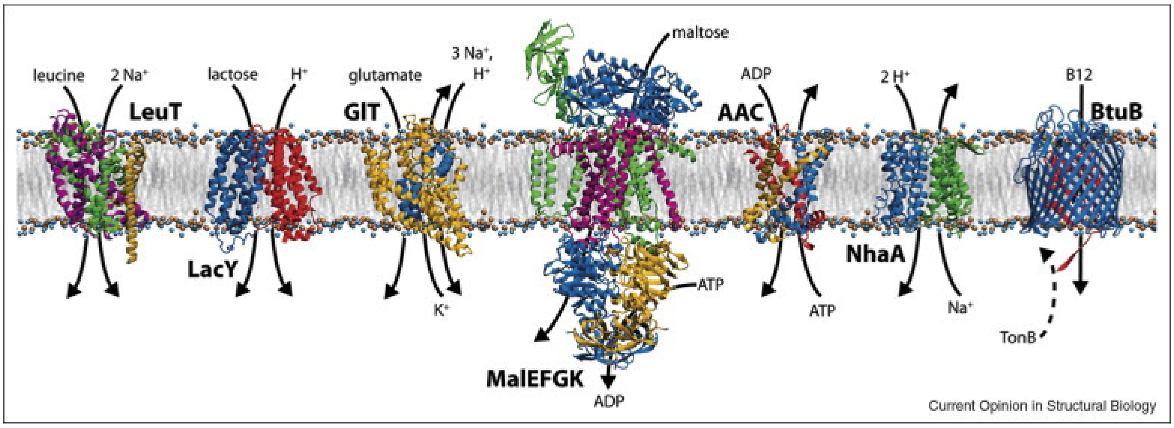

Figure 2.2 ***Bacterial carriers are integral membrane proteins.***

Carriers depend on different energy sources to drive transport across the membrane. Arrows depict the direction of movement of substrate and co-substrates (86).

From a structural point of view, it has been proposed that substrates pass through a transmembrane permeation pathway, for which the access is regulated by two "gates", one at each side of the membrane (98, 142). The gates are arranged in a way so that both are never simultaneously open. This coordination between the internal and the external gates ensures that the binding sites are only exposed at one side of the membrane at the time. The mechanism can lead to a stoichiometric coupling between the transported substrate and the conformational changes that occur during the cycle.

Based on the above brief overview, channels and carriers appear to be different and are easily distinguishable functionally by their ability to dissipate (channels) or accumulate (carriers) solutes. Nevertheless, recent discoveries have shed new light on the traditional classification.

2.1.3 Channels in carriers and carriers in channels: breaking the rules

At the beginning of 1990's a discrepancy in the channel/carrier classification became apparent. A glutamate activated Cl^- current was observed in salamander photoreceptor cells with a conductance that was considered too small to be attributed to channels and too large to be attributed to transporters (96). This discrepancy with the standard model for the electrogenic glutamate transporters was explained by the presence of an additional pathway selective to Cl^- ions associated with the transporter. Mechanistically, it was proposed that the binding of glutamate increased the open probability of a Cl^- channel intrinsic to the protein (37). After this discovery, similar *channel-like* behaviors were observed in several other transporters that belong to the sodium-coupled neurotransmitter transporter family (Neurotransmitter Sodium Symporters family, NSS). For example, glutamate and dopamine cotransporters contain a Cl^- channel (28, 76, 131); serotonin and norephinephrin cotransporters have Na^+ and Li^+ conductances, respectively (58, 124).

Another exception to the channel/carrier classification is found in the Chloride Channel family (ClC) family. Recently it was reported that a bacterial homologue of a Cl^- channel acts as a H^+-Cl^--antiporter with a strict stoichiometry of 2:1 (Cl^-:H^+) (2). A single point mutation reverts the ClC antiporter properties to channel-like features (39, 41). Yet another example is the Cystic Fibrosis Transmembrane conductance Regulator (CFTR), a Cl^- channel, which was found to be homolog to the ABC transporter family (57).

The above examples suggest that the structure of the two main classes of transmembrane proteins, channels and carriers, might be more closely related than it was originally thought (3).

2.2 CARRIER CLASSIFICATIONS

With the increasing number of data-base entries for transport proteins (protein data bank as http://cl.sdsc.edu/ce.html, http://www.ncbi.nlm.nih.gov/sites/gquery) and the description of functional information concerning transporters, it has become useful to classify these proteins according to their intrinsic characteristics. Currently several different classifications are used according the various criteria: energetics, function, genes, etc.. The major classifications described below.

2.2.1 Classical classifications

Classification according to transport energetics

In contrast to passive diffusion of solutes as displayed by channels, the term "*active*" refers a property of transporters to use a source of energy to accumulate solutes. There are three sub-classes: primary, secondary and tertiary active.

Primary active transporters (Fig. 2.3A) uses the hydrolysis of ATP to ADP (adenosine-3-phosphate to adenosine-2-phosphate) as a source of energy to transport directly solutes across the membrane. The most common examples is the Na^+/K^+-ATPase which is responsible for maintaining cell membrane potential.

Secondary-active transporters use the electrochemical potential gradient maintained by pumps (*e.g.* Na^+ and K^+ gradients across the cell-membrane by the Na^+/K^+-ATPase, acidification of synaptic vesicles by the H^+-ATPase, Fig. 2.3B) to concentrate solutes (60). For example, the Na^+-dependent glucose transporter, SGLT1 couples the movement of two Na^+ ions down their electrochemical gradient to the uphill movement of one glucose molecule into the cell (7, 36).

Finally, *tertiary-active* transporters (Fig. 2.3C) are typically exchangers that work in partnership with secondary-active cotransporters having a common substrate. The common substrate (substrate 2 in Fig. 2.3) is accumulated in the cell by the cotransporter. The chemical free energy gained is then used to drive the exchange process and accumulate a third substrate (substrate 3 in Fig. 2.3) (*e.g.* amino acid exchanger for L-cystine/L-Glu (135)).

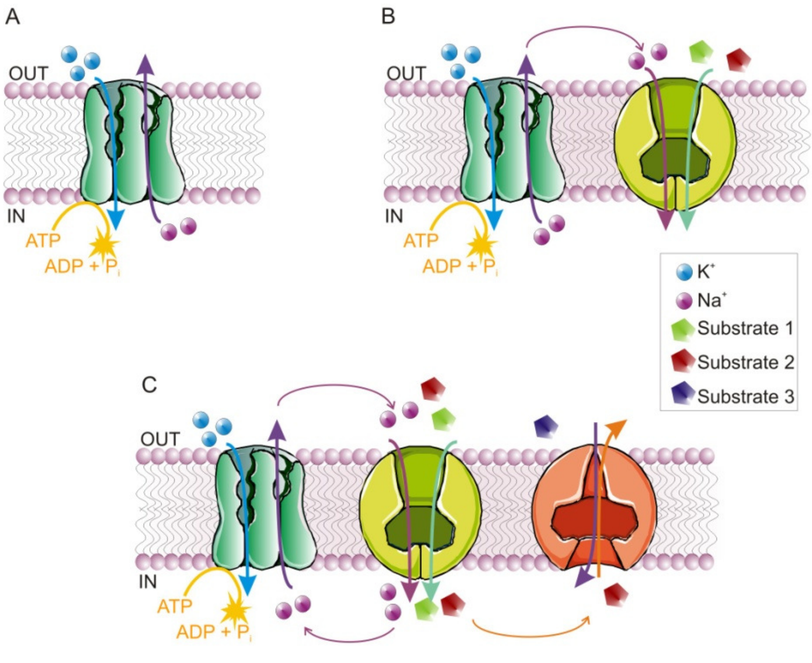

Figure 2.3 Energetics of active transport.

A. Primary active transporters use the hydrolysis of a high energy phosphate bond to move substrates across the membrane; B. Secondary-active transporters use the electrochemical gradient established by primary active systems to accumulate substrates; C. Tertiary-active transporters use the accumulated substrates from secondary-active transport to exchange substrates.

Classification according to function

Traditionally the functional classification refers to membrane transport proteins (excluding primary active transporters) as being either uniporters, symporters or exchangers (Fig. 2.4).

Uniporters (*e.g.* glucose facilitator, GLUT1) use the chemical gradient of the substrate as the driving force (19).

Symporters (or cotransporters) and *antiporters* (or exchangers) are able to use the electrochemical gradient of an ion to transport a solute into the cell. For symporters, the transport of both species is in the same direction (*e.g.* Na^+-dependent glucose cotransporter, SGLT). For antiporters, the species move in opposite directions (*e.g.* Na^+/H^+ exchanger, NHE1) (19).

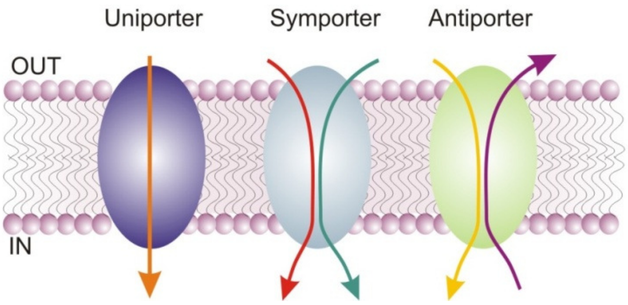

Figure 2.4 Cartoon depicting three types of transport.
The uniporters allow the diffusion of a solute in one direction depending on the chemical gradient for that solute. The symporters mediate the transport of at least two solutes in the same direction. The antiporters exchange at least one solute for another across the plasma membrane.

Classifications according to gene product

A new nomenclature for transporters was initiated by the Human Genome Organization (HUGO) in 2004 (67). SoLute Carrier (SLC) includes 378 transporters and is composed by 51 families (Fig. 2.5). General information about the transporters included in this classification is found in a table available in internet (http://www.bioparadigms.org/slc/menu.asp). This table contains different information: the human gene name, the protein name, the predominant substrates, the transport type (cotransporters, exchangers, facilitated transporters and orphan transporters) as well as the tissue distribution and the sequence accession ID. For example, although SLC5 is termed the sodium-glucose cotransporter family (SGLT1, 2, 3, 4), it also includes genes that encode for transporters of iodide (Na^+/I^- cotransporter, NIS) and choline

(CHT1) as the members within the SLC family have greater than 20-25% sequence homology to each other.

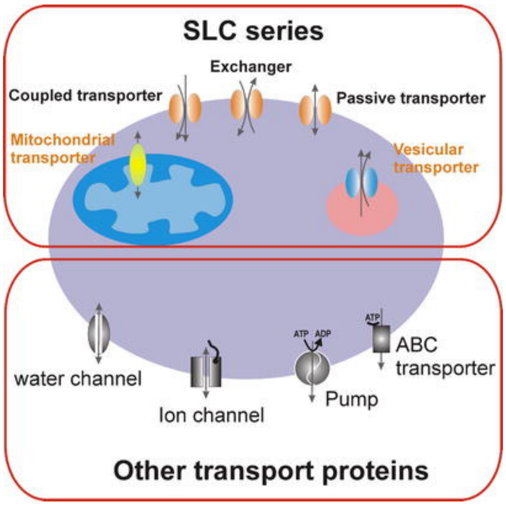

Figure 2.5 The SoLute Carrier (SLC) family.

Scheme showing a cell with solute carrier (SLC)- and non-SLC- membrane proteins present in the plasma membrane and in intracellular compartment. From (67).

A more general classification is available in the Transporter Classification DataBase (TCDB, http://www.tcdb.org/). This data-base is approved by the International Union of Biochemistry and Molecular Biology and it includes transporters as well as ion channels. It incorporates both functional and phylogenic information (132).

Another classification is given by Pfam data-base (http://pfam.sanger.ac.uk/) where proteins are classified by domains and provide a genetic classification useful for phylogenetic studies (45).

2.2.3 Classifications based on 3-D structures

Substrate Binding Proteins (SBPs) classification is one of the first classifications that consider the structure of binding sites (56). It was introduced in 1999 and includes several types of transmembrane and soluble proteins that are characterized by having a binding domain for a particular substrate. The classification follows structural differences and recently an updated classification was proposed (15). The new SBP classification takes into account all crystal structures available at the beginning of 2010. Different sizes and sequences characterize SBPs and they can be discriminated by their three-dimensional structural folds. These folds are classified into six clusters based on structure similarity. In each cluster, proteins with similar structure, but not necessarily with the same ligand, are grouped. For example, cluster D is characterized by a scaffold that contains two relative short hinges but the cluster members can bind quite different ligands (*e.g.* phosphate and iron). This classification allows comparing proteins from a structural point of view, in particular in terms of common structural *motifs*.

Folding classification

In 2002, the first crystal structure of a secondary-active transporter (proton-driven multidrug exporter, AcrB, (116)) was resolved. Since then, a large number of 3-D structures for transporters have been successfully obtained. Despite a large variability in transporter structure (*i.e.* number of TransMembrane Domains -TMD-) and function, the repetition of common structures in the protein functional core has become evident. Therefore, transporters with a low sequence similarity assume the same structural fold. By looking at the available resolved crystal structures, at least five major different core folding architectures can be distinguished (21, 48, 138): (i) LeuT$_{Aa}$ fold; (ii) LacY fold; (iii) Glt$_{Ph}$ fold; (iv) NhaA fold; (v) ATP/ADP carrier fold (Fig. 2.6).

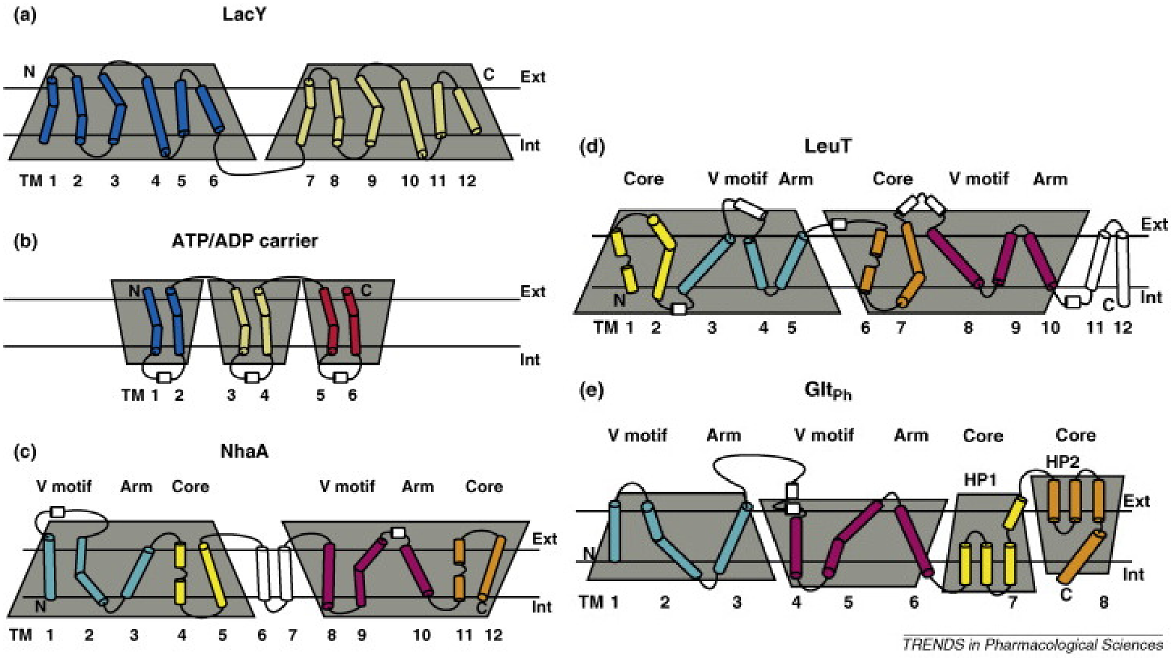

TRENDS in Pharmacological Sciences

Figure 2.6 Membrane topology of transporters with parallel and inverted structural repeats.

Modified from (21).

The presence of repeats, which comprise several contiguous TMDs, has become evident from 3-D structures. Parallel or anti-parallel orientations of repeats are related by a pseudo-symmetry axis that can be perpendicular or parallel to the plane of the membrane. It is thought that these structural repeats arise from gene duplication followed by fusion and sequence divergence.

In the LacY fold, representative of the MFS (Major Facilitator Superfamily), two repeats have a parallel orientation with respect to the plain of the membrane and const in 6 TMDs, each containing 3 TMDs that are anti-parallel suggesting a 3 TMDs ancestral form (Fig. 2.6a). The ATP/ADP mitochondrial carrier fold contains three identical units, each composed by 2 TMDs, to give a threefold pseudo-symmetric structure (Fig. 2.6b).

The other three folds depicted in Fig. 2.6c, 2.6d, 2.6e, are characterized by inverted structural repeats with anti-parallel orientation and a pseudo-symmetry axis parallel to the plane of the membrane. The $\mathrm{Glt}_{\mathrm{Ph}}$ fold shows a 3 TMDs repeat whereas NhA and $\mathrm{LeuT}_{\mathrm{Aa}}$ folds contain two 5 TMDs repeats. The majority of secondary-active transporters appear to belong to one of the three latest folds structure family. In the next two subsections, the $\mathrm{LeuT}_{\mathrm{Aa}}$ and $\mathrm{Glt}_{\mathrm{Ph}}$ folds will be described in detail.

Hairpin-like non-transmembrane discontinuous helices

The $\mathrm{Glt}_{\mathrm{Ph}}$ (that is an aspartate transporter) has a core folding that is so-called hairpin-like fold and is formed by non-transmembrane discontinuous helices. The folding architecture (Fig. 2.7c) shows 6 TMDs. They surround the core of the transport machinery composed by two re-entrant hairpin loops (HP1 and HP2) and transmembrane helix (TM7 and first part of TM8) that are orientated in an anti-parallel manner (169). This core folding is a characteristic of the glutamate transporters as well as H^+/Cl^- exchangers (40).

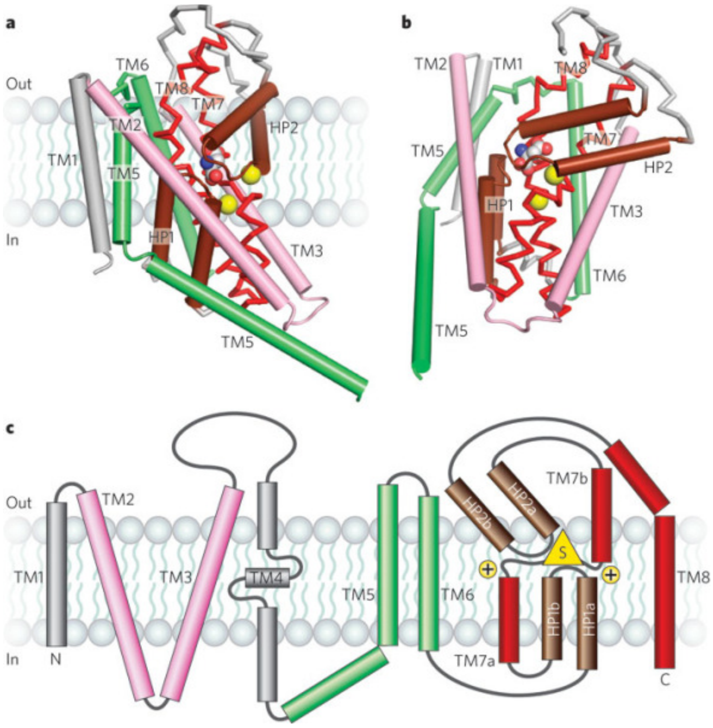

Figure 2.7 Architecture of the Glt$_{Ph}$ fold.

a. View parallel to the membrane. b. View approximately perpendicular to the membrane. c. Topological model. Brown: the hairpin loops that form the binding core of the monomer; pink/green: the inverted motif that protect the binding core, yellow: substrate (S) and co-substrates (+). From (91).

Transmembrane discontinuous helices

The folding architecture that is observed in LeuT$_{Aa}$ (the bacterial leucine transporter) is named architecture at transmembrane discontinuous helices (Fig. 2.8). Its structure shows a 5+5 TMDs repeat structure (light orange and light blue triangles in Fig. 2.8c). The functional core of the transport machinery is composed of two re-entrant loops (EL4-IL1) (167). The helices that span the membrane are orientated in an anti-parallel way. This folding is also found in other secondary-active transporters such as vSGLT (*vibrio* Na-glucose transporter) (43), MhP1 (benzyl-hydantoin transporter) (163) and BetP (Na-betaine symporter) (130).

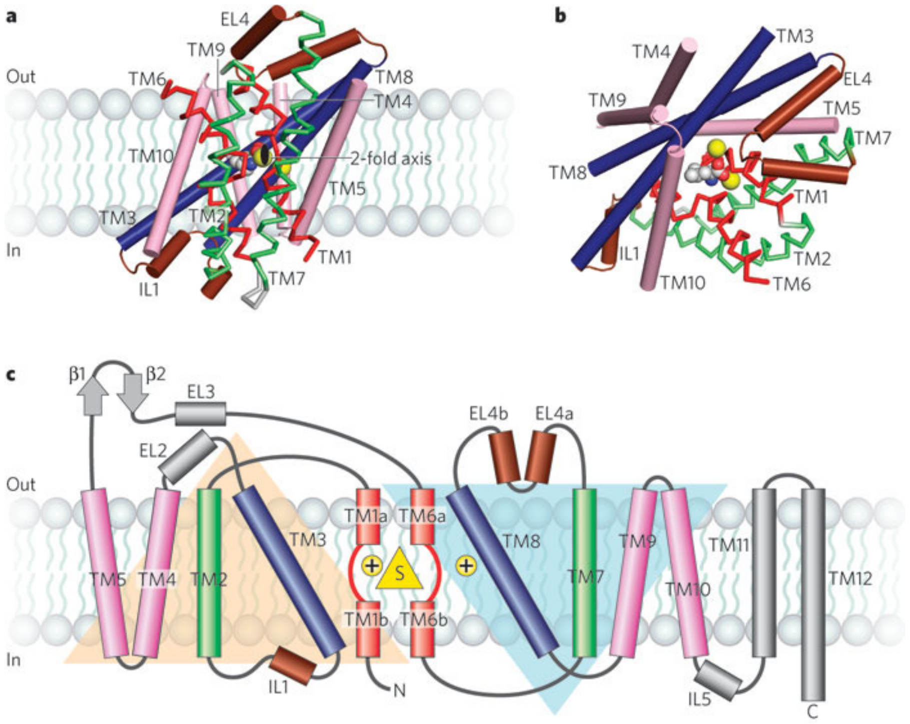

Figure 2.8 Architecture of the LeuT$_{Aa}$ fold.

a. View parallel to the membrane. b. View approximately perpendicular to the membrane. c. Secondary topology. Red, the binding core; green, pink, blue: the two inverted repeats; brown: the pseudo-two-fold loops are shown; yellow: substrate (S) and co-substrates (+). From (65).

The unexpected similarity in the folding of these cotransporters suggests common properties including transport mechanism, substrate/co-substrate binding sites and conformational changes associated with the transport activity.

2.3 MODELS OF TRANSPORT MECHANISM

Before the availability of 3-D structural information, a number of transport models had been proposed to explain the transport mechanism in carriers by integration of several functional studies (Fig. 2.9):

(i) the elevator mechanism, proposed for the multidrug transporter AcrB (Fig.2.9a);

(ii) the alternating access mechanism, originally proposed for Na^+/K^+ pumps, but also applied to cotransporter families (Fig. 2.9b);

(iii) the facilitated diffusion mechanism through a pore in the membrane (Fig. 2.9c, *e.g.* GLUT1);

(iv) the alternate gate mechanism where the binding pocket access is regulated by gates (Fig. 2.9d, proposed for Glt_{Ph} transporters).

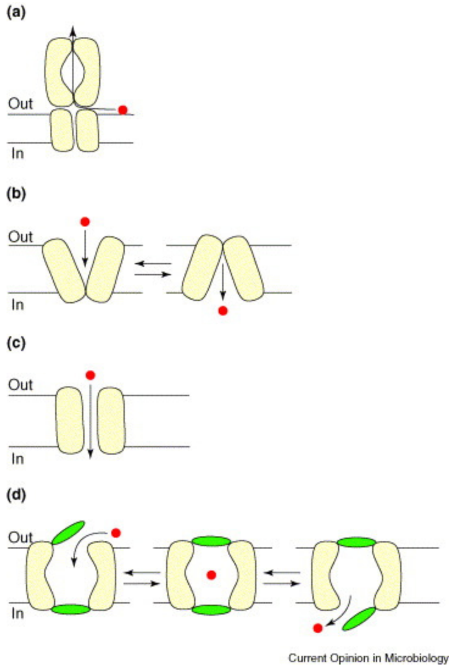

Figure 2.9 Schematic representation of four different types of translocation mechanisms proposed from functional studies as well as from recent transporters structures.
From (142).

The most important models that have emerged to explain the mechanism of secondary-active transporters are the alternating access model and the single-file model. The alternating access model was first proposed in 1966 (78). Thirty years later, the multi-substrate single-file model was described in detail (147) explaining new functional data that could not be simply explained with the alternating access model.

2.3.1 Alternating access model

In 1966 O. Jardetzky proposed for the first time a transport mechanism that is now known as the "alternating access model" (78). The model could explain the transmembrane transport of ions by "chemically activated" pumps such as the Na^+/K^+-ATPase. It shows a sequence of events occurring at every transport cycle. Jardetzky proposed three criteria that a transport protein should fulfill:

- it should contain a cavity (*permeation pathway*) that could admit the substrate;
- it should be able to present two different configurations (or two *conformations*), one in which the cavity was open to one compartment and another where the cavity was open to the second compartment (*i.e.* binding sites have to be accessible from only one side of the membrane at the time);
- it should contain binding sites for the substrates in the cavity that differed in affinity for the substrates depending on the carrier conformation.

This model fully explained many of the functional properties of the Na^+/K^+-ATPase such as a fixed stoichiometry (*e.g.* $3Na^+:2K^+$, which was already established from experimental data obtained for the pump expressed in red blood cells (125, 139)).

Later on, the determination of the fixed stoichiometry of GAT1 (Na^+-dependent γ-amino butyric acid transporter) in a heterologous expression system (*X. laevis* oocytes) (105), together with comparison between experimental data and model prediction (70) offered compelling evidence in favor of the alternating access model applied to cotransporters. From these studies, it was possible to predict that ordered partial reactions (or transitional states) have to occur to couple the transport of two or more substrates.

The scheme in Fig. 2.10 shows the conformations of a cotransporter during a complete transport cycle. All three original criteria postulated by Jardetzky are fulfilled: the permeation pathway is accessible from only one side of the membrane at the time. The cycle starts and ends at same state. The transporter has two main conformations: the outward and the inward.

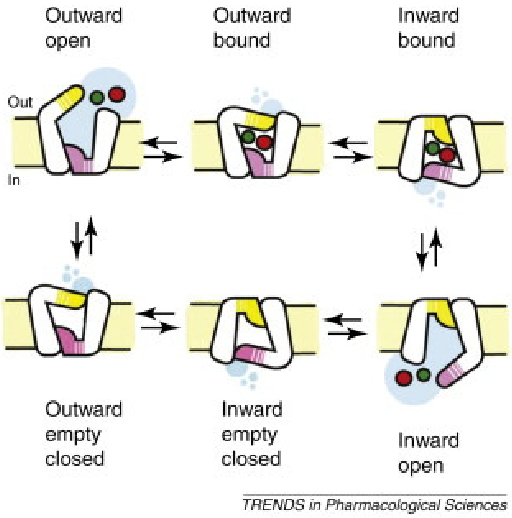

Figure 2.10 Alternating access mechanism for a symporter.
The cartoon shows the conformational transitions which a symporter undergoes during the transport cycle. From (21).

The alternating access model is currently the starting point to describe transport mechanisms of many transporters.

2.3.2 Single-File Model

The multi-substrate single-file transport model (Fig. 2.11) was proposed to take into account some of the properties that the alternating access model could not explain: namely uncoupled currents and variable stoichiometry (147). This model, considers the transport pathway structure as a single alignment of binding sites with ends exposed either to the extracellular or intracellular solutions. This structural view was borrowed from ion channel models in which the pathway is composed of a series of simultaneously bound ions (71). A substrate can be loaded from the solution to the first binding site (Fig. 2.11A). Once a substrate occupies the first binding site the “allowed” movements are from the binding site back into the solution or from the first to the second binding site (Fig. 2.11B).

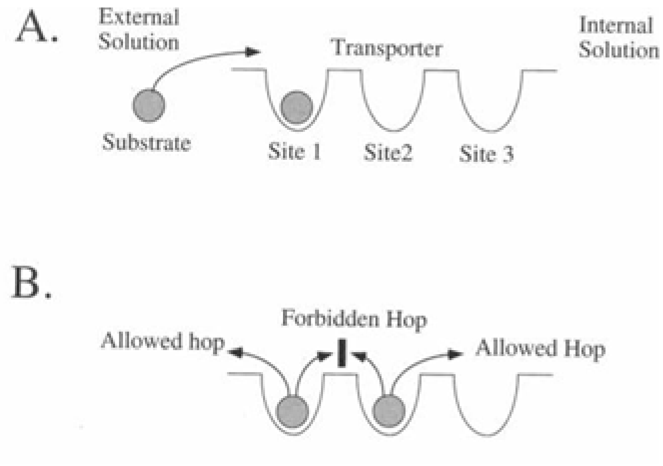

Figure 2.11 Single-file hopping model.

A. The substrate can access the first binding site from the extracellular solution. B. When a second substrate occupies the first binding site (site 1) the substrate that occupies the second binding site (site 2) cannot move back; the only possibility is to go toward the third binding site (site 3). Modified from (147).

The kinetic parameters are the result of all the possible transitions that can take place during the substrate transport. Fig. 2.11B depicts the hopping event when two substrates are bound in the transporter. Special rules are imposed on sites that are in direct contact with the solutions (internal or external). A substrate that is in the solution can “hop” to site 1 only when the site is empty, whereas the substrate that occupied the site 1 can always hop into the solution. The hopping frequency, given by the rate constants of the transporter kinetic cycle, describes the probability of individual hopping events.

This model describes all the major features of some transporters: leakage current, variable stoichiometry, substrate flux coupling and voltage-dependent transients. The major limitation is that the model cannot easily account for antiport, countertransport (the ability of the transporter to work in reverse mode) and solute exchange that can take place in some transporters (147).

Both models are conceptually based on experimental findings and they are important to understand the function of carriers.

2.3.3 Confirmation of alternating access model by 3-D structure

Transporter crystal structures, which have been resolved in the past decades, provide compelling evidence in support of the alternating access model. An evidence came from the first crystal structure of $\mathrm{LeuT_{Aa}}$ (167) showing that the binding sites were only exposed to the extracellular side of the membrane. The transporter structure contains a topologically inverted repeat of two structural elements (1-5 and 6-10) that are pseudosymmetrical with respect to the plane of the membrane (Fig. 2.12). Molecular dynamic (MD) simulations suggest that the conformational change of the bundle (TMDs 1-2-6-7) gives rise to the alternatively exposure of the binding sites (47).

The discovery of these features strongly supports the original idea of Jardetzky (78) whereby the substrate translocation relies on the binding sites being exposed to only one side of the membrane at a time. Moreover, the conformational rearrangement, necessary to allow the alternative exposure of binding sites, takes place without disrupting the substrate and co-substrate binding core in accordance also with the Single-Binding Center Gated Pore model (SBCGP), proposed to describe ADP/ATP carrier kinetic (49, 162).

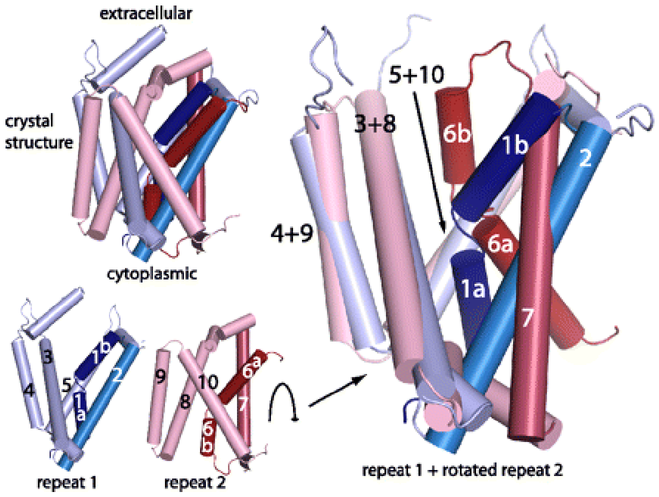

Figure 2.12 Structural asymmetry of repeats in LeuT.

TMs 1–10 of the LeuT crystal structure (upper left panel) were separated into the two structural repeats (lower left panel). The repeats can be superimposed by applying a 180° rotation (From (49)).

Support for the alternating access model and SBCGP were also founded in the 3-D structure of another cotransport: the sodium-benzylhydantoin transport protein (Mhp1) as the Mhp1 crystal structures of inward, outward and occluded states have been resolved (140).

MD simulations describe the main conformational change that occurs during the transition from the outward-facing state to the inward-facing state as a rotation of two rigid domains (the so-called bundle and hash domains) similarly to a “rocker-switch” mechanism (proposed also for LeuT$_{Aa}$). In the MD simulation, the opening and the closing of the “gates”, structurally corresponding to the helices that connect the bundle and the hash domains, is synchronized (or coupled) as described for the alternating access model (140).

Recently, the mechanistic model proposed for the proton/sugar cotransport (LacY) confirmed the validity of the alternating access model for the representative of the MFS family. This confirms that, also for this cotransporter family, the presence of inverted-domains is a key element to allow alternating access to the substrate binding pockets (127).

Research in the field of transmembrane proteins has been mainly focused on structure/functional characterization of transporters. The crystal structures emerging for many of the membrane proteins have increased our understanding of the actual transport process. The information obtained from functional and crystallographic data can be now combined to explore, in more detail, the transport mechanism of both channels and transporters using molecular dynamics simulations. *In silico* simulations can provide a temporal and spatial resolution of ion movements throughout the permeation pathway. This method relies on the determination of forces between individual atoms and this relationship with the phospholipid bilayer. Accumulation of inaccuracies in the determination of the forces describing the physical interactions limit the time of simulations to the microsecond range (86, 97).

Although these models provide a concept for how the proteins may function, the predicted behavior of these models always needs to be confirmed by functional studies.

2.4 FUNCTIONAL CHARACTERIZATION OF ELECTROGENIC TRANSPORTERS.

Over the last 50 years, the concepts derived from enzyme kinetics have successfully been applied to the characterization of membrane transport *via* carriers. For example, the movement of solutes from one compartment to another across the membrane can be considered as a reaction that is catalyzed by transport proteins acting as enzymes. Indeed, a transport system is described by some of the following properties for solutes, which are common to enzymatic processes:

- substrate specificity;
- apparent affinity for solutes ($K_{0.5}^{S}$);
- stoichiometry: a fixed number of solutes are involved in each transport cycle;
- binding mechanism: interactions on the transporter with solutes can be described as an ordered sequence of events;
- turnover rate: number of transport cycles *per* unit time;
- inhibitors and the mechanism of interaction with the transporter: substances that inhibit the transport function according to competitive, non-competitive or mixed competitive/non-competitive schemes.

2.4.1 Two-Electrode Voltage Clamp (TEVC): a method to study electrogenic cotransport

Advances of molecular biology techniques such as cloning and over-expression of a specific protein allowed the use of heterologous expression systems to explore protein functions. Moreover, the development of electrophysiological techniques, in combination with molecular biology, opened new frontiers for the investigations of electrogenic transporters. The main requirement to study electrogenic transport processes is to have a means to control the membrane potential (V_m) changes due to translocation of charges inside the cell, *i.e.* to achieve voltage clamping of the membrane. Indeed, in absence of V_m control, the driving force for the transport would be reduced. The electrogenic partial reactions (the transitions from one state to another of the protein that are sensitive to the voltage) would eventually change, over the time, their rate constant. Both driving force and time variation of the rate constant would contribute to alter the overall transport kinetics.

Therefore, electrophysiological techniques to study electrogenic transporters need:

- a control of the driving force (by controlling V_m);
- a high temporal resolution measurement of transmembrane charge movement (µs to ms range);
- real-time measurements;
- a detection of protein activity (by steady-state currents).

A commonly used heterologous expression system is the *X. laevis* oocyte. These cells have a number of advantages, including ease of handling (a large diameter, 1 mm) and are therefore easy to inject with either RNA into the cytoplasm or DNA into the nucleus (20). The oocyte translates the exogenous injected cRNA into protein, which is targeted to the plasma membrane in the case of membrane transport proteins.

The two-electrode voltage clamp (TEVC) technique uses two intracellular microelectrodes (Fig. 2.13) that impale the oocyte: one of these measures the intracellular membrane potential (V_m) compared to the bath (or extracellular medium). The other delivers current (*I*) to the oocyte. The actual membrane voltage (V_m) is compared with the desired potential as defined by the experimenter (V_{cmd}, which is typically in the range from -200 mV to +200 mV). Both signals (V_m and V_{cmd}) are compared by a differential amplifier that continuously corrects any differences between V_m and V_{cmd} by passing current (*via* the "*I*" electrode) into the oocyte. This negative feedback arrangement allows changes in membrane conductance to be followed in real-time.

As the membrane potential influences the conformational states of some electrogenic membrane proteins, a fast, accurate and homogeneous control of the V_m should be achieved by the TEVC. Typically, the TEVC can change the membrane potential of an oocyte with a temporal accuracy of 1-2 ms.

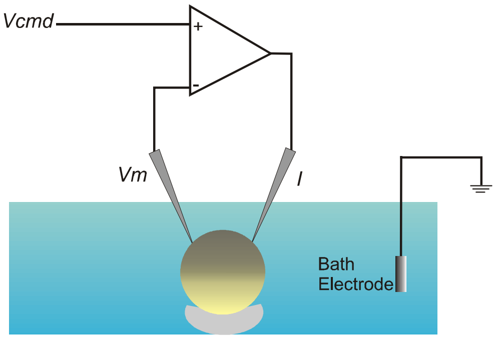

Figure 2.13 Two-Electrode Voltage-Clamp (TEVC).

Electrophysiological techniques offer a fast and indirect method to study membrane transport in electrogenic transporters. The recording of movement of ions as a current flow can be used to study functional characteristics of electrogenic cotransporters. The following section will focus on the functional characterization of electrogenic cotransporters using the TEVC by studying two types of experimental conditions:

(i) steady-state, which gives information about the electrogenic activity under steady state where the driving forces and the state variables (*e.g.* charge translocated) are constant;

(ii) presteady-state, which gives information about how the system responds to a change of state induced by a change in an external variable such as V_m.

2.4.2 Characterization of transport related currents

The transporter-associated currents that can be investigated with the voltage clamp technique are:

- steady-state substrate-induced currents;
- presteady-state currents;
- steady-state uncoupled leak currents.

The majority of the electrogenic transporters, depending on the experimental conditions, show all three currents. Nevertheless, some exceptions were observed, for example SLC20 Na^+-dependent P_i co-transporter, PiT-1, shows only transport-induced steady-state current with no evidence of uncoupled leak currents (129).

Steady-state substrate-induced currents

Steady-state substrate-induced currents are movement of charges across the membrane that accompany the transport of substrates. These currents reflect the transport of specific substrate and co-substrate (molecules and ions), if we assume a fixed stoichiometric relationship between charges and substrates translocated. As example of an electrogenic cotransporter I have chosen to illustrate this with published data from the sodium-dependent iodide symporter (NIS, SLC5A5).

Representative data obtained from oocytes expressing NIS are depicted in Fig. 2.14. A series of voltage-steps were applied to obtain steady-state current traces in presence of a solution containing Na$^+$ as main cation, (Fig. 2.14A). Application of 500 µM iodide (I$^-$) activates the cotransporter (Fig. 2.14B). An increase of the currents in the steady-state region (inset in Fig. 2.14) is seen when the cotransport is activated. The subtraction of traces recorded in absence of I$^-$ from the ones obtained in presence of I$^-$ gives the net current activated by I$^-$. This calculation allows to eliminate the endogenous currents present in both conditions. These steady-state currents can be plotted as function of voltage in an I/V plot shown in Fig. 2.14C.

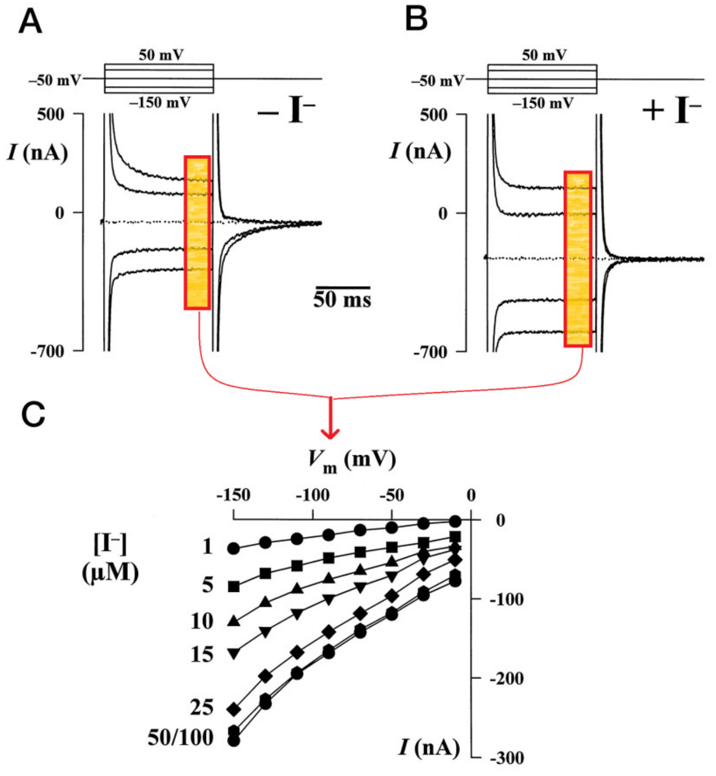

Figure 2.14 Steady-state currents in NIS.

A. Original recordings from an oocyte expressing the NIS transporter in absence of iodide. The traces were recorded at five different membrane potentials as shown in the upper part of the panel. B. Recorded traces obtained in presence of 500 µM I$^-$. C. I/V plot representing the transport activation by application of different concentrations of substrate (from 1 to 100 µM I$^-$). The curves were obtained by subtracting the steady-state current in absence of substrate from the one recorded in presence of the substrate. Modified from (42).

Increasing concentrations of I$^-$ in the extracellular solution showed different I/V curves (Fig. 2.14C) and it allows the determination of different parameters regarding substrate binding and substrate binding order: (i) apparent substrate affinity ($K_{0.5}^{S}$), (ii) Hill coefficient (nH) and (iii) maximum transport rates (I_{max}). The transport activity (current, I) plotted as a function of substrate concentration can be fitted with a form of the Hill equation (Eqn. 2.1):

$$I_0 = \frac{I_{max}[S]^{nH}}{[S]^{nH} + \left[K_{0.5}^{S}\right]^{nH}} \qquad \text{Eqn. 2.1}$$

where I_0 is the recorded response, I_{max} is the maximum predicted response and *[S]* is the substrate concentration. $K_{0.5}^{S}$ is the apparent affinity constant and it represents the substrate concentration at which the response is half of the maximal. In the case of a cotransporter with fixed driving substrate (A), this is termed the apparent affinity for substrate S, as its value will generally depend on A.

The Hill coefficient (nH), gives a lower estimation of the number of interacting molecules when they bind with positive cooperativity (161). If nH =1 the relationship between I and the substrate concentration loses its sigmoidicity and this corresponds to the classical Michaelis-Menten kinetics.

The dependence of I_{max} on fixed solute concentrations (or activities) is essential to determine the substrate binding order. In fact a reduction in the I_{max}, caused by changing the concentration of one substrate at the time is a strong indication that this substrate is the last to bind to the transporter.

Presteady-state currents

In addition to steady-state currents, it is possible to detect another type of transporter-associated current typically observed in absence of the saturating concentrations of substrate. These currents, termed presteady-state currents (Fig. 2.15A and B), are transient currents recorded in response to rapid changes in the V_m. They arise from intrinsic charge movements (charged or polar residues) of the protein in the membrane electrical field (*i.e.* charge movements resolved in the empty carrier) as well as the movement of ions entering the transmembrane electrical field and their binding, unbinding to the protein (*i.e.* Na^+ as shown in Fig. 2.15A).

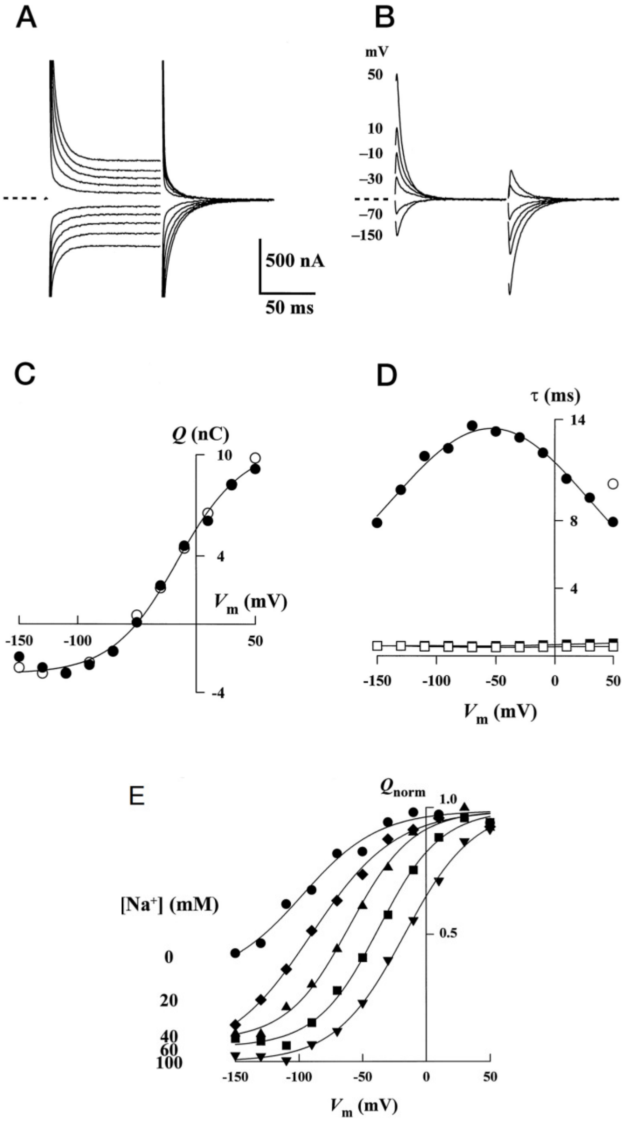

Figure 2.15 Presteady-state currents in NIS.

A. Current traces obtained by perfusing an oocyte expressing NIS with 100 mM Na$^+$ as main cation. B. traces obtained by subtraction of capacitative and steady-state components from the total current traces (represented in A). C. Q/V relationship. D. τ/V plot showing the two time constants derived from the fitting of traces in A. E. Q/V relationship at different [Na$^+$] in absence of substrate. Modified from (42).

The traces in Fig. 2.15A comprise two components: (i) a fast relaxation component that represents the charging of the membrane capacitance (τ_f). The speed of relaxation is determined by the voltage-clamp performance. The amount of charge displaced varies linearly with the size of the voltage-step and does not depend on the V_m (Fig. 2.15D, open squares); (ii) a slow relaxation (τ_s) component represents the charge movement associated with the transporter and it shows a non-linear dependence on the voltage (Fig. 2.15D, filled circles). One method of separating these components involves the application of a double exponential curve fitting procedure. The quantification of the charges that move in the membrane electrical field in response to voltage-jump can be obtained by integration over time of the transient current. The charge-voltage relationships obtained (*Q/V*, Fig. 2.15C) are further analyzed by fitting with a Boltzmann function. This function describes a simple two-state system in which each transporter is assumed to have an effective mobile charge (ze) that can be displaced across the whole of the transmembrane electrical field (Fig. 2.16):

$$Q = Q_{hyp} + \frac{Q_{max}}{1+e^{(-ze(V-V0.5)/kT}} \qquad \text{Eqn. 2.2}$$

where Q_{max} is the maximum charge translocated, Q_{hyp} is the steady-state charge at the hyperpolarizing potential limit that depends on the holding potential, $V_{0.5}$ is the voltage at which 50% of the charges have been displaced, z is the apparent valence obtained from the maximum slope of the fitted function. "e" is the elementary charge, k is the Boltzmann's constant and T is the absolute temperature.

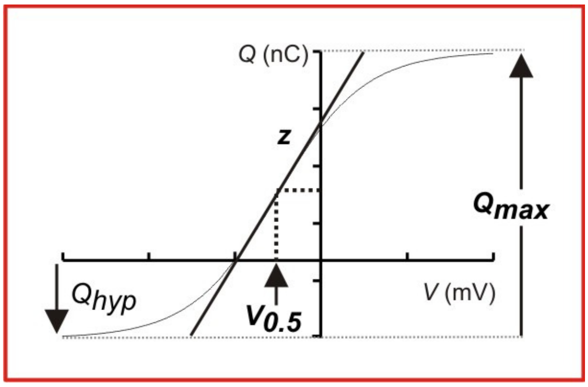

Figure 2.16 Schematic representation of the Boltzmann function used to describe the steady-state distribution of mobile charges.

Parameters obtained by fitting the data with a Boltzmann equation are indicated.

Steady-state uncoupled leak currents

Leak or *slippage* current arises from a deviation in the tightness of the coupled electrogenic behavior. The terminology that describes this current is taken from enzymes and pumps, where the *leak* is defined as a property of the membrane (*i.e.* permeability) and the *slip* concerns the molecule (in our case the transporter) that deviates from the strict dependence on the driven and driving substrates (119). Many transporters are characterized by these uncoupled currents (see Table 2.1). An important distinction can be made between *transport-dependent* and *transport-independent* leak currents.

The *transport-dependent* leak current is detected in presence of driving and driven substrates as a current in excess of that associated with the stoichiometric charge translocation.

A representative example is the glutamate transporter (EAAT family, SLC1). Glutamate transport requires 3 Na^+ together with a H^+ and counter transport of one K^+. In the presence of all these ions and the substrate, movement of anions (Cl^-) also occurs (160). This leak mode is only observed when all the substrates and co-substrates are present in the solution and is due to the presence of a ligand gated chloride channel associated with the transporter.

Transport-independent leak currents are detected in absence of driven substrates and may or may not involve the driving substrate.

The investigation of the transport-independent leak current is often difficult because more than one ionic species can contribute to the total leak current. The ions contributing to the leak current can be either the same as the ions that preferentially drive cotransport (*e.g.* SGLT1 a leak of Na^+ (31, 106)) or different (*e.g.* GAT1 is characterized by an uncoupled Li^+ current (26)). Leak current can also be anionic as shown for the sodium-coupled neutral amino acid transporter: SNAT2 (174) and EAAT5. In particular, for EAAT5 the appearance of an anionic conductance that was larger than that associated with the transport substrate, hinted at the presence of a leak mode (8).

The leak current of the Na-iodide sympoter (NIS) represents a good example of transport-independent mode. In oocytes expressing NIS it was observed that the perfusion with 100 mM Na^+ alone induces a large inward current (> 100 nA at -50 mV, Fig. 2.17) with respect to H_2O-injected oocytes (<20 nA at -50 mV). The addition of 500 μM of I^- causes a further inward directed current ($Na^+ + I^-$, Fig. 2.17). The Na^+-induced current represents the leak of Na^+ in the oocytes when NIS is expressed in the membrane. The Na^+-leak in NIS was found to be saturable with increasing Na^+ concentration in the extracellular solution. Therefore, the data were best fitted with the Hill equation to predict the *nH* = 1, indicating that at least one Na^+ ion *per* cycle *per* transporter contributes to the leak through the transporter.

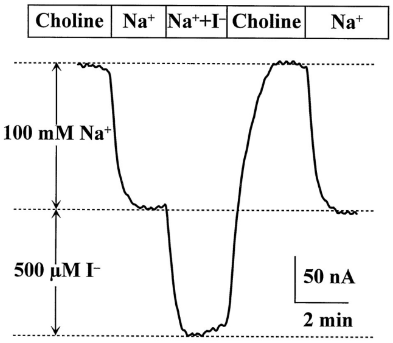

Figure 2.17 Na^+-leak current in NIS.

Current recorded from a NIS injected oocyte with the membrane potential clamped at -50 mV. The tested solutions are shown in the upper part of the figure. 100 mM Na^+ indicate the Na^+ leak current; 500 µM I^- indicate the substrate-induced steady-state current. Modified from (42).

SLC	Gene Name	Substrates		Type of uncoupling	Selected references
		Coupled	Uncoupled		
1	EAAT1,2,3,4,5	Na$^+$/H$^+$/K$^+$/Glu	Cl$^-$	T	(8)
	EAAC1		Na$^+$	L	(81)
	ASCT1, 2	Na$^+$/Neutral aa	Cl$^-$	T	(173)
5	SGLT1	Na$^+$/Glucose	Na$^+$	L	(31, 106)
	NIS	Na$^+$/I$^-$	Na$^+$	L	(42)
	SMIT	Na$^+$/myoinositol	Na$^+$	L	(33)
	SMCT	Na$^+$/monocarboxylate	Anions	L	(34)
	CHT	Na$^+$/Choline	Na$^+$	L	(77)
6	GAT1,4	Na+/Cl-/GABA	Li$^+$, Cs$^+$, Cl$^-$	L	(83, 111)
	SERT	Na$^+$/Cl$^-$/K$^+$/5HT	Na$^+$,Li$^+$,K$^+$,H$^+$,Cl$^-$	L/T	(27, 59, 112)
	DAT	Na$^+$/Cl$^-$/Dopamine	Na$^+$,Li$^+$,K$^+$,H$^+$,Cl$^-$	L/T	(114, 144)
11	DMT1	H$^+$/divalent cations	H$^+$	L	(107)
13	NaDC	Na$^+$/dicarboxylate	Na$^+$	L	(168)
15	PepT2	H$^+$/peptides	H$^+$	L	(30)
34	NaPi-IIa	Na$^+$/Phosphate	Na$^+$	L	(52)
38	SNAT1	Na$^+$/Neutral aa	Na$^+$	L	(108)
	SNAT2	Na$^+$/Neutral aa	Cl$^-$	L	(174)
	SNAT3	Na$^+$/Neutral aa	K$^+$, H$^+$, Na/H$^+$ Exchange Cations	T L	(136)

Table 2.1 Transporter families show uncoupled leak.

T: transport-dependent leak and L: transport-independent leak mode. Modified from (6).

2.4.3 Stoichiometry determination

To characterize the transport mechanism it is important to estimate the solute concentrating ability of the transport system. Ideally, cotransporters should display a fixed stoichiometry, *i.e.* between the number of moles of driving and driven substrates transported. Considering the alternating access model for substrate transport, it is easy to imagine that the binding sites for the substrates are limited in number. It is therefore useful to establish the stoichiometry to develop a transporter kinetic model.

Several approaches to estimate the stoichiometry are possible:

(i) *Tracer methods* use radioactive substrates for both substrates/co-substrates. Samples are incubated in a solution containing radioactive solutes; they will be then quantified separately for the radioactivity accumulated in the cell in the unit of time. The ratio between the amounts of the two species will give the stoichiometry. To use this approach, we assume that flux of driving and driven substrates is tightly coupled, *i.e.* the uncoupled flux (or leak current) in the electrogenic transporters is negligible. This method can also be used to establish the stoichiometry in both electroneutral and electrogenic transporters (79, 81).

(ii) *Substrate activation method* involves the quantification of the substrate flux as function of the co-substrate, or activator. Here, the concentration of one of the substrates is varied and the transport activity measured with radiotracer assays or by electrophysiology (153). The stoichiometry is indirectly estimated from the determination of the Hill coefficient (see above Eqn. 2.1). The Hill equation can be used to estimate the minimum number of binding molecules that are required to activate the protein (transporter or enzyme) but this only provides a measure of the degree of cooperatively during the binding process (161).

(iii) *Simultaneous electrophysiology and radiotracer assays.* This technique is applicable to electrogenic transport systems and it involves the quantification of charges in combination with radiotracer for a single species that are translocated during the transport. If two species are transported it is necessary to quantify the substrate/charge ratio for each. The combination of the two ratios (*i.e. nA/nS*, number of moles of driving substrate (*A*)/ number of moles of driven substrate (*S*)) gives the stoichiometry (22, 38, 42, 50). In NIS, the stoichiometry estimation gave a ratio of $I^-/Q = 0.76$ and a $Na^+/Q = 0.42$. The combination of these results gave a ratio of 1.8 (Na^+/I^-) suggesting a $Na^+:I^-$ stoichiometry of 2. The underestimation of the ratio is most likely due to the contribution of the leak Na^+ current which was not accounted for the determination of the Na^+/ charge ratio (42).

(iv) in *thermodynamic equilibrium techniques*, the membrane current is clamped to zero and the membrane potential (V_m) is measured while external substrate and cation concentrations are varied. The stoichiometry is estimated from the ratio between the changes in V_m when either co-substrates or substrates are reduced by half. For this method to be applicable, endogenous responses must be small and the leak current negligible (31, 34, 95, 141).

2.4.4 Turnover Rate

The determination of the number of transport cycles *per* unit time (the turnover rate) is an important kinetic parameter because it is an indication of the transport capacity of a transporter. Moreover, it gives the upper limit for the prediction of the rate-limiting partial reaction in the transport cycle. Under defined conditions (*e.g.* saturating substrate) and knowing the number of active transporters, it is possible to determine the transport turnover rate using steady-state and presteady-state currents. The method uses presteady-state charge movements to estimate the number of active transporters. The assumption of this method comes from studies made on channels where the measure of gating charge was proportional to the number of activated channels (71).

Like the gating charges intrinsic to the voltage-gated channels, we can use the presteady-state charge movements of electrogenic cotransporters to estimate the number of active cotransporters.

For a given transporter, the steady-state current, the current associated to the transport of substrate, can be expressed as:

$$I_S = N \ \varphi \, q \, e \qquad \text{Eqn. 2.3}$$

where N is the number of active transporters, φ is the unitary turnover rate (transport cycles *per* unit time), q is the number of charges translocated *per* cycle and e is the electronic charge (1.602 10^{-19} C).

The number of transporters (N) can then be estimated using presteady-state charge measurements:

$$N = \frac{Q_{max}}{ze} \qquad \text{Eqn. 2.4}$$

where z is the apparent valence of the moveable charge. Q_{max} is the total charge that can be moved. Both Q_{max} and z can be found by fitting the presteady-state *Q/V* data with single a Boltzmann function (see above Eqn. 2.2 in section 2.4.2).

Rearranging Eqns. 2.3 and 2.4 we obtain the turnover rate as:

$$\varphi = \frac{I_S\, z}{q\, Q_{max}} \qquad \text{Eqn. 2.5}$$

This approach is based on the following assumptions:

1. I_s represents the maximum current mediated by the transporter, it must be recorded in saturating substrate concentrations and saturating voltages.
2. Q_{max} represents the maximal number of mobile charges.
3. The number of active transporter determination (*N*) assumes that z, obtained from the Boltzmann fit, represents accurately the apparent displacement charge *per* carrier.

In different studies, the apparent valence of the moveable charge, *z*, was found to be underestimated: *e.g.* SGLT1(172), GAT1 (62) and NIS (42). For example in NIS, the Boltzmann fit gave a $z \approx 1$. By means of freeze-fracture (172), it was possible to count the number of particles and estimate the transporter density. Using this method to calculate *N* the estimation gave $z \approx 3$.

For GAT1, using the I_s/Q_{max} linear regression, the predicted turnover rate was 15.2 cycles/sec. With freeze-fracture method (172) the turnover rate was ≈4.6 cycles/sec confirming the importance of the accuracy in the determination of *N* (62). Several sources of errors were noted in the freeze-fracture method: quantification of particles, determination of Q_{max}, accuracy of membrane area.

Recently it was shown that also the estimations of turnover rates for SGLT1 (57 s^{-1} (101) and 28 s^{-1} (103)) were not correct when correlated with the particle count obtained by the freeze-fracture method (172). In this study, a new technique was used to estimate the turnover rate: the so-called Ion-Trap Technique (ITT) (18). This technique uses an ion-selective microelectrode (ISE) to measure directly the ionic activity. To have a high noise-signal ratio the ISE was pushed close to the oocyte surface (5 μm) to isolate a small volume of extracellular solution from which the cation and the solute were depleted during transport. The turnover rate of SGLT1 was estimated to be 13.3 s^{-1} in presence of 90 mM Na^+ and 5 mM α-methyl-D-glucose (99) the main limitation of this method is that high levels of expression are needed to measure the change in the ion concentrations in the trap.

2.4.5 Cation specificity

The majority of cotransporters use Na^+ electrochemical gradient as energy to transport substrates across the plasma membrane. Nevertheless, other cations, as Li^+ and H^+, can substitute for Na^+ as driving force although changing substrate affinities and transporter rates.

Illustrative examples are the sodium-coupled glucose transporters (SGLT1) and bacterial melibiose (MelB). In absence of Na^+ (the preferred co-substrate), can use Li^+ and H^+ as driving force to accumulate substrates into the cell. For these transporters the binding of cations induces conformational changes that allow the activation of the sugar transport (73, 152). In SLGT expressing oocytes, Li^+ or H^+ can be used as co-substrates but giving a different apparent affinity $K_{0.5}^{sugar}$ and maximal rate I_{max}^{sugar}. Fig. 2.18 illustrates steady-state substrate-induced currents normalized by the substrate-induced current obtained in presence of Na^+. It is evident that both H^+ and Li^+ can activate the transport (activation represented by the substrate-induced current curve) albeit with a different voltage-dependence.

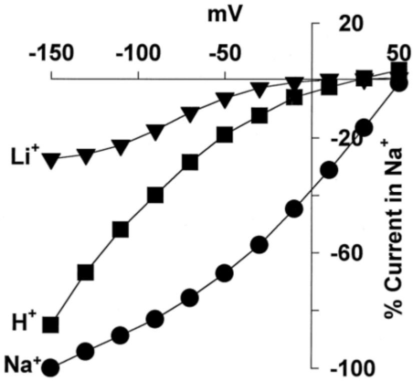

Figure 2.18 Sugar-induced current/voltage (I/V) relationships.

Currents induced by 5 mM α-methyl-D-glucoside (αMG) were measured in presence of 100 mM Na^+ *or* Li^+*, pH 7.5, or 100 mM choline chloride, pH 5.5, are plotted against the membrane potential. Modified from (73).*

The cation specificity for GABA-transporters is isoform-dependent (46, 63, 113). Protons can interact with GAT isoforms in a different manner but they are not able to activate the transporter preventing the GABA transport across the membrane. Cations can also influence the kinetics of presteady-state relaxations, *e.g.* Li^+ reduces the relaxation time at negative potential in GAT1 when Na^+ is not present (64).

2.5 PHOSPHATE TRANSPORTERS

This dissertation will focus on the functional properties of a particular secondary-active membrane protein: sodium-dependent phosphate transporters (NaPi-II). In particular, certain questions regarding the nature of the uncoupled current and the interaction of cations with the transporter are addressed. In this chapter, functional properties of NaPi-II will be described in detail.

2.5.1 Phosphate homeostasis

To place these transporters in a physiological context a brief overview on phosphate homeostasis is presented.

Phosphorus is an essential element for life: it is found in nucleic acids (DNA and RNA), it is important for signal transduction; it is an essential component of the phospholipid bilayers and it is involved in energy metabolism (as the energy source in the form of ATP) (13).

Phosphorus is widely distributed in the body, in the extracellular fluid (~500 gr.) in the inorganic form (phosphate, P_i); it is present in the soft tissues in organic form (~100 gr. as a component of phospholipids and phospho-proteins) as well as in the bone matrix (~600 gr.) where phosphate is stored as hydroxyapatite (19, 44).

In humans, dietary intake of P_i amounts to 1400 mg *per* day, once P_i is absorbed in the gut, it reaches the circulation where it is essential to buffer the blood pH. Serum P_i concentration varies from 0.8 to 1.5 mM. Finally, all the absorbed phosphate is excreted in the urine (900 mg/day) and feces (500 mg/day) to give an average balance between intake and excretion (19).

P_i absorption occurs in the small intestine by active transport process as well as free diffusion. P_i excretion occurs in the colon during feces formation as well as in kidneys in during urine formation. As kidneys filter around 7000 mg/day of phosphate its reabsorption is essential to maintain the correct homeostasis. The first part of the nephron (the proximal tubule) is involved in the reabsorption of 80% of the P_i *via* a secondary-active transport process (19).

2.5.2 Renal sodium-coupled phosphate cotransporters

P_i excretion is regulated by modification of the apical expression of the Na^+-coupled phosphate cotransporters present in the convoluted proximal tubules (154); these membrane proteins are secondary active transporters that use the electrochemical potential gradient of Na^+ to accumulate P_i inside proximal tubule cells. The pathway responsible for the basolateral exit of P_i is not yet known, but it has been hypothesized that the accumulation of P_i inside the cells is enough to drive its exit through facilitative membrane proteins by diffusion (Fig. 2.19).

Proteins from two different gene families mediate the Na^+-coupled P_i transport in the proximal tubule, namely the Type-II Na^+-dependent phosphate cotransporters, SLC34 (NaPi-II) and Type-III Na^+-dependent phosphate cotransporters, SLC20 (PiT).

The products of the gene family SLC34 encode three NaPi-II isoforms; two of them are present in the proximal tubule: NaPi-IIa (SLC34A1) and NaPi-IIc (SLC34A3). The third isoform (NaPi-IIb, SLC34A2) is localized in the small intestine, as well as other epithelia-like tissues *e.g.* in lung and testis ,where is responsible for the active absorption of phosphate (68).

Gene products of SLC20 family include two isoforms: PiT-1 and PiT-2. These phosphate transporters were originally identified as retroviral receptors, namely for the gibbon ape leukemia virus (Glvr-1, (120)) and for the rat amphotropic virus (Ram-1, (115)). Their strong identity with a phosphate permease from *Neurospora crassa* (80), was a strong indication that they were involved in phosphate transport, which was then shown to be the case by heterologous expression (84). The wide distribution (*i.e.* kidney, brain, heart, liver, muscle, and bone marrow) of both PiT-1 and PiT-2 suggests that they play a housekeeping function in several different types of cells. Recently, it was reported that PiT-2 (SLC20A2) is present in the brush border membrane in proximal tubule and contributes to the overall phosphate reabsorption in the kidney (Fig. 2.19) (156).

The main functional difference between NaPi-II and PiT is that NaPi-II prefers divalent phosphate (HPO_4^{2-}, (32)) whereas PiT prefers monovalent phosphate ($H_2PO_4^-$, (129)) and hence the transport of P_i by the latter is not strongly affected by acidification (see below). This suggests that the role of PiT in the proximal tubular cells is to compensate for the strong dependence of P_i reabsorption by SLC34 when the glomerular filtrate became acidotic (156).

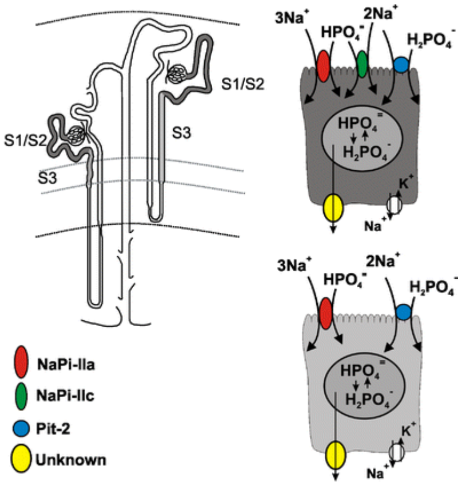

Figure 2.19 NaPi-II localisation.

Na^+-coupled P_i cotransporters are found in the apical membranes of proximal tubular brush border epithelia. Transporters are localized in the proximal tubule, specifically the S1, S2 and S3 segments. NaPi-IIc is particularly abundant in S3 segment. From (17).

NaPi-II family

Native brush border membrane preparations were used to demonstrate that phosphate transport across the proximal tubule epithelia was mediated by a secondary-active transport process (74). Furthermore, the effect of pH variations was studied in "*in vivo*" experiments (25, 134). In these early studies it was observed that the presence of P_i caused a variation in the membrane potential and therefore the presence of an electrogenic transport mechanism was proposed (23, 134). After the cloning of the NaPi-IIa (SLC34A1) transporter (110) it was possible to perform functional studies on NaPi-IIa heterologously expressed, *e.g.* in *X. laevis* oocytes, to define kinetic characteristic of this transporter. Electrogenic cotransport of P_i was demonstrated unambiguously for the first time using the TEVC (24, 66). Moreover, some of the transport properties (*e.g.* pH dependence, apparent substrate affinities) previously determined using membrane preparations were recapitulated under *in vitro* conditions, which confirmed the role of SLC34 proteins in P_i transport *in vivo.*

Our current knowledge about the structure of NaPi-II in the membrane is based on hydrophobicity profiles of the primary structure, site-directed mutagenesis and SCAM (Substituted Cysteine Accessibility Method, (5)). These techniques together with structure-function studies and *in vitro* transcription/translation investigations (93, 126) allow a more precise topology to be predicted than that obtained from solely hydrophobicity analysis of the primary sequence. Information about the 3-D structure of the NaPi-II is still lacking.

The current model for NaPi-II proposes 12 transmembrane domains (TMDs), 8 of which are most likely true membrane spanning TMDs and 4 are forming two so-called re-entrant loops. One re-entrant loop is internal (formed by TMDs 3-4) and the other one is external (formed by TMDs 8-9). These two re-entrant loops are preserved in all NaPi-IIa/b/c isoforms suggesting that they are linked to an essential functional role. According to several studies, these two regions form the putative pathway for the transport (88, 89, 94, 126). The N- and C- termini are located on the cytoplasmic face and a large extracellular loop (between TMDs 5-6) contains two N-glycosylation sites (92, 126). This loop contains a critical disulfide bridge that is believed to link the two protein regions (from TMD 1-5 and from TMD 6-12). Each of these halves of the protein contains regions that are believed to move relative to one another in a complementary manner during the transport cycle (158) (Fig. 2.20).

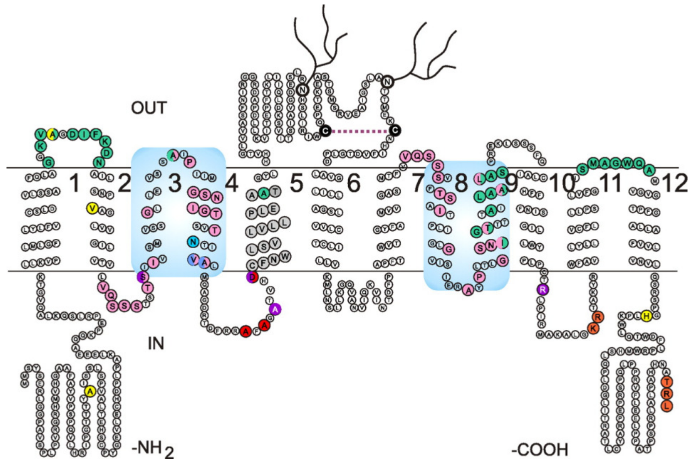

Figure 2.20 Secondary topology for rat NaPi-IIa.

The 12 transmembrane domains are shown; the light blue boxes highlight the two re-entrant loops. Two N-glycosylation sites and a disulfide bridge have been identified in the large extracellular loop between TMDs 5-6. From (159).

The electrogenic as well as the electroneutral isoforms preferentially transport divalent phosphate (HPO_4^{2-}), which is present in a ratio of 4:1 with the monovalent form ($H_2PO_4^-$) at physiological pH (pH 7.4). P_i is cotransported together with Na^+ with different stoichiometries: $3Na^+$:$1P_i$ for the electrogenic NaPi-IIa/b (52) and $2Na^+$:$1P_i$ for the electroneutral NaPi-IIc (9).

As already indicated above, P_i transport by NaPi-II is affected by extracellular pH. At low pH the transport activity (measured as P_i-induced current under voltage-clamp, I_{Pi}) decreases, which suggests that an altered acid-base status might influence the phosphate homeostasis in the body (51). Phosphonoformic acid (PFA or foscarnet) was shown in BBMVs to be a competitive inhibitor of Na^+-driven P_i cotransport (148) and was also shown to be a competitive inhibitor of NaPi-IIa expressed in *X. laevis* oocytes (apparent K_i 3.6 mM) (25).

2.5.3 NaPi-II: electrophysiological characterization

By means of heterologous expression of NaPi-IIa/b (electrogenic isoforms) in *X. laevis* oocytes, transport activity studies have been conducted using both radiotracer and voltage-clamp techniques, in particular the TEVC. In the presence of external Na^+, the application of 1mM P_i causes an inwardly directed current. This phosphate-induced current (I_{Pi}), can be seen as an increased inward current with respect to baseline holding current, I_h (Fig. 2.21). I_{Pi} is voltage-dependent, it is due to one net charge being translocated *per* transport cycle *per* transporter and it was found to be Na^+-dependent with an apparent affinity for Na^+ comparable to the value found in vesicles experiments (~50 mM) (66). The apparent affinity for P_i is $\leq$ 0.1 mM and below the normal physiological concentrations (phosphate serum level 0.8-1.5 mM). The upward deflection of I_{h} caused by the superfusion of 1 mM PFA is due to the inhibitory effect of this compound on electrogenic NaPi-II isoforms. The PFA-sensitive current (I_{PFA}), is believed to be a Na^+-leak passing though the transporter in absence of P_i (*i.e.* transport-independent leak mode, section 2.4.2).

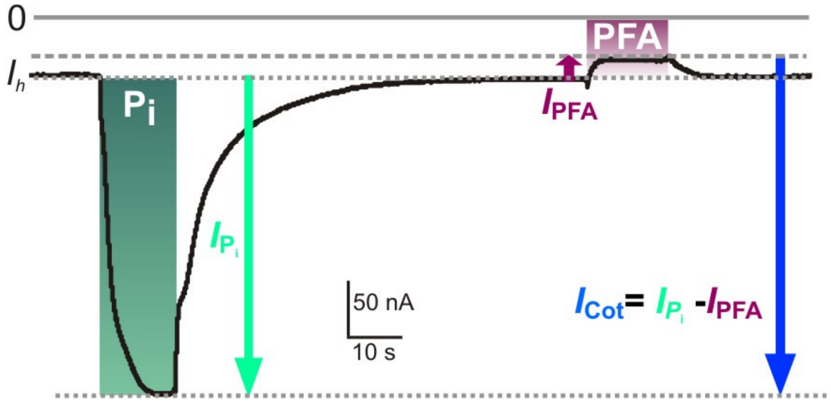

Figure 2.21 Electrophysiological responses of NaPi-IIa under voltage clamped conditions.
A voltage clamped (-50 mV) oocyte superfused with a solution containing 100 mM of Na^+ is successively exposed to saturating concentration of 1mM P_i (green) and 3 mM PFA (violet). The predicted electrogenic cotransport activity is given by I_{Cot}. Modified from (6).

In a previous study it was established that the presence of saturating P_i suppresses the Na^+-leak mode and therefore it was proposed that the leak and cotransport modes are mutually exclusive (88). Hence, it was convenient to refer to the true cotransport electrical activity defined (I_{Cot}) obtained from the sum of the absolute values of I_{PFA} and I_{Pi} (Fig 2.21 blue arrow).

The stoichiometry of electrogenic NaPi-IIa/b was determined from data obtained by studying the relationships between the translocated charge (*Q*) and the substrate (P_i) as well as between the charge and the co-substrate (Na^+). The ratio between the molar equivalent of charge translocated (n^{Qt}) and number of moles of P_i ($n^{\mathrm{HPO_4^{2-}}}$) was established, giving a n^{Q}: $n^{\mathrm{HPO_4^{2-}}}$ ratio of 1:1 (Fig. 2.22 filled circles). This result alone suggests that one P_i was transported together with one charge *per* transport cycle *per* transporter. In addition, the ratio between the number of moles of Na^+ ($n^{\mathrm{Na^+}}$) and molar equivalent of charge translocated (n^{Qt}) was established. This experiment gave n^{Qt}: $n^{\mathrm{Na^+}}$= 1:3 (Fig. 2.22 open circles). The combination of these two results established that the NaPi-IIa/b stoichiometry was $3Na^+$:$1P_i$ (50).

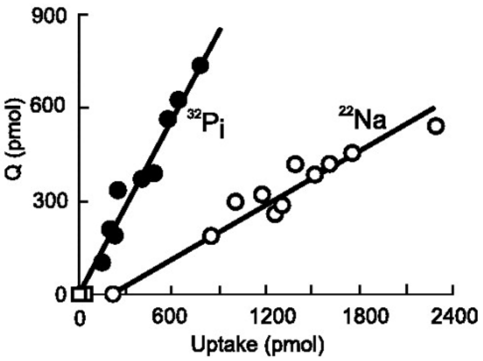

Figure 2.22 Stoichiometry determination of NaPi-IIa and NaPi-IIb.
Single oocytes were voltage clamped at -50 mV and superfused with a radioactive solution containing either ^{32}P or ^{22}Na. In the same oocyte, the charge, Q, associated with the substrate transport and the accumulated amount of radiotracer were calculated. Modified from (159).

Steady-state currents

The application of P_i induces an inwardly directed current due to the transport of 3 Na^+ together with one divalent P_i into the cell (Fig 2.23). By application of a voltage-step protocol, the P_i-induced current (I_{Pi}) can be recorded over a range of potentials (from -160 mV to +80 mV). Fig. 2.23A and B show original current traces recoded from oocytes expressing NaPi-IIb. To obtain I_{Pi}, the traces recorded in 100Na are subtracted from the traces recorded in 100Na + P_i

to eliminate endogenous oocytes currents (Fig. 2.23C). The subtracted current traces are then plotted as function of voltage (*I/V* plot Fig. 2.23D).

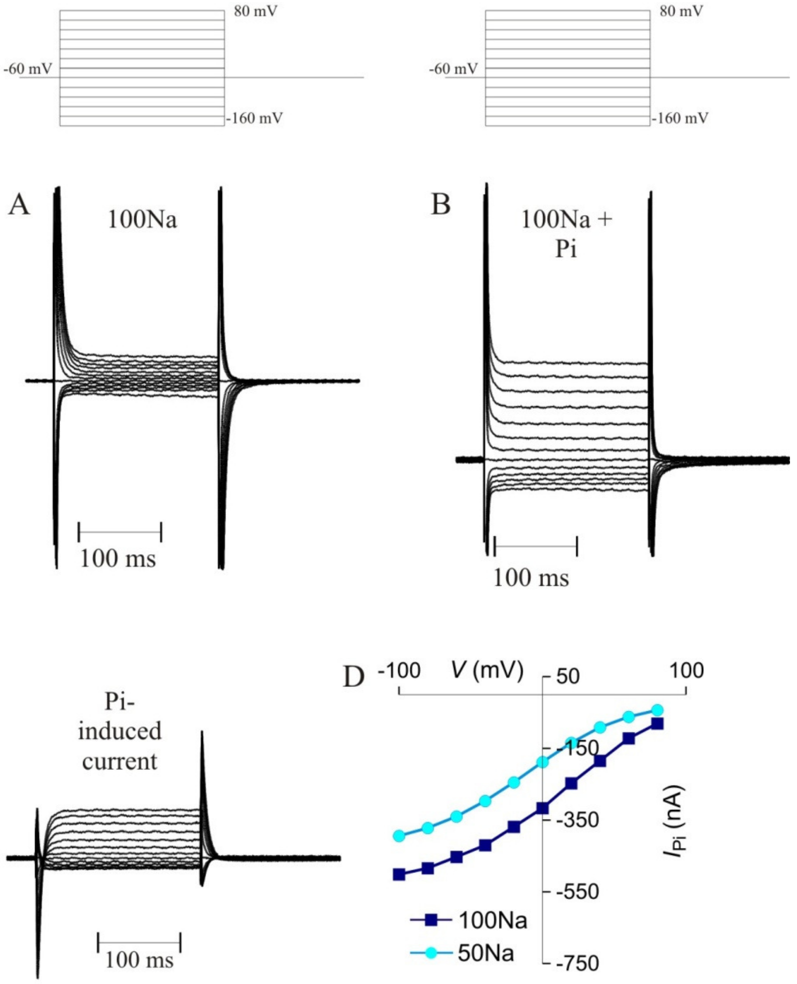

Figure 2.23 Steady-state substrate-induced current in flNaPi-IIb.

A: traces recorded in presence of 100 mM NaCl (100Na). B. Traces recorded in presence of 100 mM NaCl and 1 mM P_i *(100Na+*P_i*). C. Traces obtained by subtraction of A from B. D. I/V plot showing phosphate-induced current (*I_{Pi}*) for two* Na^+ *concentrations (squares 100 mM* Na^+*, circles* I_{Pi} *at 50 mM* Na^+*).*

As mentioned above, I_{Pi} is Na^+-dependent as seen from comparing *I/V* relationships obtained in 100Na (Fig. 2.23D, dark blue symbols) with 50Na (Fig. 2.23D, light blue symbols).

The voltage-dependence of the I_{Pi} is isoform-specific meaning that the kinetic rates are different between the isoforms. An illustrative example is depicted in Fig. 2.24, I_{Pi} is obtained applying voltage-step protocol from -140 mV to +40 mV. NaPi-IIa isoform shows the “S” shaped voltage-dependence with rate limiting behavior for potentials more negative than -100 mV (54).

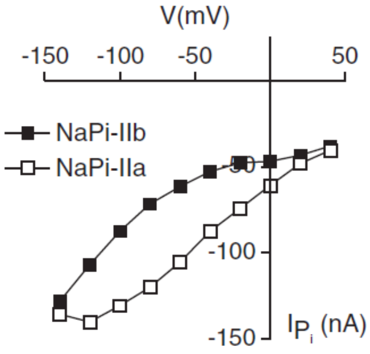

Figure 2.24 Comparison of steady-state P_i-induced current for two NaPi-II isoforms.
Modified from (54).

These characteristics suggest that the overall transport cycle includes both electrogenic (voltage-dependent) and electroneutral (voltage-independent) transitions.

Presteady-state relaxations

An understanding of the overall transport cycle can be gained by examining the behavior of the transient currents. This allows us to distinguish electrogenic from electroneutral partial reactions as well as characterize electrogenic partial reactions.

Presteady-state charge movements evoked by the voltage-step protocol (Fig. 2.25) are detected in oocytes expressing electrogenic isoforms of NaPi-II. These charge movements are dependent on the presence of Na^+ in the extracellular medium and are strongly suppressed in presence of saturating P_i (55) (see 2.4.2, presteady-state).

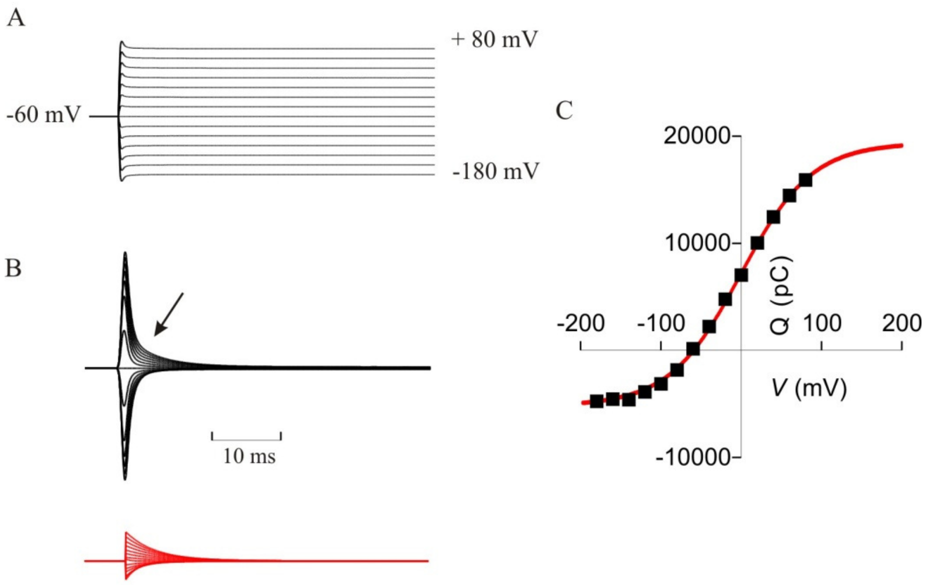

Figure 2.25 Analysis of presteady-state transients.

A. Original record of the voltage-step protocol. B. Current traces in response to voltage-step protocol. The arrow indicates the presteady-state relaxations due to NaPi-II expression. The red traces represent the slower component associated with NaPi-II obtained from the two exponential fit. C Q/V plot from the traces represented in panel B, the Boltzmann fit is represented by the red curve.

Leak mode

As already mentioned, a leak mode in the electrogenic NaPi-IIa/b is detectable by perfusing a clamped oocyte with a solution containing PFA (see Fig. 2.21). Application of voltage-step protocol shows that the voltage-dependence of I_{PFA} matches the voltage-dependence found for I_{Pi}, this support the evidence that the two currents are associated. I_{PFA} is an apparent outwardly directed current with a reversal potential (E_r) around -20 mV (Fig. 2.26). Previous studies showed that NaPi-II E_r follows a Nernstian shift according to the change in Na^+ concentrations, and confirming the cationic nature of Na^+-dependent PFA-sensitive current (52). However, the negative E_r is not consistent with what would be predicted from the Nernst equation for Na^+ (*i.e.* with ~10 mM $[Na^+]_I$ and 100mM $[Na^+]_O$ we would predict $E_r \approx +60$ mV). This discrepancy will be discussed in detail in the results chapter.

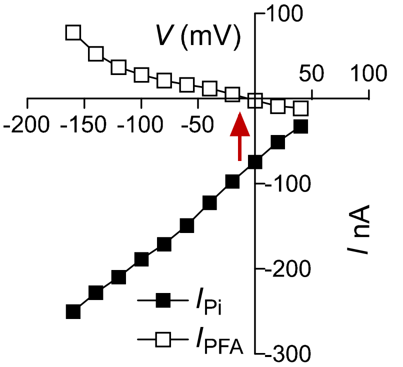

Figure 2.26 NaPi-II leak mode.

The leak current, I_{PFA} *(open squares), is obtained by subtraction of traces recorded in presence of 100Na from traces obtained in the presence of 100Na +1 mM PFA. Filled squares represent the* I_{Pi} *from the same oocyte.*

Mechanistically, the translocation of Na^+ *via* the leak pathway can occur by two ways:

- *via* a process that is independent of the cotransport cycle;
- by sharing some partial reactions with the cotransport cycle.

Important evidence in support of the notion that the leak current was directly associated with the NaPi-II protein came from mutagenesis studies on NaPi-IIa (88, 89, 94). Here, novel cysteines were introduced in the reentrant loop regions (TMD3-4 and TMD8-9) that were thought to be associated with the transport pathway. These cysteines were modified by exposure to methanethiosulfonate (MTS) reagents (94) to obtain functional data. For example, if oocytes expressing the functional mutant A453C were exposed to increasing concentrations of MTSEA (2-aminoethyl methanethiosulfonate hydrobromide), the initially inward directed I_{Pi} changed sign and became equal to I_{PFA} (Fig. 2.27). Moreover, the magnitude of the leak current increased. These effects could be reversed by exposing the oocyte to the reducing agent DTT. This was the first suggestion of a shared pathway between cotransport and leak modes (94).

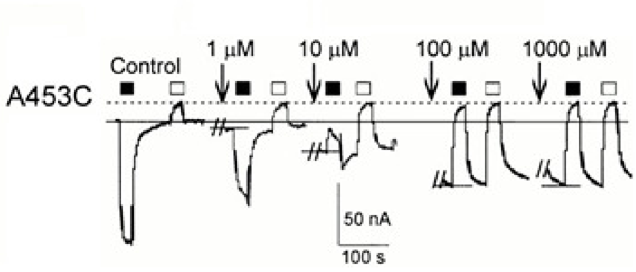

Figure 2.27 Effect of application of MTS reagents on electrogenic response.

Continuous current record obtained at -50 mV showing the response of the NaPi-IIa A435C mutant to 1 mM P_i (filled bars) or 3 mM PFA (open bars). After a control application of P_i and PFA, the substrate and the blocker were applied after successively application of MTSEA at the indicated concentrations. Modified from (94).

In another study that focused on first re-entrant loop (TMD3-4) an Ala-Cys substitution at site 203 caused an increase of the turnover rate of the leak mode, although for this particular mutant, the novel cysteine was not amenable to MTS modification. The characterization of this mutant also gave a clue about the Na^+-leak functional sites because of the alteration in the turnover rate (89).

The generation of the A203C-S460C mutant confirmed the result obtained with A453C. In this double mutant the P_i transport kinetics were comparable to the wild-type (WT), however, the Na^+-leak was significantly increased: up to six-fold with respect to the WT as for the A203C alone. Application of MTSEA modified the Cys 460, which in the single mutant (S460C) abolished both I_{Pi} and I_{PFA}, The modification leads to the suppression of the I_{Pi} and to the increase of the I_{PFA} (88). These observations suggested that the substrates (P_i and PFA) were able to interact with A203C-S460C after MTS modification but only the leak mode was active (Fig. 2.28).

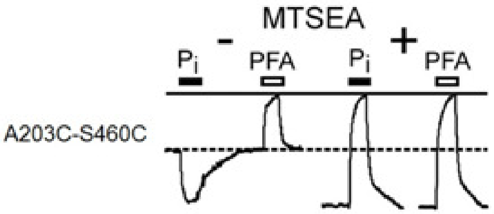

Figure 2.28 Properties of the double mutant A203C-S460C.

Oocytes expressing the construct were voltage clamped at -50 mV and 1 mM P_i or 3 mM PFA was applied as indicated. After application of MTSEA, the leak increased and the responses to P_i and PFA were the same. Modified from (88).

Applications of low concentrations of MTS reagents (5µM) over the time gave an important clue about the existing relationship between cotransport and leak modes for the A203C-S460C mutant. Cysteine modification by MTS showed a decrease in I_{Pi} and concomitantly, a corresponding increase of I_{PFA}. The modification of the two current modes was reciprocal, and this confirmed that the loss of cotransport activity is directly correlated with the gain in the leak mode activity (Fig. 2.29).

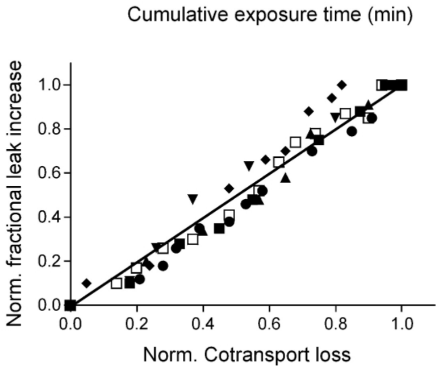

Figure 2.29 Leak cotransport relationship in A203C-S460C.

Relationship between the fraction of leak gained and the cotransport loss at the cumulated time of exposure to MTSEA or MTSET. Each symbol corresponds to a single oocyte. Modified from (88).

Taken together, these findings established that the leak is intrinsic in the electrogenic NaPi-II and that cotransport mode and leak modes are mutually exclusive (88).

Further investigations were conducted to understand the mechanism behind the leak mode. By determining the activation energy (E_a) used to translocate the substrates it is possible to distinguish between the channel-like activity (*e.g.* E_a ~6 kcal/mol) or a carrier-like uniport Na^+ pathway (*e.g.* E_a ~18 kcal/mol) (71). Both I_{PFA} and I_{Pi} were very sensitive to temperature changes. From calculations of the activation energy the I_{Pi} (E_a ~16 kcal/mol) and I_{PFA} (E_a ~11 kcal/mol) had similar E_as. This result confirms that both leak and cotransport modes are typical for enzyme-mediated processes (10).

A kinetic model

The transport of substrates across the membrane can be represented by a kinetic scheme that describes the transport cycle as a sequence of partial reactions that involve substrate binding and de-binding, as well as movement of the empty and fully loaded carrier across the membrane.

For NaPi-IIa/b an eight state kinetic model have been proposed (Fig. 2.30). Five states are considered to be "outward" facing states (*1, 2a, 2b, 3, 4*), corresponding to protein conformations where the substrate binding sites are exposed to the extracellular medium. If Na^+ is present in the extracellular solution, it can bind to the protein and allow a conformational change toward state *2a*. Another binding site for the second Na^+ is now accessible from the extracellular solution, inducing yet another conformational change moving the protein into the *2b* state. The successive partial reaction (*2b* → *3*) is accomplished by the P_i binding (state *3*). The last state of the sequence of outward facing partial reactions is reached when also the third Na^+ binds to the transporter. The *4* → *5* partial reaction describes the transition between the "outward" facing to the "inward" facing states, and allows the translocation of P_i and three Na^+ cross the membrane. The remaining five states correspond to the "inward" facing conformations (*5, 6, 7, 7a, 8*). These transitions have not yet been characterized because the TEVC technique precludes controlled exchange of the intracellular solution.

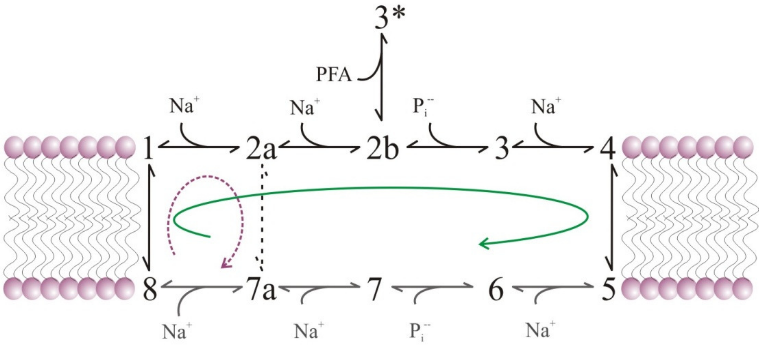

Figure 2.30 Kinetic scheme of electrogenic NaPi-II.
See text for details.

The voltage-dependence that characterizes the I_{Pi} (steady-state currents) originated from two of the partial reactions that precede P_i interaction:

- the empty carrier moving from inward to outward (*8*↔*1*);
- first Na^+ binding partial reaction (*1*↔*2*).

These two partial reactions give rise to capacitative currents: they involve the movement of mobile charges within transmembrane field (charge associated with the protein itself and one Na^+). Presteady-state relaxations are described by these two conformational changes.

The leak mode (dotted violet line Fig. 2.31) is represented by the partial reactions *1* → *2a*, *2a* → *7a*. The partial reaction *2a* → *7a* corresponds to the release of one Na^+ inside the cell. The inhibitory effect of PFA is represented as an extra partial reaction (*2b* → *3**, where *3** is the state where PFA is bound to the transporter instead of P_i.). This places the protein in a blocked state so that the normal cotransport cycle is prevented.

2.6 Open questions

A consideration of our present knowledge of the kinetics and structure-function relationships of electrogenic sodium-coupled phosphate cotransporters (NaPi-IIa/b) revealed three unanswered questions that I will address in the following sections:

1. *What is the ionic basis for the leak mode in electrogenic NaPi-II transporters?*
2. *How does lithium interact with NaPi-IIa/b?*
3. *How do substrates interact with NaPi-IIb on the cytosolic side?*

1. What is the ionic basis for the leak mode in electrogenic NaPi-II transporters?

As indicated above, there is compelling experimental evidence that the leak mode in NaPi-II is intrinsic to the protein and that leak and cotransport mode are mutually exclusive (88). However, one unresolved issue concerning the leak current the possible involvement of anions as the underlying reason for the negative reversal potential of I_{PFA} (~-30 mV). If the leak current is carried exclusively by Na^+ ions, thermodynamic equilibrium predicts a reversal potential determined by Nernst equation. Considering that the internal Na^+ concentration ($[Na^+]_I$) is ~10 mM and the $[Na^+]_O$ is 100 mM, the calculated reversal potential (E_r) is ~+60 mV. Given that the intracellular chloride concentration for a typical oocyte is Cl^- ~60 mM and the extracellular is $[Cl^-]$ ~100mM an E_r of ~-20 mV can be predicted. Accordingly, one hypothesis to explain the negative E_r could be that there is also an anionic permeation pathway associated with electrogenic NaPi-IIs as found for other transporters (*e.g.* EAAT (160)). Together with the Na^+ permeation, this shift the reversal potential to <0 mV. A detailed study of the effect of anions on the leak mode was performed and incorporated as new results in a review on the leak of NaPi-II cotransporters (6).

2. How does lithium interact with NaPi-IIa/b cotransport mode?

Lithium (Li^+) is well known to interact with cation-driven cotransporters. Li^+ can either give rise to currents (*e.g.* GAT-1 (83)) or act as inhibitor of the cotransport (*e.g.* sodium-dependent succinate cotransporter NaDC-1, (166)) or act as a co-substrate in absence of Na^+ (*e.g.* PiT-1, (129)). Possible effects of Li^+ on NaPi-II kinetics have only be studied indirectly and to a limited degree by using voltage-clamp fluorometry (61, 157). Using steady-state, presteady-state and radioactivity functional assays, a complete study of these interactions was performed.

3. How do substrates interact with NaPi-IIb on the cytosolic side?

The kinetic scheme (Fig. 2.31) describes well the forward cotransport mode of NaPi-II, however nothing is known about the partial reactions occurring on the cytosolic side. In a study on the electroneutral NaPi-IIc, evidence was presented that this isoform can operate in the reverse mode, however the order of substrate interactions was not determined (61). To address questions about internal substrate interaction and reverse mode, access to the cytosol is necessary, which means that the TEVC technique is not applicable. I therefore decided to exploit the potential of the Cut-Open Voltage-Clamp technique (COVC) that allows internal perfusion of the oocyte cytosol.

During my doctoral period, several technical changes were made that led to a significant improvement in the internal perfusion system. Moreover, the system now allows rapid superfusion of the extracellular face of the oocyte with a much higher degree of mechanical stability. The improvements of the technique provide an opportunity to study intracellular Na^+ interactions on the electrogenic NaPi-II.

3. METHODS and RESULTS

3.1 Publications that contribute to this work:

3.1.1 Paper 1: "The leak mode of type II Na^+-P_i cotransporters."

Channels (Austin). 2008 Sep 20;2(5).
Andrini O, Ghezzi C, Murer H, Forster IC.
Institute of Physiology and Center of Integrative Human Physiology (ZIHP), University of Zurich, Zurich, Switzerland.

Methods used:

- two-electrode voltage-clamp technique (TEVC);
- radiolabeled tracer assay;
- single point mutagenesis;
- voltage-clamp fluorometry (VCF).

My experimental contribution focused on the study of anionic replacement effect on leak mode.

[Channels 2:5, 346-357; September/October 2008]; ©2008 Landes Bioscience

Review

The leak mode of type II Na$^+$-P$_i$ cotransporters

Olga Andrini, Chiara Ghezzi, Heini Murer and Ian C. Forster*

Institute of Physiology and Center of Integrative Human Physiology; University of Zurich; Zurich Switzerland

Abbreviations: I_{Pi}, P$_i$-dependent change in holding current; I_{PFA}, PFA-dependent change in holding current; MTS, methanethiosulfonate; MTSEA, 2-aminoethyl MTS hydrobromide; MTSES, (MTS ethylsulfonate); MTSET, 2-(triethylammonium)ethyl MTS bromide; NaPi-IIa/b/c, type IIa/b/c sodium phosphate cotransporter; PFA, phosphonoformic acid; P$_i$, inorganic phosphate; SCAM, substituted cysteine accessibility method; TMD, transmembrane domain; WT, wild-type; SLC34, solute carrier family 34

Key words: phosphate, sodium, cotransport, leak current, *Xenopus* oocyte, electrophysiology

Na$^+$-coupled phosphate cotransporters of the SLC34 gene family catalyze the movement of inorganic phosphate (P$_i$) across epithelia by using the free energy of the downhill electrochemical Na$^+$ gradient across the luminal membrane. Electrogenic (NaPi-IIa/b) and electroneutral (NaPi-IIc) isoforms prefer divalent P$_i$ and show strict Na$^+$:P$_i$ stoichiometries of 3:1 and 2:1, respectively. For electrogenic cotransport, one charge is translocated per transport cycle. When NaPi-IIa or NaPi-IIb are expressed in *Xenopus* oocytes, application of the P$_i$ transport inhibitor phosphonoformic acid (PFA) blocks a leak current that is not detectable in the electroneutral isoform. In this review, we present the experimental evidence that this transport-independent leak originates from a Na$^+$-dependent uniport carrier mode intrinsic to NaPi-IIa/b isoforms. Our findings, based on the characteristics of the PFA-inhibitable leak measured from wild type and mutant constructs, can be incorporated into an alternating access class model in which the leak and cotransport modes are mutually exclusive and share common kinetic partial reactions.

Introduction

Secondary-active cotransporters catalyze uphill solute movement across membranes by using the free energy available from the electrochemical gradient of the driving substrate, usually a monovalent cation (Na$^+$, H$^+$ or K$^+$). The transport cycles of many members of this class are electrogenic, whereby net charge transfer accompanies cotransport and the partial reactions that constitute the transport cycle show voltage dependent kinetics. We can investigate the kinetics of these carriers by electrophysiological techniques, as ideally the substrate-induced current is an indirect measure of the transport rate for a constant number of charges translocated per cycle. Uncoupled currents give rise to deviations from the tightly coupled electrogenicity and strict stoichiometry between driving and driven substrates that is expected of the ideal secondary-active carrier. They are also referred to as leak or slippage currents (reviewed in refs. 1 and 2) and are intimately associated with the heterologous expression of the carrier protein. Their co-existence alongside the coupled transport electrogenic activity has led to a reassessment of the traditional view of channels and carriers as unique molecular entities (reviewed in ref. 3).

*Correspondence to: Ian C. Forster; Institute of Physiology; University of Zurich; Winterthurerstrasse 190; Zurich CH-8057 Switzerland; Tel.: +41.44.635.5059; Fax: +41.44.635.5025; Email: IForster@access.unizh.ch

Submitted: 10/20/08; Accepted: 10/20/08

Uncoupled currents are commonly sub-classified as transport-dependent and transport-independent currents, depending on whether they are detectable in the absence or presence of substrate. Cotransporters can exhibit one or both types of uncoupled current with different contributing ions. Uncoupled currents appear to be ubiquitous among electrogenic carriers and they have been described for gene products of at least nine solute carrier families identified in the human genome[4] (Table 1). Within a given solute carrier family, the properties of the uncoupled currents can also vary considerably for different isoforms, measured under the same experimental conditions. For example, in the biogenic amine transporter subgroup of the SLC6 family, GAT4 is reported to have two transport independent, mutually exclusive Na$^+$-dependent conductances that are permeable to Li$^+$ or Cl$^-$, both of which are present only in the absence of external Na$^+$ and GABA.[5] In contrast, the human GAT1 isoform displays only a Li$^+$-dependent uncoupled leak [Uncoupled currents are not exclusively associated with electrogenic transport. Electroneutral transporters show uncoupled currents, for example, Na$^+$-coupled glutamine transporter (SNAT3)].[5]

Transport-dependent uncoupled currents are observed in the *presence* of both driven and driving substrates and manifest themselves as currents in excess of those associated with the stoichiometric charge translocation. The most notable examples are members of the excitatory amino acid transporter family (EAAT's of the SLC1 family) that catalyze transport of glutamate driven by two Na$^+$ ions. For these carriers, experimental manipulations allow separation of the transport-dependent current to be separated into a stoichiometric component and a thermodynamically uncoupled anion selective component that is only activated in the presence of Na$^+$ and the amino acid (e.g., glutamate, aspartate).[10] This uncoupled current has been likened to that of ligand-gated channel that is gated by the driven substrate.[2,11] Although the presence of Cl$^-$ is not essential for cotransport, it is accelerated by Cl$^-$ ions[12,13] and studies suggest

Table 1 **Examples of gene products of the solute carrier families[1] that mediate uncoupled currents**

SLC	Example proteins	Coupled substrates	Un-coupled current[2]	Ions carried by uncoupled currents	Selected references[3]
1	EAAT1,2,3,4	$Na^+/H^+/K^+$/Glu	T	Cl^-	(11, 69)
	EAAC1		L	Na^+	(70)
	ASCT1,2	Na^+/neutral amino acids (exch)	T	Cl^-	(8, 9)
5	SGLT1	Na^+/glucose	L	Na^+	(17, 67, 71)
	NIS	Na^+/I^-	L	Na^+	(15)
	SMIT	Na^+/myoinositol	L	Na^+	(72)
	SMCT	Na^+/monocarboxylate	L	Anions	(73)
	CHT	Na^+/choline	L	Na^+	(74)
6	GAT-1,4	Na^+/Cl^-/GABA	L	Li^+,Cs^+, Cl^-	(5, 19, 75)
	SERT	$Na^+/Cl^-/K^+$/5HT	T/L	Na^+, Li^+, K^+, H^+	(7, 75, 76)
	hDAT	$Na^+/Cl^-/DA^+$	T/L	Na^+, Li^+, K^+, H, Cl^-	(20, 77)
11	DMT1	H^+/divalent cations	L	H^+	(34, 49)
13	NaD (NaC)	Na^+/dicarboxylates	L	Na^+	(78)
15	PepT2	H^+/peptides	L	H^+	(79)
23	SVCT1,2	Na^+/ascorbic acid	L	Na^+	(16, 80)
34	NaPi-IIa/b	Na^+/P_i	L	Na^+	(41, 45)
38	SNAT3	Na^+/glutamine	T	K^+, H^+, Na^+/H^+ exch.	(6)
			L	Cations	

[1]Nomenclature according to Human Genome Organisation Database (4). [2]According to the nomenclature of Sonders and Amara (2): L(eak) = transport-independent currents, T(ransport) = transport-dependent currents respectively. [3]Only studies using the *Xenopus* oocyte expression system are cited.

that the negative charge acts as a counterbalance to the excess charge associated with cotransported Na^+ ions.[14]

In contrast, transport-independent uncoupled currents are observed in the *absence* of the driven substrate and represent a constitutive leak that may or may not involve the driving substrate. In some cases, for example the Na^+/I^- cotransporter (NIS)[15] and the Na^+/L-ascorbic acid transporters (SVCT1,2),[16] the leak currents measured when the transporter is heterologously expressed in *Xenopus* oocytes are significantly larger than those observed for control oocytes and comparable in magnitude to the substrate-induced current. For other cotransporters, the currents can only be quantified with confidence by the application of substrates or blockers that bind specifically to the transporter, but which themselves are not transported. Characterization is further complicated by the finding that the cation species contributing to the leak current can either be the same or different from the cation that preferentially drives cotransport. For example, the leak associated with the sodium glucose cotransporter (SGLT1) is mediated by Na^+ ions,[17,18] whereas for GAT1 from the same gene family, alkali metal cations such as K^+ and Li^+, which do not drive transport, can nevertheless permeate.[2,5,19-21]

Several questions arise with respect to the identity and underlying mechanism of uncoupled currents:

(i) Are they an intrinsic property of the carrier or an artifact of the heterologous expression system?

(ii) Given that they are constitutive to the carrier, do they share either the same permeation pathway as the cotransported substrates, or are the ions conducted via a separate pathway, for example through a pore established by oligomerization of functional subunits?

(iii) Is the leak better described as a channel (gated pore) or a uniport (carrier) type mechanism?

(iv) Do they play mechanistic or physiological roles?

It has been challenging to answer these questions unambiguously, in part because of possible artifacts of the expression systems, the small size of the currents compared with the cotransport mode currents and given that the same ions are cotransported and permeate the leak pathway. Evidence from structure-function studies on heterologously expressed, as well as functionally reconstituted carriers, together with 3-D crystallographic data from bacterial homologs, is helping to provide clearer answers to these questions.

Indirect support that uncoupled currents are intrinsic to carriers comes from the observation that their magnitude correlates strongly with that of the substrate-induced electrogenic response, which should reflect the number of active transporters expressed in the membrane. However, it has been reported that heterologous expression of proteins in *Xenopus* oocytes can lead to the upregulation of endogenous Cl^- and non-specific hyperpolarization-activated cation channels (reviewed in refs. 22–25). Therefore, the number of upregulated endogenous channels might still correlate with the activity of the heterologously expressed protein. More compelling evidence that leak currents are intrinsic to the carrier protein comes from studies in which the leak is modified or even "uncoupled" from the cotransport mode activity through mutations of the protein, or by in situ modification of specific residues. These studies establish a direct link at the molecular level between the leak current and the heterologously expressed protein (reviewed in refs. 26–34). The most convincing approach to confirm the intrinsic nature of the leak current is to purify and reconstitute the protein in a membrane preparation. Transport assays can then be performed to identify the leak and transport related fluxes. For example, compelling evidence for a constitutive Cl^- conductance was found for the bacterial glutamate transporter homolog (Glt_{Ph}) reconstituted in proteoliposomes.[12]

As some cotransporters are known to form homo-oligomers, there has been speculation that leak pathways could be created at the interface between the subunits analogous to the structure of multimeric ionotropic proteins (reviewed in ref. 35). However, recent studies on the neuronal EAAT3,[36] and its bacterial homolog Glt$_{Ph}$ [12] suggest that the translocation pathways for the substrate itself and transport-dependent leak are colocalized to individual subunits and function independently. On the other hand, direct structural evidence concerning the localization of the permeation pathway for transport-independent uncoupled currents is lacking.

The Uncoupled Leak of SLC34 Proteins

Introduction. Members of the SLC34 family of Na$^+$-coupled inorganic phosphate (P$_i$) transporters play a vital physiological role in P$_i$ homeostasis, particularly in the kidney, where they are responsible for P$_i$ reabsorption from the glomerular filtrate across the apical membrane of proximal tubule epithelia. They are also expressed in epithelial membranes in the small intestine and other organs (testes, lung, liver), where their physiological function is less well understood (reviewed see ref. 37). The family comprises three isoforms that prefer divalent P$_i$ as the driven substrate: NaPi-IIa, NaPi-IIb catalyze electrogenic transport with a Na$^+$:P$_i$ stoichiometry of 3:1 and one net charge is translocated per transport cycle;[38,39] NaPi-IIc is electroneutral and therefore cotransports with a Na$^+$:P$_i$ stoichiometry of 2:1.[40]

Based on kinetic studies of WT isoforms and structure-function studies of mutant constructs, we have developed a kinetic scheme for the cotransport cycle (Fig. 1A) that comprises a sequence of partial reactions representing the transitions between unique conformational states of the protein.[37,41-43] Under normal physiological conditions, the cotransport cycle begins in the outward facing conformation of the empty carrier (state 1), which favors ordered binding of two Na$^+$ ions, followed by binding of one divalent P$_i$ and a 3rd Na$^+$ ion from the external medium. A translocation partial reaction of the fully loaded carrier (transition 4↔5) occurs, followed by release of substrates to the cytosol to leave the carrier in state 8. The normally negative intracellular potential is now sensed by the now free mobile charges intrinsic to the empty carrier, the movement of which effects a conformational change from state 8 to state 1. In its simplest form, only two electrogenic partial reactions (8↔1, 1↔2a) are sufficient for the model to account for voltage dependent kinetics and translocation of one net charge/cycle: the empty carrier and 1st Na$^+$ interaction. In this model, the translocation of the fully loaded carrier is electroneutral. The scheme is consistent with an alternating access mechanism that excludes translocation of substrates from intermediate states. In this scheme, membrane potential contributes a source of free energy to drive cotransport, but is not essential: the cycle can also proceed with membrane potentials ≥0, albeit at a lower turnover rates, driven by the difference in free energy for Na$^+$ ions between the external and internal mediums. Support for this prediction was first provided by studies on renal brush border membrane vesicles, in which the initial rate of ^{32}P uptake by renal brush border membrane vesicles is reduced, but not eliminated, when the vesicle membrane potential is changed from hyperpolarizing to depolarizing in the presence of an inward Na$^+$ gradient.[44] Experimental evidence also strongly supports the ordered substrate binding for the outward facing conformations (1↔4), however evidence is lacking with respect to order of substrate interaction for the inward facing conformations (5↔8).

Although the cotransport cycle is probably the normal physiologically relevant transport process, electrogenic NaP-IIa/b isoforms also exhibit a leak current in the absence of P$_i$ when expressed in *Xenopus* oocytes. This is incorporated in the kinetic scheme as second transport cycle that resembles a Na$^+$-dependent uniporter and shares three of the partial reactions of the cotransport cycle (Fig. 1A). In this model, both the cotransport and leak modes mediate the net movement of one charge per cycle (Fig. 1A, *inset*). For the cotransport mode, this has been established by simultaneous isotope flux and electrophysiological recording.[38,39] For NaPi-IIa/b isoforms, it has not been feasible to apply the same approach to establish the stoichiometry of the leak because the corresponding cation flux is at the limit of experimental resolution using isotopes. Therefore, our current understanding of the leak mechanism and the evidence to support of its inclusion in the kinetic scheme as a uniporter has come from the integration of findings from electrophysiological studies using both WT and mutant constructs as described below.

Properties of the uncoupled leak for WT NaPi-IIa/b. We have found no evidence of significant electrogenic activity in excess of the stoichiometrically coupled components for three electrogenic isoforms of the SLC34 family[38,39] when expressed in *Xenopus* oocytes. However, a transport-independent leak current was postulated by comparing the electrogenic responses of oocytes heterologously expressing NaPi-IIa or NaPi-IIb isoforms to P$_i$ or the P$_i$-transport inhibitor phosphonoformic acid (PFA). Figure 1B depicts a representative recording from an oocyte expressing rat NaPi-IIa when voltage was clamped to -50 mV using a two-electrode voltage clamp (*inset*). In contrast to the electrogenic response to a saturating concentration of P$_i$ (1 mM), which results in a downward deflection in the holding current corresponding to the inward movement of charge (I_{Pi}, Fig. 1B), 3 mM PFA induces a small upward deflection of the steady-state holding current (I_{PFA}). This is interpreted as evidence of block of an intrinsic leak,[41] analogous to the phlorizin-dependent block of the leak intrinsic to the Na$^+$-coupled glucose transporter (SGLT1), first described by Umbach et al.[17] The holding current level reached during PFA superfusion is not zero, but is given by the endogenous leak current of the oocyte (I_{Endog}), which at a membrane potential of -50 mV, is usually inward but its magnitude can vary widely both between and within batches of oocytes. In the absence of external Na$^+$, PFA like P$_i$, does not induce a change in holding current, which underscores the Na$^+$-dependence for the electrogenic responses to P$_i$ and PFA. At -50 mV, I_{PFA} accounts for approx 10–20% of I_{Pi}, although we have documented larger PFA-induced changes in holding current for constructs that contain point mutations at sites associated with the putative transport pathway (see below). We have also observed a PFA-dependent block of holding current in all characterized electrogenic NaPi-II isoforms, however at a given membrane potential its magnitude relative to I_{Pi} can vary, which is also reflected in differences in steady-state voltage dependence of the cotransport mode (see Fig. 5C).

As we first reported,[41] the magnitude of I_{PFA} correlates with I_{Pi} under the same voltage clamp conditions (Fig. 1C). For the rat NaPi-IIa isoform I_{Pi} is typically < -200 nA at -100 mV, whereas the magnitude of the leak current is comparable to I_{Endog} and therefore could not be easily detectable without using PFA as a blocking substrate. As illustrated for a representative oocyte expressing rat NaPi-IIa (lower, Fig. 1D), the current-voltage (*I-V*) relation for

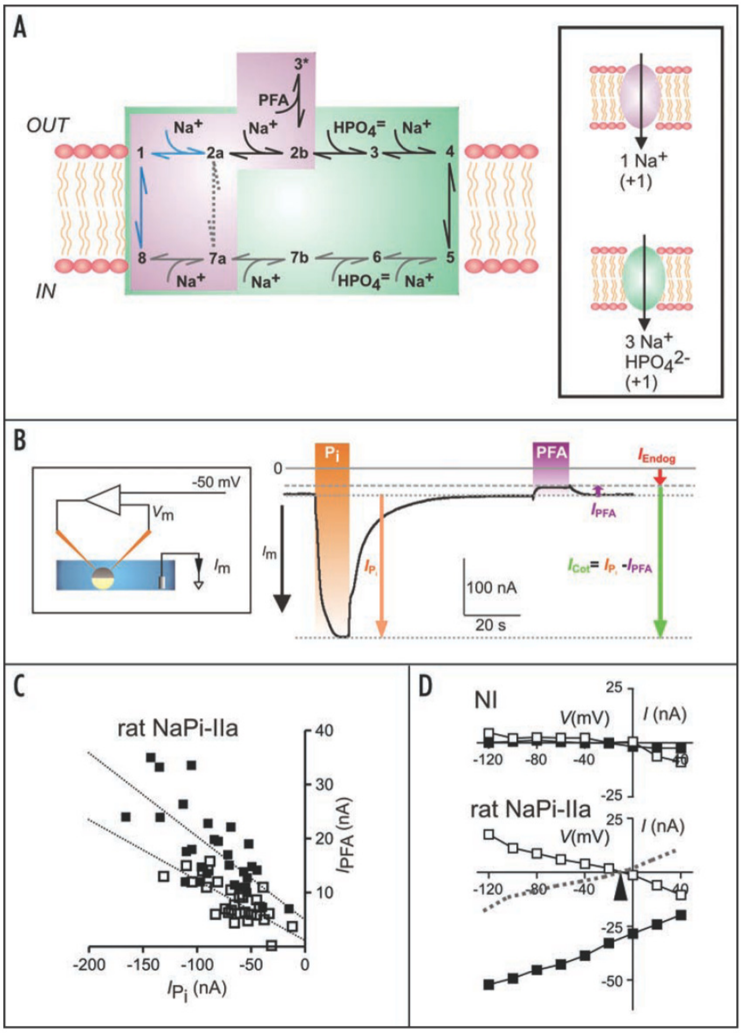

Figure 1. The transport modes of electrogenic SLC34 proteins. (A) Kinetic scheme showing the ordered sequence of partial reactions that result in net charge translocation for the cotransport mode (green shading) and leak mode (violet shading). Two electrogenic partial reactions (blue) account for the voltage dependence of transport. All other partial reactions are assumed to be electroneutral. Inset shows the two modes of electrogenic transport: cotransport and leak. Both involve the translocation of one net charge per cycle. Only the stoichiometry of the cotransport mode has been determined experimentally by simultaneous uptake and voltage clamp.[38] (B) Electrogenic responses of an oocyte expressing the rat NaPi-IIa isoform to saturating P_i (1 mM) (I_{Pi}) and PFA (3 mM) (I_{PFA}) in the presence of 100 mM Na^+. Oocyte is voltage clamped using a two-electrode voltage (inset) and the membrane clamped to -50 mV. I_{Endog} represents the endogenous oocyte current. If the leak is fully suppressed by saturating P_i, the predicted electrogenic cotransport activity is given by I_{Cot}. (Forster IC, unpublished data). (C) Correlation of I_{PFA} with I_{Pi} shown for oocytes harvested from >5 donor frogs at two holding potentials (-100 mV, filled squares; -60 mV, open squares). Linear regression lines have slopes -0.16 ± 0.03 (-100 mV); -0.11 ± 0.02 (-60 mV) but were not statistically significant (n = 29). (D) Typical steady-state voltage dependence of I_{Pi} and I_{PFA} for a representative oocyte expressing rat NaPi-IIa (lower) and a non-injected (NI) oocyte from the same donor frog as control (upper). Each data point is obtained by subtracting the oocyte holding current in the control solution from the current with 1 mM P_i or 1 mM PFA added to the control solution. Note that I_{PFA} reverses at ~-10 mV for the NaPi-IIa expressing oocyte (arrow). Dotted line indicates the apparent PFA-inhibitable leak current ($-I_{PFA}$, see text). An endogenous response to PFA is also observed for NI for $V > 0$ mV (filled squares: I_{Pi}; open squares: I_{PFA}). (Andrini O and Forster IC, unpublished data).

I_{Pi} shows an inward current for all test potentials, consistent with cotransport cycling clockwise in Figure 1A. In contrast, I_{PFA} is outward for hyperpolarizing potentials and typically reverses at potentials between -30 mV to -10 mV (arrowed, Fig. 1D). This apparently anomalous *I-V* behavior for a substrate-dependent current is simply a result of subtracting the holding current at each potential in the absence of PFA from the response in the presence of PFA to eliminate I_{Endog} [We adopt the convention that I_{Pi} and I_{PFA} indicate the change in holding current caused by the addition of P_i or PFA to the control superfusate. For steady-state *I-V* curves, data points were obtained by subtracting currents recorded in response to voltage steps in the presence of substrate, from the corresponding records in the control solution, thereby eliminating endogenous currents. The validity of this method rests on the assumption that substrates do not modulate endogenous currents]. The apparent leak current, which we assume PFA fully inhibits, is therefore $-I_{PFA}$ (dotted line, Fig. 1D). Non-injected or H_2O-injected oocytes showed either no response to PFA or a consistently smaller change in holding current for holding potentials <0 mV, (upper, Fig. 1D). Thus, the scatter in the I_{PFA} - I_{Pi} correlation most likely arises from contamination from endogenous responses to either P_i or PFA.[41,45] For $V > 0$ mV, control (non-injected or H_2O injected) oocytes sometimes also show an endogenous response to PFA, which resembles the response of injected oocytes in the same voltage range (Fig. 1D) (see below).

Our original analysis of I_{PFA} using the rat NaPi-IIa isoform documented a Nernstian shift in its reversal potential with external $[Na^+]$

from which we concluded that $-I_{PFA}$ is a measure of the permeation of Na^+ ions through the transporter. Furthermore, the dependence of $-I_{PFA}$ on external $[Na^+]$ shows Michaelian kinetics (apparent K_m = 128 mM), which suggests that one Na^+ ion interacts with the carrier.[41] Taken together, these findings offer compelling evidence that the underlying transport mechanism is more akin to that of a uniport class of carrier rather than a channel.

Under the tacit assumption that I_{PFA} reflects the inhibition of an intrinsic transport-independent leak mode of NaPi-IIa, we postulated an electroneutral Na^+ translocation partial reaction (2a↔7a) takes place in the absence of P_i (Fig. 1A). The leak and cotransport modes share common partial reactions (empty carrier and Na^+ binding/debinding on the external and internal faces of the membrane) and this model predicts that at saturating P_i, when the forward partial reaction 2b→3 is favored, the leak mode will be inactive. When PFA is bound, the protein occupies a unique blocked conformation (3^*). This is similar to schemes proposed for the Na^+ glucose cotransporter SGLT1 (reviewed in refs. 18 and 46). Importantly, if the leak and cotransport modes are mutually exclusive, the true baseline for quantitating the electrogenic activity of the cotransport mode for saturating P_i (I_{Cot}) is given by the holding current in the presence of PFA and *not* the holding current in the control solution (Fig. 1B).

In this model, the rate of translocation of Na^+ via the leak pathway is also predicted to be very slow. We have estimated the turnover rates for the cotransport cycle of electrogenic SLC34 proteins to lie in the range 4–13 s^{-1} (47). Therefore, if one net charge is translocated in the leak mode, the magnitude of I_{PFA} suggests that the leak turnover rate will be <1 s^{-1}.

The carrier mechanism for the leak mode has gained further support from a study on the temperature dependence of I_{Pi} and I_{PFA} of the flounder NaPi-IIb isoform, which was chosen because of its large transport activity, up to 5-fold greater than mammalian isoforms.[40] As illustrated in Figure 2A, both I_{Pi} and I_{PFA} show strong temperature dependencies that when fit with the Arrhenius equation yield activation energies (E_a) at -100 mV of ~16 kcal mol^{-1} and ~11 kcal mol^{-1} for I_{Pi} and I_{PFA} , respectively (Fig. 2B). The estimate of E_a for I_{PFA} is consistent with that expected for a carrier type mechanism involving large conformational changes, rather than a channel. The latter should have an activation energy closer to that for free diffusion of ions (e.g., reviewed in ref. 48), for example, as reported for the Cl^- leak of GAT4.[5] The activation energy for I_{PFA} is the same as that reported for the H^+-mediated leak of the divalent metal ion transporter DMT1,[49] but significantly less than 26 kcal mol^{-1} reported for the Li^+-activated leak of GAT1,[21] and 21 kcal $mole^{-1}$ for the Na^+-activated leak of SGLT1.[50] These data show that among members of different solute carrier families there is varying complexity of conformation changes that accompany the uncoupled leak mode. Furthermore, we found that E_a for both cotransport and leak modes is only weakly sensitive to membrane potential (Fig. 2B), which supports the assumption that the rate-limiting substrate translocation partial reactions for each mode (2a↔7a; 4↔5) are electroneutral.[51] Analysis of the temperature dependence of the partial reactions associated with the empty carrier and lumped Na^+ binding interactions, which are manifest experimentally as presteady-state charge movements (see below), also revealed activation energies >10 kcal mol^{-1}.[51] It is therefore conceivable that the temperature dependence of I_{PFA} reflects molecular rearrangements associated with the empty carrier and Na^+ binding events and not translocation per se.

In other studies, we have documented the insensitivity of I_{PFA} to changes in external pH.[45,52] As illustrated in Figure 3A, when the external medium is acidified, I_{Pi} at all potentials decreases, in part due to the reduced availability of the preferred divalent P_i and also because protons interact with partial reactions in the transport cycle.[39,45] It is noteworthy that at pH 5, I_{Pi} closely matches I_{PFA} at pH 7.4 (Fig. 3B), which suggests that there is a progressive pH-dependent shift from the cotransport mode to the leak mode. Moreover, these data indicate that even in its monovalent form at pH 5.0, P_i can interact with the carrier to inhibit both leak and

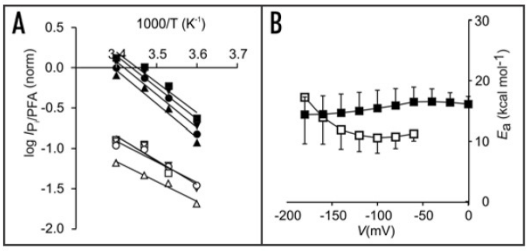

Figure 2. Temperature dependence of I_{PFA} suggests that it arises from a carrier-mediated conductance. (A) Arrhenius plots of the normalized magnitude of I_{Pi} (filled symbols) and I_{PFA} (open symbols) for the membrane potentials indicated. Straight lines represent linear regression fits to the data points to yield the apparent activation energy (E_a) given by: $\log [I_{Pi}, _{PFA}] = -E_a/(2.303\ R)\ (1/T) + \log A$, where E_a is the activation energy, R the gas constant, T temperature (K) and A a constant. (Squares*:* -180 mV*; inverted triangles:* -140 mV*;* circles*:* -100 mV*;* triangles: -60 mV). (B) E_a plotted as a function of membrane potential, I_{Pi} (filled squares) and I_{PFA} (open squares). Modified from ref. 51 with permission.

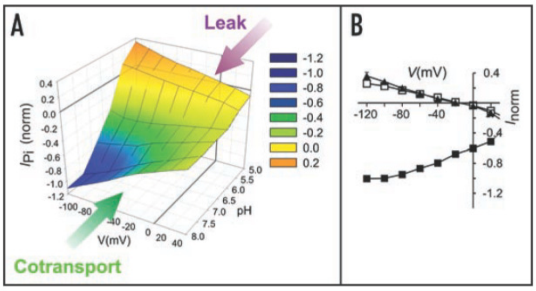

Figure 3. Acidification transforms the electrogenic transport modes of rat NaPi-IIa. (A) Evidence for "mode" switching from cotransport to leak as the external medium is acidified. Steady-state pH-V profile of WT showing I_{Pi} (1 mM total P_i) as a function of external pH and V. Currents were normalized to the magnitude of I_{Pi} at -100 mV, pH 7.4 and pooled (n = 4). Error bars omitted for clarity. Legend indicates color and corresponding normalised I_{Pi}. (B) Normalized, pooled (n = 5) I-V data for WT that compares I_{Pi} at pH 5.0 (open squares) with I_{PFA} at pH 7.4 (filled triangles), normalized to the magnitude of I_{Pi} at -100 mV, pH 7.4 (filled squares). The superposition of I_{Pi} at pH 5.0 and I_{PFA} at pH 7.4 suggests that at pH 5.0 only the leak mode is operational. © Ehnes et al., adapted from Figure 3 originally published in The J Gen Physiol 2004;124: 489–503.

cotransport modes.[52] The robust nature of I_{PFA} is also underscored by its insensitivity to the arginine modifying reagent, phenolglyoxal, which typically reduces I_{Pi} by 50%.[53]

Leak and electrogenicity go hand in hand in SLC34 proteins. Although PFA inhibits Na^+-coupled P_i cotransport mediated by both electrogenic and electroneutral SLC34 isoforms (Ghezzi C and Stange G, unpublished data), a PFA-dependent change in holding current is only detectable in electrogenic NaPi-IIa/b isoforms (Fig. 4A and B). This suggests that the putative Na^+-leak pathway is absent in NaPi-IIc. Evidence to support this conclusion comes from studies on the WT NaPi-IIc and the WT NaPi-IIc backbone engineered to restore electrogenicity.

First, WT NaPi-IIc is proposed to lack a Na^+-binding site within the transmembrane electric field, consistent with its Na^+:P_i stoichiometry of 2:1,[40] (lower, Fig. 4B). Binding of one Na^+ ion at this site would correspond to the 1st Na^+ interaction of the transport cycle (1↔2a) (Fig. 1A). For electrogenic NaPi-IIa/b, voltage steps induce presteady-state charge movements in 0 mM P_i. These are considered to originate in part from the movement of one Na^+ ion per transporter with the transmembrane electric field, as well as the movement of mobile charges associated with the empty carrier, observed in the absence of external Na^+.[42,43] As neither component of charge movement is detectable in oocytes that express functioning NaPi-IIc, this may indicate that in the electroneutral transport cycle, partial reaction 1↔2a is absent, and the reorientation of the empty carrier is electroneutral. Moreover, voltage clamping NaPi-IIc oocytes at different potentials does not alter the rate P_i uptake, which indicates that the electroneutral isoform lacks voltage-dependent partial reactions in its transport cycle.[40]

Second, by comparing the sequences of the electrogenic and electroneutral isoforms, we identified a critical three amino acid motif conserved in all electrogenic isoforms that includes an aspartic acid (Fig. 6), which is absent in all electroneutral isoforms. When the residues comprising this motif, are substituted at the equivalent sites in the electroneutral backbone, the resulting mutant (AAD-IIc) displays electrogenic behavior (Fig. 4A). One net charge is transported per P_i (Fig. 4B, upper) and the Na^+:P_i stoichiometry of cotransport is increased from 2:1 to 3:1 (Fig. 4B, lower).[40] Moreover, presteady-state charge movements are detectable, both in the presence and absence of external Na^+ (data not shown). The former finding is consistent with the re-establishment of a Na^+ binding site within the transmembrane field.[40] The latter finding indicates that the effective mobile charge, which confers voltage dependence to the empty carrier partial reaction (Fig. 1A), is present in AAD-IIc, possibly contributed by the substituted Asp-224. Application of PFA induces an upward deflection of the steady-state holding current (arrowed, Fig. 4A) similar to that observed for the WT electrogenic isoforms, however the *I-V* relationship (Fig. 4C) reveals a weaker voltage dependence for both I_{Pi} and I_{PFA} compared to the WT over the same voltage range. Thus, the substituted motif is essential, but not exclusively involved in determining the voltage dependence.[40] Like the WT, for AAD-IIc the magnitude of I_{PFA} correlates with I_{Pi} (Fig. 4D), which supports our view that I_{PFA} reflects electrogenic activity intrinsic to the expressed protein.

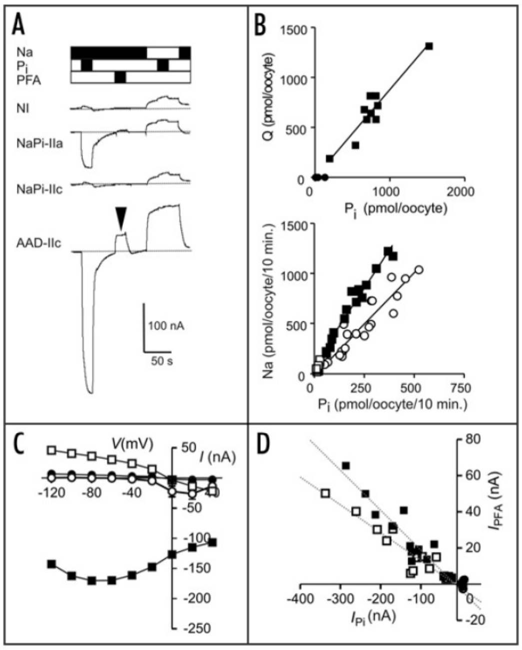

Figure 4. Conferring electrogenicity and leak to the electroneutral NaPi-IIc. (A) Representative current tracings of oocytes from the same donor frog, comparing non-injected (NI), mouse NaPi-IIa, mouse NaPi-IIc and AAD-IIc under different superfusion conditions as indicated. Na: Control buffer; P_i: Control + 1 mM P_i; PFA: Control + 1 mM PFA. Control buffer contains either 100 mM NaCl (filled bar) or 100 mM CholineCl (empty bar). Oocytes were voltage clamped at -50 mV. Arrow indicates response of AAD-IIc to 1 mM PFA in 100 mM NaCl buffer. (B) Upper: Charge translocation (Q) correlates with P_i uptake for AAD-IIc. Each point is from an individual oocyte. AAD-IIc (filled squares); NI (filled circles) from same donor frog. Slope of linear regression line (0.9 ± 0.1) indicates that one charge is translocated per P_i molecule as for WT NaPi-IIa/b.[38] Lower: Dual uptake (^{22}Na, $^{32}P_i$,) for WT NaPi-IIc and AAD-IIc demonstrate that the Na^+:P_i stoichiometry is increased in the AAD-IIc. AAD-IIc (filled squares); NaPi-IIc (open circles); NI (open squares) from the same donor frog. Data points for NaPi-IIc and AAD-IIc are fit with linear regression lines that give slopes of: 3.0 ± 0.2 (AAD-IIc) and 2.0 ± 0.2 (NaPi-IIc). Figure 4A and B are adapted from © Bacconi et al., Figure 3 originally published in Proc Natl Acad Sci USA 2005; 102:489–503. (C) Representative *I-V* data for AAD-IIc (squares) and WT NaPi-IIc (circles). I_{Pi} (filled symbols; I_{PFA} (open symbols). (Bacconi A, Forster IC, unpublished data). (D) Correlation between I_{PFA} and I_{Pi}. Data for oocytes expressing AAD-IIc (squares, n = 15) and NI (circles, n = 4) from different donor frogs for currents measured for the same oocyte at two holding potentials (-60 mV: open symbols; -100 mV: filled symbols). Lines are linear regression fits with slopes: -0.154 ± 0.015 (-60 mV) and -0.221 ± 0.021 (-100 mV). (Bacconi A, Forster IC, unpublished data).

In summary, these findings offer compelling evidence that the presence of a leak current and the electrogenic interaction of one Na^+ ion with the empty carrier are not coincidental. As this Na^+ interaction is absent in the electroneutral isoform, the leak current displayed by electrogenic isoforms seems to be a direct consequence of their electrogenic transport kinetics.

Anion replacement experiments. The small magnitude of I_{PFA} and potential for contamination by endogenous currents that are also modulated by the specific substrates of the SLC34 family proteins

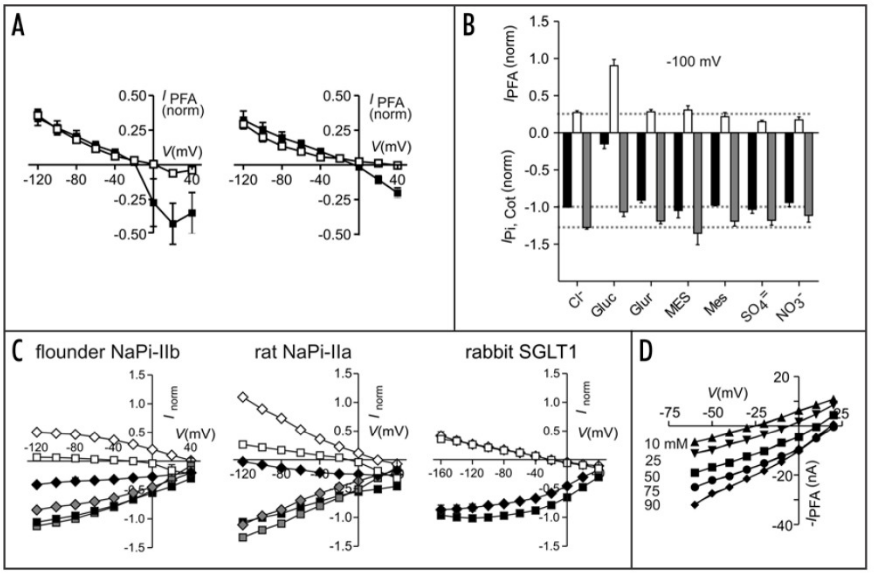

Figure 5. Effect of external anion substitution on I_{Pi} and I_{PFA}. (A) Upper: Steady-state *I-V* data for rat NaPi-IIa expressing oocytes showing I_{PFA} with external Cl^- = 107 mM (filled squares) and morpholineethanesulfonate (MES) (100 mM) + 7 mM Cl^- (open squ*ares*) in the external solution. Data were normalized to I_{Pi} (1 mM P_i, 107 mM Cl^-, -100 mV) and pooled (n = 3). Lower: Steady-state *I-V* data for rat NaPi-IIa expressing oocytes, showing I_{PFA} with external Cl^- = 107 mM (filled squares) and glucuronate (100 mM) + 7 mM Cl^- (open squ*ares*) in the external solution. Data were normalized to I_{Pi} (1 mM P_i, 107 mM Cl^-, -100 mV) and pooled (n = 5). (Andrini O and Forster IC, unpublished data). (B) Summary of substituting 100 mM of external Cl^- with indicated anions showing I_{Pi} (filled bars); I_{PFA} (open bars) and I_{Cot} (= I_{Pi} - I_{PFA}) (grey bars*)* at -100 mV, normalized to I_{Pi} in 107 mM Cl^- at -100 mV. Gluc, gluconate, Glur, glucuronate; Mes, methanesulfonate; MES, morpholineethansulfonate. Data are pooled using oocytes expressing rat NaPi-IIa (n ≥ 5). (Andrini O and Forster IC, unpublished data). (C) Left: Steady-state *I-V* data for flounder NaPi-IIb (n = 3); center: rat NaPi-IIa (n = 4); right: rabbit SGLT1 (n = 5). In each case, normalized data are shown for superfusion in 107 Cl^- (*squares*) and 100 mM gluconate + 7 mM Cl^- (*diamonds*). For flounder NaPi-IIb, rat NaPi-IIa: I_{Pi} (1 mM)—filled symbols; I_{PFA} (1 mM)—open symbols, I_{Cot} (= I_{Pi} - I_{PFA})—grey symbols; for rabbit SGLT1: $I_{\alpha\text{-MDG}}$ (1 mM) (filled symbols), phlorizin (100 μM) (open symbols). (Ghezzi C and Forster IC, unpublished data). (D) Dependence of the PFA-inhibitable current on external [Na^+] in 100 mM gluconate superfusate confirms the [Na^+]-dependent shift in reversal potential. Data are from a representative oocyte expressing the human NaPi-IIa isoform. Na^+ was replaced equimolarly with Li^+. The hyperpolarizing shift in reversal potential followed a Nernstian relation with a slope 54.2 ± 4.0 mV/log[Na^+] (Forster IC, unpublished data).

has prevented its full characterization over a wide range of experimental conditions, particularly for membrane potentials close to 0 mV, unless cells with high expression (I_{Pi}) are selected. One feature of I_{PFA} that was not fully resolved in the above studies was thatif the PFA-inhibitable leak reflects the activity of a Na^+-dependent conductance, equilibrium thermodynamics predicts that its reversal potential (E_r) should be given by the Nernst potential. For example, if we assume a typical oocyte cytosolic [Na^+] <10 mM (reviewed in ref. 54), with an external [Na^+] = 100 mM, E_r > +60 mV. In practice, we consistently document E_r in the range -10 to -30 mV (for example see Fig. 1D), which might be expected for a Cl^- conductance and suggests that PFA inhibits more than one permeating ion species. Interestingly, the reversal potential for I_{PFA} was similar to that of phlorizin-inhibitable leak current of Na^+-coupled glucose transporter (SGLT-1) (see Fig. 5C), which was shown to be dependent on internal sugar.[17] Initially, we therefore adopted a similar strategy for simulations using the kinetic model for NaPi-IIa/b, by assuming a finite internal P_i (reviewed in refs. 45 and 53).

Experiments in which we replaced ~90% of external Cl^- with other anions have now shed new light on the origin of the negative E_r. Substitution with the large polyatomic anions like morpholineethanesulfonate (MES) (upper, Fig. 5A) and glucuronate (lower, Fig. 5A) cause a depolarizing shift of E_r and suppression of I_{PFA} for $V > 0$ mV. This behaviour is consistent with the partial suppression of an inward Cl^- flux (in all anion replacement experiments, the external [Cl^-] = 7 mM). Moreover, a comparison of the responses of non-injected or H_2O-injected oocytes to PFA indicates that it suppresses an endogenous outward rectifying current that varies considerably between oocyte batches and according to the number of days after retrieval from the ovary. This endogenous current, which can be larger than the transporter-associated leak could therefore account for the negative E_r in NaPi-IIa/b expressing oocytes. In contrast, for $V < 0$ mV we observe only a small change in the I_{PFA} when Cl^- is removed from the external medium. Moreover, I_{PFA} was little affected when oocytes were dialysed in a low Cl^- medium to reduce the internal [Cl^-] (reviewed in ref. 10) compared to non-dialysed oocytes, thereby confirming that outward movement of Cl^- ions does not contribute significantly for hyperpolarizing potentials.

With the notable exception of gluconate, equimolar replacement of 100 mM external chloride with a selection of anions

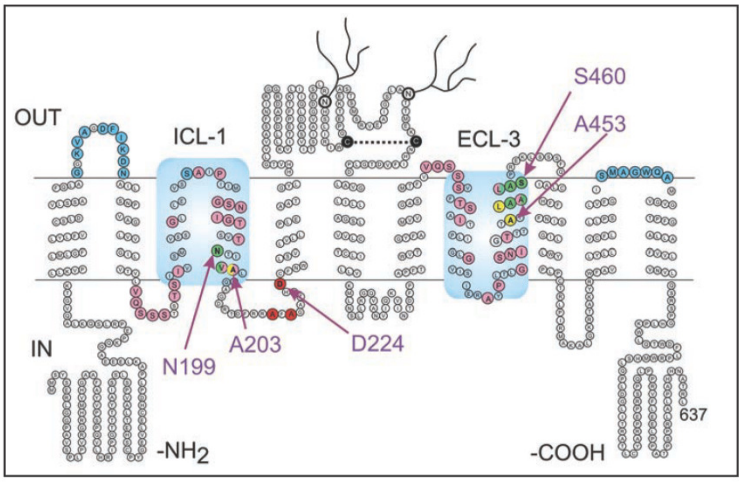

Figure 6. Secondary topology of SLC34 family proteins. Topology is based on the rat NaPi-IIa sequence and predicted according to (81). One essential cysteine bridge (black, dashed line) links the N- and C-terminal halves of the protein and there are two N-glycosylation sites in the large extracellular loop. The two re-entrant loops, proposed to form the transport pathway, are shaded (light blue) contain repeat residues (pink). Selected sites, relevant to leak and cotransport modes, which have been identified from structure-function studies, in which either the leak mode or cotransport mode or both are affected by MTS incubation are indicated as follows; blue: leak unchanged; green: cotransport fully suppressed, leak unchanged; yellow: cotransport fully suppressed, leak increased. In addition, sites critical for electrogenicity are shown (red). © Virkki et al., adapted from Figure 3 originally published in AJP-renal Physiol 2007; 293:643–54.

(Fig. 5B) had only minor effects on the magnitude of I_{Pi} and I_{PFA} at hyperpolarizing potentials, and the variations in I_{PFA} for the different conditions therefore most likely reflect the influence of endogenous currents. Gluconate substitution resulted in a significant increase in I_{PFA}, a concomitantly smaller I_{Pi} relative to the holding current in the gluconate control solution, yet only a small reduction (17% at -100 mV) in the apparent cotransport activity ($I_{\mathrm{Cot}} = I_{\mathrm{Pi}} - I_{\mathrm{PFA}}$) (Fig. 5B). The increased I_{PFA} with gluconate superfusion was documented also for human NaPi-IIb and flounder NaPi-IIb. Significantly, its voltage dependence mirrors that of I_{Pi} in 107 mM Cl^-, as illustrated in Figure 5C for the flounder NaPi-IIb (left) and rat NaPi-IIa (center). These isoforms show characteristically different voltage dependencies for I_{Pi} (1 mM) (e.g., Forster 2006): for hyperpolarizing potentials down to -120 mV, rat NaPi-IIa shows no rate-limiting behavior compared with the flounder NaPi-IIb. The similarity of the voltage dependence of I_{Pi} and I_{PFA} for each isoform supports our notion that the leak and cotransport modes share common voltage dependent processes (Fig. 1A). Moreover, in both cases, the reduced I_{Pi} in gluconate superfusion appears as a direct consequence of the subtraction procedure used to eliminate endogenous currents in which the leak is, in effect, subtracted from the response to $\mathrm{P_i}$. The increase in leak with gluconate superfusion appears to be a unique property of NaPi-IIa/b proteins expressed in *Xenopus* oocytes. We examined the effect of gluconate substitution on the intrinsic leak of SGLT1, using phlorizin to block its uncoupled leak.[17] Here, we documented no significant difference between the phlorizin-dependent currents in 107 mM Cl^- or with 100 mM gluconate and no shift in the reversal potential (right, Fig. 5C) unlike the behavior observed for NaPi-IIa/b expressing oocytes from the same donor frog. Gluconate replacement slightly reduced the α-MNG-dependent cotransport mode current, as previously reported and indicates that Cl^- ions can interact with SGLT1 and alter its voltage dependent kinetics.[55] However, the negative E_r for SGLT1 cannot be explained simply by the involvement of Cl^- ions. Finally, we also confirmed that PFA-inhibitable current measured with gluconate replacement has the properties of Na^+-dependent conductance (Fig. 5D). Equimolar replacement of Na^+ with Li^+, which does not drive transport in SLC34 transporters, shifted the E_r of $-I_{\mathrm{PFA}}$ according to the Nernstian relationship with slopes of 54.9 ± 6.5 mV/log[Na^+] (rat NaPi-IIa, n = 3) and 51.9 ± 2.4 mV/log[Na^+] (human NaPi-IIa, n = 3) (Forster IC, unpublished data). These data strongly suggest that the main permeating ion in the leak mode is Na^+, in agreement with our earlier findings.[41]

The mechanism by which gluconate increases the PFA-inhibitable leak of NaPi-IIa/b is unclear and will require further investigation. As gluconate is a known chelator of divalent cations,[56] we confirmed that the appropriate reduction of free [Ca^{2+}] and [Mg^{2+}] in the external buffer, to simulate chelation by gluconate, was not the underlying cause. The main effect of gluconate substitution on NaPi-IIa/b kinetics is to increase the leak current, most likely by altering the rate of the Na^+-translocation step 2a↔7a (Fig. 1A), whereas the predicted cotransport activity is only marginally affected. In this respect, the behaviour of NaPi-IIa/b with gluconate superfusion supports the notion that $\mathrm{P_i}$ induces a switch from the leak to cotransport cycle.

New insights from structure-function studies- evidence that leak and cotransport share the same pathway. The current secondary topology of SLC34 proteins (Fig. 6) is based on prediction algorithms and structure-function studies (reviewed in refs. 37 and 43). The functional unit of NaPi-IIa is a monomer,[57] however there is also evidence that it may dimerize in the membrane.[58] Each monomer comprises a core backbone of eight transmembrane domains interspersed with two repeat regions in the C- and N-terminal halves of the protein. We propose that they form two reentrant loops that associate to constitute the transport pathway. Cysteine scanning studies have confirmed that parts of loop ECL-3 and ICL-1 are accessible from the external and internal sides of the membrane, respectively. In ECL-3, evidence of a partial α-helical structure was obtained from cysteine scanning,[27] however no detailed topological features have been identified for the outwardly oriented ICL-1. As no 3-D structure for members of the SLC34 family or its bacterial homologs currently exist and there is no homology with available 3-D structures of other Na^+-dependent cotransporters, this functional assignment of

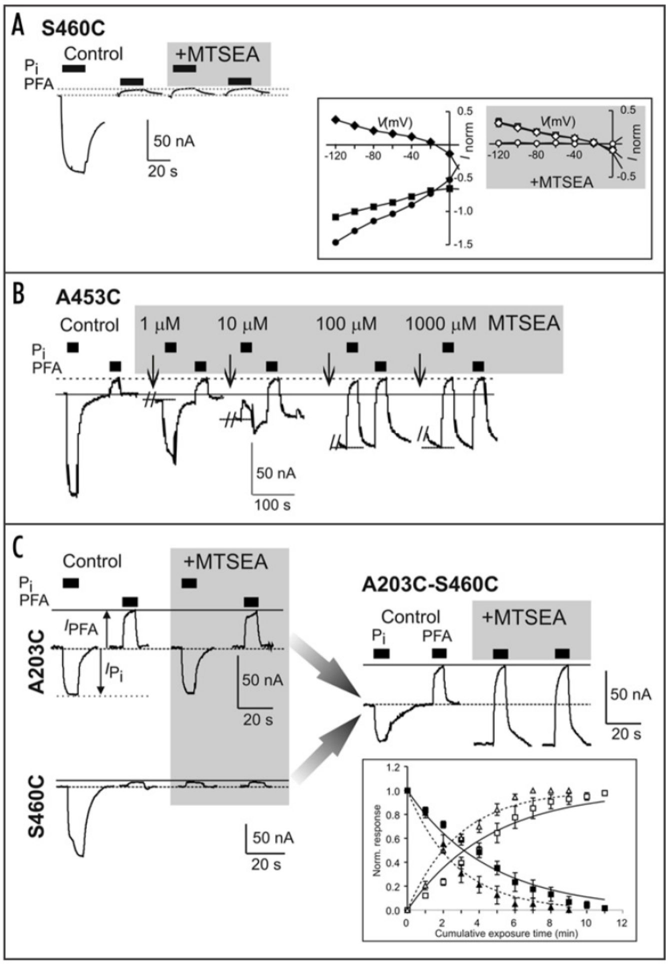

Figure 7. Structure function studies separate leak from cotransport activity. (A) S460C mutant. Representative current recording at -50 mV showing response to P_i (1 mM) and PFA (3 mM) under control conditions. The oocyte was then exposed to the methanethiosulfonate reagent MTSEA (1 mM) for 3 minutes and then the measurement was repeated. © Lambert et al., adapted from Figure 6 originally published in The J Gen Physiol 1999; 114:637–51. Inset shows *I-V* data for S460C and establishes that I_{Pi} after and I_{PFA} before and after MTSEA exposure are almost identical over a wide range of test potentials. Data points normalised to I_{Pi} at -100 mV before MTSEA exposure (n = 4). Filled symbols: control; empty symbols: after MTSEA exposure; squares: I_{Pi}; diamonds: I_{PFA}; circles: I_{Cot}. (Forster IC, unpublished data). (B) A453C mutant. Representative recording at -50 mV showing response to P_i (1 mM) and PFA (3 mM) under control conditions and after exposure to MTSEA for 3 min at the indicated concentrations. Only the baseline that immediately preceded application and washout of the test substrates is shown. The dashed line indicates holding current reached during control PFA application. Continuous line indicates initial holding current in control superfusate. No external adjustment of current offset was made during the recording. After 100 μM MTSEA application there is little change in the responses to P_i and PFA. © Lambert et al., adapted from Figure 3 originally published in The J Gen Physiol 2001; 117:533–46. (C) The double mutant A203C-S460C. Representative recording at -50 mV showing response to P_i (1 mM) and PFA (3 mM) under control conditions and after exposure to MTSEA (1 mM for 3 min) for mutant A203C (upper) and S460C (lower) and A203C-S460C. Inset shows the reciprocity of transport mode activity as A203C-S460C is progressively modified using MTS reagents MTSEA (squares) and MTSES (triangles). Loss of cotransport function (filled symbols) and gain in leak (open symbols) follow reciprocal time courses suggesting that the two processes are linked. Continuous (MTSEA) and dotted (MTSES) lines are fits to the data with a single exponential function to give modification rates for MTSEA (leak gain: $7.3 \times 10^{-4}\ s^{-1}\ \mu M^{-1}$; cotransport loss: $7.2 \times 10^{-4}\ s^{-1}\ \mu M^{-1}$) an MTSES (leak gain: $1.1 \times 10^{-3}\ s^{-1}\ \mu M^{-1}$; cotransport loss: $1.2 \times 10^{-3}\ s^{-1}\ \mu M^{-1}$). Each data point represents mean ± SEM (n = 6). (For further details see ref. 29.) © Kohler et al., adapted from Figures 2 and 6 originally published in The J Gen Physiol 2002; 120:693–705.

the reentrant segments remains speculative. Nevertheless, the repeat regions are also conserved in the prokaryotic homolog from *Vibrio cholera*.[43,59] Moreover, recent 3-D structures of Na^+-driven cotransporters[60-63] have highlighted the importance of the inverted repeat structure that defines the substrate binding region and which could well apply to SLC34 proteins.

Insights into the nature and localization of the leak pathway for SLC34 proteins have come from structure-function studies in which cysteine residues are substituted at functionally important sites. This involves determining accessibility by methanethiosulfonate (MTS) reagents of the novel cysteine and characterizing the effect of the cys-substitution and MTS-modification on the I_{Pi} and I_{PFA}.[26-29,64,65] In these studies, a number of mutants show full suppression of cotransport activity after MTS modification, which confirms their accessibility. These can be further distinguished according to the effect cys-modification has on the PFA-inhibitable leak: constructs in which the leak is unchanged after cys-modification and those in which the leak activity is increased.

Mutant S460C exemplifies the first type of behavior, which has a Ser-Cys substitution at a site in the C-terminal end of reentrant loop ECL-3 (Fig. 6). The substitution alone does not alter the basic kinetic properties compared to the WT.[26] However, after exposure to MTS reagents that increase the residue bulk and alter the charge at the substitution site, cotransport activity is inhibited, and the electrogenic responses to P_i (1 mM) and PFA (3 mM) are identical (Fig. 7A). This behavior can readily be understood in terms of the kinetic scheme (Fig. 1A), whereby P_i and PFA compete for the same binding site, thus blocking the leak mode. In the case of S460C, after MTS exposure, the substrate binding partial reactions for binding of Na^+ (1-2a, 2a-2b) and P_i (2b-3) still occur, however subsequent partial reactions in the transport cycle are excluded because the modified cysteine restricts the possible conformational states the protein can occupy. With respect to the leak mode, state 3* (PFA bound) and state 3 (P_i bound) are therefore indistinguishable, in agreement with the equivalence of I_{Pi} and I_{PFA} over a wide range of test potentials(inset, Fig. 7A). At least one site has also been identified that shows similar behavior to S460C in the predicted reentrant loop ICL-1.[28] The cotransport activity of this mutant N199C (Fig. 6) is modified using the partially membrane permeable reagent MTSEA, whereas the impermeable MTSET has no effect. In addition to providing confirmation of the predicted topology, this finding is a first, albeit indirect hint that these reentrant loops might contribute to a common transport pathway for both the leak and cotransport modes. The critical importance of Asn-199 was demonstrated by making other substitutions at this site. Mutants in which the native Asn is substituted with the amide derivative of glutamate (Gln) or other basic or acidic amino acids (Asp, His, Arg) show only leak (PFA response), whereas substituting with Cys, Ala and Thr is tolerated and the corresponding mutants show both leak and cotransport activity.[28]

Mutant A453C also with a cys-substitution in ECL-3, exemplifies the second type of behavior. MTSEA treatment induces a large Na^+-dependent leak that, like S460C, is equally suppressed by both PFA and P_i (Fig. 7B).[27] As the MTSEA concentration is increased, a progressively greater fraction of transporters is modified and I_{Pi} changes from the initial downward deflection, characteristic of cotransport, to an upward deflection, which represents inhibition of the leak current. Note that the holding current reached during PFA application remains the same and corresponds to I_{Endog} (Fig. 1A). In the GABA transporter GAT1 a similar phenotype of increased leak after MTS modification of Cys-74 in the first reentrant loop region[33] which, according to the 3-D structure of the bacterial homolog $LeuT_{Aa}$, forms part of the substrate binding domain.[63,66]

These findings provide compelling evidence for an interaction between ICL-1 and ECL-3, which was further investigated by examining the effect on the Cys-Ser substitution at site 460 by making a second cys substitution at site Ala-203 in ICL-1.[29] The single mutant (A203C) exhibits a significantly larger I_{PFA} compared with the WT[28] (Fig. 7C). As expected, the double mutant (A203C-S460C) displays the phenotype of A203C, which indicates that the Cys-460 does itself alter the electrogenic activity. However, after exposure to MTSEA, the leak increases and P_i induces the same change in holding current as PFA,[29] thus recapitulating the phenotype observed for Ala-Cys substitution in ECL3 (Fig. 7B). Based on the behavior of this and other mutants, our current view is that the leak and cotransport pathways share common structural elements. Whether one or both novel Cys in A203C-S460C are modified remains to be determined, however we currently favor a steric interaction between Cys-203 and Cys-460, in which only Cys-460 is modified, based on the behavior of other substitutions at these sites and a comparison of the rates of modification (Fig. 7C, inset).[29] The A203C-S460C double mutant also provides a useful tool to demonstrate the close interrelationship between leak and cotransport modes. The progressive growth in leak and decrease in cotransport activity over the time course of cys-modification is reciprocal (Fig. 7C, inset). This is the behavior expected of two populations of transporters: those that are modified and mediate only leak and those that are unmodified and can still mediate cotransport.[29]

Transport kinetics and leak. Transport-independent leak currents can introduce a source of error and lead to data misinterpretation when characterizing the transport kinetics of electrogenic carriers. As noted above, some WT cotransporters display leak currents that are comparable in magnitude to the substrate-induced change in holding current, (e.g., NIS,[15] and SVCT1,-2, [ref. 16]). If our model of mutual exclusivity of the leak and cotransport modes is valid also for other electrogenic carriers, large leak currents should be taken into account when deriving phenomenological kinetic parameters, such as apparent substrate affinities. Errors will arise when the substrate-induced currents are measured relative to the leak current (i.e., the baseline current in the absence of substrate, see Fig. 1A), which would substantially underestimate the magnitude of the cotransport mode current.[43] At non-saturating $[P_i]$, the overall electrogenic activity will be contributed by both leak and cotransport modes: depending on the probability of occupancy of the associated states, a fraction of the transporters will translocate charge in the leak mode and others in the cotransport mode.

For cotransporters like NaPi-IIa/b, and SGLT1, where the leak typically accounts for ≤20% of substrate induced current, this error is small. For SGLT1, it was estimated that the leak contribution to electrogenic activity is negligible for glucose concentrations well below the apparent affinity for glucose cotransport[18] and a similar analysis has yet to be undertaken for NaPi-IIa/b. However, for NaPi-IIa/b, the error can become larger under specific conditions, such as low pH (Fig. 2A) or gluconate perfusion (Fig. 5C), where the relative contribution of the two transport modes to electrogenic activity changes significantly. This could account a significant deviation in stoichiometry of NaPi-IIa/b observed at pH < 6.8 determined by simultaneous uptake and charge measurements on single oocytes. Here, the transported charge is quantified by integrating the steady-state response to substrate (e.g., I_{Pi} in Fig. 1B), using the control solution as baseline (reviewed in refs. 15, 38 and 67). At pH 7.4 and 6.8, the $Q:P_i$ ratio for rat NaPi-IIa expressing oocytes is ~1.0,[38] whereas at pH 6.2, where I_{Pi} is significantly smaller but the leak is unchanged, $Q:P_i = 0.5 \pm 0.1$ (n = 13) (Forster IC, Loo DDF, Eskandari S, unpublished experiments). It may also explain the non-integer estimate of stoichiometry reported for the Na^+-coupled iodide cotransporter (NIS).[15]

Conclusions

The physiological significance the NaPi-IIa/b leak is unclear: for example, along the length of the renal proximal tubule, NaPi-IIa in the brush border membrane is mostly exposed to Pi levels that exceed K_m^{Pi} and therefore we would not expect the substrate-independent leak to contribute to a significant inward Na^+ flux. However, in the context of structure-function investigations, the leak mode offers a useful phenotype for gaining insight into transport mechanisms. Whereas many transporters exhibit channel-like (gated pore) behavior with complex permeation phenotypes (see Table 1), the Na^+-dependent leak current of SLC34 proteins appears to result from the intrinsic translocation of one charge per transport cycle and is specific for Na^+. Although we cannot exclude a leak mechanism in which Na^+ itself gates a thermodynamically uncoupled Na^+-selective pore, the evidence we have obtained so far from WT and mutant constructs is consistent with the leak being intimately associated with the electrogenic interaction of a single Na^+ ion, and its subsequent translocation via a uniport mechanism. In this respect, the term "uncoupled" leak should be used with reservation. Importantly, the leak and cotransport modes of NaPi-IIa/b appear to be mutually exclusive: the behavior of the Cys mutants provides strong evidence that the leak mode is fully suppressed when substrate is bound. Here, we assume that the mutant behavior reflects the transitions between a subset of conformational states also occupied in the WT. Therefore, according to the transport scheme (Fig. 1A), for a given external [Na$^+$], the concentration of P$_i$ will determine whether the protein translocates only Na$^+$ ions via the leak loop (transition 2↔7), or binds P$_i$ and cotransports 3 Na$^+$ ions and P$_i$ (transition 4↔5), with the same Na$^+$ ion common to both modes.

Finally, we note that our data are based exclusively on experiments with intact oocytes and constant intracellular environment. To test the validity of the alternating access model implied by the kinetic scheme of Figure 1A, further investigations would benefit from the cut-open oocyte technique, to allow access to the intracellular medium (reviewed in ref. 68).

Acknowledgements

This work was supported by the Swiss National Science Foundation and the Gebert-Ruf Foundation. The rabbit SGLT1 cDNA was a kind gift of Professor Ernest M. Wright, UCLA.

References

1. Nelson N, Sacher A, Nelson H. The significance of molecular slips in transport systems. Nat Rev Mol Cell Biol 2002; 3:876-81.
2. Sonders MS, Amara SG. Channels in transporters. Curr Opin Neurobiol 1996; 6:294-302.
3. DeFelice LJ, Goswami T. Transporters as channels. Ann Rev Physiol 2007; 69:87-112.
4. Hediger MA, Romero MF, Peng JB, Rolfs A, Takanaga H, Bruford EA. The ABCs of solute carriers: physiological, pathological and therapeutic implications of human membrane transport proteinsIntroduction. Pflugers Archiv Eur J Physiol 2004; 447:465-8.
5. Karakossian MH, Spencer SR, Gomez AQ, et al. Novel properties of a mouse gamma-aminobutyric acid transporter (GAT4). J Memb Biol 2005; 203:65-82.
6. Schneider HP, Broer S, Broer A, Deitmer JW. Heterologous expression of the glutamine transporter SNAT3 in *Xenopus* oocytes is associated with four modes of uncoupled transport. J Biol Chem 2007; 282:3788-98.
7. Cao Y, Mager S, Lester HA. H$^+$ permeation and pH regulation at a mammalian serotonin transporter. J Neurosci 1997; 17:2257-66.
8. Zerangue N, Kavanaugh MP. ASCT-1 is a neutral amino acid exchanger with chloride channel activity. J Biol Chem 1996; 271:27991-4.
9. Broer A, Wagner C, Lang F, Broer S. Neutral amino acid transporter ASCT2 displays substrate-induced Na$^+$ exchange and a substrate-gated anion conductance. Biochem J 2000; 346:705-10.
10. Wadiche JI, Amara SG, Kavanaugh MP. Ion fluxes associated with excitatory amino acid transport. Neuron 1995; 15:721-8.
11. Fairman WA, Vandenberg RJ, Arriza JL, Kavanaugh MP, Amara SG. An excitatory amino-acid transporter with properties of a ligand-gated chloride channel. Nature 1995; 375:599-603.
12. Ryan RM, Mindell JA. The uncoupled chloride conductance of a bacterial glutamate transporter homolog. Nat Struct Mol Biol 2007; 14:365-71.
13. Miller C. A leak in the EAATs. Nat Struct Mol Biol 2007; 14:356-7.
14. Zomot E, Bendahan A, Quick M, Zhao Y, Javitch JA, Kanner BI. Mechanism of chloride interaction with neurotransmitter:sodium symporters. Nature 2007; 449:726-30.
15. Eskandari S, Loo DD, Dai G, Levy O, Wright EM, Carrasco N. Thyroid Na$^+$/I$^-$ symporter. Mechanism, stoichiometry and specificity. J Biol Chem 1997; 272:27230-8.
16. Tsukaguchi H, Tokui T, Mackenzie B, et al. A family of mammalian Na$^+$-dependent L-ascorbic acid transporters. Nature 1999; 399:70-5.
17. Umbach JA, Coady MJ, Wright EM. Intestinal Na$^+$/glucose cotransporter expressed in *Xenopus* oocytes is electrogenic. Biophys J 1990; 57:1217-24.
18. Chen XZ, Coady MJ, Jalal F, Wallendorff B, Lapointe JY. Sodium leak pathway and substrate binding order in the Na$^+$-glucose cotransporter. Biophys J 1997; 73:2503-10.
19. Mager S, Kleinberger-Doron N, Keshet GI, Davidson N, Kanner BI, Lester HA. Ion binding and permeation at the GABA transporter GAT1. J Neurosci 1996; 16:5405-14.
20. Sonders MS, Zhu SJ, Zahniser NR, Kavanaugh MP, Amara SG. Multiple ionic conductances of the human dopamine transporter: the actions of dopamine and psychostimulants. J Neurosci 1997; 17:960-74.
21. MacAulay N, Zeuthen T, Gether U. Conformational basis for the Li$^+$-induced leak current in the rat gamma-aminobutyric acid (GABA) transporter-1. J Physiol 2002; 544:447-58.
22. Shimbo K, Brassard DL, Lamb RA, Pinto LH. Viral and cellular small integral membrane proteins can modify ion channels endogenous to *Xenopus* oocytes. Biophys J 1995; 69:1819-29.
23. Tzounopoulos T, Maylie J, Adelman JP. Induction of endogenous channels by high levels of heterologous membrane proteins in *Xenopus* oocytes. Biophys J 1995; 69:904-8.
24. Buyse G, Voets T, Tytgat J, et al. Expression of human pICln and ClC-6 in *Xenopus* oocytes induces an identical endogenous chloride conductance. J Biol Chem 1997; 272:3615-21.
25. Broer S, Schuster A, Wagner CA, et al. Chloride conductance and Pi transport are separate functions induced by the expression of NaPi-1 in *Xenopus* oocytes. J Memb Biol 1998; 164:71-7.
26. Lambert G, Forster IC, Stange G, Biber J, Murer H. Properties of the mutant Ser-460-Cys implicate this site in a functionally important region of the type IIa Na$^+$/P$_i$ cotransporter protein. J Gen Physiol 1999; 114:637-52.
27. Lambert G, Forster IC, Stange G, Kohler K, Biber J, Murer H. Cysteine mutagenesis reveals novel structure-function features within the predicted third extracellular loop of the type IIa Na$^+$/P$_i$ cotransporter. J Gen Physiol 2001; 117:533-46.
28. Kohler K, Forster IC, Stange G, Biber J, Murer H. Identification of functionally important sites in the first intracellular loop of the NaPi-IIa cotransporter. Am J Physiol 2002; 282:687-96.
29. Kohler K, Forster IC, Stange G, Biber J, Murer H. Transport function of the renal type IIa Na$^+$/P$_i$ cotransporter is codetermined by residues in two opposing linker regions. J Gen Physiol 2002; 120:693-703.
30. Ryan RM, Mitrovic AD, Vandenberg RJ. The chloride permeation pathway of a glutamate transporter and its proximity to the glutamate translocation pathway. J Biol Chem 2004; 279:20742-51.
31. Borre L, Kavanaugh MP, Kanner BI. Dynamic equilibrium between coupled and uncoupled modes of a neuronal glutamate transporter. J Biol Chem 2002; 277:13501-7.
32. Ryan RM, Vandenberg RJ. Distinct conformational states mediate the transport and anion channel properties of the glutamate transporter EAAT-1. J Biol Chem 2002; 277:13494-500.
33. Yu N, Cao Y, Mager S, Lester HA. Topological localization of cysteine 74 in the GABA transporter, GAT1, and its importance in ion binding and permeation. FEBS Letters 1998; 426:174-8.
34. Mackenzie B, Ujwal ML, Chang MH, Romero MF, Hediger MA. Divalent metal-ion transporter DMT1 mediates both H$^+$-coupled Fe^{2+} transport and uncoupled fluxes. Pflugers Archiv. Eur J Physiol 2006; 451:544-58.
35. Eskandari S, Kreman M, Kavanaugh MP, Wright EM, Zampighi GA. Pentameric assembly of a neuronal glutamate transporter. Proc Natl Acad Sci USA 2000; 97:8641-6.
36. Leary GP, Stone EF, Holley DC, Kavanaugh MP. The glutamate and chloride permeation pathways are colocalized in individual neuronal glutamate transporter subunits. J Neurosci 2007; 27:2938-42.
37. Virkki LV, Biber J, Murer H, Forster IC. Phosphate transporters: a tale of two solute carrier families. Am J Physiol Renal Physiol 2007; 293:643-54.
38. Forster IC, Loo DD, Eskandari S. Stoichiometry and Na$^+$ binding cooperativity of rat and flounder renal type II Na$^+$-P$_i$ cotransporters. Am J Physiol 1999; 276:644-9.
39. Virkki LV, Forster IC, Biber J, Murer H. Substrate interactions in the human type IIa sodium-phosphate cotransporter (NaPi-IIa). Am J Physiol 2005; 288:969-81.
40. Bacconi A, Virkki LV, Biber J, Murer H, Forster IC. Renouncing electrogenicity is not free of charge: switching on electrogenicity in a Na$^+$-coupled phosphate cotransporter. Proc Natl Acad Sci USA 2005; 102:12606-11.
41. Forster I, Hernando N, Biber J, Murer H. The voltage dependence of a cloned mammalian renal type II Na$^+$/P$_i$ cotransporter (NaPi-2). J Gen Physiol 1998; 112:1-18.
42. Virkki LV, Murer H, Forster IC. Voltage clamp fluorometric measurements on a type II Na$^+$-coupled P$_i$ cotransporter: shedding light on substrate binding order. J Gen Physiol 2006; 127:539-55.
43. Forster IC, Kohler K, Biber J, Murer H. Forging the link between structure and function of electrogenic cotransporters: the renal type IIa Na$^+$/P$_i$ cotransporter as a case study. Prog Biophys Mol Biol 2002; 80:69-108.
44. Beliveau R, Ibnoul-Khatib H. Electrogenicity of phosphate transport by renal brush-border membranes. Biochem J 1988; 252:801-6.
45. Forster IC, Biber J, Murer H. Proton-sensitive transitions of renal type II Na$^+$-coupled phosphate cotransporter kinetics. Biophys J 2000; 79:215-30.
46. Parent L, Supplisson S, Loo DD, Wright EM. Electrogenic properties of the cloned Na$^+$/glucose cotransporter: II. A transport model under nonrapid equilibrium conditions. [erratum appears in J Membr Biol 1992; 130:203]. J Memb Biol 1992; 125:63-79.
47. Forster IC, Virkki LV, Bossi E, Murer H, Biber J. Electrogenic kinetics of a mammalian intestinal Na$^+$/P$_i$-cotransporter. J Memb Biol 2006; 212:177-90.
48. van Winkle L. Biomembrane Transport. San Diego: Academic 1999.
49. Mackenzie B, Takanaga H, Hubert N, Rolfs A, Hediger MA. Functional properties of multiple isoforms of human divalent metal-ion transporter 1 (DMT1). Biochem J 2007; 403:59-69.
50. Loo DD, Hirayama BA, Meinild AK, Chandy G, Zeuthen T, Wright EM. Passive water and ion transport by cotransporters. J Physiol 1999; 518:195-202.
51. Bacconi A, Ravera S, Virkki LV, Murer H, Forster IC. Temperature-dependency of steady-state and presteady-state kinetics of a type IIb Na$^+$/P$_i$ cotransporter. J Memb Biol 2007; 215:81-92.
52. Ehnes C, Forster IC, Kohler K, et al. Structure-function relations of the first and fourth predicted extracellular linkers of the type IIa Na$^+$/Pi cotransporter: I. Cysteine scanning mutagenesis. J Gen Physiol 2004; 124:475-88.

53. Forster IC, Kohler K, Stange G, Biber J, Murer H. Modulation of renal type IIa Na^+/P_i cotransporter kinetics by the arginine modifier phenylglyoxal. J Memb Biol 2002; 187:85-96.
54. Sciortino CM, Romero MF. Cation and voltage dependence of rat kidney electrogenic Na^+-HCO(-)(3) cotransporter, rkNBC, expressed in oocytes. Am J Physiol 1999; 277:611-23.
55. Loo DD, Eskandari S, Boorer KJ, Sarkar HK, Wright EM. Role of Cl^- in electrogenic Na^+-coupled cotransporters GAT1 and SGLT1. J Biol Chem 2000; 275:37414-22.
56. Kenyon JL, Gibbons WR. Effects of low-chloride solutions on action potentials of sheep cardiac Purkinje fibers. J Gen Physiol 1977; 70:635-60.
57. Kohler K, Forster IC, Lambert G, Biber J, Murer H. The functional unit of the renal type IIa Na^+/Pi cotransporter is a monomer. J Biol Chem 2000; 275:26113-20.
58. Forster IC, Hernando N, Biber J, Murer H. Proximal tubular handling of phosphate: A molecular perspective. Kidney Intl 2006; 70:1548-59.
59. Werner A, Kinne RK. Evolution of the Na-P_i cotransport systems. Am J Physiol 2001; 280:301-12.
60. Boudker O, Ryan RM, Yernool D, Shimamoto K, Gouaux E. Coupling substrate and ion binding to extracellular gate of a sodium-dependent aspartate transporter. Nature 2007; 445:387-93.
61. Faham S, Watanabe A, Besserer GM, et al. The crystal structure of a sodium galactose transporter reveals mechanistic insights into Na^+/sugar symport. Science 2008; 321:810-4.
62. Yernool D, Boudker O, Jin Y, Gouaux E. Structure of a glutamate transporter homologue from Pyrococcus horikoshii. Nature 2004; 431:811-8.
63. Yamashita A, Singh SK, Kawate T, Jin Y, Gouaux E. Crystal structure of a bacterial homologue of Na^+/Cl^--dependent neurotransmitter transporters. Nature 2005; 437:215-23.
64. Kohler K, Forster IC, Stange G, Biber J, Murer H. Essential cysteine residues of the type IIa Na^+/P_i cotransporter. Pflugers Archiv. Eur J Physiol 2003; 446:203-10.
65. Virkki LV, Forster IC, Bacconi A, Biber J, Murer H. Functionally important residues in the predicted 3rd transmembrane domain of the type IIa sodium-phosphate co-transporter (NaPi-IIa). J Memb Biol 2005; 206:227-38.
66. Kanner BI. Structure and function of sodium-coupled GABA and glutamate transporters. J Memb Biol 2006; 213:89-100.
67. Mackenzie B, Loo DD, Wright EM. Relationships between Na^+/glucose cotransporter (SGLT1) currents and fluxes. J Memb Biol 1998; 162:101-6.
68. Adams SV, DeFelice LJ. Ionic currents in the human serotonin transporter reveal inconsistencies in the alternating access hypothesis. Biophys J 2003; 85:1548-59.
69. Wadiche JI, Arriza JL, Amara SG, Kavanaugh MP. Kinetics of a human glutamate transporter. Neuron 1995; 14:1019-27.
70. Kanai Y, Nussberger S, Romero MF, Boron WF, Hebert SC, Hediger MA. Electrogenic properties of the epithelial and neuronal high affinity glutamate transporter. J Biol Chem 1995; 270:16561-8.
71. Chen XZ, Coady MJ, Jackson F, Berteloot A, Lapointe JY. Thermodynamic determination of the Na^+: glucose coupling ratio for the human SGLT1 cotransporter. Biophys J 1995; 69:2405-14.
72. Coady MJ, Wallendorff B, Gagnon DG, Lapointe JY. Identification of a novel Na^+/myo-inositol cotransporter. J Biol Chem 2002; 277:35219-24.
73. Coady MJ, Wallendorff B, Bourgeois F, Charron F, Lapointe JY. Establishing a definitive stoichiometry for the Na^+/monocarboxylate cotransporter SMCT1. Biophys J 2007; 93:2325-31.
74. Iwamoto H, Blakely RD, De Felice LJ. Na^+, Cl^- and pH dependence of the human choline transporter (hCHT) in *Xenopus* oocytes: the proton inactivation hypothesis of hCHT in synaptic vesicles. J Neurosci 2006; 26:9851-9.
75. Mager S, Min C, Henry DJ, et al. Conducting states of a mammalian serotonin transporter. Neuron 1994; 12:845-59.
76. Galli A, Petersen CI, deBlaquiere M, Blakely RD, DeFelice LJ. Drosophila serotonin transporters have voltage-dependent uptake coupled to a serotonin-gated ion channel. J Neurosci 1997; 17:3401-11.
77. Meinild AK, Sitte HH, Gether U. Zinc potentiates an uncoupled anion conductance associated with the dopamine transporter. J Biol Chem 2004; 279:49671-9.
78. Yao X, Pajor AM. The transport properties of the human renal Na^+-dicarboxylate cotransporter under voltage-clamp conditions. Am J Physiol Renal Physiol 2000; 279:54-64.
79. Chen XZ, Zhu T, Smith DE, Hediger MA. Stoichiometry and kinetics of the high-affinity H^+-coupled peptide transporter PepT2. J Biol Chem 1999; 274:2773-9.
80. Mackenzie B, Illing AC, Hediger MA. Transport model of the human Na^+-coupled L-ascorbic acid (vitamin C) transporter SVCT1. Am J Physiol Cell Physiol 2008; 294:451-9.
81. Radanovic T, Gisler SM, Biber J, Murer H. Topology of the type IIa Na^+/P(i) cotransporter. J Memb Biol 2006; 212:41-9.

3.1.2 Paper 2: “Lithium interactions with the type II Na$^+$-coupled inorganic phosphate cotransporters.”

Andrini O., Meinild A.K., Ghezzi C., Murer H., Forster I.C.
Institute of Physiology and Center of Integrative Human Physiology (ZIHP), University of Zurich, Zurich, Switzerland.

Methods used:

- Two-electrode voltage-clamp technique (TEVC);
- Radiolabled tracer assay;
- Single point mutagenesis.

I characterized the effect of Li$^+$ ions on cotransport. The functional studies lead to the development of a revised kinetic scheme for NaPi-II.

Abstract

Type IIa/b Na^+-coupled inorganic phosphate cotransporters (NaPi-IIa/b) are generally considered to be exclusively Na^+ dependent. Here we show that Li^+ can substitute for Na^+ as a driving cation. We expressed NaPi-IIa/b in *X. laevis* oocytes and performed two-electrode voltage-clamp electrophysiology and uptake assays to investigate the effect of external Li^+ on their kinetics. Substitution of 50% external Na^+ with Li^+ reduced the maximum transport rate but increased apparent affinity for P_i. Moreover, the steady-state voltage dependence of the P_i-induced current was significantly weaker in the presence of external Li^+. By means of simultaneous electrophysiology and ^{22}Na uptake on single oocytes, we show that Li^+ ions can substitute for at least one of the 3 Na^+ ions necessary for cotransport. To identify which partial reactions in the transport cycle involved Li^+ interactions we performed presteady-state assays. They provide compelling evidence that Li^+ ions, in the absence of external Na^+ can interact with the empty carrier, however the total charge displaced was 70% of that in the presence of Na^+ or when 50% of the Na^+ was replaced by Li^+. If Na^+ and Li^+ were both present, the voltage dependence of the mobile charges was shifted in the depolarizing direction, which was also consistent with the altered steady-state voltage dependence of phosphate induced current. Our presteady-state data suggest that charge movement in the presence of Li^+ alone reflects the interaction of a single Li^+ ion with the transporter, in contrast to 2 Na^+ ions when only Na is present. To account for our findings, we propose an ordered binding scheme for cotransport in which one Li^+ ion can bind with high affinity at the putative 1st cation interaction site. This is followed by the cooperative binding of one Na^+ ion, one divalent P_i anion and a 3rd Na^+ ion to complete the loading of the carrier before translocation. When Li^+ is bound, the backward transitions of voltage dependent partial reactions in the cotransport cycle are altered to account for the lower turnover rate.

Introduction

Secondary-active cotransporters use the free energy available from downhill cation electrochemical gradients to catalyse uphill transport of specific solutes into the cell. The majority of mammalian cotransporters use Na^+ as their preferred driving cation under physiological conditions, yet in some cases other cations (Li^+, H^+) can substitute for Na^+, albeit with altered apparent cation and substrate affinities, and transport rates. For example, Li^+ or H^+ can drive glucose transport catalysed by the sodium-coupled glucose cotransporter (SGLT1) (16, 17) and Li^+ can substitute for Na^+ as the driving cation of the sodium-coupled dicarboxylate transporter (NaDC-1) (23) and the excitatory amino acid transporter (EAAT1) (2). Such cation substitutions can have significant clinical consequences. For example, therapeutic doses of orally administered LiCl, used to treat bipolar disorder, result in the rapid onset of increased renal excretion of Krebs cycle intermediates (30). Typically, the concentration of Li^+ in both serum and glomerular filtrate is in the mM range. Although this is at least 10-fold smaller than the prevailing Na^+ concentration, it is sufficient to compete with Na^+ for one of the 3 cation binding sites postulated for NaDC-1 (23), and thereby inhibit reabsorption. On the other hand, some cotransporters show no detectable transport activity if Li^+ fully replaces Na^+, yet when both cations are available, potent stimulation of transport can occur at membrane potentials in the physiological range, as reported for the γ-amino acid transporter GAT1 (18, 32).

Type-II Na^+-coupled inorganic phosphate (P_i) cotransporters (NaPi-IIa,c; SLC34A1,A3) are both expressed in the apical membrane of mammalian proximal tubule epithelia where they mediate P_i reabsorption (7, 21). Although genetically unrelated to NaDC-1, their 3:1 (for electrogenic NaPi-IIa) and 2:1 (for electroneutral NaPi-IIc) Na^+:P_i stoichiometries imply the existence of multiple Na^+ binding sites that could also be potential targets for Li^+ interaction in the kidney. In one of the few reports that has addressed the effects of Li^+ on renal P_i handling, it appears that P_i clearance and tubular reabsorption are normal in humans undergoing chronic Li^+ therapy (24), unlike the case for dicarboxylates. Moreover, in two animal studies, the effect of high doses of Li^+ on P_i handling would appear to result from an indirect action on PTH regulation of NaPi-II abundance in the brush border membrane, as opposed to an interaction with cation binding sites within the transport protein (1, 31).

In contrast to the lack of any clinically significant effect of Li^+ on renal P_i transport, biophysical studies on heterologously expressed NaPi-II proteins in *Xenopus* oocytes reveal direct interactions of Li^+ on the protein (13, 28, 29). By labeling the electrogenic isoform flounder NaPi-IIb with a fluorophore at functionally important sites, voltage dependence changes in fluorescence intensity that depend on the $[Li^+]$, offer compelling evidence that before P_i binding, one Li^+ interacts with the protein. The induced conformational changes, as reflected in fluorescence intensity changes, were comparable to those reported for Na^+ over the same concentration range (28), however no evidence for the cotransport of Li^+ was presented. Similar Li^+-dependent changes in fluorescence emissions were reported for the electroneutral NaPi-IIc (13). It was also significant that in that study no change in ^{32}P uptake was observed when 50% of the Na^+ was replaced with Li^+. This finding suggested, at least for the electroneutral NaPi-IIc isoform, that Li^+ does not readily substitute for Na^+ in the complete cotransport cycle.

Taken together, these findings prompted us to undertake a rigorous biophysical investigation of the effects of Li^+ on NaPi-II transport kinetics using electrogenic NaPi-II isoforms expressed in *X. laevis* oocytes. Our findings provide compelling evidence that Li^+ ions compete with Na^+ ions at the cation binding site that is initially occupied by external cations in the ordered cotransport cycle. Moreover, we demonstrate that at sufficiently high concentrations, one Li^+ can substitute for one Na^+ to drive cotransport of P_i. These findings offer valuable insight into how different cations interact with NaPi-II protein to drive coupled transport.

Materials and Methods

Solutions and reagents

Three standard extracellular solutions were used, each containing (in mM) KCl, 2; $CaCl_2$, 1.8; $MgCl_2$, 1; HEPES-TRIS, 10; adjusted to pH 7.4 with either 100 mM NaCl, 100 mM LiCl or 100 mM choline Cl, and are referred to as 100Na, 100Li or 100Ch solutions, respectively. In cation substitution experiments NaCl was equimolarly replaced with either ChCl or LiCl and solutions with intermediate extracellular [Na^+] and [Li^+] were obtained by mixing 100Na with 100Ch or 100Li in appropriate proportions to maintain the same ionic strength. P_i was added from a 1M K_2HPO_4/ KH_2PO_4 stock premixed to give pH 7.4. Modified Barth's solution for storing oocytes contained (in mM): NaCl, 88; KCl, 1; $CaCl_2$, 0.41; $MgSO_4$, 0.82; $NaHCO_3$, 2.5; $Ca(NO_3)_2$, 2; HEPES, 7.5; pH 7.5 adjusted with TRIS and supplemented with 5 mg/l doxycyclin and 5 mg/l gentamicin.

All standard reagents were obtained from either Sigma-Aldrich or Fluka (Buchs, Switzerland).

Site-directed mutagenesis and cRNA preparation

cDNA encoding wild-type (WT) flounder NaPi-IIb (GenBank/EMBL/DDBJ accession n. AAB16821) rat NaPi-IIa and human NaPi-IIa were subcloned into KSM expression vector containing the 5' and 3' UTRs from *Xenopus* β-globin to improve its expression in oocytes, described in (27). The plasmids were linearized with *XbaI* (Promega) and used a template for synthesis of capped cRNA using Message Machine T3 kit (Ambion).The cDNA preparation for the A175C mutant of flNaPi-IIb was done as previously described in (14)

Expression in Xenopus laevis oocytes

Female *X. laevis* frogs were purchased from *Xenopus* Express (France). Portions of ovaries were surgically removed from frogs anesthetized in MS222 (tricaine methansulphonate) and cut in small pieces.After suturing the incision the frog was placed in a separate tank for at least 2 days in order to fully recover from the surgery and returned to a larger tank. A minimum of 8 weeks were allowed before re-operation on the same animal. All animal handling was in full compliance with the regulations and recommendations of the University and Federal Veterinary Offices with written approval. Oocytes were typically treated for 45 min with collagenase (crude type 1A) 1 mg/ml in 100Na solution (without Ca^{2+}) in presence of 0.1 mg/ml trypsin inhibitor type III-O. Healthy stage V-VI oocytes were selected, maintained in modified Barth's solution at 16°C and injected with 10 ng of cRNA. Experiments were performed 4-7 days after injection.

Two-electrode Voltage Clamp

The standard two-electrode voltage clamp (TEVC) technique was used using either Geneclamp (Molecular Devices, Inc., USA); Turbo TEX10 (NPI Electronics, Tamm, Germany) or a laboratory built TEVC instrument (4). Oocytes were mounted in a small recording chamber (volume: 100µl) and continuously superfused (5ml/min) with the test solution pre-cooled to

20°C. For constant voltage recordings, currents were acquired at 20 samples/s and filtered at 10 Hz (3 dB, 8 pole Bessel characteristic). Faster sampling rates (up to 20k samples/s) were used for voltage-step recordings with low-pass filtering adjusted accordingly (typically at 500 Hz).

Steady-state P_i activation of electrogenic transporters was determined by varying the P_i concentration in presence of the same background solution and subtracting the respective currents in the control solution alone from those in control solution+$P_{i.}$ Steady state Na^+ activation was similarly determined by subtracting the respective responses in the control solution from those in control+P_i and $[P_i]$=1mM.

Steady-state P_i-induced currents (I_{P_i}) were fit with a form of the modified Hill Equation:

$$I_{Pi} = I_{Pi}^{\max}\left([S]^{n_H}/\left([S]^{n_H}+(K_{0.5}^{S})^{n_H}\right)\right)+K \qquad (1)$$

where [S] is the concentration of variable substrate (Na^+ or P_i), $\boldsymbol{I_{P_i}}^{\max}$ is the maximal P_i-induced current, $K_{0.5}{}^{S}$ is the apparent affinity constant for substrate S, n_H is the Hill coefficient and K is a constant that take in account of uncoupled leak effects (3). For P_i activation n_H=1 and equation 1 reduces to a Michaelian form.

Presteady-state relaxations were recorded using voltage steps from V_h=-60 mV to voltages in the range of -180 to +80 mV. Unless otherwise stated, relaxations were quantified by fitting with a two-component exponential function starting approximately 4 ms after the commencement of the voltage step to allow the linear components of charge movement arising from charging the oocyte capacitance to have fully decayed. The fitted curve was then extrapolating back to the time at which 70% of the membrane was charged (typically 1 ms after pulse onset), estimated by integrating the capacity transient for a 20 mV step from the holding potential. This time point was used as the reference time zero for numerical integration of the total relaxation to obtain the charge moved (Q) for a step from the holding potential to the test potential.

The Q-V data were fitted with a Boltzmann function of the form:

$$Q = Q_{hyp} + Q_{\max}/\left(1+\exp(ze(V_{0.5}-V)/kT)\right) \qquad (2)$$

where $V_{0.5}$ is the voltage at which the charge is distributed equally between two hypothetical states, z is the apparent valency of an equivalent charge that moves through the whole of the membrane field, $Q_{\max}$ is the total charge available to move, Q_{hyp} is the charge of the hyperpolarizing limit and is a function of V_h, and e, k and T have their usual meanings.

Radiolabelled tracer experiments

^{32}P uptake assay: Oocytes expressing flNaPi-IIb and not injected oocytes (6-10 oocytes/group) were first equilibrating in 100Na solution without tracer. After aspiration of this solution, oocytes were incubated in 100Na solution containing 1mM cold P_i and ^{32}P (final specific activity 10 mCi/mmol, Perkin Elmer, Switzerland). Uptake proceeded for 10 min and then oocytes were washed 3 or 4 times with 5 ml of ice-cold 100Ch solution containing 2 mM P_i, and lysed individually in 250 µl of 4% SDS. The amount of radioactivity in each oocyte was measured by scintillation counting (Tri-Carb 2900TR, Packard). The uptake time was chosen to be short enough to assume that initial rate conditions were satisfied so that uptake/unit time is a

direct measure of transport velocity, without compromising measurement reliability, based on previous studies (19). The data were normalized for the uptake obtained from oocytes expressing flNaPi-IIb Wild Type (WT), in standard condition (100Na or 50Na50Ch) as indicated.

Simultaneous voltage-clamp and ^{22}Na uptake: standard TEVC was used as described previously (26). The oocyte was impaled and clamped at a constant voltage and than superfused with a solution 40Na60Ch or 40Na60Li until a stable base line was reached. The oocyte was exposed to the corresponding solution containing 1mM P_i cold and ^{22}Na (final specific activity 1.5 mCi/mmol, Perkin Elmer, Switzerland) for 10 min. After the base line was returned at the starting level the oocyte was removed from the chamber and washed 3 times in 100Ch solution ice-cold. This experiment was repeated using a solution containing 20 mM Na^+ and 80 mM Li^+ or 80 mM choline Cl.

The oocyte was lysed in a vial containing 250 µl of 4% SDS to which scintillation cocktail was added. The net charge (*Q*) was calculated from the current traces by subtracting the endogenous holding current and numerically integrating the area under the baseline-corrected curve. Uptake and charge were expressed as their molar equivalents, by assuming monovalency for the charge.

Data analysis and software.

Data analysis was performed with Clampfit V. 10.2 (Molecular Devices, Inc., USA) and Prism V. 4.03 (Graphpad Software, La Jolla, USA). Data points are shown as mean+/-sem.

Results

The effect of Li^+ substitution on ^{32}P uptake in oocytes expressing rat and flounder isoforms

For oocytes expressing the flounder NaPi-IIb isoforms, replacement of NaCl with 100 mM LiCl (100Li) gave a small uptake amounting to 3.0±0.1% of that measured in 100Na (Fig. 1A, *upper panel*). A similar behavior was observed in oocytes expressing the rat NaPi-IIa isoform (data not shown). Non-injected (NI) oocytes from the same donor animals showed no significant difference between Li^+ and Na^+ incubation, which suggested that the small uptake in 100 mM Li^+ for the NaPi-IIa/b expressing oocytes was not an endogenous artifact (Fig. 1A, *lower panel*).

In a second series of uptake experiments, we replaced 50% of external NaCl with either LiCl (50Na50Li) or choline Cl (50Na50Ch) and compared the uptake for each isoform. The uptake in the presence of Li^+ was reduced by approximately 50% (Fig. 1B) which suggested a possible interaction of Li^+ with the transporter. The effect of Li^+ appeared to be common to all electrogenic isoforms, as we obtained similar results using the human NaPi-IIa (data not shown).

Steady-state electrophysiology

To gain further insight into the underlying mechanism of Li^+ ions interactions with NaPi-II proteins, we used the two-electrode voltage clamp (TEVC) to define the electrical driving force and measure the steady-state phosphate induced current (I_{P_i}) under different external perfusion conditions, in response to 1 mM P_i (pH 7.4) (Fig. 2). All these and subsequent assays were performed on oocytes expressing the flounder NaPi-IIb isoform because it gave a more robust expression. We also performed control measurements using either the rat or human NaPi-IIa isoforms and we observed qualitatively similar behavior (data not shown).

Current-voltage (*I-V*) data pooled from oocytes expressing the flounder NaPi-IIb were normalized to I_{P_i} at V= -100 mV to take account of different expression levels and aid comparison of the responses for each superfusion condition. As shown in Fig. 2A, 100% replacement of Na^+ with Li^+ gave no significant electrogenic response and this was indistinguishable from the electrogenic response to P_i in 100Ch (data not shown). At hyperpolarizing potentials, replacement of 25%, 50% or 75% of external Na^+ with choline caused a concomitant reduction in I_{P_i} compared with 100Na, as we have previously reported (6, 26). The equivalent Li^+ substitution further reduced I_{P_i} compared to the choline case, which was also consistent with the reduced ^{32}P uptake observed for superfusion with 50Na50Li (Fig. 1B).

A comparison of I_{P_i} for the same choline and lithium replacements also revealed that the presence of Li^+ did not simply result in a dose-dependent scaling of the *I-V* data as might be expected for a simple voltage-independent competitive inhibition of transport function. Instead, we found that increasing the external [Li^+] also altered the voltage-dependence such that the voltage-independent, rate-limiting P_i-induced current normally seen at hyperpolarizing potentials now occurred at more depolarizing potentials. For example, with 25Na75Li, I_{P_i} was voltage independent for V<0 (Fig. 2A *right panel*).

By transposing the data of Fig. 2A at each membrane potential to give the cation activation dose-dependence we could compare the effect of equimolar choline (Fig. 2B) or lithium (Fig. 2C) replacement. In these experiments the total external monovalent cation strength was maintained at ~100 mM. For choline replacement, these data resembled the typical Na^+ activation for NaPi-IIb and showed the expected tendency to saturate at high $[Na^+]$ (4, 6). In contrast, we observed no saturation for equimolar Li^+ replacement. At low $[Na^+]$ the relative change in electrogenic response over the voltage range from -160 to 0 mV was smaller when Li^+ replaced Na^+ than for choline replacement. Moreover, in the former case there was a strong activation of the response for $[Na^+] \geq 75$ mM, particularly at hyperpolarizing potentials.

To better understand the underlying mechanism by which Li^+ affected the transport kinetics, we determined the P_i and Na^+ activation characteristics with and without a constant $[Li^+] = 50$ mM. We chose this concentration to ensure that on the one hand the Li^+-effect was readily detectable and on the hand to have resolvable currents at low $[P_i]$. Fig. 3A compares the pooled *I-V* data for P_i-activation with a background of either 50Na50Ch or 50Na50Li. Two effects of Li^+ substitution were readily apparent: (i) the voltage dependence was suppressed over the voltage range assayed (-140 mV to 0 mV) and (ii) I_{P_i} showed saturation at a lower $[P_i]$ compared with superfusion in 50Na50Ch. These effects were better visualized by transposing the data (Fig. 3B). We then fit these data with the Michaelis-Menten equation (Eqn 1, with $n_H = 1$) to estimate the maximum P_i-induced current ($I_{P_i}^{max}$) and the apparent affinity constant for P_i ($K_{0.5}^{P_i}$).

The predicted $I_{P_i}^{max}$ plotted as a function of V (Fig. 3C) confirmed the weaker voltage dependence for 50Na50Li for $V<0$ and at the hyperpolarizing extreme, the maximum predicted electrogenic transport rate was significantly reduced compared to the 50Na50Ch case. At strongly hyperpolarizing potentials, the predicted $K_{0.5}^{P_i}$ (Fig. 3D) for the 3 superfusion conditions was similar, however the data sets deviated from one another as V became more polarized. For 50Na50Li, $K_{0.5}^{P_i}$ decreased with depolarization, which implied that the apparent P_i affinity increased, compared to superfusion with either 100Na or 50Na50Ch, for which we observed the opposite trend.

We next compared the effect of Li^+ on Na^+ activation of cotransport by determining I_{P_i}while varying $[Na^+]$ with 50 mM Li^+ present in all solutions (Fig. 4). To quantify the Na^+-activation, we used 6 Na^+ concentrations in the range 3 mM to 100 mM. The pooled, normalized, *I-V* data for this experiment showed the weak voltage dependence for all $[Na^+]$ and saturation at high $[Na^+]$ (Fig. 4A). When these data where transposed (Fig. 4B), we observed no sigmoidicity at low $[Na^+]$ in contrast to the normal behavior for all electrogenic NaPi-IIa/b isoforms when equimolar choline replaced Na^+ (e.g. (4, 6, 9, 26)). This can be readily seen when the data obtained from a representative oocyte expressing flNaPi-IIb are superimposed (shown for a membrane potential =-100mV) (Fig. 4B). The fit using Eqn. 1 with free parameters yielded Hill coefficients (n_H) that were close to unity (Fig. 4C) over the voltage range investigated and contrasted with representative data for choline substitution for which $n_H>1$. Moreover, the apparent affinity constant for Na^+ activation ($K_{0.5}^{Na}$) in the presence of 50 mM Li^+ was smaller compared with the Li^+-free case over the range of test potentials (Fig. 4D). Finally, as expected, the predicted $I_{P_i}^{max}$ showed less voltage dependence than in the Li^+-free case and at V=0, $I_{P_i}^{max}$ was independent of Li^+ (Fig. 4E).

For the complementary experiment (Fig. 5), we maintained $[Na^+]$ = 50 mM and varied $[Li^+]$ from 0 to 75 mM. In this experiment, increasing external $[Li^+]$ caused a dose-dependent inhibition of I_{P_i} over the entire experimental voltage range (Fig. 5A). The transposed data (Fig. 5B) revealed that at high $[Li^+]$ the predicted I_{P_i} asymptoted to a constant level that depended weakly on V. These data were best fit using the Michaelian form of Eqn 1 (n_H=1) with a variable offset to take account of the electrogenic response at $[Li^+]$=0.. The predicted apparent Michaelis constant for the inhibition ($K_{0.5}^{Li}$) showed strong voltage dependence and decreased at hyperpolarizing potentials (Fig 5D).

Li^+ ions and transport stoichiometry

The preceding results established that Li^+ interacted with NaPi-IIb in the presence of Na^+ to alter the maximum transport rate and apparent affinities for P_i and Na^+. That significant electrogenic activity remained even for high $[Li^+]$ indicated that Li^+ did not simply compete for occupancy of Na^+ interaction sites and thereby block electrogenic, Na^+-driven cotransport. One possible interpretation of these data could be that one or more Li^+ ions substituted for Na^+ and were cotransported, but possibly at a lower turnover rate than with Na^+ alone, consistent with our uptake data (Fig. 1A). To test this hypothesis, we performed simultaneous ^{22}Na uptake and recording, under voltage clamp, of I_{P_i} from individual oocytes as previously described (9, 11, 26) (see Materials and Methods). This allowed the determination of the ratio of number of moles of Na^+ (n^{Na^+}) to the molar equivalent of charge translocated (n^{Q_t}) for individual oocytes. If indeed Li^+ substituted for Na^+ as a driving cation, we would predict that the 3:1 cotransport stoichiometry, given by the ratio $n^{Na^+}:n^{HPO_4^{2-}}$ (where $n^{HPO_4^{2-}}$ is the number of moles of divalent P_i transported) would be reduced. Moreover, this decrease should depend on the relative availability of each cation. On the other hand, if bound Li^+ prevented the completion of the cotransport cycle for a given fraction of transporters, the $n^{Na^+}:n^{Q_t}$ ratio should remain unchanged. Fig. 6 shows the combined results of this assay with a fixed $[Na^+]$ = 20 mM or 40 mM and with $[Li^+]$ and [Ch] =80 mM, or 60 mM, respectively. As previously shown (9, 26), when Na^+ was the only cation interacting with NaPi-II the $n^{Na^+}:n^{Q_t}$ ratio was close to 3:1 and this was independent of the external $[Na^+]$ (Fig. 6A). When Li^+ was substituted for choline, there was a significant reduction in $n^{Na^+}:n^{Q_t}$ for 40Na60Li from 3.1±0.5 to 2.2±0.13 (Students t-test, $p<0.01$) and this was further reduced from 2.8±0.18 to 1.6±0.23 with 20Na80Li (Students t-test $p<0.004$) (Fig. 6B).

These findings established that Li^+ reduced the $n^{Na^+}:n^{Q_t}$ ratio and suggested that Li^+ ions may substitute for Na^+ ions in the transport cycle.

Na^+- and Li^+-dependence of presteady-state kinetics

The steady-state findings indicate that Li^+ ions alter the steady-state voltage dependence of cotransport, and can substitute for Na^+ as the cotransported cation species, however these data offer little insight into which of the 3 cation binding sites are involved. The altered voltage dependence suggested that Li^+ ions interact with one or more voltage-dependent partial reactions that constitute the NaPi-II transport cycle, nevertheless it is possible that electroneutral partial reactions may also be the target, because the overall steady-state kinetics is a function of all transport cycle-associated rate constants. To determine which partial reactions were involved, we investigated the effect of cation substitutions on presteady-state charge movements that we have previously shown reflect voltage dependent partial reactions of the transport cycle (4-6, 8, 10).

Fig. 7 shows representative original records membrane current relaxations under different superfusion conditions for voltage steps from a -60 mV holding potential (V_h) to test voltages in the range -180 mV to +80 mV. For a representative non-injected oocyte this protocol induced linear transient current relaxations that typically lasted 1-2 ms with low-pass filtering at 500Hz (Fig. 7A). For a flNaPi-IIb-expressing oocyte from the same donor frog and superfusion in 100 mM NaCl (100Na), 100 mM choline Cl (100Ch) and 100 mM LiCl (100Li) respectively, voltage steps gave rise to relaxations that were superimposed on the endogenous transients (Fig. 7B). The presence of relaxations for superfusion in 100Li suggested that, like Na^+, Li^+ ions were able to interact with the expressed protein in a voltage dependent manner. We also observed relaxations if the oocyte was superfused in 50:50 mixtures of the superfusates (Fig. 7*C*). Remarkably, for the case of superfusion in 50%NaCl, 50%LiCl (50Na50Li), the relaxations for steps to potentials >0 were significantly slower than those in the absence of Li^+.

To quantify these observations, we determined the charge (Q) associated with NaPi-IIb by fitting the relaxations to exponentially decaying functions (see Materials and Methods). For superfusion in Na^+ and choline, the relaxations were well described by fitting a single exponential to the relaxation after the linear capacitive component was complete (see Materials and Methods). However, when both Li^+ and Na^+ were present, a double exponential fit was found to describe more accurately the current decay (see Materials and Methods and Fig S1, Supporting material). The faster time constants (Fig. 7D, *left panel*) were typically <10 ms over the test voltage range and showed a "bell-shaped" dependence on V as previously reported for the flNaPi-IIb (4, 6). The slow time constant observed for superfusion with 50Na50Li showed a strong voltage dependence but no maximum was observed for test potentials up to +80 mV (Fig 7D, *right panel*). For V<-60 mV, although the fitting algorithm reported a slow component, the poor signal-to-noise ratio for hyperpolarizing steps meant that there was greater uncertainty in the fit (Fig 7D, *right panel*).

Fig 8 shows normalized Q-V data obtained from the exponential fit for each of the superfusion conditions. These data were fit with a single Boltzmann function (Eqn. 2, Materials and Methods) to obtain 3 phenomenological parameters: $Q_{\max}$, the predicted maximum charge displaced, $V_{0.5}$ the voltage at which 50% of the charge is displaced and z the effective valency factor (Fig. 8B-D). Given the significantly different time constant associated with the 50Na50Li superfusion, we took pains to ensure that this was not artifactual. To this end, we confirmed that the charge movement due to the presence of Li^+ fulfilled 3 properties expected for a fixed number of mobile charges that can move within the transmembrane electric field and are directly associated with functionally expressed NaPi-IIb. These properties are: (i) the total charge displaced was proportional to the I_{P_i} (see Fig S2A, Supporting material); (ii) the charge movement was reversible over the test voltage range-i.e. the magnitude of charge induced by the

ON step (from V_h to the test potential) and OFF step (from the test potential to V_h) were in good agreement (see Fig S2B, Supporting material); and (iii) the charge movement was the result of memoryless process: i.e. by changing V_h to +40 mV the *Q*-*V* was displaced along the *Q* axis (see Fig S2B, Supporting material) and, moreover, we obtained comparable estimates of the Boltzmann parameters (Q_{max}, $V_{0.5}$, *z*).

To compare the effects of cation substitution in more detail, we normalized the *Q*-*V* data to Q_{max} in 100Na and offset each set to superimpose at the depolarizing limit (Fig. 8A). The total detectable mobile charge approximately doubled when Na^+ (50 mM or 100 mM) alone was added to the medium compared to the 100Ch case (Fig. 8B) and doubling [Na^+] caused a depolarizing shift for $V_{0.5}$ of ~25 mV (Fig. 8C), consistent with previous reports (6, 28). However, replacement of 50% of Na^+ with Li^+ caused a further depolarizing shift of ~50 mV relative to the 100Na case (Fig. 8C). This finding provided further support for the notion that Li^+ ions interacted with the NaPi-IIb protein and altered the voltage dependent kinetics. Moreover, although we were unable to apply voltage steps beyond +80 mV because of contamination of the records from the activation of endogenous Cl^- channels, the Q_{max} prediction from the Boltzmann fits strongly suggested that this parameter remained reasonably constant for the 3 conditions: 100Na, 50Na50Ch and 50Na50Li (Fig. 8B). Finally, the apparent valency (*z*) increased above that of the empty carrier value (0.40±0.04) when Na^+, Li^+ or both Na^+ and Li^+ were present in the superfusate (Fig. 8D). With only Li^+ present, the valence increased to 0.52±0.04, whereas when Na^+ it varied from 0.56±0.02 (50Na50Ch) to to 0.65± 0.02 (100Na).

Qualitatively similar behavior was observed for the human and rat NaPi-IIa isoforms (data not shown), which confirmed that the effect of Li^+ on the voltage dependence of presteady-state kinetics was not unique to the WT NaPi-IIb. Moreover, the generality of the effect was demonstrated using a mutant NaPi-IIb isoform (A175C) that shows a significantly different voltage dependence from the WT (14). In 100Na, its presteady-state voltage dependence is shifted towards hyperpolarizing potentials compared to the WT, however, in 50Na50Li, we observed a ~50 mV depolarizing shift in $V_{0.5}$ relative to the estimate in 100Na as for the WT (see Fig. S3, Supporting Material). These findings indicated that independent of the intrinsic voltage dependence of the NaPi-II protein, the effect of Li^+ ions was the same and supported the notion that like Na^+ ions, Li^+ ions bind to one or more sites located within the transmembrane electric field (8). When Li^+ was the only alkali metal cation present in the superfusate, the total detectable mobile charge increased over that for 100Ch (Fig. 8B). Moreover, there was a concentration dependent shift in the charge distribution, qualitatively similar to Na^+ (Fig. 8A, *right panel*). However, a doubling of [Li^+] resulted in a smaller depolarizing shift in $V_{0.5}$ (~15 mV) compared to the Na^+ case. Moreover, Q_{max} was approximately 70% of that obtained with 100Na (Fig. 8B).

We also investigated if other monovalent cations could also induce similar effects, we made 100% substitutions with Rb^+, Cs^+ and K^+, however no additional charge movement was observed (see Fig. S4, Supporting material). This suggested that the size of the cation was of critical importance for interactions with NaPi-IIb as Na^+ and Li^+ have comparable but smaller atomic radii compared with the other cations investigated (e.g. (15))

To gain further insight into the Li^+ interactions, we performed a detailed analysis of the presteady-state charge movements with varying $[Li^+]$ in the presence and absence of fixed $[Na^+]$ and the converse. Fig. 9 shows the variation of Boltzmann parameters for varying cation concentrations with equimolar choline substitution. For Q_{max} (Fig. 9A), all fit estimates were normalized to the predicted Q_{max} at 100Na for each cell and then pooled (Fig. 9A). This fit parameter remained reasonably constant for $[Na^+]$ or $[Li^+]$> 10 mM and the maximum displaceable charge in the presence of Li^+ remained at approximately 70% of that obtained in Na^+. Both z (Fig. 9B) and $V_{0.5}$ (Fig. 9C) increased with cation concentration. Whereas z was similar for each cation, we observed a significant difference between the respective dose-dependent behavior of $V_{0.5}$. This became more evident when these data were replotted on a $\log_{10}$[X!scale, where X= Na^+ or Li^+ (Fig. 9D). At high cation concentrations, $V_{0.5}$ then varied linearly and the limiting slopes were 118± 8mV/decade and 64±3 mV/decade for Na^+ and Li^+, respectively. For $[Li^+]$ <25 mM, $V_{0.5}$ deviated from the linear behavior and showed less dependence on $[Li^+]$.

In the final series of experiments, we repeated these measurements and varied one cation in the presence of a constant concentration (10mM and 50 mM) of the other (Fig. 10). For variable $[Na^+]$, Q_{max} , normalized to the value estimated for each cell at 100Na, was close to unity for $[Li^+]$= 10 mM and 50 mM (Fig. 10A, *left panel*), whereas for variable $[Li^+]$ it depended on $[Na^+]$. We could attribute the large error in normalized Q_{max} for $[Na^+]$=50 mM and variable $[Li^+]$ to the lack of saturation of the *Q-V* at depolarizing potentials for this condition (see Fig. 8A). This also had consequences for the uncertainty in predictions for z and $V_{0.5}$. By constraining the fits with a fixed Q_{max} obtained from 100Na fit, the Boltzmann fits to the *Q-V* data for the variable $[Na^+]$ case were not compromised and the respective uncertainties in z and $V_{0.5}$ were reduced. The effective valence (z) for both variable $[Na^+]$ and $[Li^+]$ (Fig. 10B) showed a small concentration-dependent increase. Moreover, $V_{0.5}$ for all conditions showed a characteristic linear dependence on $\log_{10}$ $[Na^+]$ or $\log_{10}$ $[Li^+]$. For variable $[Na^+]$, the limiting slopes in the presence of external Li^+ were significantly smaller (56 ±4 mV/decade -10 mM Li^+) and 58± 6 m /decade-50 mM Li^+) compared with the slope in the absence of external Li^+ (118±8 mV/decade). Moreover, the intercept on the $[Na^+]$ axis shifted to the left as $[Li^+]$ increased. In contrast, the addition of a fixed $[Na^+]$ to the external medium with $[Li^+]$ variable (Fig. 10C, *right panel*) the slopes were 64±3 mV/decade (0 mM Na^+); 79±3 mV/decade (10 mM Na^+) and 61±3 mV/decade (50 mM Na^+). For this experimental protocol, the intercept on the $[Li^+]$ axis also shifted to the left as $[Na^+]$ increased. This apparent reciprocity of the influence of one cation species on the voltage dependence of the other cation suggested a reciprocal interaction between Na^+ and Li^+ ions competing for occupancy of the same site(s) in the protein.

Discussion

Does Li^+ alone act as a driving cation?

Uptake assays in which we replaced external Na^+ with Li^+ suggested that Li^+ may also drive P_i cotransport, albeit at a significantly lower turnover rate than for Na^+ (Fig.1A). The low uptake activity precluded a more detailed kinetic analysis to determine if this resulted from a reduced maximum transport rate, reduced substrate apparent affinity (Li^+ or P_i) or combination of both. Based on the uptake data, we would predict that voltage clamped oocytes expressing flNaPi-IIb with typical P_i-induced currents (I_{P_i}) > -200 nA at -100mV (1 mM P_i) would therefore give correspondingly small $I_{P_i} \approx -6$ nA in 100 mM Li^+. By means of electrophysiological assays, we were unable to detect a significant inward current in the presence of 100 mM Li^+. Although currents in the nA range are certainly detectable with the TEVC, we routinely observed that non-injected oocytes could also display an electrogenic response to P_i within this range. This is thought to be related to endogenous chloride channels (I:C: Forster, unpublished observations) and could easily mask any NaPi-IIb dependent P_i response in 100 mM Li^+. Based on the uncertainties in resolving such small currents, we were unable to conclude definitively that Li alone can induce an electrogenic response from NaPi-IIb. We also obtained evidence that Li^+ ions alone can specifically interact with NaPi-IIb from the presteady-state assays in this present study (see below) as well as from voltage clamp fluorometry studies on both NaPi-IIb (28, 29) as well as the electroneutral NaPi-IIc (13).

It could also be hypothesized that the ^{32}P uptake measured in 100 mM Li^+ was the result of transport via endogenously expressed proteins from the SLC20 family (e.g. PiT-1,2), given that in oocytes overexpressing the *Xenopus* PiT-1 a resolvable electrogenic response was found in 100 mM Li^+ (25). In the present study, there was indeed a significantly higher uptake in 100Li compared with 100Ch for non-injected oocytes, which could suggest the involvement of endogenous PiT, however the overall levels were 10-fold lower than in oocytes expressing NaPi-IIb. Given the significance of the uptake data with 100 mM Li^+, we therefore conclude that Li^+ ions can fully substitute for Na^+. A clearer role for Li^+ as a driving cation was obtained in assays performed in the presence of Na^+.

Steady-state kinetics reveal complex interactions of Li^+ in the presence of Na^+.

Our uptake assays in which 50% of the external Na^+ was equimolarly replaced with Li^+ gave the first hint of a direct influence of Li^+ ions on the cotransport cycle and suggested that when Li^+ was present, transport was inhibited (Fig 1 B). We obtained further insight into this phenomenon from electrophysiological assays. A comparison of the current-voltage (*I-V*) data (I_P) when choline or Li^+ replaced Na^+ and the total cation concentration remained constant (Fig. 2A), confirmed the apparent inhibitory effect of Li seen in the uptake experiments. We also observed a clear alteration in the steady-state voltage dependence, whereby the normal rate-limiting, voltage-independent behavior observed at hyperpolarized potentials occurred at less negative potentials as $[Li^+]$ increased. This was accompanied by a concomitant decrease in the electrogenic response. These altered steady-state kinetics suggested that Li^+ ions could influence one or more partial reactions in the transport cycle that determine the overall voltage dependence of transport as well as the turnover rate (cotransport rate) of the protein.

An additional indication that membrane potential-dependent partial reactions should be considered in explaining the uptake data (Fig 1B) came from a recent study on the electroneutral isoform, NaPi-IIc (13). This protein shows no steady-state or presteady-state charge movement, and ^{32}P uptake is voltage-independent, which led us to conclude that no voltage-dependent partial reactions contribute to the transport cycle. Furthermore, it was reported that there was no significant change in uptake when 50% of Na^+ was replaced with Li^+ (13). This finding could suggest that the Li^+ effects reported in the present study were unique to the electrogenic NaPi-IIa/b and implied an interaction of Li^+ ions with voltage-dependent partial reactions only.

When choline progressively replaced Na^+, the electrogenic response tended to saturate at high $[Na^+]$ as previously reported (e.g. (4, 6, 26)). In contrast, Li^+ replacement revealed a more complex behavior, as might be expected for an interaction between different cations at intermediate concentrations (Fig. 2B,C). Surprisingly, although Li^+ reduced the electrogenic activity, it increased the apparent affinity for P_i (Fig 3B). This behavior would not be expected for a simple competitive inhibition of transport by Li^+, for which we would expect a decrease in the apparent affinity for P_i and an unchanged maximum transport rate.

It was previously reported for the Na^+-coupled succinate transport (NADC-1) (23) that Li^+ ions, in the presence Na^+ ions, caused a mixed type inhibition to account for the reduced apparent succinate affinity and reduced maximum transport rate for that transporter. Moreover, the effects of Li^+ on NaDC-1 were observed at relatively low $[Li^+]$ (5 mM). For NaPi-IIb, our steady-state data also suggest a complex Li^+ interaction. For the Na^+-activation experiments with fixed $[P_i]$, the apparent affinity for Na^+ increased in the presence of 50 mM Li compared with choline substitution (Fig 4D). Moreover, these experiments revealed that the normally sigmoidal behavior observed for Na^+-activation with choline replacement was best described by a Michaelian function. This suggested that if Li^+ ions modulated the transport cycle, but did not participate as a driving cation, their presence significantly reduced the cooperativity of Na^+ interactions. Alternatively, we could explain this behavior if Li^+ ions replaced one or more Na^+ ions in the transport cycle.

When we maintained a constant $[Na^+]$ = 50 mM and determined the Li^+-activation with 1 mM P_i, (Fig 5B) we also found that the Li-dependence could best be described by a Michaelian function, which suggest that one Li^+ ion interacted with the protein. Moreover, these data provide further confirmation that Li^+ does not act as a simple competitive inhibitor of P_i transport because as $[Li^+]$ increased, the transport rate reached a plateau that was weakly voltage dependent. We might expect this behavior if two cotransport pathways were possible: one involving Na^+ ions alone with a high transport turnover rate and another in which both Li^+ and Na^+ ions participated and with a lower turnover rate. We would then predict that the latter pathway would progressively dominate as $[Li^+]$ increased until a limiting transport rate was reached. Interestingly, the normalized *I-V* data reported in Fig 5A for each $[Li^+]$ were the same at V= 0 mV. This indicated that in the absence of membrane potential as a driving force, cotransport activity was unaffected by the presence of external Li^+. Moreover, Michaelian behavior for Li^+ interaction was consistent with voltage clamp fluorometry (VCF) data obtained from the same isoform (29), which indicated that one Li^+ ion interacted with the protein in the absence of P_i. For NaDC-1, similar behavior was reported whereby the inhibition by Li^+ was best described by a Michaelian function and the maximal inhibition ranged from 54% at -150 mV and 76% at -10 mV (22).

Stoichiometry determination establishes that Li^+ can substitute for Na^+ in the transport cycle.

The correlation between charge translocated (Q_t) and Na+ uptake under voltage clamp conditions provided strong experimental evidence that Li^+ ions can substitute for Na^+ as a driving cation. Although there was some experimental scatter in the data, equimolar Li^+ substitution for choline resulted in a statistically significant reduction in the stoichiometry ratio, which would be expected if Li^+ substituted for one or more Na^+ ions in the transport cycle. It is tempting to conclude from these data that in the presence of Li^+, the ratio $n^{Na}:n^{Q_t} = 2$ implying that one Li^+ ion has substituted for one of the 3 Na^+ ions cotransported. However, uncertainties in the data do not allow us to rule out that >1 Na^+ ion is replaced by Li^+. Indeed, the non-integer stiochiometry we observed at the macroscopic level could arise from a mixed population of proteins operating with $n^{Na}:n^{Q_t} =3$, 2 or 1, depending on the occupancy of cation binding sites on a cycle-to-cycle basis.

Despite these uncertainties, these findings did allow us to rule out two hypotheses for the mechanism of Li^+ interaction. First, if Li^+ suppressed electrogenic cotransport but the protein completed the transport cycle in an electroneutral mode, we would expect the ratio $n^{Na}:n^{Qt}$ to increase above the 3:1 obtained for superfusion with only Na^+ present. Second, if Li^+ competitively inhibited cotransport, this would not result in a change in stoichiometry.

Presteady-state analysis reveals separate cation interactions that precede P_i binding

The above findings suggest an involvement of voltage-dependent partial reactions explaining the Li^+ effects. However, it is difficult from steady-state data alone to make clear predictions as to which partial reactions are Li^+-dependent because the electrogenic response is a function of all partial reactions in the transport cycle. To identify the partial reactions involved it was necessary to exploit the power of presteady-state analysis, whereby we could investigate cation interactions for a limited set of partial reactions in the transport cycle (see Fig 11).

When Li^+ ions alone were present in the external medium there was an increase in the detectable charge movement that was significantly greater than that measured in 100Ch, which we attribute to voltage-dependent conformational changes associated with the empty carrier (e.g. (8)). These findings contrast with those of a previous study where we reported that there was only a marginal difference between the Q_{max} predicted in 100Ch and 100Li for the flNaPi-IIb mutant S448C (29): this led us to conclude that Li^+ ions did not enter the transmembrane electric field. In the present study, we found a ~50% increase in total mobile charge movement (Q_{max}) compared to that of the empty carrier (100Ch). This discrepancy might be attributable to the effect of the cysteine mutation on cation interactions or that in the present study we chose high expressing cells with an electrogenic response < -400 nA (1 mM P_i) , which facilitated more precise estimation of charge movement.

In the present study, we found that $Q_{\max}$ in 100Li was only ~70% of that obtained in 100Na. One interpretation of this finding, based on the predictions of a simple two-state model for charge displacement that the Boltzmann function describes (e.g.(8)) would be that in 100Li, the lumped mobile charges in each protein (in this case Li^+ ions) move through a smaller fraction of the transmembrane electric field to reach their binding site compared with the 100Na case. This is also consistent with the Boltzmann fit estimate of the apparent valence (z) for 100Li being less than that found for 100Na or 50Na50Ch (Fig 8D) and the finding that the apparent valence is smaller in 100 mM Li. If both Na^+ and Li^+ were present in the external medium (50Na50Li), $Q_{\max}$ was similar to the 100Na case, which suggested that the charge contribution due to the Li^+ alone was not the result of Li^+ interacting with the protein at an independent site. In that case, we would expect $Q_{\max}$ to exceed that for 50Na50Ch, where $Q_{\max}$ was close to that in 100Na. Another explanation for our finding could be one Li^+ ion can bind with high affinity to the 1st cation binding site leaving the 2nd cation binding site free for Na^+ occupancy.

Our initial presteady-state analysis (Fig 8) also revealed that the steady-state mobile charge distribution (Q-V) was significantly affected by the cation species present in the external medium (Fig 8A). This could be quantified in terms of the midpoint voltage ($V_{0.5}$) at which 50% of the charge was displaced (Fig 8C). When Na^+ was the only cation present, a 50% reduction in $[Na^+]$ resulted in a $V_{0.5}$ hyperpolarizing shift ≈27 mV, whereas when Li^+ was the only cation present the shift was in the same direction but significantly smaller (≈15 mV). However, the most dramatic effect was observed for 50Na50Li, which resulted in ≈ 81 mV depolarizing shift relative to 50Na50Ch.

For the case with only one cation species present, the basic interpretation of these shifts with changes in cation activity can be obtained by considering a 2-state model in which the cation is either bound or unbound and it must cross an energy barrier to reach the binding site (see Appendix 1). This model predicts a linear relationship between $V_{0.5}$ and $[X]$ plotted logarithmically with slope $S_X = kT/(e\delta_X)$ where δ_X is the electrical depth of the binding site within the transmembrane electrical field and the apparent cation affinity (K_x) can be found from the intercept on the log[X] axis. For Na^+ or Li^+ as the only cations, (Fig 9) linearity between $V_{0.5}$ and log[X] was obtained (Fig 9) for $[Na^+]$ or $[Li^+] \geq 50$ mM and the limiting slopes were significantly different. For Na+ alone, the slope is approximately 120 mV/log [Na] , consistent with 2 Na^+ ions interacting before P_i binding (29). Using the derived expressions for the slope and total charge displacement (see Appendix), the ratio of limiting slopes is given by:

$$\frac{S_{Li}}{S_{Na}} = \frac{Q_{\max}^{Na} n_{Li}}{Q_{\max}^{Li} n_{Na}} \qquad (3)$$

Substituting the measured slopes and $Q^{X}_{\max}$, for the respective ions, we obtain the ratio $n_{Li}/n_{Na} = 0.35$. This indicates that the number of Li^+ ions that interact with the transporter is less than the number of Na^+ ions. Given that our current model predicts that $n_{Na}=2$, this result would be consistent with $n_{Li}= 1$. Furthermore, the intercepts on the $\log[Na^+]$ and $\log[Li^+]$ axes were 100 mM and 75 mM respectively, suggesting that Li^+ ions interacted with a greater affinity than Na^+

ions. It must be noted that this 2-state model neglects the charge contributions from the empty carrier, which explains the lack of linearity for $V_{0.5}$ data at low [X] and the model also assumes that the ions bind simultaneously, which may also explain why the ratio $n_{\mathrm{Li}}/n_{\mathrm{Na}}$ is not closer to the expected 0.5, suggested by our model.

We obtained further insight into the cation interactions by determining the Boltzmann parameters from the *Q*-*V* data when one cation was varied with the other fixed at 10 mM or 50 mM (Fig. 10). These data confirmed that for variable [Na$^+$] ≥ 10 mM, Q_{max} was independent of [Na$^+$] and appeared to be unaffected by 10 mM or 50 mM Li , despite a large uncertainty in the fit parameters due to the lack of saturation at depolarizing potentials. In contrast, for variable [Li$^+$], whereas Q_{max} was independent of [Li$^+$] for [Li$^+$]≥ 10 mM, but increased with [Na$^+$] = 10 , 50 mM, respectively. With Na$^+$ as the variable cation, the limiting slope was ≈60 mV/log$_{10}$[Na$^+$] for [Li$^+$]=10 mM and 50 mM; with Li$^+$ as the variable cation, the limiting slope varied between 61 mV/log$_{10}$[Na$^+$] (50 mM Na$^+$) and 79 mV/log$_{10}$[Na$^+$] (10 mM Na$^+$). For both sets of data, an increasing concentration of the fixed cation shifted the intercept on the log$_{10}$[X] axis to the left. According to the 2-state model (see above) this indicated that the apparent affinity of the variable cation increased with the fixed cation concentration. The reciprocal behavior would not be expected if both cations competed for the same binding site, but suggests a cooperative interaction, whereby the binding of one cation increases the apparent affinity for the other.

A revised kinetic scheme for electrogenic NaPi-II transporters

The interpretation of the presteady-state data in terms of a 2-state model for cation interaction gave some insight into the complexity of the Na$^+$ and Li$^+$ interactions but was obviously of limited value considering the underlying assumptions. A more realistic, but algebraically complex, model for Na$^+$ interactions has been proposed (e.g. (12)) that comprises 4 states and two sequential partial reactions to account for the 2 Na$^+$ ions predicted to bind before P$_i$ binds ((29)). This model also takes into account the role of the empty carrier in determining the voltage dependent kinetics in the transport cycle, and for simplicity, assumes the 2nd Na$^+$ partial reaction is electroneutral. To account for the present findings, we propose that this model be extended to incorporate two cotransport cycles depending on whether Li$^+$ is present or not (Fig 11). We assume that Li$^+$ can only bind at the first cation binding site, which becomes available when the empty carrier occupies state 1. When Li$^+$ is bound, a 2nd Na$^+$ ion binds cooperatively and cotransport proceeds such that 2 Na$^+$ ions and 1 Li$^+$ ion are cotransported with P$_i$. This would account for the reduced stoichiometry that we observed. The probability of this cycle occurring depends on the relative concentrations of Li$^+$ and Na$^+$ in the external medium. With Li$^+$ as the only monovalent cation in the external medium, cotransport is unfavoured because 2 or 3 Li$^+$ ions cannot easily bind to the transporter. This situation, not shown in the scheme, would account for the low uptake reported in 100Li. In the absence of external Na$^+$ and P$_i$, we therefore predict that Li$^+$ can preferentially only occupy the first cation binding site and therefore this accounts for the lower Q_{max} observed and reduced apparent valence compared with the case when Na$^+$ is also present. This also implies that there must be some charge movement associated with the 2nd cation (Na$^+$) interaction and therefore our original electroneutral kinetics predicted for this partial reaction (2a↔2b, Fig 11) would need to be revised accordingly. If this is the case, then the presteady-state kinetics obtained in 100mM Li offer a valuable insight into the cation interactions with NaPi-IIa/b at the molecular level for they reflect the voltage dependent interactions of a single cation with the protein.

Finally, to account for the altered voltage dependence of presteady-state *Q*-*V* when both Li and Na^+ are present, we predict that the backward rate constant for the 2nd Na^+ binding partial reaction (2b’→2a) will become much slower than when Na^+ occupies the first cation binding site, thereby conferring an apparent increase in Na^+ and P_i affinity.

Appendix 1. Two state barrier model for cation interaction

We consider a simple 2-state model in which the cation is either bound (state 2) or unbound (state 1) and it must cross a sharp energy barrier to reach the binding site. We can apply Eyring transition state theory (e.g. (15)), to express the rate constants associated with the forward (binding) and backward (dissociation) reactions as functions of membrane potential (V). Assuming pseudo 1st order kinetics, the forward rate is proportional to the activity (concentration) of the ion (X) according to the law of mass action. The rates for a symmetrical barrier are then given by:

$$k_{12} = [X]^{n_X} k_{12}^0 \exp(-n_X \delta_X eV/2kT) \qquad \text{(A1a)}$$

$$k_{21} = k_{21}^0 \exp(n_X \delta_X eV/2kT) \qquad \text{(A1b)}$$

where n_X= number of cations of X binding simultaneously at a site located an equivalent electrical distance δ_X through the transmembrane electric field, k^0_{12} and k^0_{21} are the forward and backward rates with V=0. Then for N transporters, the total charge displaced is given by:

$$Q^X_{\max} = N\, e\, n_X\, \delta_X \qquad \text{(A1c)}$$

and $V_{0.5}$ can be expressed as

$$V_{0.5} = \frac{kT}{e n_X \delta_X} \ln\left(\frac{k_{12}^0}{k_{21}^0}\right) + \frac{kT}{e\delta_X} \ln[X] \qquad \text{(A1d)}$$

or

$$V_{0.5} = \frac{kT}{e\delta_X} \ln\left(\frac{[X]}{K_X}\right) \qquad \text{(A1e)}$$

and $$K_X = \left(\frac{k_{21}^0}{k_{12}^0}\right)^{n_X} \qquad \text{(A1f)}$$

where K_x is the apparent affinity constant for X (at V=0) and k, T, e have their usual meanings (e.g. (20)). Thus, there is a linear relationship between $V_{0.5}$ and [X] plotted logarithmically with slope S_X= kT/($e\delta_X$) and K_x can be found from the intercept on the log[X] axis.

Figure legends

Figure 1. Evidence of Li^+ interaction with NaPi-IIa/b from ^{32}P assays.

(A) For oocytes expressing flounder NaPi-IIb, replacement of Na^+ with Li^+ (open bars) in the uptake medium gave significantly greater uptake (*upper panel*) than for non-injected (NI) oocytes from the same donor animal (*lower panel*). Note the 10-fold difference in ordinate scales in the two panels. Data pooled from n=9 oocytes (2 animals). Data were normalized to the mean uptake in 100Na for each isoform.

(B) Comparison of ^{32}P uptake when 50% of Na was equimolarly replaced with choline (50Na50Ch, black bars) or Li^+ (50Na50Li, open bars). Data pooled from n=21 oocytes from three donor frog. Data were normalized to mean uptake in 50Na50Ch for each isoform.

Figure 2. Partial replacement of Na^+ with Li^+ alters the voltage dependence of phosphate induced current

(A) Normalized current-voltage (I-V) data showing the voltage dependence of phosphate dependent current (I_{P_i}) in response to 1 mM P_i for different cation replacements: 25%, 50%, 75% choline Cl (gray circles) and LiCl (open circles). The black squares represent the I_{P_i} recorded in 100Na and the open squares the recorded I_{P_i} in 100Li. In each case the data points were normalized to I_{P_i} at -100 mV (100Na) in response to the superfusion of 1 mM P_i. Continuous lines are the result of fitting the data with a sigmoidal function to indicate voltage-independent rate limiting behavior at hyperpolarizing V. Data pooled from n=7 oocytes. Typical I_{P_i} at -100 mV in 100Na in response to 1 mM P_i was -200 nA.

(B) Transposed I-V data showing the dependence of normalized I_{P_i} on external $[Na^+]$. Data points are joined by straight lines for visualization. Data from n=8 oocytes normalized to the response at 100Na, -100 mV.

(C) Transposed I-V data showing the dependence of normalized I_{P_i} on external $[Li^+]$. Data points are joined by straight lines. Data from n=10 oocytes normalized to the response at 100Na, -100 mV.

Figure 3. Effect of Li^+ on P_i-activation

(A) Comparison of I-V data showing variation of I_{P_i} with V for 5 concentrations P_i indicated with 50% choline replacement (*upper panel*) or 50% Li^+ replacement (*lower panel*). Data points normalized to I_{P_i} at -100mV in 100Na, 1 mM P_i and joined for visualization.

(B) Transposed data from (A) fitted with Eqn 1.

(C) I-V of predicted maximum electrogenic response to P_i ($I_{P_i}^{max}$) obtained from fits in (B). Data points joined for visualization.

(D) Comparison of voltage dependence of the apparent affinity constants ($K_{0.5}^{P_i}$) for each superfusion condition.

Normalised substrate activation data were pooled from n= 7 cells. Error bars in fit parameters represent SE reported by fitting algorithm.

Figure 4. Effect of Li^+ on Na-activation with 1 mM P_i

(A) *I-V* showing variation of I_{P_i} with *V* for 6 [Na^+]. Data points normalized to I_{P_i} at -100mV, 1 mM P_i and joined for visualization.

(B) Transposed data from (A) fitted with Eqn. 1. Data is also shown for a representative oocyte with choline replacement.

(C) Comparison of Hill coefficient (n_H) plotted as a function of membrane potential, or 0 mM Li^+ and 50 mM Li^+. Error bars represent SE reported by fit using Eqn. 1 to data in (B).

(D) Comparison of apparent affinity ($K_{0.5}^{Na}$) plotted as a function of membrane potential for 0 mM Li^+ and 50 mM Li^+. Error bars represent SE reported by fit using Eqn. 1 to data in (B)

(E) Comparison of maximum P_i-induced current ($I_{P_i}^{max}$) for 0 mM Li^+ and 50 mM Li^+.

Figure 5 Li^+ inhibition of P_i-activation at 50 mM Na

(A) *I-V* showing dependence of I_{P_i} on *V* for 5 [Li^+] indicated. Data points normalized to I_{P_i} at -100mV, 1 mM P_i in 100Na (not shown) and joined for visualization.

(B) Transposed data from (A) fitted with Eqn. 1 (n_H=1) with a variable offset to take account of I_{P_i} with [Li^+]=0.

(C) Comparison of apparent Michaelis constant for inhibition by Li^+ ($K_{0.5}^{Li}$) plotted as a function of membrane potential. Error bars indicate SE reported by fit using Eqn. 1.

Figure 6. Lithium alters flNaPi-IIb stoichiometry

(A) Relationship between net charge transfer (Q_t) and radiolabeled Na^+ uptake for oocytes expressing the flounder NaPi-IIb isoform and voltage clamped at -50 mV in the presence of 40 mM and 20 mM Na^+ together with 60 mM and 80 mM choline Cl respectively. Both Qt and Na^+ uptake were expressed as their molar equivalents (n^{Na^+}, n^{Q_t}). Each point was obtained from a single oocyte. The respective data sets were fit with a linear regression line with variable slope and Y-axis intercept to take account of endogenous uptake in control oocytes. Slopes shown were not significantly different and support n^{Na^+}:n^{Q_t} stoichiometry of 3:1, as previously reported (9).

(B) Relationship between Q_t and radiolabeled Na^+ uptake as in (A) in the presence of 40 mM and 20 mM Na^+ together with 60 mM and 80 mM LiCl respectively. Each point was obtained from a single oocyte. Linear regression fitting as in (A). The slopes were statistically different from each other (Student's t-test $p<0.03$) and indicate a reduction of stoichiometry due to the presence of Li^+ in the medium. The gray dotted line represents the ratio equal to 3.

Figure 7. Li^+ substitution and presteady-state charge movement

(A) Voltage step protocol used for inducing presteady-state charge relaxations (*left*) and response of a representative non-injected (NI) oocyte (*right*). For this cell, large positive voltages also evoked a response from endogenous Cl^- channels (red trace). The maximum and minimum of each capacitive charging transient have been clipped graphically.

(B) Current traces recorded from a representative oocyte expression flNaPi-IIb (from same donor frog as in (A)) in response to the protocol in (A) under three superfusion conditions: 100 mM NaCl (100Na); 100 mM LiCl (100Li) and 100 mM choline Cl (100Ch). The red trace corresponds to a voltage step to +80 mV.

(C) Current traces from the same cell as in (B) superfused as indicated.

(D) Voltage dependence of time constants obtained from fitting the ON relaxations (steps fromV_h= -60 mV to test potential) in (B) and (C) to single (100Na, 50Na50Ch) and double (50Na50Li) exponential functions. Note the different scales for the 50Na50Li data. Each data point is mean ±SEM for 6 cells. Data points are joined to aid visualization.

Figure 8. Analysis of presteady-state charge movement for different cation substitutions.

(A) Normalized charge-voltage (Q-V) data pooled from n= 6 oocytes for the superfusion conditions indicated. Continuous lines are fits using Eqn 2. Data were normalized to Q_{max} predicted from 100Na fit. All data sets were adjusted so that they were superimposed at the depolarizing limit predicted by the fit.

(B) Comparison of normalized maximum charge movement (Q_{max}) for each superfusate. Dashed line indicates reference value (100Na).

(C) Comparison of midpoint voltage ($V_{0.5}$) for each superfusate.

(D) Comparison of apparent valence (z) for each superfusate. Dashed line indicates mean z estimated for empty carrier (100Ch).

In B-D, Bars indicate mean±SEM reported by fit to pooled data (n= 9).

Figure 9. Boltzmann parameters reported by fits to *Q-V* data with varying [Li^+] or [Na^+] with equimolar choline.

(A) Pooled Q_{max} data plotted as a function of [Na^+] (*filled symbols*) or [Li^+] (*open symbols*). normalized to Q_{max} estimated for each cell in 100Na and 0 mM Li. Dotted line indicates normalization level. Each point is mean±SEM for n>6 cells. Data points joined for visualization.

(B) Pooled effective valence (z) for same cells as in (A) plotted as a function of [Na^+] (*filled symbols*) or [Li^+] (*open symbols*). Data points joined for visualization.

(C) Pooled midpoint potential ($V_{0.5}$) for same cells as in (A) plotted as a function of [Na^+] (*filled symbols*) or [Li^+] (*open symbols*). Data points joined for visualization.

(D) Data in (C) replotted on a $\log_{10}$[Na^+] or $\log_{10}$[Li^+] scale. Linear regression lines are plotted on points that showed an obvious linear relationship. Note the strong deviation from linearity for the Li^+ data at low [Li^+].

Figure 10. Boltzmann parameters reported by fits to *Q-V* data for varying [Li^+] or [Na^+] in the presence of fixed concentrations of the other cation

(A) Pooled Q_{max} data plotted as a function of [Na^+] (*left panel*) or [Li^+] (*right panel*). normalized to Q_{max} estimated for each cell in 100Na^+ and 0 mM Li^+. In each case, the constant cation concentration is indicated. Dotted lines indicate normalization level. Each point is mean±sem for n>4 cells. Data points joined for visualization.

(B) Pooled effective valence (*z*) for same cells as in (A) plotted as a function of [Na^+] (*left panel*) or [Li^+] (*right panel*). In each case, the constant cation concentration is indicated. Data points joined for visualization.

(C) Pooled midpoint potential ($V_{0.5}$) for same cells as in (A) plotted as a function of $\log_{10}[Na^+]$ (*left panel*) or $\log_{10}[Li^+]$ (*right panel*). Each point is mean±SEM for n>4 cells. Data points joined for visualization. Linear regression lines are plotted on points that showed an obvious linear relationship. In each case, the constant cation concentration is indicated.

In each plot, the data points from Fig 9 corresponding to 0 mM Li^+ or Na^+ have been replotted to aid comparison

Figure S1. Comparison of exponential fits to presteady-state relaxations recorded in 50Na50Li.

Presteady-state relaxations for voltage steps indicated and superfusion in 50Na50Li were fit with a single exponential decay (*left panel*) or 2 exponential decay (*right panel*). The residuals show difference between original data trace and respective fits.

Figure S2. Characteristics of charge displacement associated with NaPi-IIb expression.

(A) Total displaceable charge (Q_{max}), detected in 100Na, 50Na50Ch and 50Na50Li, is proportional to I_{P_i} at -100 mV. Each point was obtained from a single oocyte. Linear regression lines indicate that the slopes are significantly different for each superfusion condition

(B) *Q-V* for ON (from holding potential, V_h = -60 mV, +40 mV) to test potential (*V*) and OFF (from *V* to V_h) obtained from the same oocyte superfused with 100Na (*left panel*) and 50Na50Li (*right panel*).

Figure S3. Li substitution and presteady-state behavior of mutant A175C

(A) Pooled *Q-V* data for mutant A175C (*n* = 5) normalized to predicted Q_{max} for 100Na superfusion. Continuous lines are fits with Eqn. 2 with Q_{max} constrained to 1. Data points were shifted so that all fits superimposed at the depolarizing limit.

(B) Apparent valence (*z*) for 3 superfusion conditions indicated. Bars indicate mean±sem reported by fit to pooled data.

(C) Midpoint voltage ($V_{0.5}$) reported from Boltzmann fits for 3 superfusion conditions indicated. Bars indicate mean±SEM reported by fit to pooled data.

Figure S4. Substitution of Rb, Cs or K does not evoke additional charge movement.

Normalized *Q*-*V* data pooled from *n*= 5 oocytes for superfusion with 100% replacement (100 mM) of Na with choline, Rb^+, Cs^+, Li^+ and K^+. Continuous lines show Boltzmann fits (Eqn. 2). Only Li^+ showed a significantly increased detectable charge movement compared with 100Ch.

References

1. Arruda JA, Richardson JM, Wolfson JA, Nascimento L, Rademacher DR, Kurtzman NA (1976) Lithium administration and phosphate excretion. Am J Physiol 231:1140-1146
2. Borre L, Kanner BI (2001) Coupled, but not uncoupled, fluxes in a neuronal glutamate transporter can be activated by lithium ions. J Biol Chem 276:40396-40401
3. Ehnes C, Forster IC, Bacconi A, Kohler K, Biber J, Murer H (2004) Structure-function relations of the first and fourth extracellular linkers of the type IIa Na^+/P_i cotransporter: II. Substrate interaction and voltage dependency of two functionally important sites. Journal of General Physiology 124:489-503
4. Forster I, N. Hernando, et al. (1998) The voltage dependence of a cloned mammalian renal type II Na+/Pi cotransporter (NaPi-2). Journal of General Physiology 112:1-18
5. Forster IC BJ, Murer H. (2000) Proton-sensitive transitions of renal type II Na(+)-coupled phosphate cotransporter kinetics. Biophys J 79:215-130
6. Forster IC, C. A. Wagner, et al. (1997) Electrophysiological characterization of the flounder type II Na+/Pi cotransporter (NaPi-5) expressed in Xenopus laevis oocytes. Journal of Membrane Biology 160:9-25
7. Forster IC, Hernando N, Biber J, Murer H (2006) Proximal tubular handling of phosphate: A molecular perspective. Kidney Int 70:1548-1559
8. Forster IC, Kohler K, Biber J, Murer H (2002) Forging the link between structure and function of electrogenic cotransporters: the renal type IIa Na^+/P_i cotransporter as a case study. Progress in Biophysics and Molecular Biology 80:69-108
9. Forster IC, Loo DD, Eskandari S (1999) Stoichiometry and Na^+ binding cooperativity of rat and flounder renal type II Na^+-P_i cotransporters. American Journal of Physiology 276:F644-649
10. Forster IC, Virkki LV, Bossi E, Murer H, Biber J (2006) Electrogenic kinetics of a mammalian intestinal Na^+/P_i-cotransporter. Journal of Membrane Biology 212:177-190
11. Fukami-Kobayashi K TY, Nishikawa K. (1999) Domain dislocation: a change of core structure in periplasmic binding proteins in their evolutionary history. J Mol Biol 286:279-290
12. Ghezzi C MA-K, Murer H, Forster IC. (2011) Voltage- and substrate-dependent interactions between sites in putative
re-entrant domains of a Na^+-coupled phosphate cotransporter
Pflügers Arch, European Journal of Physiology
13. Ghezzi C MH, Forster IC. (2009) Substrate interactions of the electroneutral Na+-coupled inorganic phosphate cotransporter (NaPi-IIc). J Physiol 587:4293-4307
14. Ghezzi C MH, Forster IC. (2011) Voltage- and substrate-dependent interactions between sites in putative
re-entrant domains of a Na^+-coupled phosphate cotransporter
15. Hille B (2001) Ion channels of excitable membranes. Sinauer, Sunderland, Mass.
16. Hirayama BA, Loo DD, Wright EM (1994) Protons drive sugar transport through the Na+/glucose cotransporter (SGLT1). J Biol Chem 269:21407-21410

17. Hirayama BA, Loo DD, Wright EM (1997) Cation effects on protein conformation and transport in the Na+/glucose cotransporter. J Biol Chem 272:2110-2115

18. MacAulay N, Zeuthen T, Gether U (2002) Conformational basis for the Li(+)-induced leak current in the rat gamma-aminobutyric acid (GABA) transporter-1. J Physiol 544:447-458

19. Magagnin S WA, Markovich D, Sorribas V, Stange G, Biber J, Murer H. (1993) Expression cloning of human and rat renal cortex Na/Pi cotransport. Proc Natl Acad Sci U S A 90:13

20. Mager S, Cao Y, Lester HA (1998) Measurement of transient currents from neurotransmitter transporters expressed in Xenopus oocytes. Methods Enzymol 296:551-566

21. Murer H, Hernando N, Forster I, Biber J (2000) Proximal tubular phosphate reabsorption: molecular mechanisms. Physiological Reviews 80:1373-1409

22. Pajor AM HB, Loo DD. (1998) Sodium and lithium interactions with the Na+/Dicarboxylate cotransporter. J Biol Chem 273:18923-18929

23. Pajor AM, Hirayama BA, Loo DD (1998) Sodium and lithium interactions with the Na+/Dicarboxylate cotransporter. J Biol Chem 273:18923-18929

24. Perez GO, Oster JR, Magrinat G, Vaamonde CA (1977) Effect of long-term lithium administration on renal phosphorus handling. Clin Pharmacol Ther 21:449-452

25. Ravera S, Virkki LV, Murer H, Forster IC (2007) Deciphering PiT transport kinetics and substrate specificity using electrophysiology and flux measurements. Am J Physiol Cell Physiol 293:C606-620

26. Virkki L. V. FIC, et al. (2005) Substrate interactions in the human type IIa sodium-phosphate cotransporter (NaPi-IIa). American Journal of Physiology 288:F969-F981

27. Virkki LV FI, Hernando N, Biber J, Murer H. (2003) Functional characterization of two naturally occurring mutations in the human sodium-phosphate cotransporter type IIa. J Bone Miner Res 18:2135-2141

28. Virkki LV, Murer H, Forster IC (2006) Mapping conformational changes of a type IIb Na+/Pi cotransporter by voltage clamp fluorometry. J Biol Chem 281:28837-28849

29. Virkki LV, Murer H, Forster IC (2006) Voltage clamp fluorometric measurements on a type II Na+-coupled Pi cotransporter: shedding light on substrate binding order. J Gen Physiol 127:539-555

30. Wright EM, Wright SH, Hirayama B, Kippen I (1982) Interactions between lithium and renal transport of Krebs cycle intermediates. Proc Natl Acad Sci U S A 79:7514-7517

31. Yusufi AN CS, Dousa TP. (1993) Effect of chronic lithium treatment upon the Na(+)-coupled cotransporters in renal brush border membranes. Kidney Int 43:1074-1080

32. Zhou Y, Zomot E, Kanner BI (2006) Identification of a lithium interaction site in the gamma-aminobutyric acid (GABA) transporter GAT-1. J Biol Chem 281:22092-22099.

Figure 1

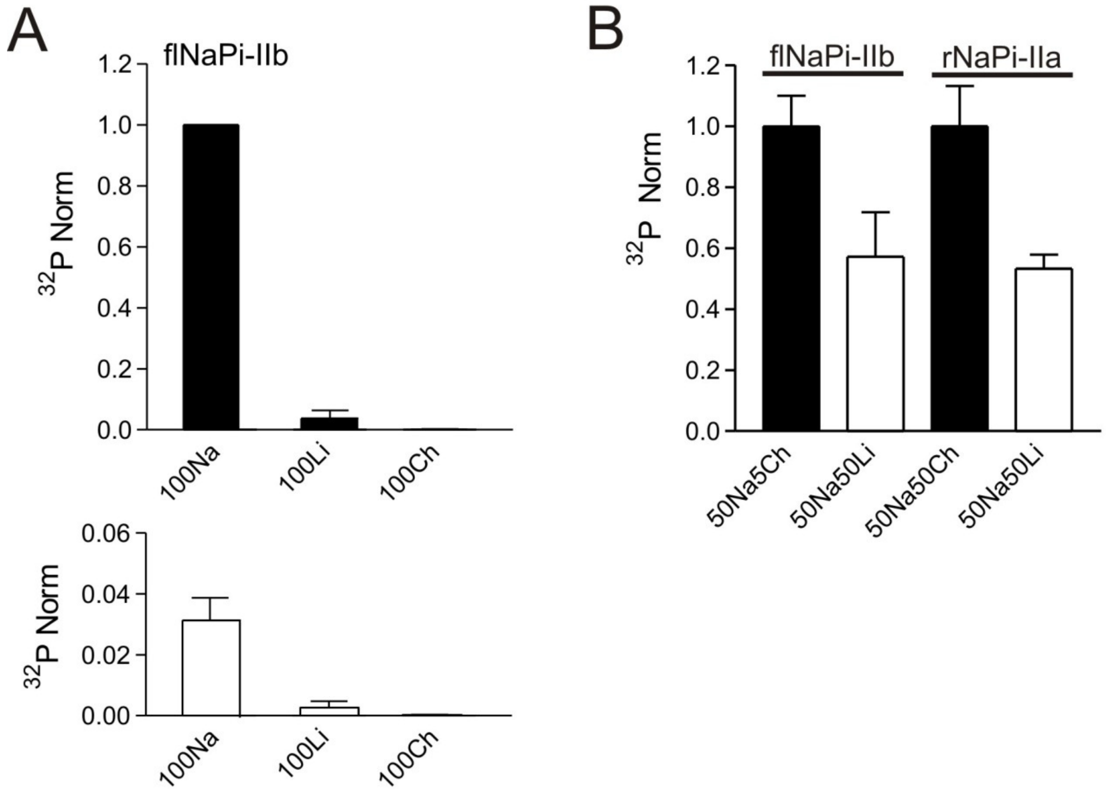
A
flNaPi-IIb
^{32}P Norm
1.2
1.0
0.8
0.6
0.4
0.2
0.0
100Na
100Li
100Ch
^{32}P Norm
0.06
0.04
0.02
0.00
100Na
100Li
100Ch
B
flNaPi-IIb
rNaPi-IIa
^{32}P Norm
1.2
1.0
0.8
0.6
0.4
0.2
0.0
50Na5Ch
50Na50Li
50Na50Ch
50Na50Li

Figure 2

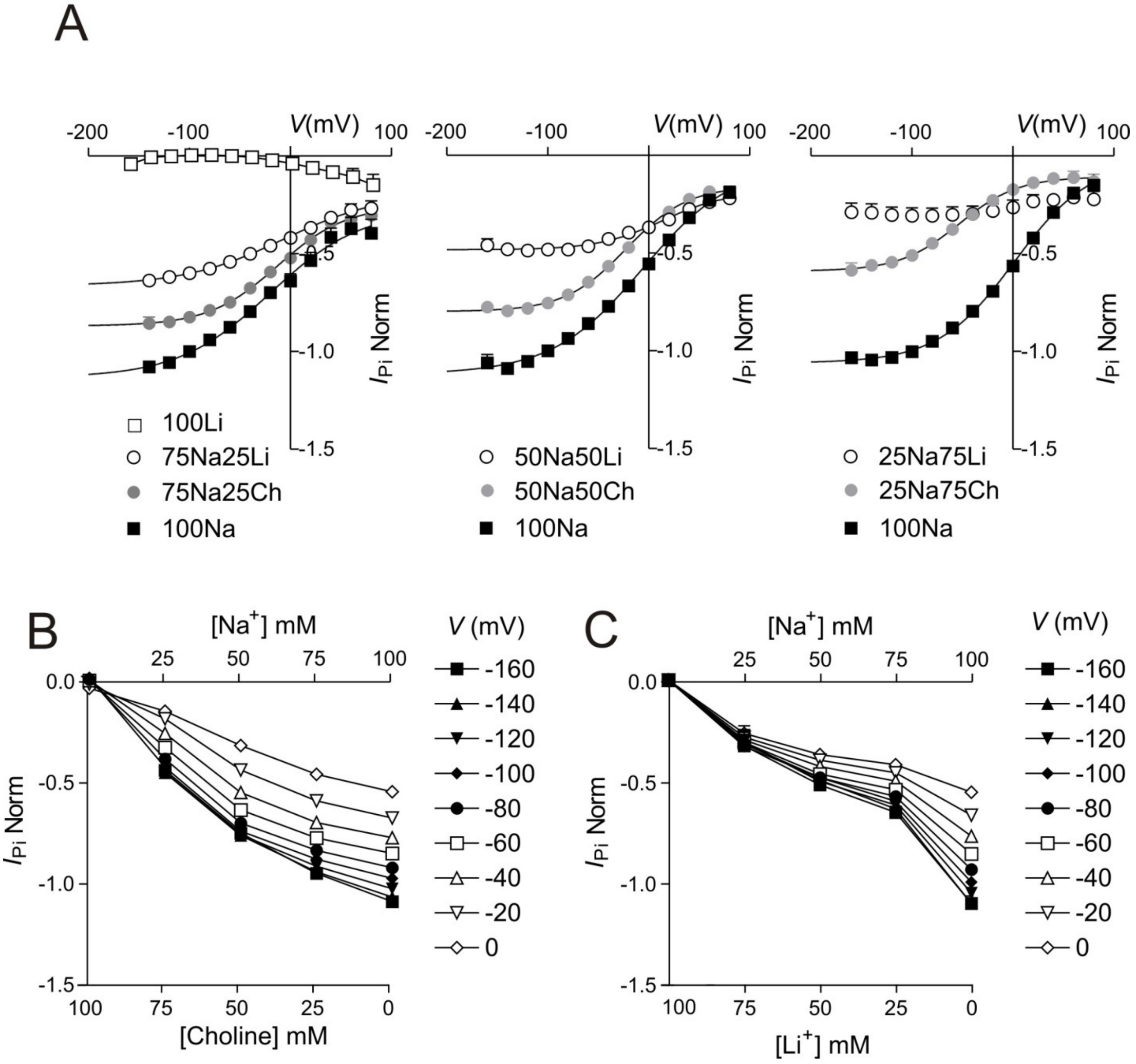
A
-200
-100
V(mV)
100
-0.5
-1.0
-1.5
I_{Pi} Norm
100Li
75Na25Li
75Na25Ch
100Na
50Na50Li
50Na50Ch
25Na75Li
25Na75Ch
B
C
[Na+] mM
25
50
75
100
0.0
-0.5
-1.0
-1.5
[Choline] mM
[Li+] mM
V (mV)
-160
-140
-120
-100
-80
-60
-40
-20
0

Figure 3

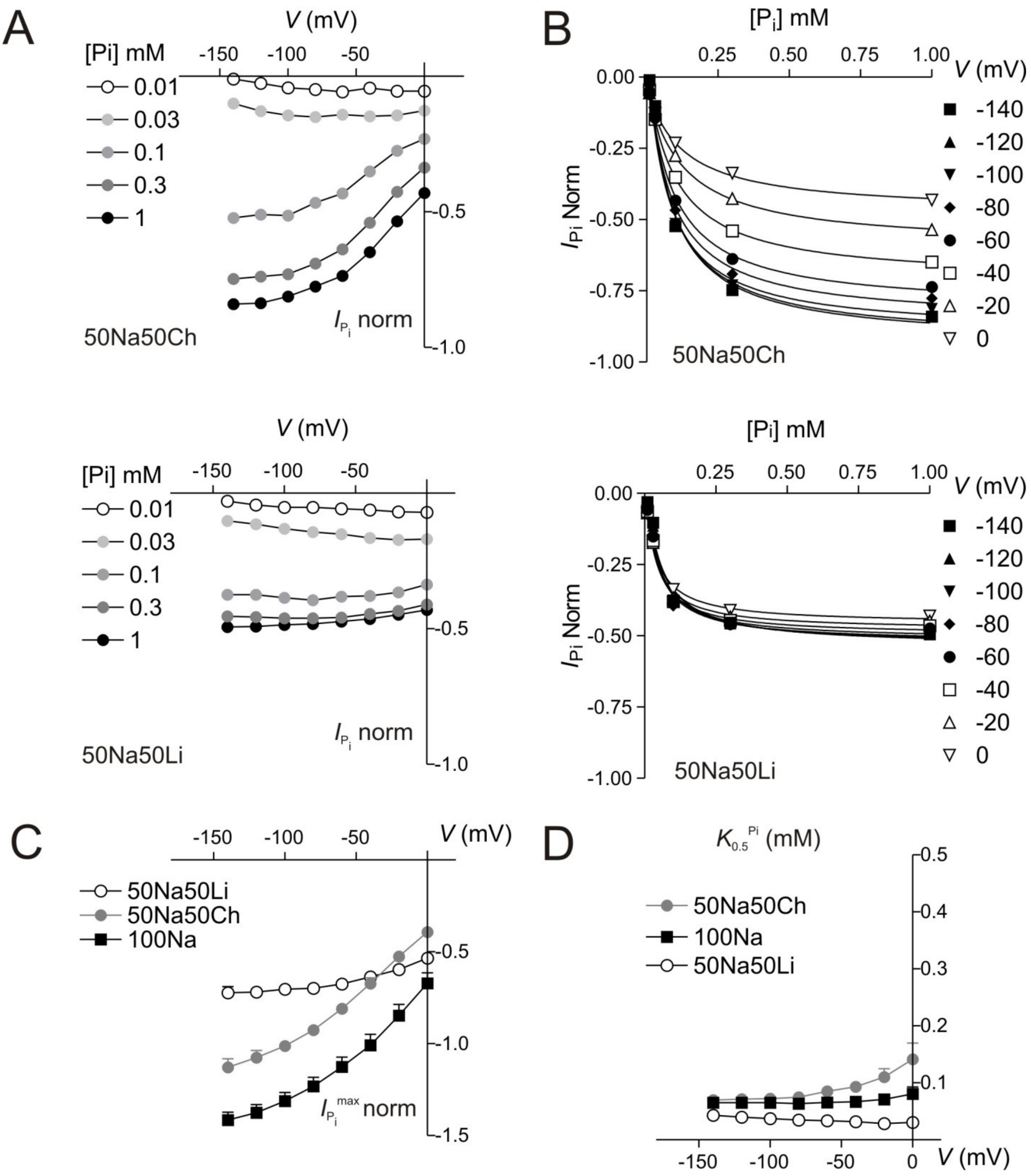
A
V (mV)
[Pi] mM
-150
-100
-50
0.01
0.03
0.1
0.3
1
-0.5
I_{P_i} norm
-1.0
50Na50Ch
B
[P$_i$] mM
0.25
0.50
0.75
1.00
V (mV)
0.00
-0.25
-0.50
-0.75
-1.00
I_{Pi} Norm
■ -140
▲ -120
▼ -100
◆ -80
● -60
□ -40
△ -20
▽ 0
50Na50Ch
V (mV)
[Pi] mM
-150
-100
-50
0.01
0.03
0.1
0.3
1
-0.5
I_{P_i} norm
-1.0
50Na50Li
[Pi] mM
0.25
0.50
0.75
1.00
V (mV)
0.00
-0.25
-0.50
-0.75
-1.00
I_{Pi} Norm
■ -140
▲ -120
▼ -100
◆ -80
● -60
□ -40
△ -20
▽ 0
50Na50Li
C
-150
-100
-50
V (mV)
50Na50Li
50Na50Ch
100Na
-0.5
-1.0
$I_{P_i}^{max}$ norm
-1.5
D
$K_{0.5}^{Pi}$ (mM)
0.5
0.4
0.3
0.2
0.1
50Na50Ch
100Na
50Na50Li
-150
-100
-50
0
V (mV)

Figure 4

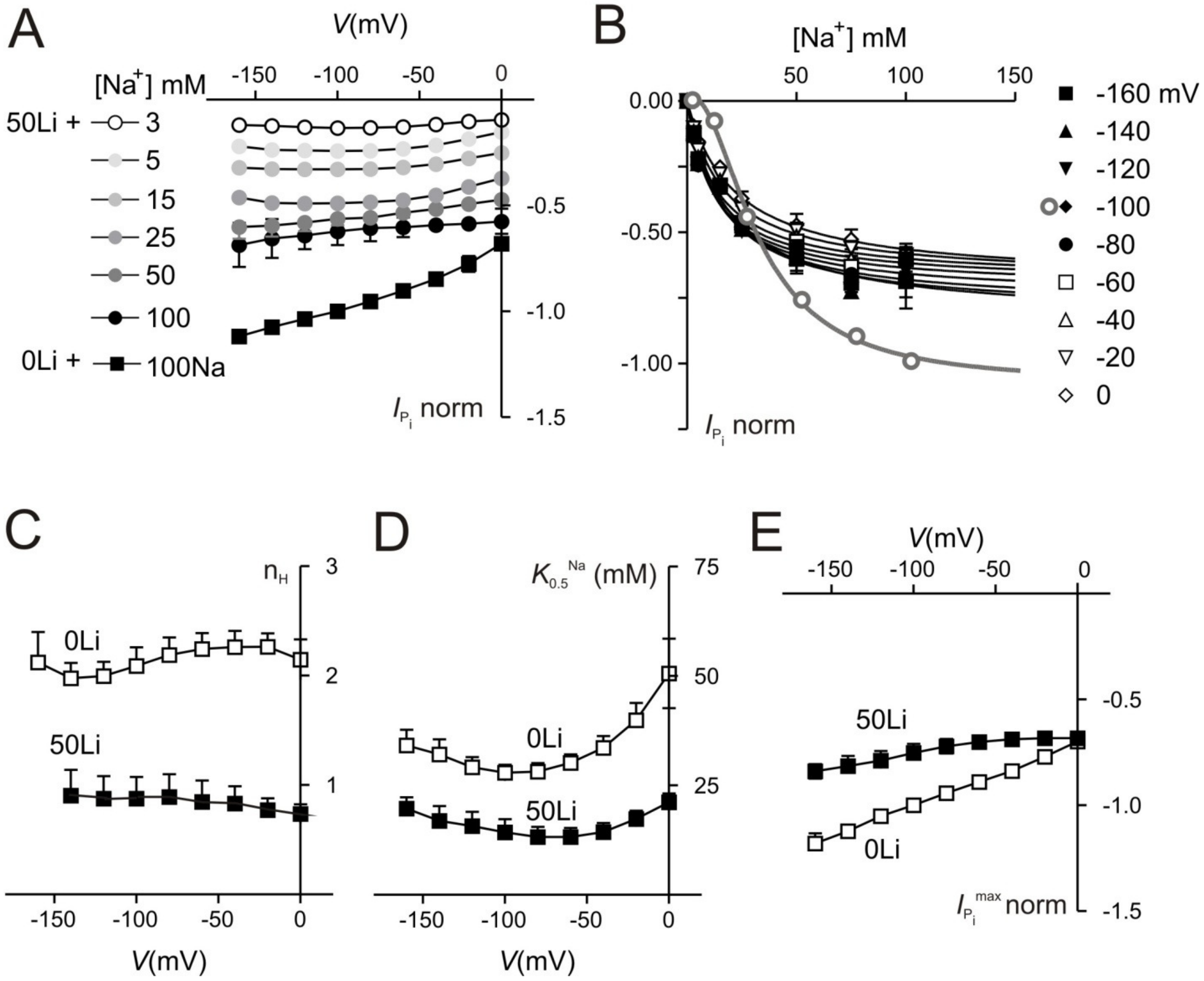
A
V(mV)
-150
-100
-50
0
[Na+] mM
50Li + 3
5
15
25
50
100
0Li + 100Na
-0.5
-1.0
-1.5
I_Pi norm
B
[Na+] mM
50
100
150
0.00
-0.50
-1.00
I_Pi norm
-160 mV
-140
-120
-100
-80
-60
-40
-20
0
C
n_H
3
2
1
0Li
50Li
-150
-100
-50
0
V(mV)
D
K_0.5^Na (mM)
75
50
25
0Li
50Li
-150
-100
-50
0
V(mV)
E
V(mV)
-150
-100
-50
0
50Li
0Li
-0.5
-1.0
-1.5
I_Pi^max norm

Figure 5

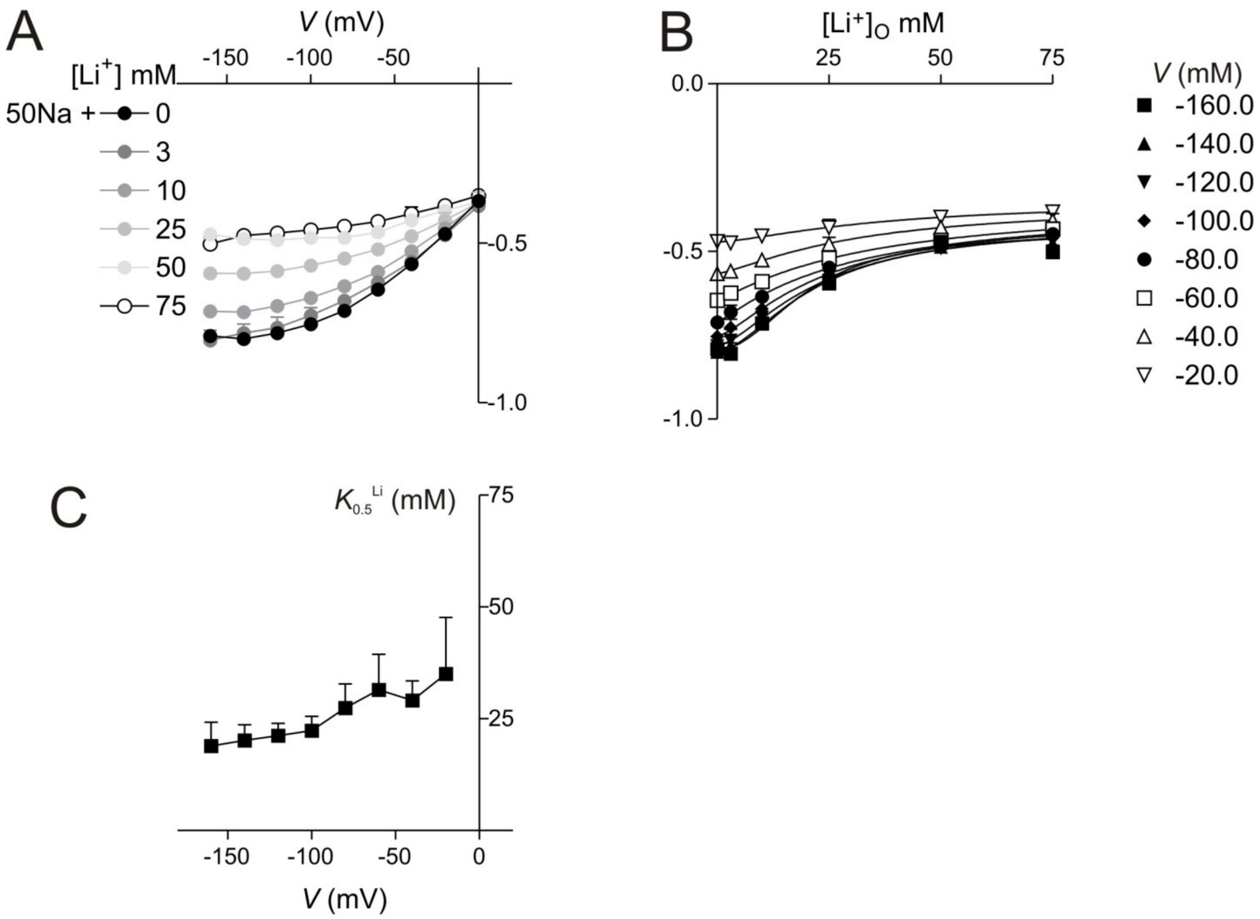
A
V (mV)
-150
-100
-50
-0.5
-1.0
[Li$^+$] mM
50Na + 0
3
10
25
50
75
B
[Li$^+$]$_O$ mM
25
50
75
0.0
-0.5
-1.0
V (mM)
■ -160.0
▲ -140.0
▼ -120.0
◆ -100.0
● -80.0
□ -60.0
△ -40.0
▽ -20.0
C
$K_{0.5}^{Li}$ (mM)
75
50
25
-150
-100
-50
0
V (mV)

Figure 6

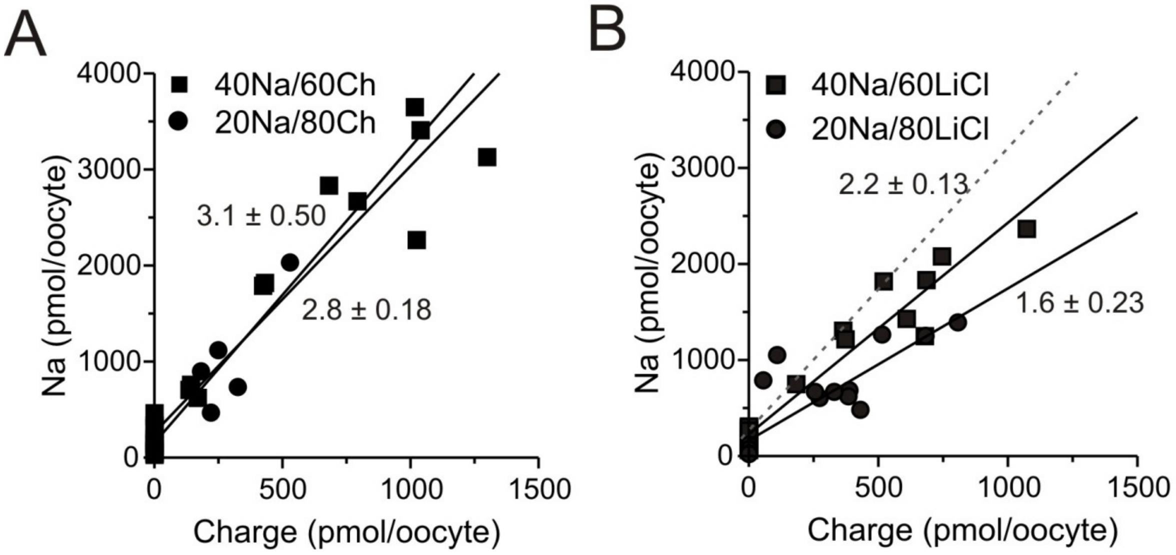
A
4000
3000
2000
1000
0
Na (pmol/oocyte)
0
500
1000
1500
Charge (pmol/oocyte)
40Na/60Ch
20Na/80Ch
3.1 ± 0.50
2.8 ± 0.18
B
4000
3000
2000
1000
0
Na (pmol/oocyte)
0
500
1000
1500
Charge (pmol/oocyte)
40Na/60LiCl
20Na/80LiCl
2.2 ± 0.13
1.6 ± 0.23

Figure 7

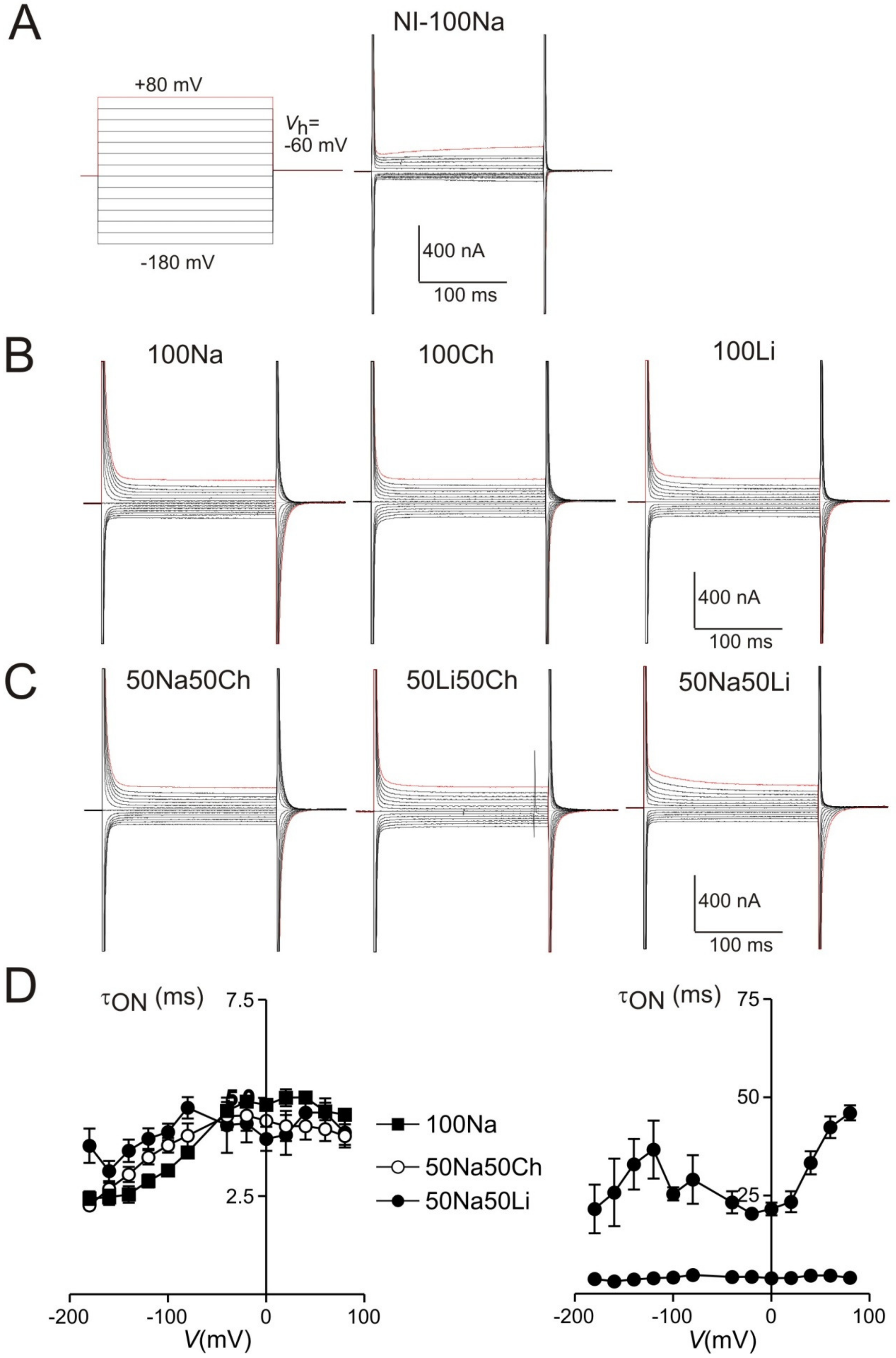
A
NI-100Na
+80 mV
Vh=
-60 mV
-180 mV
400 nA
100 ms
B
100Na
100Ch
100Li
400 nA
100 ms
C
50Na50Ch
50Li50Ch
50Na50Li
400 nA
100 ms
D
τON (ms)
7.5
5.0
2.5
-200
-100
0
100
V(mV)
100Na
50Na50Ch
50Na50Li
τON (ms)
75
50
25
-200
-100
0
100
V(mV)

Figure 8

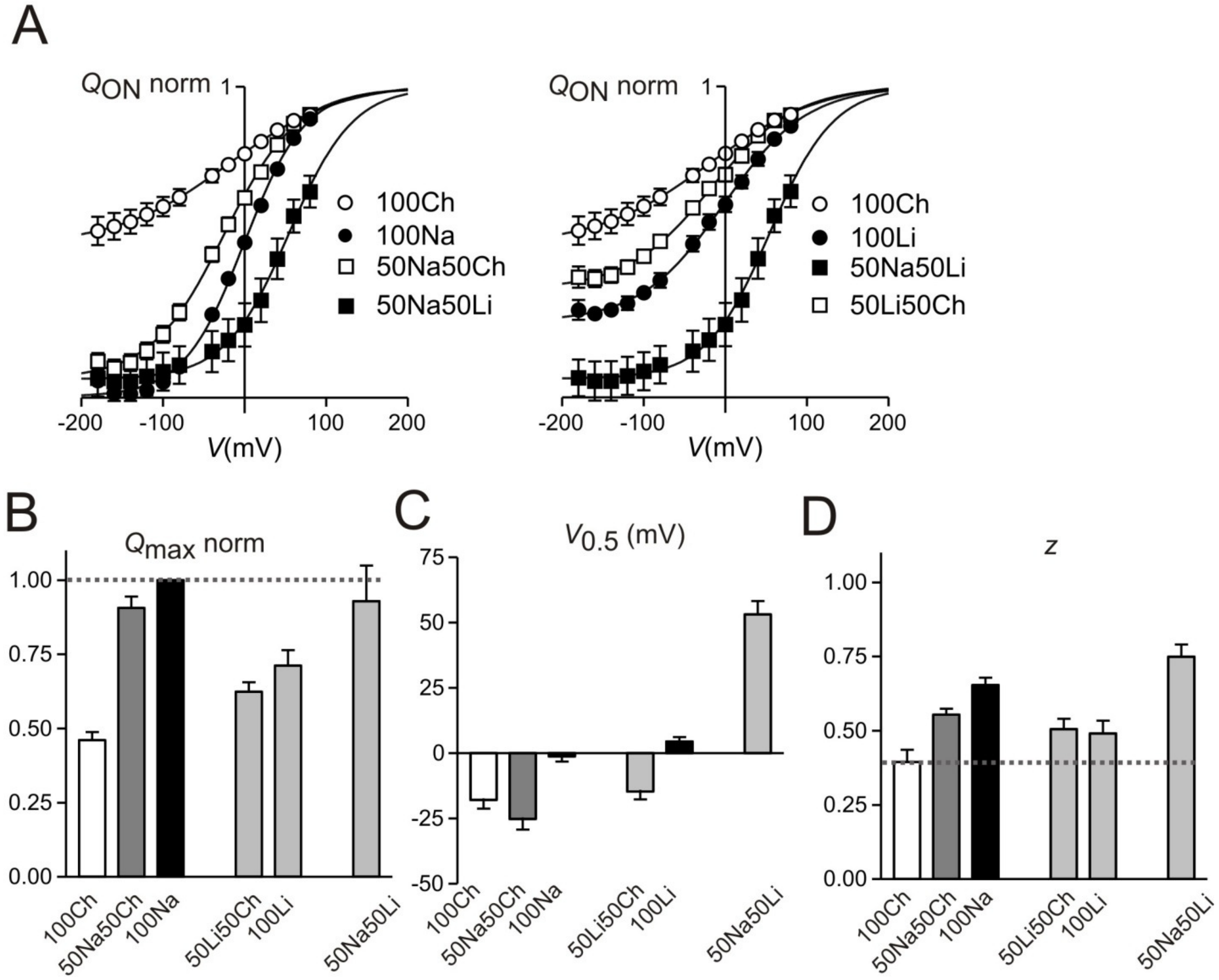
A
Q_{ON} norm
1
-200
-100
100
200
V(mV)
100Ch
100Na
50Na50Ch
50Na50Li
Q_{ON} norm
1
-200
-100
100
200
V(mV)
100Ch
100Li
50Na50Li
50Li50Ch
B
Q_{max} norm
1.00
0.75
0.50
0.25
0.00
100Ch
50Na50Ch
100Na
50Li50Ch
100Li
50Na50Li
C
$V_{0.5}$ (mV)
75
50
25
0
-25
-50
100Ch
50Na50Ch
100Na
50Li50Ch
100Li
50Na50Li
D
z
1.00
0.75
0.50
0.25
0.00
100Ch
50Na50Ch
100Na
50Li50Ch
100Li
50Na50Li

Figure 9

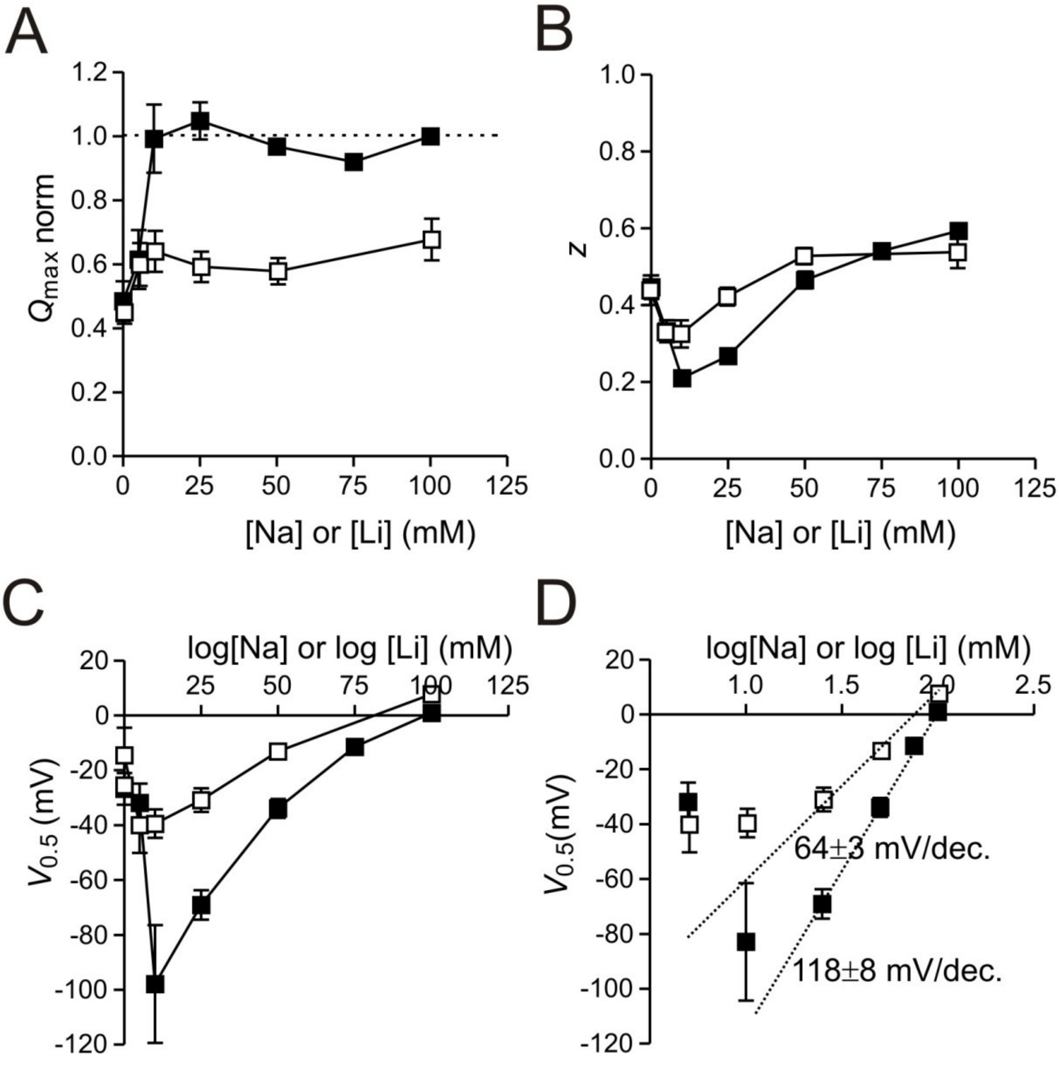
A
1.2
1.0
0.8
0.6
0.4
0.2
0.0
Q_{max} norm
0
25
50
75
100
125
[Na] or [Li] (mM)
B
1.0
0.8
0.6
0.4
0.2
0.0
z
0
25
50
75
100
125
[Na] or [Li] (mM)
C
log[Na] or log [Li] (mM)
20
0
-20
-40
-60
-80
-100
-120
25
50
75
100
125
$V_{0.5}$ (mV)
D
log[Na] or log [Li] (mM)
20
0
-20
-40
-60
-80
-100
-120
1.0
1.5
2.0
2.5
$V_{0.5}$(mV)
64±3 mV/dec.
118±8 mV/dec.

Figure 10

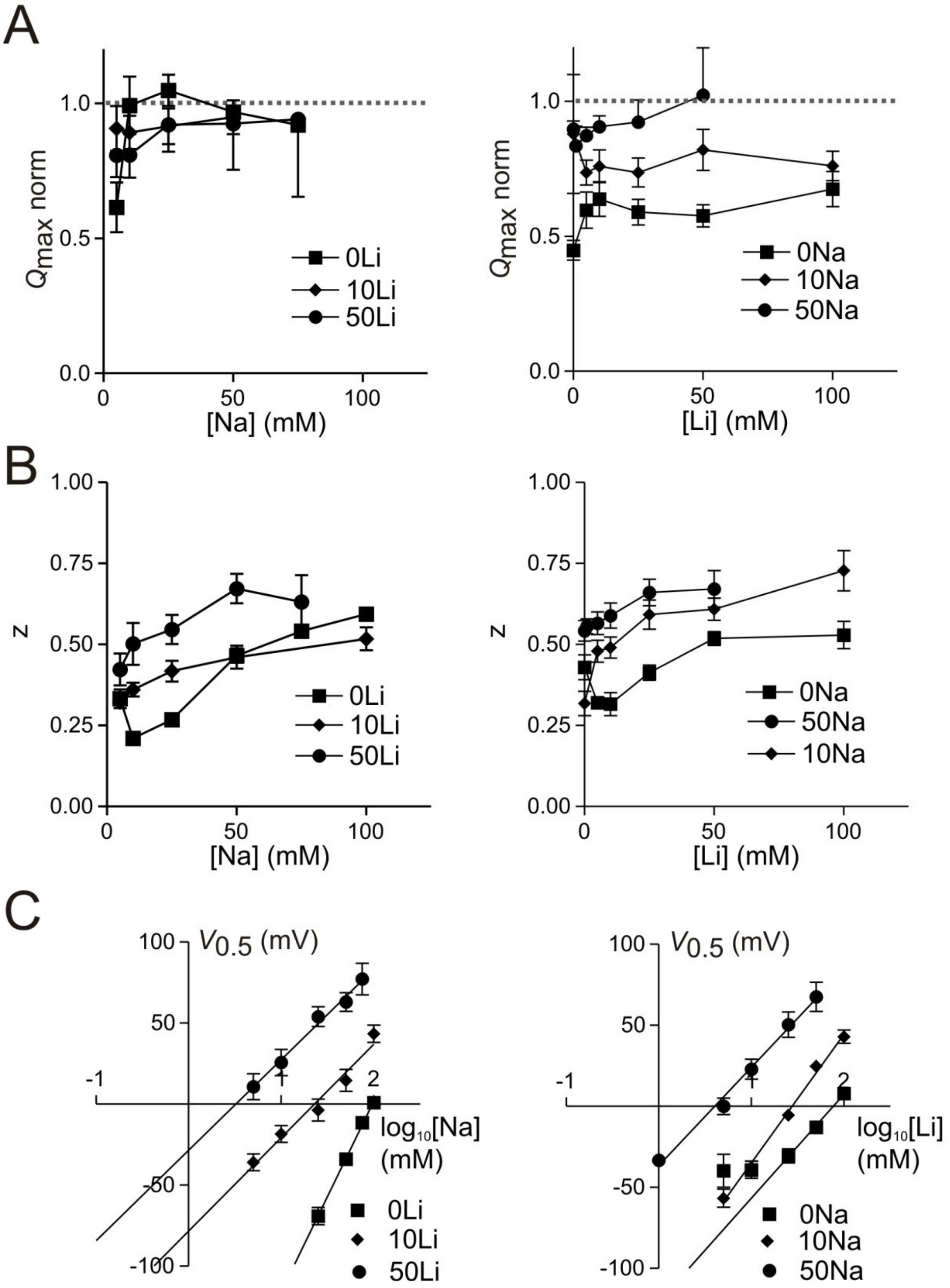
A
Q$_{max}$ norm
1.0
0.5
0.0
0
50
100
[Na] (mM)
0Li
10Li
50Li
Q$_{max}$ norm
1.0
0.5
0.0
0
50
100
[Li] (mM)
0Na
10Na
50Na
B
z
1.00
0.75
0.50
0.25
0.00
0
50
100
[Na] (mM)
0Li
10Li
50Li
z
1.00
0.75
0.50
0.25
0.00
0
50
100
[Li] (mM)
0Na
50Na
10Na
C
100
$V_{0.5}$ (mV)
50
-1
1
2
-50
-100
log$_{10}$[Na] (mM)
0Li
10Li
50Li
100
$V_{0.5}$ (mV)
50
-1
1
2
-50
-100
log$_{10}$[Li] (mM)
0Na
10Na
50Na

Figure 11

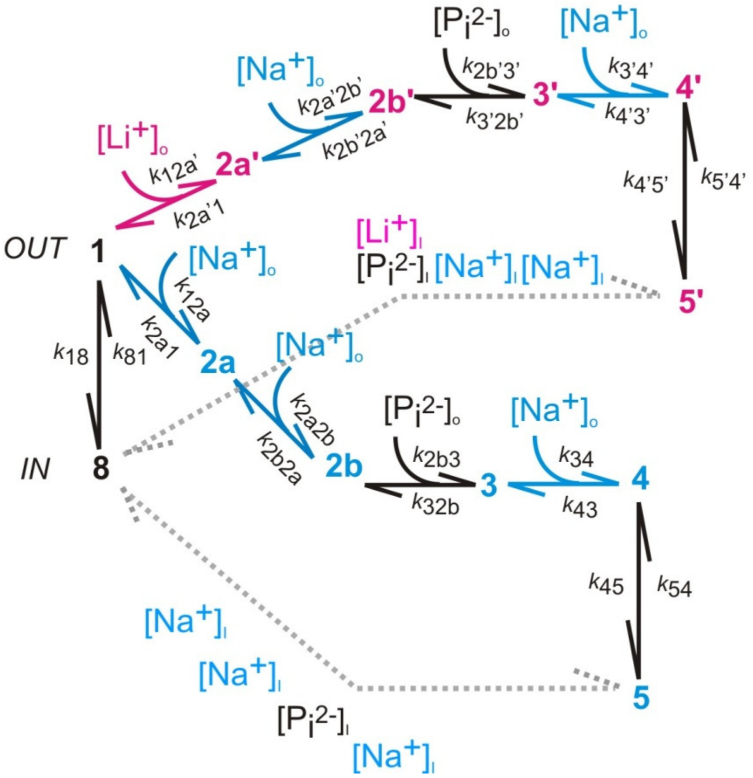
[Pi2-]o
[Na+]o
[Na+]o
k2b'3'
k3'4'
2b'
3'
4'
k2a'2b'
k3'2b'
k4'3'
[Li+]o
2a'
k2b'2a'
k12a'
k4'5'
k5'4'
k2a'1
OUT
1
[Na+]o
[Li+]i
[Pi2-]i [Na+]i [Na+]i
5'
k12a
k18
k2a1
k81
2a
[Na+]o
k2a2b
[Pi2-]o
[Na+]o
IN
8
k2b2a
2b
k2b3
3
k34
4
k32b
k43
k45
k54
[Na+]i
[Na+]i
[Pi2-]i
[Na+]i
5

Figure S1

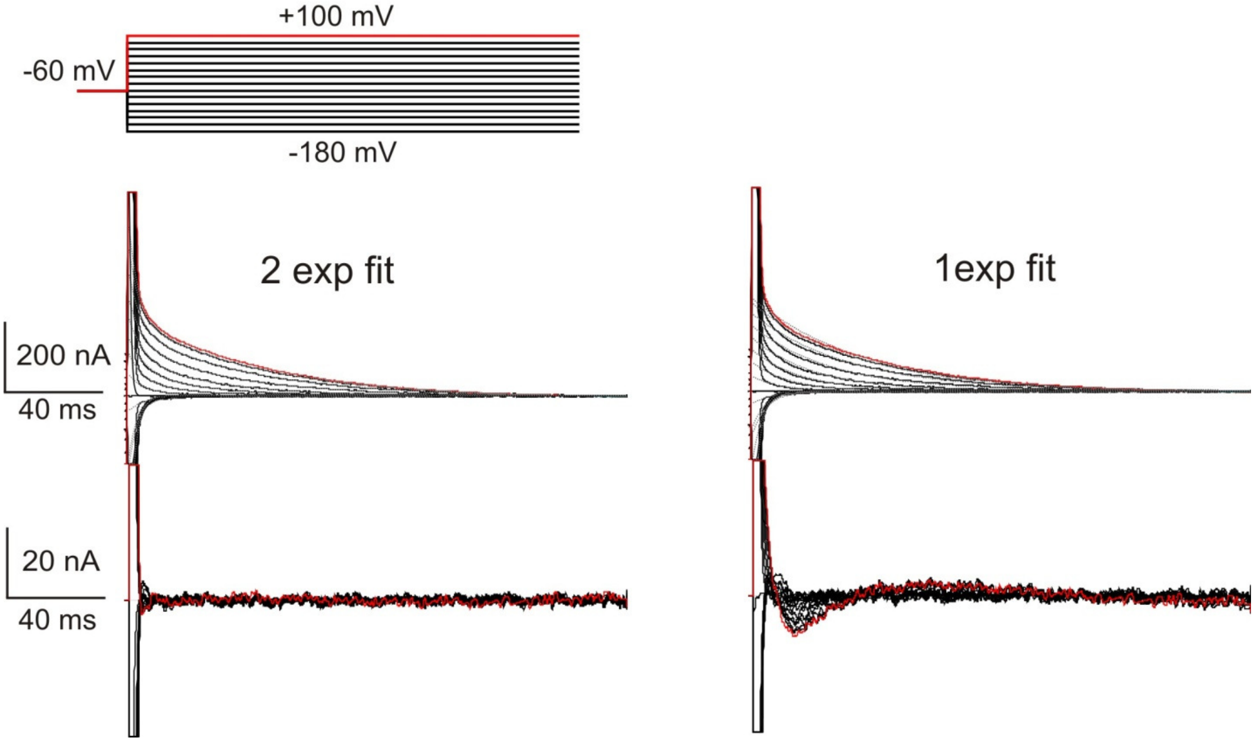

Figure S2

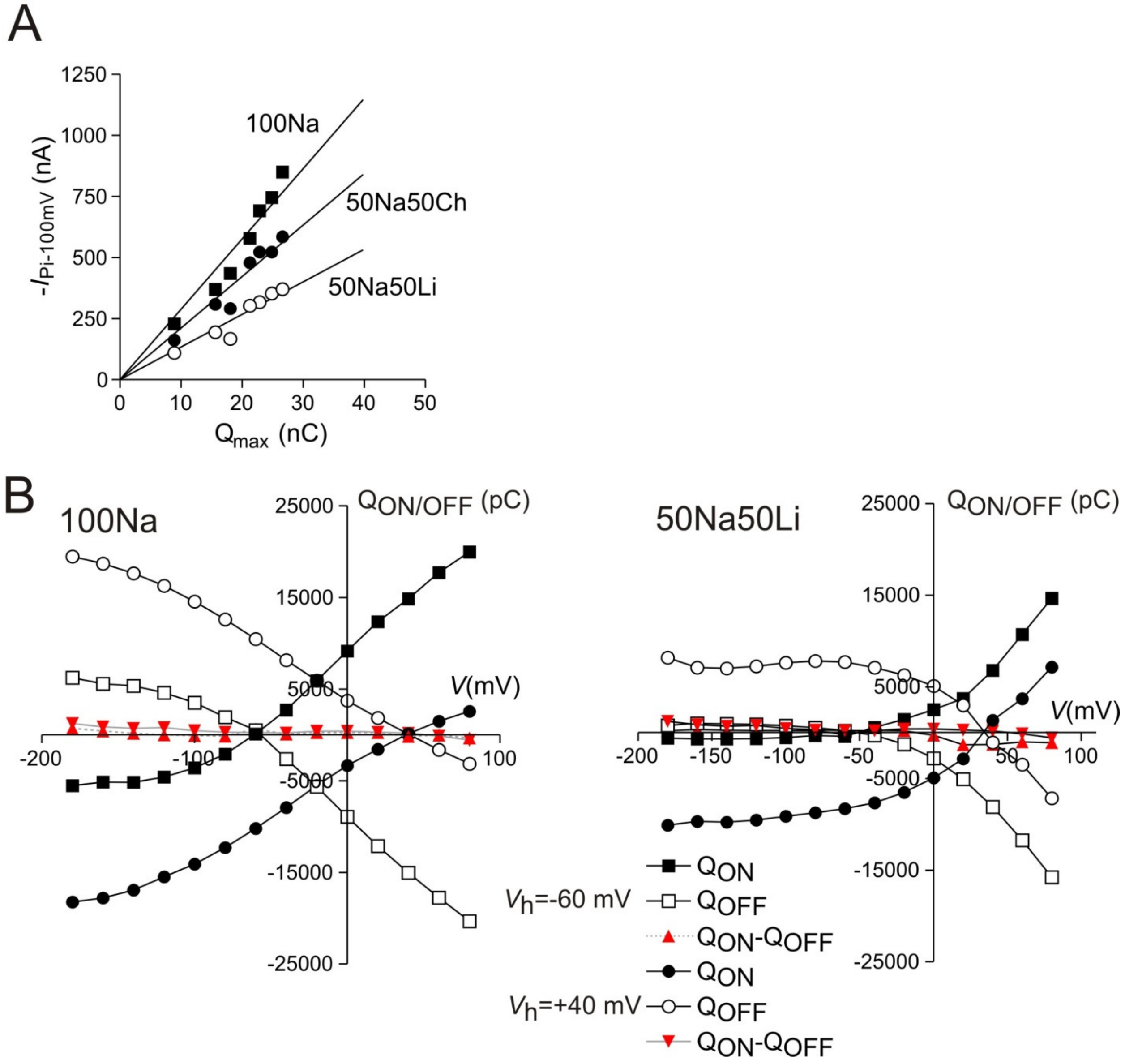
A
1250
1000
750
500
250
0
$-I_{\text{Pi-100mV}}$ (nA)
100Na
50Na50Ch
50Na50Li
0
10
20
30
40
50
Q_{max} (nC)
B
100Na
25000
$Q_{\text{ON/OFF}}$ (pC)
15000
5000
-5000
-15000
-25000
V(mV)
-200
-100
100
50Na50Li
25000
$Q_{\text{ON/OFF}}$ (pC)
15000
5000
-5000
-15000
-25000
V(mV)
-200
-150
-100
-50
50
100
V_h=-60 mV
Q_{ON}
Q_{OFF}
$Q_{\text{ON}}-Q_{\text{OFF}}$
V_h=+40 mV
Q_{ON}
Q_{OFF}
$Q_{\text{ON}}-Q_{\text{OFF}}$

Figure S3

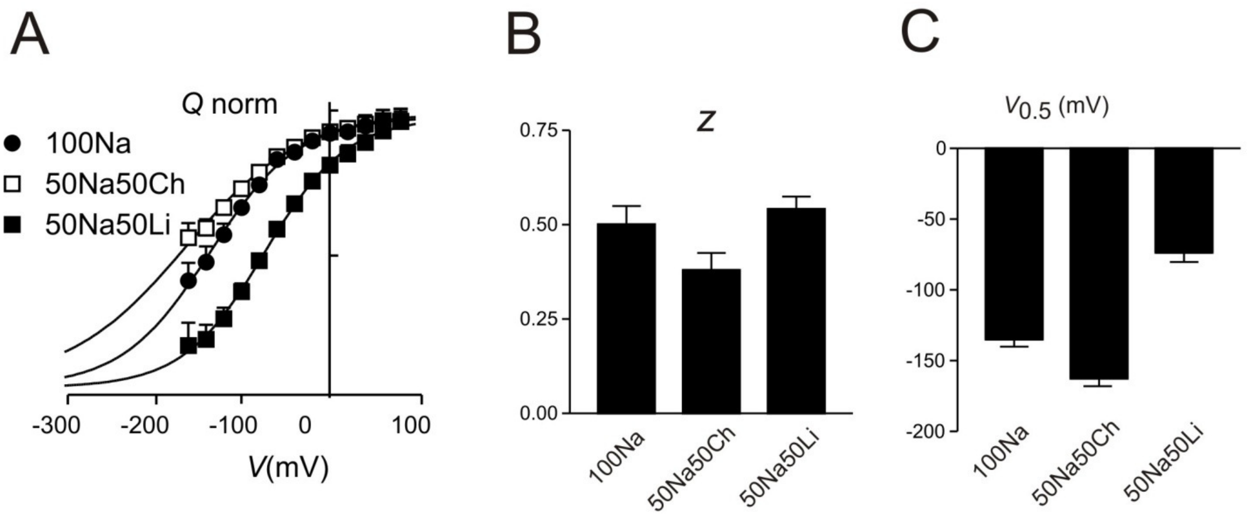
A
Q norm
● 100Na
□ 50Na50Ch
■ 50Na50Li
-300
-200
-100
0
100
V(mV)
B
z
0.75
0.50
0.25
0.00
100Na
50Na50Ch
50Na50Li
C
V0.5 (mV)
0
-50
-100
-150
-200
100Na
50Na50Ch
50Na50Li

Figure S4

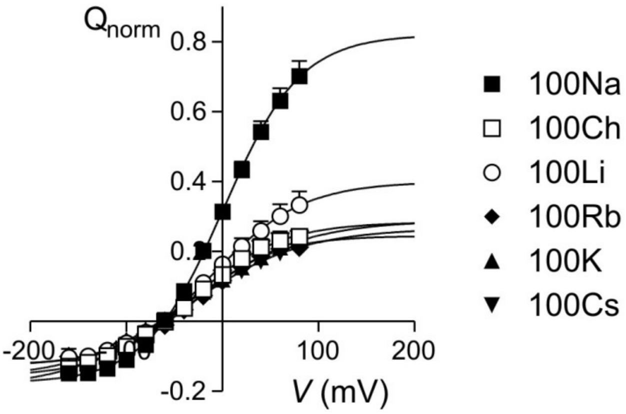
Q_{norm}
0.8
0.6
0.4
0.
-0.2
-200
100
200
V (mV)
■ 100Na
□ 100Ch
○ 100Li
◆ 100Rb
▲ 100K
▼ 100Cs

3.2 Unpublished material:

3.2.1 Cut-open voltage clamp technique (COVC): access to the cytoplasmic side of the membrane.

Introduction

As already mentioned in the previous sections, some cotransporters are electrogenic and they have been characterized by Two-Electrode Voltage Clamp technique (TEVC). This technique has three main shortcomings:

(i) lack of easy access to the cytoplasmic site of the membrane;

(ii) relative "slow" clamping speed, whereby the membrane potential cannot settle faster than a several hundred µs. Therefore, the resolution of currents with fast kinetics is limited;

(iii) relative slow extracellular perfusion systems due to the oocyte dimension (*i.e.* large sphere).

In the following section, I will give few examples of how it is possible to overcome these shortcomings and explain principles of Cut-Open Voltage Clamp as well as technical details about this system.

To overcome the inaccessibility to the cytoplasmic side of the membrane some indirect methods such as dialysis and injection of solutions are available (12, 90):

- dialysis procedures typically involve overnight incubation of oocytes in a specific medium (*e.g.* Na^+-free solution) to allow the cells to equilibrate and thereby eliminate or reduce a specific ion present inside the oocyte;
- microinjection allows studies on transport activity by cytoplasmic microinjection of a solution containing co-substrates/substrates/inhibitors (solutes).

Neither dialysis nor microinjection is suitable to investigate transporter kinetics, because the control of internal solute concentration is not precise. Moreover, microinjection of solutes during an experiment may result in significant mechano-electrical artifacts due to the damage of the oocyte membrane around the microinjection pipette and movement of the cell, especially if large volumes are injected.

None of these methods eliminates the other two shortcomings present in the TEVC, namely the slow clamp performance and speed of external solution exchange.

A more precise control of the solution exchange can be performed by using sophisticated electrophysiological techniques such as the patch-clamp method and the giant-excised membrane-patch method, where a small part of the membrane, or the entire cell, can be voltage clamped by a single glass micropipette (see Table 3.1). These two methods allow the accessibility to the internal and external media, moreover, the clamped surface is small (3-1200 μm^2) leading to an increased clamp speed performance.

The standard patch-clamp method uses patch-clamp pipette tips that are normally 0.5-2 µm diameter. This gives the possibility to have a fast clamp due to the small size of the clamped area (1-3 μm^2). Of particular interest is the inside-out configuration that gives direct access to the cytoplasmic side of the membrane. Three main problems must be addressed when this method is used to study transporters:

- magnitude of current (considering the clamped area and the transporter turnover rate, 1-10.000 cycles/sec);
- stability of the preparation (less than 1 h);
- difficult access to the extracellular medium (in inside-out configuration).

Using this method, the transport-associated current signal cannot be readily resolved. For example, assuming a typical turnover rate of 100 cycle s^{-1} and a transporter density in the patch of about ~300 particles/μm^2, the expected current signal would be ~320 fA (calculated from data reported in (62)). Moreover, in the excised patch the current signals can be difficult to measure due patch quality. Indeed a low quality seal might result in leak currents around the seal that will excess the detected signals (133).

The conventional configurations of the patch-clamp (*i.e.* whole-cell, outside-out and inside-out) were modified to compensate for some of the limitations (*i.e.* membrane patch-area and washout of cytoplasmic components). One method to overcome the washout of cytoplasmic component is the perforated-patch where the pipette solution contains a substance (*e.g* nystatin (75), anphotericin B (128)) that forms a patch with a higher resistance access in comparison to the whole-cell configuration. With the perforated-patch, the intracellular solute concentrations are preserved intact but the clamped membrane is the same as in whole-cell configuration.

The necessity to exchange the solution in the internal pipette during a whole-cell or inside-out configurations was overcome by the insertion of a capillary tube (polyethylene or quartz) in the internal pipette to change the solution within seconds or minutes (*e.g.* study of the regulation of potassium channels by acetylcholine (143)). A planar patch-clamp chip (Nanion Technologies, Germany) is now available offering an internal perfusion system in which up to eight intracellular solutions can be used (web reference: http://www.nanion.de/products/port-a-patch/port-a-patch-add-ons/internal-perfusion.html).

Another alternative to the standard patch-clamp method is the giant-excised membrane-patch method (inside-out configuration). This method uses a large pipette tip with an inner diameter of 12-40 µm (corresponding to a capacitance of ~4-15 pF) giving rise to approximately 100-fold increase in the membrane area of the patch and an additional increase in current signal size (133). This technique is useful to study exchangers and cotransporters in native tissue, as well as in expression systems like *X. laevis* oocytes (*e.g.* GAT1 (104)). Nevertheless, this technique also has some limitations (69):

- seal formation requires the presence of divalent cations and chloride;
- the seal quality has to be monitored during the experiment;
- repeatable and stable outside-out patches are sometimes difficult to obtain depending on the cell type used;

Despite the necessity to perform a seal on one side of the membrane, researchers have established a method that allows solutions changing *via* the pipette. This method is called “positive-pressure method” and consists of a flexible quartz tubing connected to a reservoir that is then connected to an air pressure system to allow solution exchanges (69).

Technique	**Clamp speed**	**Clamped membrane area**	**Perfusion exchange**		**Signal size**
			Internal	**External**	
Standard patch-clamp	5-10 µs	1-3 µm^2	Inside-out configuration: internal	Outside-out, whole cell configuration: external (133)	~320 fA
Giant membrane patches	1µs	100-1200 µm^2	Both possible with the positive pressure method (69)		~600 fA - ~11 pA
Cut-Open (COVC)	20/40 µs	> 0.2 mm^2	Both possible at the same time (145)		> 19 pA
Two-Electrode (TEVC)	200 µs	~3 mm^2		Only extracellular superfusion	~50 nA – ~1000 nA

Table 3.1 Summary of the electrophysiological techniques applied to X. laevis oocytes and their main features.

Principle and development of COVC

An alternative technique to study channels and transporters expressed in *X. laevis* oocytes is the Cut-Open Voltage Clamp (COVC) technique.

The original design, named Cut-Open Vaseline-Gap voltage clamp (COVG), was developed by Stefani and Bezanilla (16, 145), the system has been further refined by others (31, 35, 85, 149). The technique was originally developed to study potassium channels expressed in *X. laevis* oocytes in order to investigate their fast gating currents.

In the COVC technique, a small part of the oocyte membrane is electrically isolated and voltage clamped. This arrangement gives (i) a good compromise between clamp speed and size of the clamped area and (ii) access to the internal medium. In the following sections the original method, as well as the major improvements to the technique, are described (see Table 3.2).

The COVC (29, 35, 149) requires the establishment of three electrical isolated compartments that allow access to three different regions of the oocyte membrane (Fig. 3.1): (i) the top pool: gives access to the recorded membrane area; (ii) the guard pool: give access to the middle part of the oocyte; (iii) the bottom pool: provides electrical access to the interior of the oocyte.

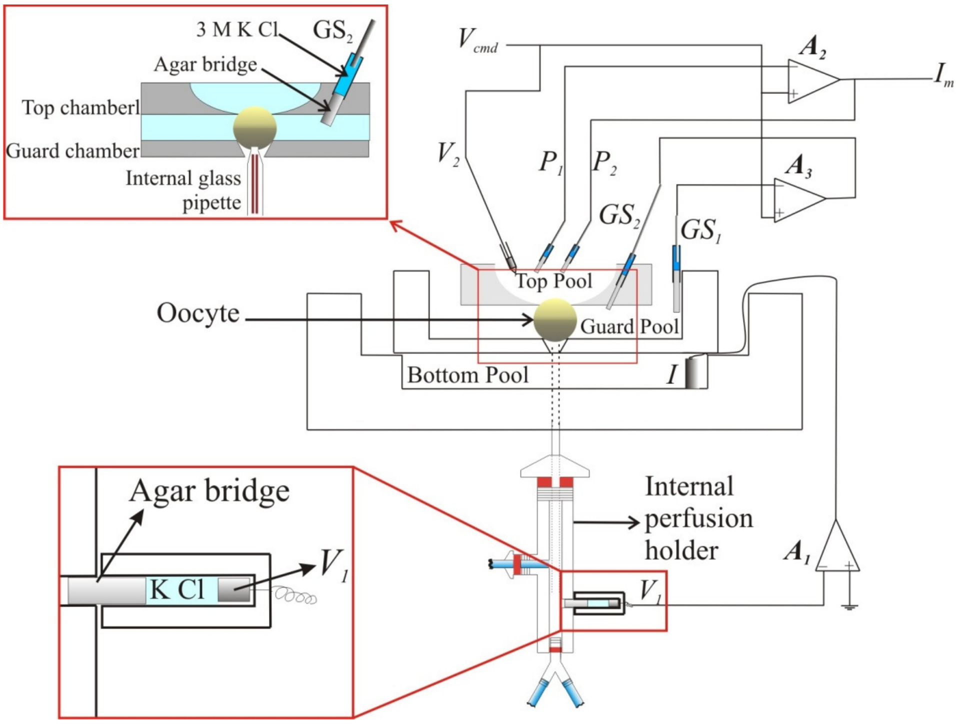

Figure 3.1 Schematic of the Cut-Open Voltage-Clamp chamber with simplified electronic components.
A_1, A_2, A_3: amplifiers, P_1, P_2, V_2, GS_1, GS_2, I: electrodes. I_m: output current. V_{cmd}: command potential.

The three voltage clamps that constitute the COVC system (controlled by three amplifiers, A_1, A_2 and A_3) work together to (i) define the potential (V_1) at the cytoplasmic side of the oocyte membrane to be at signal ground (= 0 mV) and (ii) clamp the top and guard pools to a command potential (V_{cmd}) defined by the experimenter. Note that this arrangement is the opposite of the conventional TEVC where the external potential is fixed at 0 mV and the oocyte interior is controlled by the voltage clamp. For the COVC, if $V_2 > 0$ mV, the transmembrane potential, V_m (= V_1-V_2), will be negative according to the set-up currently used in our laboratory. The middle chamber acts as an external guard to prevent leak currents flowing between the top and middle pool around the oocyte membrane.

The fast clamp performance (~20 µs) typical for the COVC is a result of the smaller clamped membrane area (> 0.2 mm^2, 10% of the total surface of a typical oocyte) compared with TEVC. For COVC, this corresponds to a membrane capacitance of approximately ~25 nF. In addition, the internal electrode must be close to the cytosolic side of the membrane.

The physical breaking of the oocyte membrane facing the bottom pool provides access to the cytoplasmic side of the upper part of the oocyte membrane. In the original technique, the electrical access to the cytosol was obtained by using either forceps or the detergent saponin. In the current set-up we penetrate the lower part of the membrane with a glass micro-capillary (OD 1 mm, ID 0.58 mm, with a tip of 100 µm) that passes through a 1 mm hole drilled in the bottom chamber.

Three electrodes are placed in the top pool: P_1 and P_2 comprise agar bridges (3% agar in 3 M KCl) in contact with chlorinated silver wire electrodes *via* 3 M KCl solution in order to eliminate junction potential (Fig. 3.1). Together with amplifier A_2, P_1 and P_2 are used to define the potential of the upper pool at the V_{cmd}. The output of A_2 is a voltage proportional to the current passing through the exposed membrane (I_m). The third electrode (V_2), placed in the top pool, is a glass capillary (resistance 0.1 MΩ) containing 3 M KCl and silver/silver chloride pellet connected to the V_2 head-stage *via* a commercial holder. This electrode senses the potential close to the external side of the cell membrane.

Two electrodes are inserted in the guard pool: GS_1 and GS_2. Each of them comprises an agar bridge (3% agar in 3 M KCl) in contact with a chlorinated silver wire electrode *via* 3 M KCl solution. Together with amplifier A_3, GS_1 and GS_2 are used to clamp the middle part of the oocyte membrane at the same potential as the top pool (V_{cmd}, Fig. 3.1).

The potential immediately under the oocyte upper membrane is sensed by electrode V_1 connected *via* 3 M KCl solution and a plexiglas support to an agar bridge (Fig. 3.1 lower inset). The agar bridge is attached to the internal perfusion capillary holder and a Ag/AgCl pellet electrode makes electrical contact with the intracellular solution *via* the bridge (Fig. 3.1). Amplifier A_1, electrode V_1 and an Ag/AgCl pellet electrode (I) in the lower pool are used to clamp the inside of the oocyte to zero (virtual ground).

Cut-Open Vaseline-Gap voltage-clamp: original design

The original COVC system (Bezenilla-Stefani (16, 145, 149)) was called Cut-Open Vaseline-Gap voltage clamp technique because vaseline rims were used to isolate the clamped portion (top pool) and the cut membrane portion (bottom pool) from the rest of the oocyte. The original idea to use the vaseline gap method was taken from the vaseline gap clamped method to study skeletal muscle fibers (72). The adaptation of this method to oocytes led to the Bezanilla-Stefani set-up shown in Fig. 3.2.

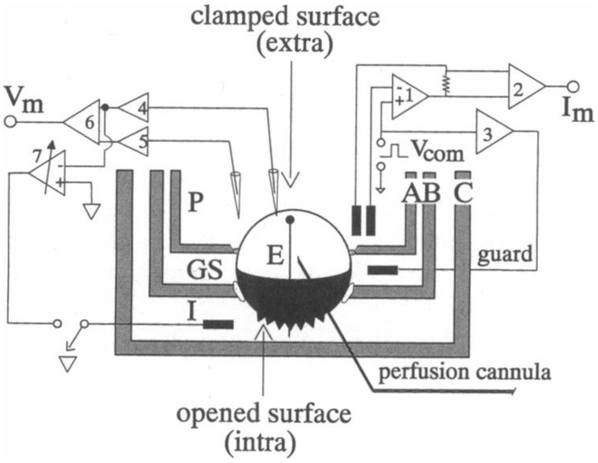

Figure 3.2 Schematization of the original Cut-Open Vaseline-Gap system.
From (149).

In this system two vaseline rims were formed manually, one rim (~300 µm) surrounded the guard chamber hole (guard shield, GS in Fig. 3.2) to isolate the part of the oocyte that is exposed to the bottom pool (I in Fig. 3.2); a second vaseline rim (~50 µm) surrounded the top pool hole and was critical for the quality of the recording (frequency response of the clamp) by preventing the recording of currents arising from the membrane under the seal (portion exposed to the middle pool, GS). In the Bezanilla-Stefani design the oocyte was held in position by applying a positive hydrostatic pressure on top of the oocyte; the positioning of the upper part (A) was done manually on top of the oocyte to create the three electrical isolated pools. The access to the cytoplasm in the bottom pool was obtained by adding saponin (0.1%) for 1 min or cutting a small part of the oocyte membrane with scissors before the oocyte mounting as noted above (Fig. 3.2).

Intracellular perfusion was achieved by introducing a perfusion canula (200 µm made of polyethylene tube) connected to a syringe perfusion system operating at a rate of 1-50 µl/h to provide internal solution exchange in ~5 min.

Several modifications to this original design were accomplished to allow faster oocyte mounting as well as easier intracellular oocyte perfusion (Table 3.2).

Major implementations of the original design, described in Costa et al. (Dani system design, (35)), concerned (i) modifications in the recording chamber and (ii) the perfusion system.

A special feature of Dani design was the enlargement of the top pool to have more space for an external superfusion and a suction systems. The second improvement made in Dani system concerned the formation of the seal between the top pool hole and the oocyte. In their design, an “elevator” wheel raised and lowered the middle chamber, which led to more reproducible and higher resistance sealing at the access holes (Fig. 3.3).

The internal perfusion system was improved by merging two functions: (i) control of intracellular medium and (ii) voltage sensing. A micropipette made from borosilicate glass (100 µm diameter) allowed the exchange of internal medium and was positioned in a commercial pipette holder. In addition, an Ag/AgCl electrode (connected to V_1) was screwed at the side of this holder to allow sensing of the intracellular voltage. This arrangement minimized the risk of puncturing the oocyte membrane because independent adjustment of the electrode position could be made. Therefore it was possible to perform long experiments (*i.e.* > 1h) (35). The extracellular perfusion system was improved by using multiple tubing connected to gravity feed syringes (109).

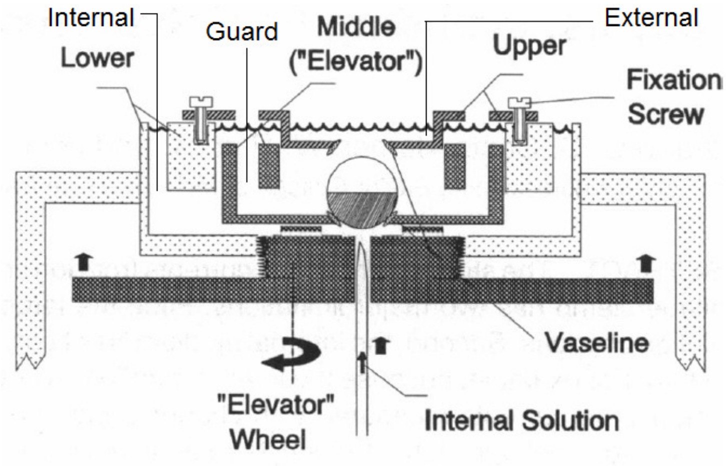

Figure 3.3 Chamber system adapted from the original COVG design.
Modified from (35).

Further modifications were reported from Lapointe system design to improve the intracellular perfusion system by changing the perfusion rate using hydrostatic pressure (70 cm H_2O and hydraulic resistance) (31). Two more improvements were then developed and merged in the Schild system design (85): first, the dead space in the internal perfusion system was reduced by using quartz microfilaments (MicroFil, MF-34G, World Precision Instruments, Sarasota, FL, USA); second, the top pool was made smaller and more mobile (movement controlled by micromanipulator) compared to previous designs (*e.g.* Horisberger system, (1)).

In our laboratory, some features of previous designs were retained (see next section).

System	**Modifications for the original design**	**Advantage**	**Disadvantage**
Stefani-Bezanilla (1992, (16, 149))	small removable top chamber.	- low signal to noise ratio (1 nA at 3 kHz); - fast time resolution (20-100 µs); (iv) stable recording (> 1h).	- fast external perfusion not available; - reproducibility of vaseline ring.
Dani (1994, (35))	- larger and fixed top pool; - elevator wheel; - internal micropipette.	- fast extracellular perfusion system; - double function of internal micropipette (change of internal solution and control of voltage).	mobile middle pool.
Lapointe (1995, (31))	- low resistance glass internal pipette; - fast internal perfusion rate with a drain system.	very fast exchange in the intracellular solution.	moveable middle pool.
Horisberger (1999, (1))	- upper hole 500 µm in direct contact with the oocyte; - reduction of the dead space at 5 µm.	reduction in the dead space for the internal perfusion system.	
Schild (2005, (85))	- moveable top chamber; - micromanipulator to control the internal pipette;	precise alignment of holes.	relatively long set up time.

Table 3.2 Summary of the modifications introduced to the original COVG design.

COVC: current design

The COVC in our lab is to a large extent based on the Schild system developed at University of Lausanne (85). We used the original oocyte voltage commercial clamp, model CA-1B, Dagan Corporation, USA. Data acquisition was performed using Digidata 1322A system with the pCLAMP 8.0 software package (Axon Instruments, Foster City, CA, USA).

The realization of the top chamber

The top chamber (Fig. 3.4) was redesigned in order to have:

- (i) a small volume to allow fast extracellular solution exchange;
- (ii) easy positioning of the chamber that allows more flexibility in aligning the top pool with respect to the oocyte;
- (iii) top pool hole manufactured with precision machining.

The slots in the circumference of the chamber were made to hold the plastic tubes for perfusion as well as agar bridges for the electrodes (red arrows in Fig. 3.4). The suction needle is mounted on the top pool plexiglas stage (see later for details). This arrangement gave good mechanical stability of the top pool assembly and allowed a clear field of view of the top hole during mounting of the oocyte.

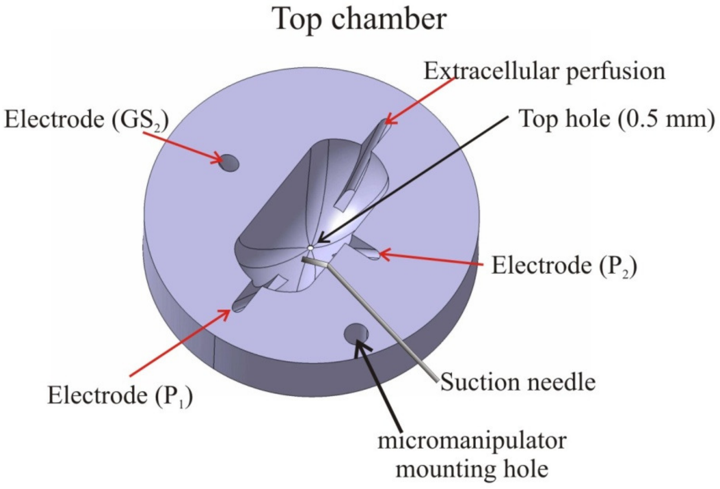

Figure 3.4 Top chamber.

CAD rendering of the new design of the top chamber. The ellipse shaped pool allows a fast exchange of solutions due to the small volume in contact with the oocyte. The slots for extracellular perfusion and for the two electrodes (P_1 and P_2) necessary to clamp the top pool are indicated. A diagonal hole (electrode GS_2, arrow) was drilled in the top chamber to allow the close proximity of the guard electrode to the oocyte in the guard pool (courtesy of Institute of Physic workshop, University of Zurich).

For ease the manipulation, the top pool was connected *via* a plexiglas support to a micromanipulator (Three Axes, Narishige, Japan). This allows fine control of the positioning of the hole with respect to the oocyte membrane and a reliable high resistance seal between the edge of the hole and the oocyte surface (Fig. 3.5).

The control of the top pool volume was achieved by a suction needle (24G, 90mm long needle, from Pajunk) attached to the top pool plexiglas support. To have the maximal flexibility, a micromanipulator (MS125-X, Newport) was attached to the plexiglas support. The introduction of this fine control (with a sensitivity of 0.5 µm and a maximum stage travel of 3.2 mm) gives the possibility of adjusting the volume in the top chamber also during the experiment (Fig. 3.5).

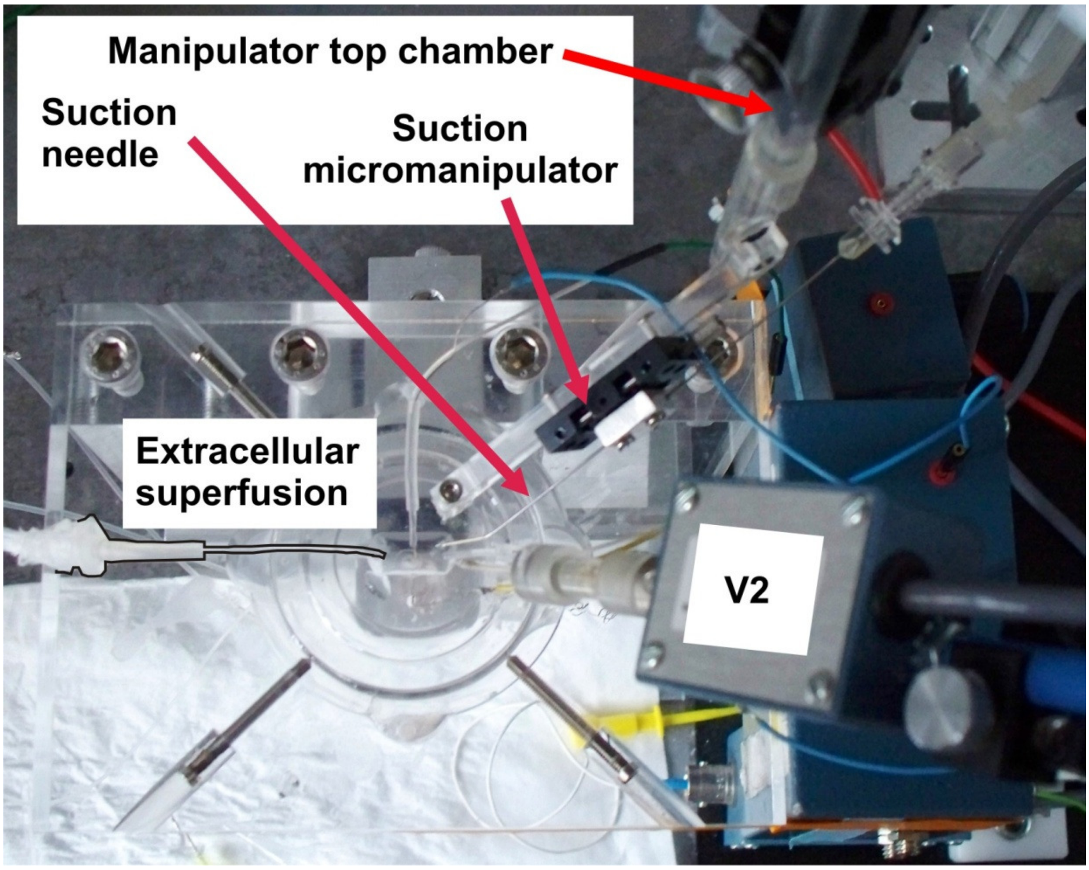

Figure 3.5 Photo showing the top part of the chamber.

Other improvements

As in the Schild design of the chamber system (85), the guard chamber was positioned within the bottom chamber and the alignment between the bottom hole (1 mm) and the guard funnel-shaped hole (bottom 0.6 mm, top 1 mm) was done by adjusting four screws located in the bottom chamber (Figs. 3.5 and 3.6). The hole in the guard chamber is funnel shaped to accommodate the oocyte without using the vaseline rim. These improvements, already used in (85), result in a faster assembling of the system and allows higher reproducibility in seal formation.

A higher and more stable bottom pool support was designed to allow correction of the position of internal pipette holder and therefore of the alignment adjustment between (i) the internal glass pipette, (ii) the bottom and guard hole and (iii) the oocyte top domus.

Positioning of the internal perfusion holder was achieved by a linear microcontrol alignment positioned at the rear of the bottom pool stage (MT MT-XY and MT-CL, Newport) (Fig. 3.6).

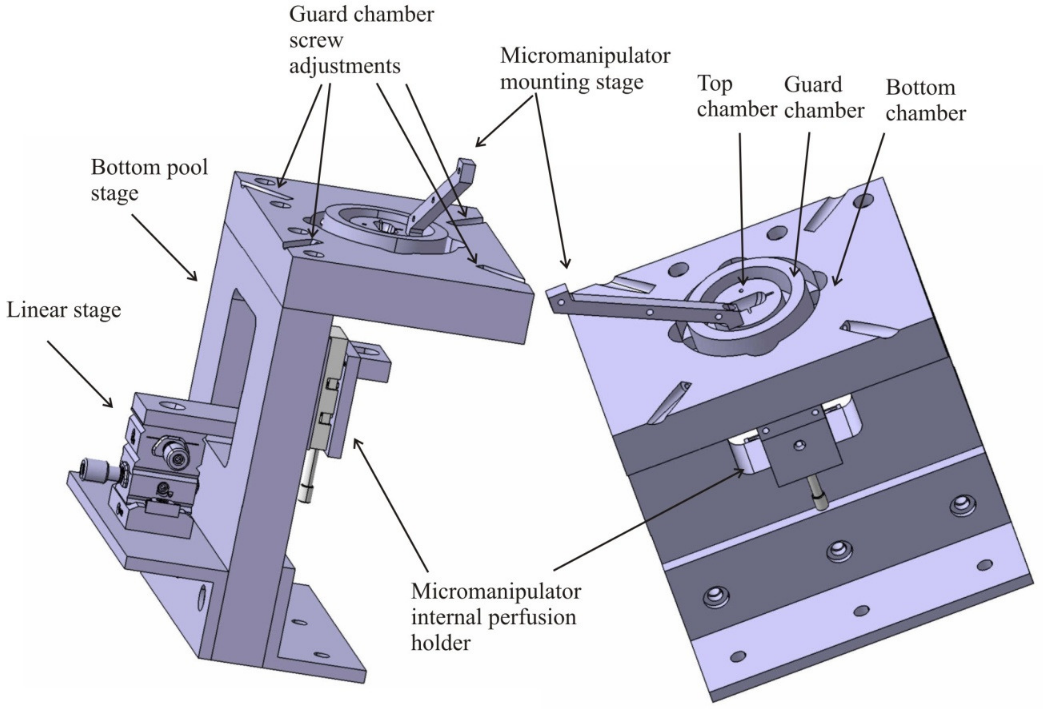

Figure 3.6 New design of the COVC system.

CAD rendering of the new design. The innovations: (i) linear microcontroller; (ii) bottom pool stage; (iii) micromanipulator for intracellular perfusion holder are indicated. This gives a good balance between flexibility and system stability (courtesy of Institute of Physics, UZH).

Perfusion system

The extracellular perfusion flow was driven by gravity and controlled manually *via* three-way valves (Fig. 3.7A). The suction was provided by a vacuum pump at a rate that matched the inflow rate and, as mentioned above, it can be regulated also during the experiment.

The internal perfusion system was constructed as shown in Fig. 3.7B. The intracellular solution was continuously perfused at the cytoplasmic side of the oocyte membrane *via* an automated delivery dual syringe pump (KD Scientific, Model 100 series). The perfused solution was exchanged by means of three-way valves and the flow rate was typically ~5 µl/min (the cytoplasmic medium exchange is achieved in ~7 sec).

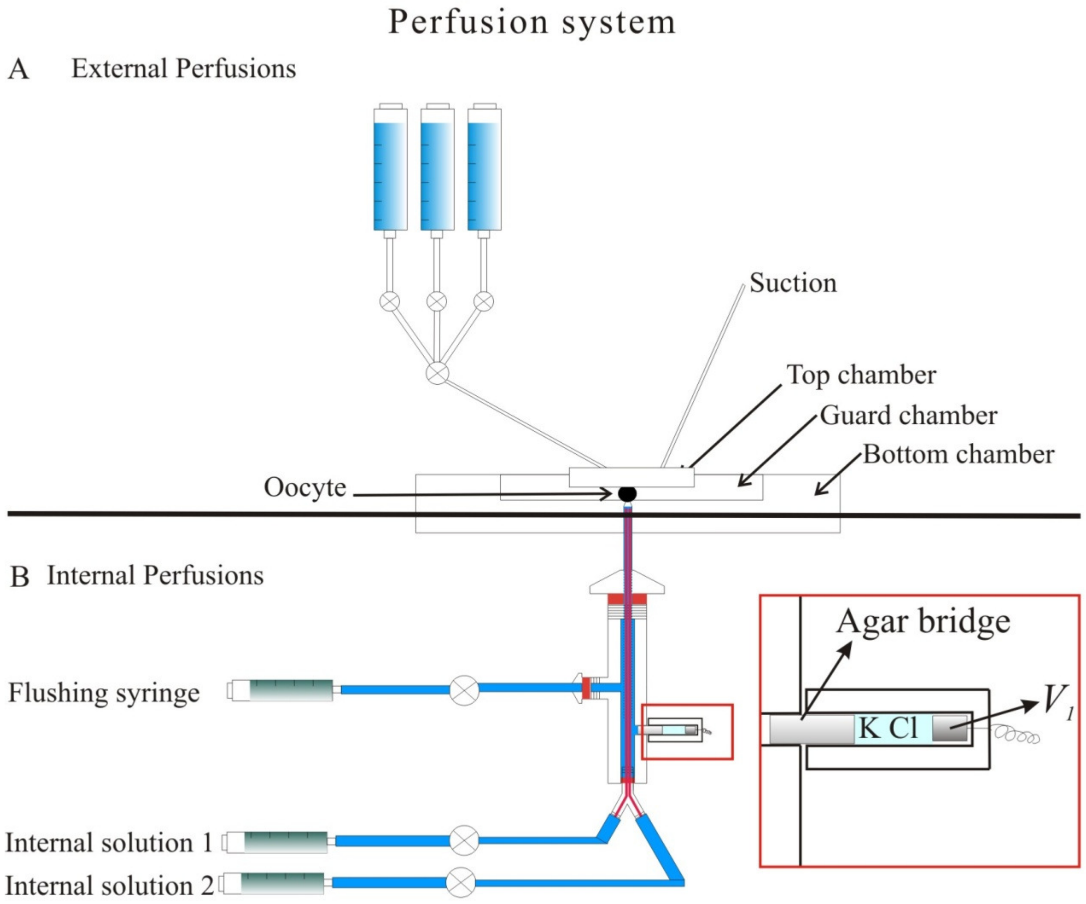

Figure 3.7 Schematic view of the perfusion system.

Extracellular (A) and intracellular (B) perfusion systems are represented. In the inset is depicted the electrical connection between V_1 and the internal perfusion system via 3 mM KCl and an agar bridge (3% agar in 3 M KCl).

Internal perfusion was achieved using a glass pipette (OD 1 mm, ID 0.58 mm, borosilicate glass capillaries, Harvard Apparatus) with a tip diameter of 100 µm tightly mounted in a commercially available electrode holder (Warner Instruments), referred to as internal perfusion holder. The glass pipette contained two microfilaments in fused silica each with an inner diameter of 100 µm (OD 170 µm, TSP100170, BGB Analytic) and cut to a length of ~8 cm.

The fused silica capillary tubes were glued to a “Y” piece support (ID 1.19 mm, OD 2.68 mm, Y barb 1/16in, Ercatech, Switzerland) to obtain maximal stability of the perfusion system and to avoid any possible leak of solution, or bubble formation. The “Y” piece was mounted in the bottom part of the internal perfusion holder using a 1 mm ID O-ring to prevent solution leak.

An additional internal solution flushing syringe was connected to the internal perfusion holder according to Lausanne design (85). This was necessary to ensure electric contact between V_1 and the bottom pool. To provide a low resistance contact between the internal solution and V_1 and to avoid contamination from 3 M KCl in the internal solution an agar bridge (3% agar in 3 M KCl) was placed between the internal perfusion holder and V_1 (inset in Fig. 3.7).

The internal perfusion holder was mounted on a miniature linear stage (MS series, MS500-X, Newport). This was essential to control the penetration of the internal pipette inside the oocyte and allow precise positioning just below the upper membrane.

Solutions

The extracellular solutions were the same as for the standard TEVC experiments (100Na), composition in mM: NaCl, 100; KCl, 2; $CaCl_2$, 1.8; $MgCl_2$, 1; HEPES-TRIS, 10; adjusted to pH 7.4. P_i was added from a 1M K_2HPO_4/ KH_2PO_4 (pH 7.4) to the 100Na solution to give the desired final concentration of P_i.

The intracellular solutions were as follows: 100Na$_i$ (in mM): NaCl, 100; KCl, 2; $MgCl_2$, 2.8; EGTA 0.1; HEPES-TRIS, 10; adjusted to pH 7.4. 100K$_i$ (in mM): NaCl, 2; KCl, 100; $MgCl_2$, 2.8; EGTA 0.1; HEPES-TRIS, 10, adjusted to pH 7.4. Internal solutions with an intermediate $[Na^+]_i$ and $[K^+]_i$ were obtained by mixing 100Na$_i$ with 100K$_i$. All the solutions were filtered before to be used.

Sequence of oocyte mounting

1. Preparation of guard and bottom pools:

The guard and the bottom pools are both filled with standard extracellular solution (100Na). The filling of the bottom pool was made *via* the hole present in the bottom of the guard chamber; this maneuver ensures the electric contact between the two pools by reducing bubble formation around the hole. The top pool is also filled with extracellular solution *via* the extracellular perfusion system to prevent the formation of air bubbles. The top pool is lowered by the micromanipulator to touch the bottom pool. This maneuver is necessary to correct for any possible offset between the electrodes (see point 3).

2. Preparation of the intracellular system:

The intracellular syringes are filled with 5 ml of intracellular solutions (*i.e.* $100K_i$) and the pump delivery is turned on to completely fill the plastic tubes and the fused capillary to eliminate air bubbles. The flushing syringe is also filled with internal solution and is used to fill the internal perfusion holder and the glass internal pipette. The pipette is raised through the bottom hole

3. Mounting electrodes and adjustments:

The electrodes are now positioned in the appropriate slots. In the top pool the agar bridges (polyethylene tubes of 1.09 mm OD, 0.38 mm ID filled with a gel made of 3% agar solved in 3 M KCl) are connected to the P_1 and P_2 wires by silicon tube (2 mm OD, 1 mm ID) filled with 3 M KCl. The immersion of P_1 and P_2 in the top bath can cause a small DC offset visible in the I_m output. This offset can be adjusted by a trim pot in the main head-stage, which contains the mains electrical connectors of P_1, P_2, GS_1 and GS_2. GS_1 and GS_2 are now connected and immersed in the guard pool. Correction for voltage offsets is achieved by a regulation of a trim pot on the main head-stage as for P_1 and P_2. GS_2 is placed in a diagonal hole drilled in the top chamber to be as close as possible to the cell. GS_1 was placed in the guard bath. Both guard electrodes are constructed as previously described for P_1 and P_2. In the bottom pool, the I Ag/AgCl pellet is used to clamp the inside of the oocyte to zero volts.

The V_2 electrode can be now connected to the head-stage and immersed in the top pool. The offset correction is nulled *via* the Dagan controller. V_1 can be connected as previously describe in the internal perfusion holder and the offset correction made by a adjustment on the Dagan controller..

4. Oocyte mounting:

The top pool is now lifted to allow the oocyte positioning. The positioning of the oocyte in the funnel shaped hole in the guard pool is a critical step. The oocyte has to be gently placed in the hole and a negative hydrostatic pressure is applied to fix the oocyte in position. The negative hydrostatic pressure is obtained manually by sucking a small amount of solution out of the bottom pool with a Pasteur pipette. The oocyte is now in position and has to be orientated in the correct way: the animal pole (or dark pole) should face down to improve visual control of the position of the internal pipette penetration during the clamp procedure.

5. Establishment of electrically separate pools:

The three electrically separate pools are obtained by lowering down the top pool using the micromanipulator and gently make contact with the oocyte membrane. This step is critical to ensure a stable experiment, because it determines the quality of the seal around of the oocyte domus. The top pool can now be re-filled with extracellular solution *via* the perfusion system described above (Fig. 3.7).

Clamp procedure

A test pulse (typically +10 mV) is applied *via* a membrane test run in the pClamp program or the internal test on the Dagan voltage clamp to monitor the different stages in the oocyte positioning and penetration.

When the three electrically separate compartments are ready, the oocyte top domus is passively charged *via* the resistance of the unpermealized membrane in the bottom pool and the cytoplasmic resistance in series. The insertion and the positioning of the internal glass capillary tip will be visible to the operator both in the microscope (as shaded ring below the oocyte membrane) and electrically on the oscilloscope (as change in the capacitive transient relaxation speed). The internal pipette tip is raised and the animal pole membrane penetrated. The capacitive transients, visualized on an oscilloscope, are now characterized by slow decay resulting from the cytoplasmic resistance and the capacitance of the oocyte membrane exposed to the top pool.

The optimal perfusion of the cytoplasmic side of the membrane is obtained by placing the intracellular pipette tip in close proximity to the upper domus membrane. The internal pipette must be as close as possible to the clamped membrane to minimize the voltage drop due to the electrical resistance of the oocyte cytoplasm. It is now possible to switch the guard clamp from passive to active and then the clamp can be turned on (A_1), which will result in very fast clamp of the upper portion of the oocyte membrane, visible with the oscilloscope by a fast decay of capacitive transients, typically <100 µs.

3.2.2 "Substrate interactions in Na$^+$-coupled P$_i$ cotransporters – a cytosolic perspective"

The COVC can be used to characterize changes in NaPi-IIb kinetics in response to changing the cytosolic substrate concentrations. This will potentially give new insights into the effect on apparent substrate affinities and order of substrate binding/de-binding at the cytosolic side.

The first aim in this work was to establish the quality of the recordable data by means of the new system by comparing the records with those obtained using TEVC.

As shown in Fig. 3.8, I_{Pi} was comparable to the TEVC data when the system was perfused on both side of the membrane (inside 100K$_i$, outside 100Na and 100Na + 1mM P$_i$). The I_{Pi} was, as expected, smaller than the signal recorded in TEVC, as only ~10 % of the membrane is accessible to the external solution exchange. However, a change in the voltage-dependence of I_{Pi} was observed. This alteration of I_{Pi} with respect to I_{Pi} recorded with TEVC, might be explained by the complete absence of Na$^+$ ions in the intracellular medium.

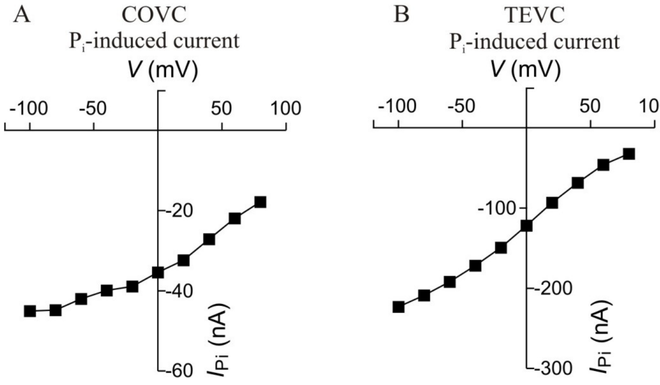

Figure 3.8 Comparison of phosphate-induced current (I_{Pi}) measured with COVC and TEVC.

A. I/V relationship of I_{Pi} obtained with COVC. The substrate-induced current was obtained by subtraction of the current recorded in 100Na from the current recorded in presence of 1 mM P_i in the extracellular solution (100Na). The oocyte cytoplasm was continuously perfused with the standard 100K$_i$ (100 mM [KCl]$_i$) via internal perfusion. B. TEVC I_{Pi} I/V data before for the substrate induced current. This record was obtained from an intact oocyte.

To confirm this hypothesis more experiments have to be performed using different Na^+ concentrations in the intracellular perfusion solution.

One general question that we would like to answer using this technique is: how a change in the ionic composition of the intracellular solution modifies the transporter kinetics?

The standard internal perfusion solution contains potassium (K^+) as the main cation ($100K_i$). In a series of experiments, this solution was exchanged with an intracellular solution containing 100 mM of NaCl ($100Na_i$). Considering NaPi-II, which is a sodium-dependent cotransporter, it is possible to envisage an effect on the transport activity due to a cation substitution on the cytoplasmic side of the membrane.

This hypothesis was first tested by determination of the apparent affinity of P_i in presence of $100Na_i$ at the cytoplasmic side of the oocyte membrane. From the $I_{Pi}/[P_i]_O$ relationship fitted with the Michaelis-Menten equation (see Fig. 3.9) we estimated the apparent affinity constant for phosphate ($K_{0.5}^{Pi}$).

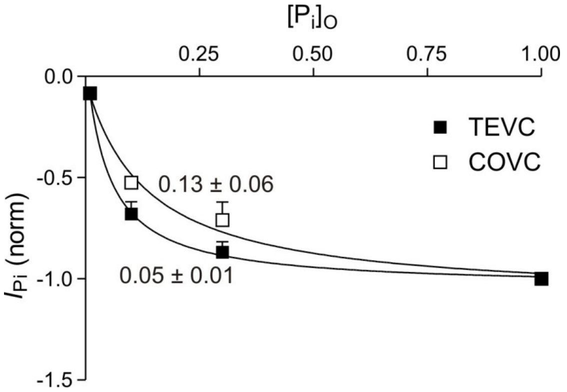

Figure 3.9 P_i dose-response recorded at V_h = -50 mV.

The two data sets were obtained using TEVC (black squares, n=5) and COVC (open squares, n=3). The data were fitted with Michaelis-Menten equation (Eqn. 2.1) and gave $K_{0.5}^{Pi}$ =f 0.05±0.01 mM (TEVC) and 0.13 ± 0.06 mM (COVC). The TEVC records were obtained from intact oocytes whereas with COVC the data were collected from internally perfused oocytes ($100Na_i$).

The $K_{0.5}^{Pi}$ obtained with TEVC and COVC with $100Na_i$ were 0.05 ± 0.01 and 0.13 ± 0.06 respectively. This difference suggests that the intracellular Na^+ might influence the internal partial reactions in NaPi-II although these are preliminary data. Further experiments, with different $[P_i]_O$ and several different intracellular solutions must be performed to fully characterize the intracellular partial reactions.

4. DISCUSSION

The detailed characterization of phosphate transport proteins is necessitated by the essential role that phosphate plays in the body. The functional mechanism of these proteins has been the subject of many studies for more than 30 years. After cloning and heterologous expression of rat NaPi-IIa (110), a characterization of the transport kinetics of the wild-type transporter (52, 118) was performed. Following the cloning of different isoforms and subtypes together with a large number of single point mutational studies (89, 93, 94), the results of two-electrode voltage clamp (TEVC), voltage clamp fluorometry (VCF) and radiotracer assays have allowed us to make some generalizations about this family of membrane transport proteins.

Three common features of the NaPi-II isoforms are (53, 159):

- their amino acid sequences. All the members of the SLC34 family (NaPi-IIa, IIb, and IIc) have a high degree of sequence identity. Taking into account the differences in sequence length, it is possible to conduct a hydrophobicity analysis, predicting a comparable secondary topology model for all three isoforms. The amino acid sequence differences appear to be mostly in the C- and N- termini as well as in the large hydrophilic extracellular loop (Fig. 2.20). The two halves of the proteins are separated by this large loop and show a high degree of similarity in the predicted membrane spanning domains (53);
- their functionally. The apparent affinity for Na^+ is ~50 mM for all three isoforms and all transporters preferably divalent phosphate with an apparent affinity <0.1 mM P_i. The transport can be inhibited by using a competitive blocker: phosphonoformic acid (PFA) (159).
- their common substrate binding order and substrate specificity for electrogenic and electroneutral isoforms: Na^+, Na^+ P_i, Na^+ (61, 157).

These commonalities suggest a similar transport mechanism among the isoforms. Nevertheless, there is also one important functional difference between the three isoforms. NaPi-IIc is electroneutral and therefore 2 Na^+ ions together with 1 HPO_4^{2-} are transported inside the cell *per* transport cycle on the other hand, the electrogenic NaPi-IIb and NaPi-IIa transport 3 Na^+

coupled with 1 HPO_4^{2-}. It was shown that the substitution of three residues with their NaPi-IIa equivalents in NaPi-IIc (S189A, S191A, and G195D) resulted in electrogenic transport with a ratio of 1:1 charge/P_i coupling, which confirmed the $3Na^+$:$1P_i$ stoichiometry observed for the electrogenic wild-type isoforms (9).

Two further properties of the electrogenic isoforms that have been addressed in this thesis are: (i) the leak mode and (ii) the interaction and participation of Li^+ ions in the cotransport mode.

4.1 Leak mode in Na^+-coupled phosphate transporters

The NaPi-II kinetic scheme (Fig. 2.30, section 2.5.3) incorporates a leak cycle in addition to the normal cotransport cycle. The leak cycle was proposed to represent a uniporter transport that allows Na^+ ions to be translocated according to their electrochemical gradient. In the kinetic scheme, the leak shares three partial reactions with the cotransport cycle (10, 88) but does not include P_i or the last Na^+. Studying the leak mode gives insight into the behavior of a subset of partial reactions.

The Na^+-coupled sugar transporter (SGLT1) is an example of a protein with transport characteristics similar to NaPi-II. SGLT1 is characterized by both cotransport and leak modes.

Both SGLT1 and NaPI-II cotransporters are Na^+-dependent, yet it is also known that Cl^- plays a role in the SGLT1 cotransport mode by increasing the apparent affinity for sugar (102). Until recently, it was still unclear why the observed reversal potential for the Na^+-dependent leak current (phlorizin-sensitive leak current) for SGLT1 was approximately -30 mV (155). A recent study showed using a mutant that displays a threefold increase in the leak current, that the leak in SGLT does not involve Cl^-. Moreover, they showed that other monovalent cations can stimulate the leak current and shift the E_r toward positive potentials (*i.e.* Li^+ ~+ 30 mV) (100).

Electrogenic isoforms of NaPi-II possess a leak current that is quantified by using phosphonoformic acid (PFA) as blocker. PFA is assumed to fully suppress this current. The PFA-sensitive current (I_{PFA}), that is believed to be solely due to permeation of Na^+ ions, is characterized by a reversal potential (E_r) that is typically between -30 mV and -20 mV. Like SGLT1, this negative E_r is inconsistent with Na^+ being the only permeant cation (Fig. 4.1).

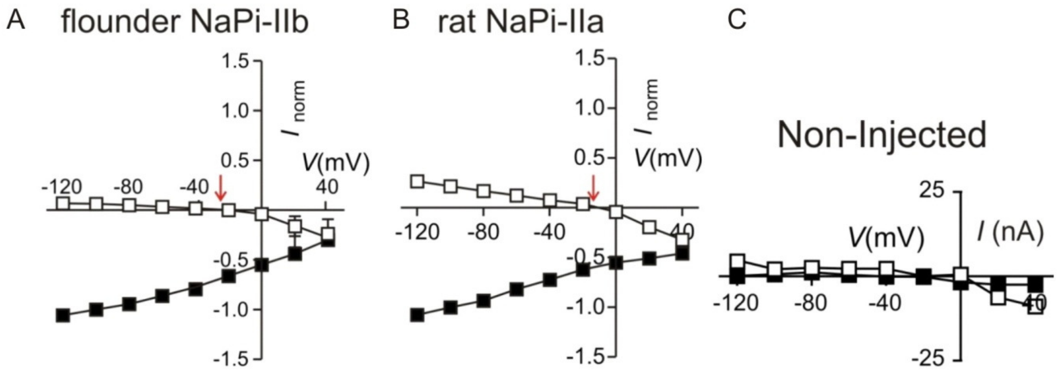

Figure 4.1. I/Vs plot of I_{Pi} and I_{PFA}.

A. and B. PFA-sensitive current (-I_{PFA}, open squares) obtained by subtraction of the current recorded in presence 100Na and 1mM PFA from the current recorded in 100Na; the normalization refers to the phosphate-induced current recorded in 100Na and in response to 1mM P_i at -100 mV. The red arrow indicates the reversal potential (E_r) for each isoform. The filled squares represent the net substrate-induced current activated by the presence of 100 mM Na^+ and 1 mM P_i (subtraction of the current recorded in 100Na from the current recorded in 100Na + $1P_i$). C. I/V traces recorded in non-injected oocytes superfused with 100Na + 1mM Pi (black squares) or 1 mM PFA (open squares). Modified from (6).

My contribution to the investigation about the nature of E_r showed, unexpectedly, that for $V > 0$ mV, PFA suppresses an endogenous outward Cl^- current (Fig. 4.2).

This endogenous component can affect our ability to resolve the leak current (-I_{PFA}) and I_{Pi} in oocytes exhibiting low expression. Variations in the endogenous component were observed in different batches of oocytes (cells coming from different donor frogs) as well as according to the number of days after injection of oocytes with cRNA.

I observed that 1 mM PFA was sufficient to block an endogenous Cl^- efflux in non-injected oocytes. This current can be larger than the I_{PFA} in low expressing cells, resulting in an inward current that gives rise to a negative E_r (Fig. 4.1C).

The observation in non-injected oocytes was confirmed in oocytes expressing NaPi-IIa. Chloride substitution with the large anion 2-(N-morpholino) ethanesulfonic (MES) as well as other anions (glucuronate, methansulfonate, sulfate, and nitrate) did not affect the magnitude of I_{PFA} at negative potentials (Fig. 4.2). The suppression of I_{PFA} at positive potentials was evident when 100 mM chloride was substituted with 100 mM of MES or glucuronate (Fig. 4.2 *left panel*) in agreement with the findings for non-injected oocytes.

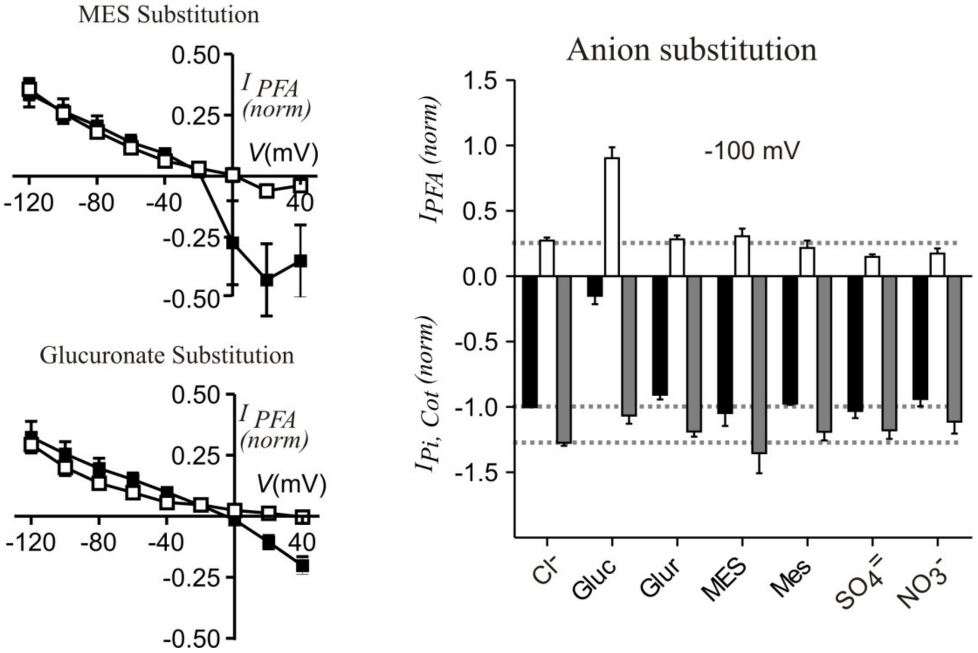

Figure 4.2 Anion substitution in rat NaPi-IIa expressing oocytes.

The currents represented in the figure are normalized for the I_{Pi} (in 100Na and 1 mM P_i) at -100 mV. Left panel show I/V curves obtained in presence of 100 mM of either MES (upper panel) or glucuronate (lower panel) where 7.6 mM of Cl^- were still present. Right panel summarises the effect of a selection of anion substitutions on the I_{PFA} and on I_{Pi}. Modified from (6).

The representative I/V for a non-injected oocyte (Fig. 4.1C) confirms that 1 mM PFA can also affect endogenous currents. Moreover, a reduction in the external Cl^- concentration, from 107.6 mM to 7.6 mM (Fig. 4.2, open squares) causes a reduction in the apparent inwardly directed current at positive potentials. This gives rise to a depolarizing shift in the E_r. The data in Fig. 4.2 (right panel) confirms that anions, with the exception of guconate, do not change the magnitude of I_{PFA} and I_{Pi}.

In the case of gluconate substitution: the I_{PFA}-sensitive is significantly larger than in standard condition. Interestingly, concomitant with the I_{PFA} increase, a decrease in I_{Pi} was observed. Moreover, the resulting total electrogenic activity ($I_{Cot} = I_{Pi} - I_{\mathrm{PFA}}$) was reduced only by 17% (Fig. 4.3). This experiment also confirms the validity of our current model for the mutual exclusivity of the leak and the cotransport modes because of the unique effect that gluconate has on the leak. In additional experiments, we could show that the voltage-dependence of the leak current was similar to that of I_{Pi}, supporting our model in which the leak and cotransport modes have the same voltage dependent partial reactions.

This behavior seems to be unique for NaPi-II transporters. When an experiment was performed using SGLT1 as control, gluconate did not affect the leak current even if the replacement slightly reduced the cotransport current due to a known involvement of Cl^- in the cotransport mode of SGLT (102).

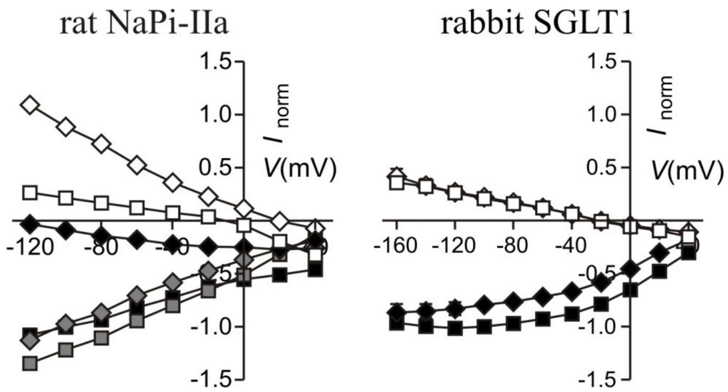

Figure 4.3 I/Vs gluconate substitution.

I/V curves obtained in presence of Cl^- *(squares) and in presence of gluconate (diamonds). Left panel:* I_{PFA} *(open squares) and* I_{Pi} *(filled squares) are added to obtain* I_{Cot} *(gray symbols) values with either* Cl^- *or gluconate.* I_{PFA} *in presence of gluconate (open diamonds) is larger than* I_{PFA} *in* Cl^-*.* $I_{Cot}^{gluconate}$ *shows only a 17% reduction of* I_{Cot} *in* Cl^-*. Right panel: the same experiment performed with SGLT1 and using phlorizin to block the leak. Gluconate does not increase the phlorizin-sensitive current (open diamonds), whereas a decrease in the glucose sensitive current can be observed (filled diamonds) in comparison to the glucose current recorded in presence of chloride (filled squares). Modified from (6).*

To investigate the behavior of gluconate in more detail, we tested the hypothesis that a reduction of Ca^{2+} or Mg^{2+} may influence the I_{PFA} given that gluconate is a well known chelator of divalent cations. The hypothesis was tested by performing two experiments. In the first experiment, we used a common Ca^{2+} chelator EDTA (ethylenediaminetetraacetic acid) at 0.5 mM to mimic the effect of the presence of 100 mM of gluconate and in the second experiment we used a solution with a 10-fold lower Ca^+ concentration (0.18 mM). In neither experiment we could not recapitulate the same behavior of I_{PFA} in presence of gluconate, therefore we could reject the divalent chelator hypothesis.

Another concern using gluconate solution is that it can change its chemical properties. We checked freshly prepared solutions containing gluconate by means of nuclear magnetic resonance, NMR, spectroscopy (performed in the lab of Prof. Robinson, Institute of Organic Chemistry, UZH) for contamination and stability. We obtained resonance frequency spectra for four consecutive days (the normal period where we keep our solutions for the experiments), and compared them. No differences in the spectra were found, indicating that the solutions did not change their properties.

From there results we concluded that the sodium gluconate solution was stable at least over a short period of time and that the effect on I_{PFA} is not influenced by Ca^{2+} or Mg^{2+}. As the gluconate effect appears to be unique to NaPi-II, we tentatively suggest that it may directly or indirectly interact with NaPi-II proteins to increase the translocation rate of Na^+ ions in the leak mode.

In both intestine and kidney, the leak mode of NaPi-II most likely has no physiological relevance because P_i is always at a high enough concentration so that the cotransport mode is favored. However, the Na^+-leak mode gives a useful phenotype to understand structure/function data.

4.2 Lithium interactions

Since 1946, lithium has been used in the treatment of psychiatric diseases (*i.e.* bipolar disorder (137)). The mechanism of the Li^+ action as a mood-stabilizer is still not well understood. The therapeutic action can involve several targets in the brain: inhibition of enzymes (*e.g.* glycogen synthase kinase 3, inositol phosphatases), modulation of glutamate receptors, modulation of monovalent cations transport (*e.g.* Na^+) (170).

When ingested, Li^+ is absorbed in the gut, distributed *via* the circulation (from which lithium will have access to the brain, its target organ *via* the blood-brain barrier) and then excreted in the urine. The kidney, Li^+ is freely filtered in the glomerula and by the time it reaches the proximal tubule, 80% is reabsorbed by Na^+-dependent transporters (151).

It has been shown that Li^+ influences the kinetics of succinate transport in the renal proximal tubule. Using rabbit renal brush border membrane vesicles, in presence of Na^+, Li^+ acts as an inhibitor (K_i of 1.2 mM) of the sodium-dependent succinate transporter (166).

The transporter was then identified through expression cloning as NaDC-1 (121) and characterized in *X. laevis* oocytes. It was demonstrated that Li^+ alone can drive succinate transport *via* NaDC-1 with a lower apparent affinity than for Na^+ (122).

As Li^+ is present in the proximal tubule and can affect the function of renal secondary-active transporters, we investigated if Li^+ also has an effect on P_i handling in the proximal tubule?

Physiological studies have shown that no changes in phosphate reabsorption occurs when Li^+ is administrated to patients (123) and rats (171). This suggests that both renal phosphate cotransporter isoforms, NaPi-IIa and NaPi-IIc are unaffected. However, it was shown that for intestinal BBMVs, Li^+ alone does support P_i uptake at pH 7.4 (14). This result can now be most likely explained by the presence of Type III phosphate cotransporters (PiT-2, SLC20) (11). After SLC20 isoforms were cloned and expressed in *X. laevis* oocytes a significant ^{32}P uptake in 100 mM LiCl was observed compared with control non-injected oocytes and a small electrogenic response was reported in response to 1 mM P_i (129), thus confirming the findings from data obtained in BBMVs.

Using Voltage Clamp Fluorometry (VCF), it was observed that at least one Li^+ ion could interact with NaPi-IIb. This study involved engineering a novel cysteine at site S448 to allow fluorescent labeling (157). In this mutant (S448C), the transport kinetics were similar to the wild type (WT), whereas the electrogenic cotransport of P_i was suppressed after exposure to thiol reactive agents such as MTS (methanethiosulfonates) (157). It was concluded that, despite the lack of cotransport activity, cations and P_i interactions still took place. In the case of labeling with the fluorophore, MTS-TAMRA, it was shown that at least one Li^+ interacted with the protein with an apparent affinity in the range of 100 - 300 mM (157). To further investigate the molecular effect of Li^+ on NaPi-II, we decided to characterize how the NaPi-II driving cation selectivity and transporter kinetics for P_i and Na^+ were affected by the presence of Li^+. In the next sections the figures indicated by * are numbered as in section 3.1.2: “Lithium interactions with the type II Na^+-coupled inorganic phosphate cotransporters.”

The effect of Li^+ substitution on ^{32}P uptake

Radioactive assays performed using oocytes expressing the electrogenic isoforms of NaPi-II showed that Na^+ replacement by Li^+ in the extracellular medium gave ^{32}P uptake (~3%) that was significantly different from when Na^+ was substituted with choline (Ch), which we assume from previous experiments, does not interact with NaPi-II (*Fig. 1A). The uptake levels observed would be expected to give an electrical response of <10 nA. This current is comparable in size to the signal obtained from endogenous currents in non-injected oocyte exposed to a solution containing 100Na + 1 mM P_i. Because of these reasons it was not possible to further characterize the P_i response in presence of 100 mM Li^+ using both radioactive assays and TEVC technique.

It was then decided to use solutions that contained both Na^+ and Li^+ and compare the results with the corresponding Na^+ and Ch mix (*i.e.* 50Na50Li compared with 50Na50Ch). ^{32}P uptake data indicated that in presence of Li^+ the uptake was decreased by ~50% (*Fig 1B), which suggested that Li^+ does indeed interact with electrogenic NaPi-II. In contrast, a previous study showed that ^{32}P uptake in oocytes expressing the electroneutral NaPi-IIc was not affected by the presence of Li^+ (50Na50Li compared with 50Na50Ch) (61). Nevertheless, in that study it was suggested that one Li^+ ion interacted with NaPi-IIc protein in an electroneutral manner. These apparently contradictory results can be explained by taking into account the hypothesis formulated in the context of that study (61). In NaPi-IIc, where 2 Na^+ ions are transported with 1 P_i, it was proposed that 3 Na^+ ions bind to the protein, but the first of these to interact does not participate in the transport cycle. It can be hypothesized that the first Na^+ binding can be affected by Li^+ ions. To obtain more evidence in support of this hypothesis, we investigated the effect of Li^+ on the electrogenic isoforms of NaPi-II cotransporters. These experiments were undertaken using mainly the NaPi-IIb isoform because of the robust P_i-induced currents (> -200 nA range at -50 mV) when expressed in *X. laevis* oocytes.

Steady-state electrophysiology

First, we studied the effect of equimolar replacement of Na^+ with either Li^+ or choline chloride on the phosphate induced current (I_{Pi}) activated by 1 mM P_i. In presence of Li^+, I_{Pi} was always smaller than in the corresponding Na^+ substitution with Ch at hyperpolarizing potentials (*i.e.* -100 mV, Fig. 4.4A). When referred to I_{Pi} at -100 mV in 100Na, we found a decrease of ~25% in presence of 50Na50Ch and a decrease of ~50% in I_{Pi} in presence of 50Na50Li. This result was confirmed also by using another NaPi-II isoform (*i.e.* hNaPi-IIa, Fig. 4.4B) even though the reduction in I_{Pi} was quantitatively different (~25% decrease in ChCl and ~30% in LiCl). Furthermore, for both isoforms the presence of Li^+ strongly affected the voltage-dependence of I_{Pi}, making the *I/V* relationship less voltage dependent in the presence of Li^+ for V<0 mV. This was most readily seen for the flNaPi-IIb isoform (see Fig 4.4A) and this was even more pronounced when 75 mM Na^+ was replaced with Li^+: the voltage-dependence of I_{Pi} for flNaPi-IIb isoform was completely suppressed for V<0 mV (*Fig. 2A).

From these steady-state electrophysiology findings, we drew the following conclusions:

1) the "Li^+ effect" was most likely general with respect to electrogenic members of the SLC34 family;

2) Li^+ substitution had a significant effect on the voltage-dependence and the rate limiting cotransport activity at hyperpolarizing *V*;

3) in the presence of Na^+ and Li^+, the electrogenicity of transport is maintained.

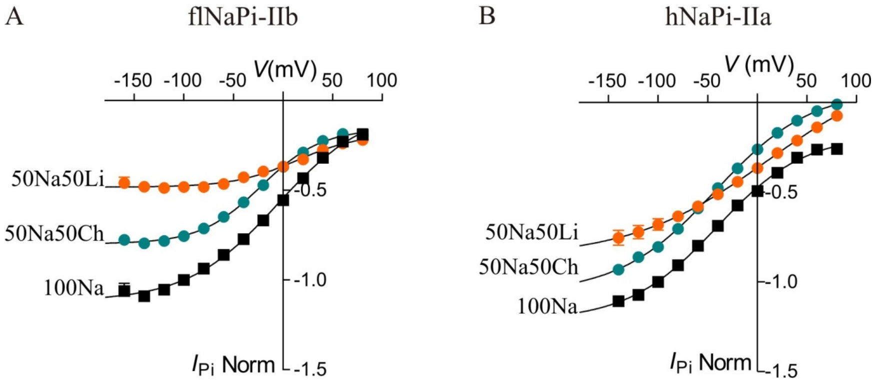

Figure 4.4 Effect of Li^+ on I_{Pi} recorded in oocytes expressing.

I/Vs relationships obtained in three different perfusion solution as indicated. A. flNaPi-IIb isoform and B. hNaPi-IIa isoform.

These findings suggest that the previously identified voltage-dependent partial reactions (*1* ↔ *2a* and *8* ↔ *1*, see Fig. 4.6) could be affected by the presence of Li^+ in the extracellular solution. Nevertheless, as these data were obtained at only one P_i concentration and with two Na^+ concentrations, we were unable to characterize the Li^+ effect. It is possible to hypothesize that Li^+ affects (i) the voltage-dependence partial reactions of the cotransport cycle alone, or (ii) it has an additional effect on the translocation of the fully loaded carrier, which has been hypothesized to be the rate limiting step in the transport cycle for NaPi-II protein.

To gain further insight into the specific partial reactions influenced by Li^+ we determined the apparent affinities for each substrate. Steady-state currents were recorded during perfusion of the oocytes with a solution containing 50 mM Li^+ and 50 mM Na^+ and different concentrations of P_i to study P_i-activation in presence of Li^+. From the data analysis (data fitted with Michaelis-Menten equation, Eqn. 2.1 with nH=1) we obtained the apparent affinity ($K_{0.5}^{Pi}$) and the maximal response for P_i (I^{Pi}_{max}). We showed that $I^{Pi}_{max}{}^{Li}$ was reduced compared to the $I^{Pi}_{max}{}^{Ch}$ (*Fig. 3C). The voltage-dependence of I^{Pi}_{max} was weaker for V<0 mV, confirming the data Fig. 4.4. The $K_{0.5}{}^{Pi}$ obtained in 50Na50Li was lower compared to the $K_{0.5}{}^{Pi}$ in 100Na and in 50Na50Ch for -100 mV < V < 0 mV (*Fig. 3D).

From these data, we concluded that in presence of Li^+, the apparent affinity of P_i for NaPi-II increased, which suggested that Li^+ interacts with NaPi-II and thereby changes the distribution of transporter state occupancies such that it is easier for P_i to bind to NaPi-II. This suggestion led to the formulation of two hypotheses: (i) Li^+ binds to the protein allosterically and can also change the Na^+ apparent affinity or (ii) Li^+ substitutes for Na^+ and is translocated during the cotransport cycle.

To decide between the two hypotheses the next question to be answered concerned the Na^+ interaction in presence of Li^+. Particular attention was paid to the prediction of the Hill coefficient (*nH*) and the apparent affinity for Na^+ because we had already observed an alteration in $K_{0.5}{}^{Pi}$ in 50Na50Li. The result of the Na^+ activation experiment showed a variation in *nH* in the 50Na50Li solution. The coefficient was found to be close to 1, whereas in absence of Li^+ the prediction gave an $nH > 2$ (*Fig. 4C). This result suggested that the presence of Li^+ changes the cooperativity of Na^+ binding to the transporter. Moreover, $K_{0.5}{}^{Na+}$ was reduced in the presence of Li^+ (*Fig. 4D). The behavior of the phosphate response in the complementary experiment, where the Li^+ concentration was changed in presence of 50 mM Na^+ (nH ~1, and $K_{0.5}{}^{Li+}$ ~25 mM, *Fig. 5C) suggested that at least one Li^+ could interact with NaPi-II.

From additional experiments (not shown), in which we kept the concentration of Na^+ (50 mM) constant and changed the Li^+ concentration (25 mM and 50 mM) we concluded that Li^+ was not the last ion to interact with NaPi-II based on the observation that no Li^+-dependent I_{max} was observed.

From these results, we concluded that the interaction of at least one Li^+ ion changes both $K_{0.5}{}^{Na+}$ and $K_{0.5}{}^{Pi}$, which indicated that the kinetics of the transporter change in presence of Li^+. It was not possible from these data to identify which partial reactions of the kinetic scheme were modulated by Li^+, or, according to our second hypothesis, if Li^+ can substitute for Na^+ at least in one of the partial reactions.

Simultaneous electrophysiology and uptake assays

Simultaneous electrophysiology and uptake experiments with ^{22}Na showed a decrease in the ratio of the number of moles of Na^+ (n^{Na+}) transported to the molar equivalent of charge translocated (n^{Qt}) in presence of Li^+.

Solution	n^{Na+}/ n^{Qt}
40Na60Ch	3.1 ± 0.5
20Na80Ch	2.8 ± 0.5
40Na60Li	2.2 ± 0.13
20Na80Li	1.6 ± 0.23

Table 4.1 Na^+ to charge ratio obtained by simultaneous electrophysiology and uptake assays.
*Values from *Fig. 6A and B.*

This result supports the hypothesis that at least one Li^+ ion can substitute Na^+ in the transport cycle at high Li^+ concentrations. Our findings do not fully exclude the possibility that more than one Li^+ ion can participate in a fraction of the transport cycles, because the Hill coefficient (*nH*) predicts the lower number of ions that interact in a cooperative manner with the transporter.

Na^+- and Li^+- dependence of presteady-state kinetics

From steady-state data analysis we saw that the voltage dependence of I_{Pi} was strongly affected by the presence of Li^+, nevertheless, some electroneutral partial reactions could also be influenced by Li^+. This led us to investigate in detail the partial reactions that precede P_i binding, namely the empty carrier (*8 ↔ 1*) and the two Na^+ binding partial reactions (*1 ↔ 2a* and *2a ↔ 2b)* (Fig. 4.5). The kinetics of these partial reactions can be investigated by removing P_i from the external medium and applying voltage steps to evoke presteady-state charge movements.

The presteady-state analysis showed that like Na^+ ions, Li^+ ions were also able to interact with the transporter in a voltage dependent manner (*Fig 7B). However, the total charge movement with 100 mM LiCl was approximately 70% of that obtained in 100 mM NaCl and the shift in the midpoint voltage of the steady-state *Q*-*V* distribution ($V_{0.5}$) with changing [Li^+] suggested that only one Li^+ ion interacted with the protein as opposed to 2 Na^+ ions.

One possible explanation for the reduced Q_{max} is that the Li^+ ions do not enter as deeply into the transmembrane electric field as Na^+ ions. A second hypothesis takes into account that, in absence of Na^+, we are observing at only two partial reactions (*8 ↔ 1* and *1 ↔ 2a*) as only one Li^+ is interacting with NaPi-II before the P_i. The partial reaction *2a ↔ 2b* were also electrogenic, the Q_{max} reduction in Li^+ alone can be explained by the fact that this transition does not take place. Compelling evidence that supports the second hypothesis is that when both Li^+ and Na^+ are present the $Q_{\mathrm{max}}^{\mathrm{50Na50Li}}$ is equal to $Q_{\mathrm{max}}^{\mathrm{100Na}}$, thereby compensating for the charge missing in 100Li. Given that the maximum charge obtained in 50Na is approximately the same as in 100Na (*Fig. 8), if Li^+ can contribute to the charge movement at a site independent of the Na^+ site, we would expect that in 50Na50Li Q_{max} would be larger. That this was not the case strongly suggests that Li^+ ions and Na^+ ions have common interaction site(s).

In the 50Na50Li solution we observed significantly slower time constants for the presteady-state currents compared to those obtained in a Li^+-free solution, particularly for voltage steps >0 mV (*Fig. 7C). Under these conditions, the time course of the presteady-state currents was best described by two time constants, one of which was in the same range (<10 ms) as normally observed for Na^+ alone and a second, the slower time constant, typically >15 ms. Importantly, the total displaceable charge was the same as when only Na^+ was present. This suggested that the number of cations contributing to the total charge movement when both Na^+ and Li^+ were in the medium was the same as when Na^+ alone was present. The slower time constant for charge movement observed for depolarizing steps suggested that if both Li^+ and Na^+ were bound, the presence of Li^+ slowed the overall release of bound charge from the protein.

To investigate the nature of Na^+-Li^+ interactions in more detail, we examined the presteady-state currents with varying $[Li^+]$ or $[Na^+]$ in the presence of a fixed concentrations of Na^+ or Li^+, respectively. When Na^+ was the variable cation, the slope of $V_{0.5}$ with respect to $\log_{10}[Na^+]$ was always significantly < 80 mV/decade except when $[Li^+]=0$. This suggested that Li^+ suppressed the normal interaction of 2 Na^+ ions that gives rise to a slope of approximately 120 mV/decade (*Fig. 9D). In the complementary set of experiments with Li^+ the variable cation, the slope remained approximately 60-70 mV/decade, consistent with one Li^+ interacting with NaPi-II (*Fig 10C).

Proposed kinetic model

A revised kinetic scheme is proposed to take account of the above results in which two cotransport cycles are possible depending on the presence or absence of Li^+.

The current model proposes that Li^+ and Na^+ compete for the same binding site (s) (at least one) in the protein. Depending on the concentration of both cations (*i.e.* Na^+ and Li^+), the probabilities to complete either the "all-Na^+-NaPi-II cotransport cycle" or the "Li^+-Na^+ cotransport cycle" change, depending on the concentration of both cations. If Li^+ is present at high concentration the probability cotransport *via* the "Li^+-Na^+ cotransport cycle" (left cycle in Fig. 4.5) increases and therefore Li^+ will bind first followed by one Na^+. If P_i is present, the transport cycle proceeds and all substrates (1Li^+, 1Na^+ 1HPO_4^{2-}, 1 Na^+) can translocate across the membrane. However, there is always a possibility for Na^+ to bind in the first Na^+ binding site and the cotransport *via* the conventional cotransport cycle, "all-Na^+-NaPi-II cotransport cycle" (right-hand loop in Fig. 4.5), will occur. To test the feasibility of this scheme, numerical simulations will be necessary.

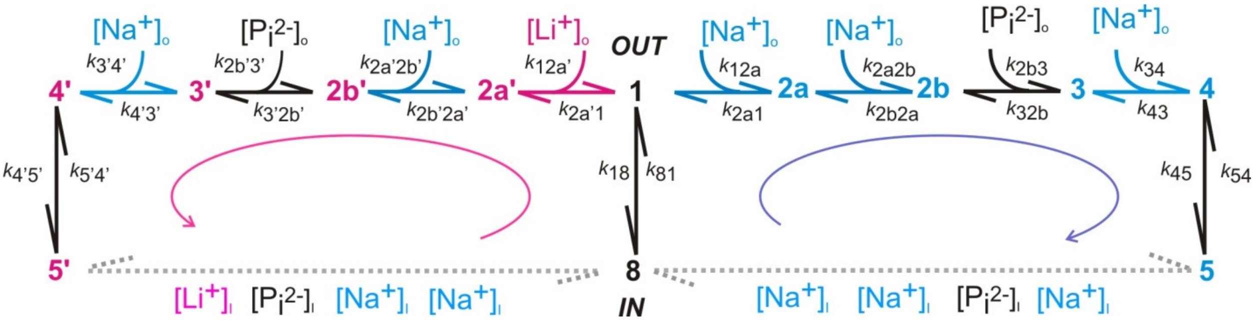

Figure 4.5 Current cotransport kinetic scheme of NaPi-IIb.

In summary, the experiments performed have provided compelling evidence in support of Li^+ ions acting as a substitute for at least for one Na^+ ion in the cotransport cycle and that their presence can significantly alter the voltage-dependence of the transport kinetics, as well as the maximum transport rate. Recent evidence from uptake experiments performed using the electroneutral NaPi-IIc strongly support the notion that Li^+ interacts only with the first cation binding site (61). In that study, it was suggested that although 2 Na^+ ions most likely interact with the protein before the P_i, only one of these (corresponding to partial reaction 2a↔2b in the scheme of Fig 4.5) participates in cotransport. For NaPi-IIc, evidence for Li^+ interactions was obtained from voltage clamp fluorometry assays, however the apparent affinity estimated from the fluorometry assays for Li^+ was even higher than that obtained from similar assays performed using the S448C mutant of the electrogenic NaPi-IIb (157).

4.3 Future perspectives

Two functional aspects of Na^+-coupled phosphate cotransporters have been investigated in this dissertation.

The ionic nature of the leak mode in NaPi-IIa/b has been studied with respect to a potential anion conduction. More information could be obtained by using COVC to gain further insight into the reversibility of the PFA-sensitive current by using mutants characterized by a larger I_{PFA}. In this study, it was not possible to clarify whether Li^+ ions were able to activate the leak mode on NaPi-IIa/b. The size of I_{PFA} was not sufficient to give a clear result. The use of mutants that show a bigger PFA-sensitive responce will then be useful to resolve this question. The ability of NaPi-II to interact with Li^+ ions rise some questions about the Na^+ binding sites that cannot be answered simply by functional studies. It will be necessary to have a 3-D structure of NaPi-II to first confirm the data obtained experimentally (*i.e.* it Li^+ occupies the 1st cation binding site) and second to clarify if one Li^+ ions can bind at more than one site. Therefore, the 3-D structure will give insight into the selectivity of the Na^+-binding sites, thereby opening the way to combine functional and structural data into a more precise structural model of NaPi-II.

Mechanistically, it is still not well understood how the intracellular release of substrates occurs due to the poor accessibility to the cytoplasmic face of the plasma membrane. By means of Cut-Open Voltage Clamp technique, it will be possible to learn about the substrate and co-substrates internal interaction. Evidence (*e.g.* human serotonin transporter (4)) suggests that changing the internal solute concentration modifies the steady-state and presteady-state characteristics. A complete set of functional experiments will be therefore necessary and useful to complete and fulfill the gaps in the knowledge about the internal (or cytoplasmic) partial reactions giving a final kinetic scheme of NaPi-II transporters.

5. REFERENCES

1. Abriel H., Horisberger J.D. (1999) Feedback inhibition of rat amiloride-sensitive epithelial sodium channels expressed in Xenopus laevis oocytes. J Physiol 516 (Pt 1):31-43

2. Accardi A., Miller C. (2004) Secondary active transport mediated by a prokaryotic homologue of ClC Cl- channels. Nature 427(6977):803-807

3. Accardi A., Picollo A. (2010) CLC channels and transporters: Proteins with borderline personalities. Biochimica et Biophysica Acta (BBA) - Biomembranes 1798(8):1457-1464

4. Adams S.V., DeFelice L.J. (2003) Ionic currents in the human serotonin transporter reveal inconsistencies in the alternating access hypothesis. Biophys J 85(3):1548-1559

5. Akabas M.H., Stauffer D.A., Xu M., Karlin A. (1992) Acetylcholine receptor channel structure probed in cysteine-substitution mutants. Science 258(5080):307-310

6. Andrini O., Ghezzi C., Murer H., Forster I.C. (2008) The leak mode of type II Na+-Pi cotransporters. Channels 2(5):346-357

7. Aronson P.S. (1981) Identifying secondary active solute transport in epithelia. Am J Physiol 240(1):F1-11

8. Arriza J.L., Eliasof S., Kavanaugh M.P., Amara S.G. (1997) Excitatory amino acid transporter 5, a retinal glutamate transporter coupled to a chloride conductance. Proc Natl Acad Sci U S A 94(8):4155-4160

9. Bacconi A., Virkki L.V., Biber J., Murer H., Forster I.C. (2005) Renouncing electroneutrality is not free of charge: switching on electrogenicity in a Na+-coupled phosphate cotransporter. Proc Natl Acad Sci U S A 102(35):12606-12611

10. Bacconi A., Ravera S., Virkki L.V., Murer H., Forster I.C. (2007) Temperature dependence of steady-state and presteady-state kinetics of a type IIb Na+/P i cotransporter. J Membr Biol 215(2-3):81-92

11. Bai L., Collins J.F., Ghishan F.K. (2000) Cloning and characterization of a type III Na-dependent phosphate cotransporter from mouse intestine. Am J Physiol Cell Physiol 279(4):(4):C1135-C1143

12. Baker P.F., D.E. Knight (1989) Experimental control of intracellular environment. Methods Enzymol 171(40):817-828

13. Berndt T. , Kumar R. (2009) Novel mechanisms in the regulation of phosphorus homeostasis. Physiology 2417-25

14. Berner W., Kinne R., Murer H. (1976) Phosphate transport into brush-border membrane vesicles isolated from rat small intestine. Biochem J 160(3):467-474

15. Berntsson R.P., Smits S.H., Schmitt L., Slotboom D.J., Poolman B. (2010) A structural classification of substrate-binding proteins. FEBS Lett 584(12):2606-2617

16. Bezanilla F., Perozo E., Papazian D.M., Stefani E. (1991) Molecular basis of gating charge immobilization in Shaker potassium channels. Science 254(5032):679-683

17. Biber J., Hernando N., Forster I.C., Murer H. (2009) Regulation of phosphate transport in proximal tubules. Pflugers Arch 458(1):39-52

18. Blanchard M.G., Longpré J.P., Wallendorff B., Lapointe J.Y. (2008) Measuring ion transport activities in Xenopus oocytes using the ion-trap technique. Am J Physiol Cell Physiol 295(5):C1464-1472

19. Boron W.F, Boulpaep E.L. (2005) Medical physiology: a cellular and molecular approach. Elseviers Saunders

20. Bossi E., Fabbrini M.S., Ceriotti A. (2007) Exogenous protein expression in Xenopus oocytes: basic procedures. Methods Mol Biol 375107-131

21. Boudker O., Verdon G. (2010) Structural perspectives on secondary active transporters. Trends Pharmacol Sci 31(9):418-426

22. Bourgeois F., Coady M.J., Lapointe J.Y. (2005) Determination of transport stoichiometry for two cation-coupled myo-inositol cotransporters: SMIT2 and HMIT. J Physiol 563(Pt 2):333-343

23. Burckhardt G., Stern H., Murer H. (1981) The influence of pH on phosphate transport into rat renal brush border membrane vesicles. Pflugers Arch 390(2):191-197

24. Busch A., Waldegger S., Herzer T., Biber J., Markovich D., Hayes G., Murer H., Lang F. (1994) Electrophysiological analysis of Na+/Pi cotransport mediated by a transporter cloned from rat kidney and expressed in Xenopus oocytes. Proc Natl Acad Sci U S A 91(17):8205-8208.

25. Busch A.E., Wagner C.A., Schuster A., Waldegger S., Biber J., Murer H., Lang F. (1995) Properties of electrogenic Pi transport by a human renal brush border Na+/Pi transporter. J Am Soc Nephrol 6(6):1547-1551

26. Cammack J.N., Schwartz E.A. (1996) Channel behavior in a gamma-aminobutyrate transporter. Proc Natl Acad Sci USA 93(2):723-727

27. Cao Y., Mager S., Lester H.A. (1997) H+ permeation and pH regulation at a mammalian serotonin transporter. J Neurosci 17(7):2257-2266

28. Carvelli L., McDonald P.W. , Blakely R.D. , L.D. DeFelice (2004) Dopamine transporters depolarize neurons by a channel mechanism. Proc Natl Acad Sci U S A 10116046-16051

29. Chen X.Z., Coady M.J., Lapointe J.Y. (1996) Fast voltage clamp discloses a new component of presteady-state currents from the Na(+)-glucose cotransporter. Biophys J 71(5):2544-2552

30. Chen X.Z., Zhu T, Smith D.E., Hediger M.A. (1999) Stoichiometry and kinetics of the high-affinity H+-coupled peptide transporter PepT2. J Biol Chem 274(5):2773-2779

31. Chen X.Z., Coady M.J., Jackson F., Berteloot A., Lapointe J.Y. (1995) Thermodynamic determination of the Na+: glucose coupling ratio for the human SGLT1 cotransporter. Biophys J 69(6):2405-2414

32. Cheng L., Sacktor B. (1981) Sodium gradient-dependent phosphate transport in renal brush border membrane vesicles. J Biol Chem 256(4):1556-1564

33. Coady M.J., Wallendorff B., Gagnon D.G., Lapointe J.Y. (2002) Identification of a novel Na+/myo-inositol cotransporter. J Biol Chem 277(38):35219-35224

34. Coady M.J., Wallendorff B., Bourgeois F., Charron F., Lapointe J.Y. (2007) Establishing a definitive stoichiometry for the Na+/monocarboxylate cotransporter SMCT1. Biophys J 93(7):2325-2331

35. Costa A.C., Patrick J.W., Dani J.A. (1994) Improved technique for studying ion channels expressed in Xenopus oocytes, including fast superfusion. Biophys J 67(1):395-401

36. Crane R.K. (1977) The gradient hypothesis and other models of carrier-mediated active transport. Rev Physiol Biochem Pharmacol 7899-159

37. DeFelice L.J., Blakely R.D. (1996) Pores medels for transporters? Biophys J 70(2):579-580

38. Díez-Sampedro A., Eskandari S., Wright E.M., Hirayama B.A. (2001) Na+-to-sugar stoichiometry of SGLT3. Am J Physiol Renal Physiol 280(2):F278-282

39. Dutzler R., Campbell E.B., MacKinnon R. (2003) Gating the selectivity filter in ClC chloride channels. Science 300(5616):108-112

40. Dutzler R., Campbell E.B., Cadene M., Chait B.T., MacKinnon R. (2002) X-ray structure of a ClC chloride channel at 3.0 A reveals the molecular basis of anion selectivity. Nature 415(6869):287-294

41. Dutzler R. (2007) A structural perspective on ClC channel and transporter function. FEBS Lett 581(15):2839-2844

42. Eskandari S., Loo D.D., Dai G., Levy O., Wright E.M., Carrasco N. (1997) Thyroid Na+/I- symporter. Mechanism, stoichiometry, and specificity. J Biol Chem 272(43):27230-27238

43. Faham S., Watanabe A., Besserer G.M., Cascio D., Specht A., Hirayama B.A., E.M. Wright., Abramson J. (2008) The crystal structure of a sodium galactose transporter reveals mechanistic insights into Na+/sugar symport. Science 321(5890):810-814

44. Farrow E.G., White K.E. (2010) Recent advances in renal phosphate handling. Nature Reviews Nephrology 6(4):207-217

45. Finn R.D., Mistry J., Tate J., Coggill P., Heger A., Pollington J.E., Gavin O.L., Gunasekaran P., Ceric G., Forslund K., Holm L., Sonnhammer E.L., Eddy S.R., Bateman A. (2010) The Pfam protein families database. Nucleic Acids Res 38(Database issue):D211-222

46. Forlani G., Bossi E., Ghirardelli R., Giovannardi S., Binda F., Bonadiman L., Ielmini L., Peres A. (2001) Mutation K448E in the external loop 5 of rat GABA transporter rGAT1 induces pH sensitivity and alters substrate interactions. J Physiol 536(Pt 2):479-494

47. Forrest L.R., Rudnick G. (2009) The rocking bundle: a mechanism for ion-coupled solute flux by symmetrical transporters. Physiology (Bethesda) 24377-386

48. Forrest L.R., Krämer R., Ziegler C. (2011) The structural basis of secondary active transport mechanisms. Biochim Biophys Acta 1807(2):167-188

49. Forrest L.R., Zhang Y.W., Jacobs M.T., Gesmonde J., Xie L., Honig B.H., Rudnick G. (2008) Mechanism for alternating access in neurotransmitter transporters. Proc Natl Acad Sci U S A 105(30):10338-10343

50. Forster I.C., Loo D.D., Eskandari S. (1999) Stoichiometry and Na+ binding cooperativity of rat and flounder renal type II Na+-Pi cotransporters. Am J Physiol 276(4 Pt 2):F644-649

51. Forster I.C., Biber J., Murer H. (2000) Proton-sensitive transitions of renal type II Na(+)-coupled phosphate cotransporter kinetics. Biophys J 79(1):215-230

52. Forster I.C., Hernando N., Biber J., Murer H. (1998) The voltage dependence of a cloned mammalian renal type II Na+/Pi cotransporter (NaPi-2). J Gen Physiol 112(1):1-18

53. Forster I.C., Köhler K., Biber J., Murer H. (2002) Forging the link between structure and function of electrogenic cotransporters: the renal type IIa Na+/Pi cotransporter as a case study. Prog Biophys Mol Biol 80(3):69-108

54. Forster I.C., Virkki L., Bossi E., Murer H., Biber J. (2006) Electrogenic kinetics of a mammalian intestinal type IIb Na(+)/P(i) cotransporter. J Membr Biol 212(3):177-190

55. Forster I.C., Wagner C.A., Busch A.E., Lang F., Biber J., Hernando N., Murer H., Werner A. (1997) Electrophysiological characterization of the flounder type II Na+/Pi cotransporter (NaPi-5) expressed in Xenopus laevis oocytes. J Membr Biol 160(1):9-25

56. Fukami-Kobayashi K., Tateno Y., Nishikawa K. (1999) Domain dislocation: a change of core structure in periplasmic binding proteins in their evolutionary history. J Mol Biol 286(1):279-290

57. Gadsby D.C., Vergani P., Csanády L. (2006) The ABC protein turned chloride channel whose failure causes cystic fibrosis. Nature 440(7083):477-483

58. Galli A., Blakely R.D., DeFelice L.J. (1996) Norepinephrine transporters have channel modes of conduction. Proc Natl Acad Sci U S A 93(16):8671-8676.

59. Galli A., Petersen C.I., deBlaquiere M., Blakely R.D., DeFelice L.J. (1997) Drosophila serotonin transporters have voltage-dependent uptake coupled to a serotonin-gated ion channel. J Neurosci 17(10):3401-3411

60. Geck P., Heinz E. (1989) Secondary active transport: introductory remarks. Kidney Int 36(3):334-341

61. Ghezzi C., Murer H., Forster I.C. (2009) Substrate interactions of the electroneutral Na+-coupled inorganic phosphate cotransporter (NaPi-IIc). J Physiol 587(Pt 17):4293-4307

62. Gonzales A.L., Lee W., Spencer S.R., Oropeza R.A., Chapman J.V., Ku J.Y., Eskandari S. (2007) Turnover rate of the gamma-aminobutyric acid transporter GAT1. J Membr Biol 220(1-3):33-51

63. Grossman T.R., Nelson N. (2002) Differential effect of pH on sodium binding by the various GABA transporters expressed in Xenopus oocytes. FEBS Lett 527(1-3):125-132

64. Grossman T.R., Nelson N. (2003) Effect of sodium lithium and proton concentrations on the electrophysiological properties of the four mouse GABA transporters expressed in Xenopus oocytes. Neurochemistry International 43(4-5):431-443

65. Harini Krishnamurthy Chayne L. Piscitelli, Eric Gouaux (2009) Unlocking the molecular secrets of sodium-coupled transporters. Nature 459347-355

66. Hartmann C.M., Wagner C.A., Busch A.E., Markovich D., Biber J., Lang F., Murer H. (1995) Transport characteristics of a murine renal Na/Pi-cotransporter. Pflugers Arch 430(5):830-836

67. Hediger M.A., Romero M.F., Peng J.B., Rolfs A., Takanaga H., Bruford E.A. (2004) The ABCs of solute carriers: physiological, pathological and therapeutic implications of human membrane transport proteins. Pflugers Arch - Eur J Physiol 447465-468

68. Hilfiker H, Hattenhauer O., Traebert M, Forster I., Murer H., Biber J. (1998) Characterization of a murine type II sodium-phosphate cotransporter expressed in mammalian small intestine. Proc Natl Acad Sci U S A 95(24):14564–14569

69. Hilgemann D.W., Lu C.C. (1998) Giant membrane patches: improvements and applications. Methods Enzymol 293267-280

70. Hilgemann D.W., Lu C.C. (1999) GAT1 (GABA:Na+:Cl-) cotransport function. Database reconstruction with an alternating access model. J Gen Physiol 114(3):459-475

71. Hille B. (2001) Ion channels of excitable membreanes. Sinauer Associates, Inc 3rd edition

72. Hille B., Campbell D.T. (1976) An improved vaseline gap voltage clamp for skeletal muscle fibers. J Gen Physiol 67(3):265-293.

73. Hirayama B.A., Loo D.D., Wright E.M. (1997) Cation effects on protein conformation and transport in the Na+/glucose cotransporter. J Biol Chem 272(4):2110-2115

74. Hoffmann N., Thees M., Kinne R. (1976) Phosphate transport by isolated renal brush border vesicles. Pflugers Arch 362(2):147-156

75. Horn R., Marty A. (1988) Muscarinic activation of ionic currents measured by a new whole-cell recording method. J Gen Physiol 92(2):145-159

76. Ingram S.L., Prasad B.M., Amara S.G. (2002) Dopamine transporter-mediated conductances increase excitability of midbrain dopamine neurons. Nat Neurosci 5(10):971-987

77. Iwamoto H., Blakely R.D., DeFelice L.J. (2006) Na+, Cl-, and pH dependence of the human choline transporter (hCHT) in Xenopus oocytes: the proton inactivation hypothesis of hCHT in synaptic vesicles. J Neurosci 26(39):9851-9859.

78. Jardetzky O. (1966) Simple allosteric Model for membrane pumps. Nature 211969-970

79. Jennings M.L., Adame M.F. (2001) Direct estimate of 1:1 stoichiometry of K(+)-Cl(-) cotransport in rabbit erythrocytes. Am J Physiol Cell Physiol 281(3):C825-832

80. Johann S.V., Gibbons J.J., O'Hara B. (1992) GLVR1, a receptor for gibbon ape leukemia virus, is homologous to a phosphate permease of Neurospora crassa and is expressed at high levels in the brain and thymus. J Virol 66(3):1635-1640

81. Kanai Y., Nussberger S., Romero M.F., Boron W.F., Hebert S.C., Hediger M.A. (1995) Electrogenic properties of the epithelial and neuronal high affinity glutamate transporter. J Biol Chem 270(28):16561-16568

82. Kanner B.I. (1978) Active transport of gamma-aminobutyric acid by membrane vesicles isolated from rat brain. Biochemistry 17(7):1207-1211

83. Karakossian M.H., Spencer S.R., Gomez A.Q., Padilla O.R., Sacher A., Loo D.D., Nelson N., Eskandari S. (2005) Novel properties of a mouse gamma-aminobutyric acid transporter (GAT4). J Membr Biol 203(2):65-82

84. Kavanaugh M.P., Kabat D. (1996) Identification and characterization of a widely expressed phosphate transporter/retrovirus receptor family. Kidney Int 49(4):959-963

85. Kellenberger S., Gautschi I., Pfister Y., Schild L. (2005) Intracellular thiol-mediated modulation of epithelial sodium channel activity. J Biol Chem 280(9):7739-7747

86. Khalili-Araghi F. , Gumbart J., Wen P.C. , Sotomayor M., Tajkhorshid E. , Schulten K. (2009) Molecular dynamics simulations of membrane channels and transporters. Curr Opin Struct Biol 19(2):128-137

87. Kippen I., Hirayama B., Klinenberg J.R., Wright E.M. (1979) Transport of tricarboxylic acid cycle intermediates by membrane vesicles from renal brush border. Proc Natl Acad Sci U S A 76(7):3397-3400

88. Köhler K., Forster I.C., Stange G., Biber J., Murer H. (2002) Transport function of the renal type IIa Na+/P(i) cotransporter is codetermined by residues in two opposing linker regions. J Gen Physiol 120(5):693-705

89. Köhler K., Forster I.C., Stange G., Biber J., Murer H. (2002) Identification of functionally important sites in the first intracellular loop of the NaPi-IIa cotransporter. Am J Physiol Renal Physiol 282(4):F687-F696

90. Kostyuk P.G. (1982) Intracellular perfusion. Ann Rev Neurosci 5107-120

91. Krishnamurthy H., Piscitelli C.L., Gouaux E. (2009) Unlocking the molecular secrets of sodium-coupled transporters. Nature 459(7245):347-355

92. Lambert G., Traebert M., Hernando N., Biber J. , Murer H. (1999) Studies on the topology of the renal type II NaPi-cotransporter. Pflugers Arch 437(6):972-978

93. Lambert G., Forster I.C., Stange G., Biber J., Murer H. (1999) Properties of the mutant Ser-460-Cys implicate this site in a functionally important region of the type IIa Na(+)/P(i) cotransporter protein. J Gen Physiol 114(5):637-652

94. Lambert G., Forster I.C., Stange G., Köhler K., Biber J., Murer H. (2001) Cysteine mutagenesis reveals novel structure-function features within the predicted third extracellular loop of the type IIa Na(+)/P(i) cotransporter. J Gen Physiol 117(6):533-546

95. Lapointe J.Y., Hudson R.L., Schultz S.G. (1986) Current-voltage relations of sodium-coupled sugar transport across the apical membrane of Necturus small intestine. J Membr Biol 93(3):205-219

96. Larsson H.P., Picaud S.A., Werblin F.S., Lecar H. (1996) Noise analysis of the glutamate-activated current in photoreceptors. Biophys J 70(2):733-742

97. Läuger P. (1987) Dynamics of ion transport systems in membranes. Physiol Rev 67(4):1296-1331

98. Lester H.A., Cao Y., Mager S. (1996) Listening to neurotransmitter transporters. Neuron 17(5):807-810

99. Longpré J.P., Lapointe J.Y. (2011) Determination of the Na(+)/glucose cotransporter (SGLT1) turnover rate using the ion-trap technique. Biophys J 100(1):52-59

100. Longpré J.P., Gagnon D.G., Coady M.J., Lapointe J.Y. (2010) The actual ionic nature of the leak current through the Na+/glucose cotransporter SGLT1. Biophys J 98(2):231-239

101. Loo D.D., Hazama A., Supplisson S., Turk E., Wright E.M. (1993) Relaxation kinetics of the Na+/glucose cotransporter. Proc Natl Acad Sci USA 90(12):5767-5771

102. Loo D.D., Eskandari S., Boorer K.J., Sarkar H.K., Wright E.M. (2000) Role of Cl- in electrogenic Na+-coupled cotransporters GAT1 and SGLT1. J Biol Chem 275(48):37414-37422

103. Loo D.D., Hirayama B.A., Cha A., Bezanilla F., Wright E.M. (2005) Perturbation analysis of the voltage-sensitive conformational changes of the Na+/glucose cotransporter. J Gen Physiol 125(1):13-36

104. Lu C.C., Hilgemann D.W. (1999) GAT1 (GABA:Na+:Cl-) cotransport function. Kinetic studies in giant Xenopus oocyte membrane patches. J Gen Physiol 114(3):445-457

105. Lu C.C., Hilgemann D.W. (1999) GAT1 (GABA:Na+:Cl-) Cotransport Function. Steady Sate Studies in Giant Xenopus Oocytes Membrane Patches. J Gen Physiol 114429-444

106. Mackenzie B., Loo D.D., Wright E.M. (1998) Relationships Between Na+/Glucose Cotransporter (SGLT1) Currents and Fluxes. Journal of Membrane Biology 162(2):101-106

107. Mackenzie B., Ujwal M.L., Chang M.H., Romero M.F., Hediger M.A. (2006) Divalent metal-ion transporter DMT1 mediates both H+ -coupled Fe2+ transport and uncoupled fluxes. Pflugers Arch 451(4):544-558

108. Mackenzie B., Schäfer M.K., Erickson J.D., Hediger M.A., Weihe E., Varoqui H. (2003) Functional properties and cellular distribution of the system A glutamine transporter SNAT1 support specialized roles in central neurons. J Biol Chem 278(26):23720-23730

109. Maconochie D.J., Knight D.E. (1989) A method for making solution changes in the sub-millisecond range at the tip of a patch pipette. Pflugers Arch 414(5):589-596

110. Magagnin S., Werner A., Markovich D., Sorribas V., Stange G., Biber J., Murer H. (1993) Expression cloning of human and rat renal cortex Na/Pi cotransport. Proc Natl Acad Sci U S A 90(13):5979-5983

111. Mager S., Kleinberger Doron N., Keshet G.I., Davidson N., Kanner B.I., Lester H.A. (1996) Ion binding and permeation at the GABA transporter GAT1. J Neurosci 16(17):5405-5414

112. Mager S., Min C., Henry D.J., Chavkin C., Hoffman B.J., Davidson N., Lester H.A. (1994) Conducting states of a mammalian serotonin transporter. Neuron 12(4):845-859

113. Matskevitch I., Wagner C.A., Stegen C., Bröer S., Noll B., Risler T., Kwon H.M., Handler J.S., Waldegger S., Busch A.E., Lang F. (1999) Functional characterization of the Betaine/gamma-aminobutyric acid transporter BGT-1 expressed in Xenopus oocytes. J Biol Chem 274(24):16709-16716

114. Meinild A.K., Sitte H.H., Gether U. (2004) Zinc potentiates an uncoupled anion conductance associated with the dopamine transporter. J Biol Chem 279(48):49671-44979

115. Miller D.G., Edwards R.H., Miller A.D. (1994) Cloning of the cellular receptor for amphotropic murine retroviruses reveals homology to that for gibbon ape leukemia virus. Proc Natl Acad Sci U S A 91(1):78-82

116. Murakami S., Nakashima R., Yamashita E., Yamaguchi A. (2002) Crystal structure of bacterial multidrug efflux transporter AcrB. Nature 419(6907):587-593

117. Murer H., Hopfer U. (1974) Demonstration of electrogenic Na+-dependent D-glucose transport in intestinal brush border membranes. Proc Natl Acad Sci U S A 71(2):484-488

118. Murer H., Hernando N., Forster I., Biber J. (2000) Proximal tubular phosphate reabsorption: molecular mechanisms. Physiol Rev 80(4):1373-1409

119. Nelson N., Sacher A., Nelson H. (2002) The significance of molecular slips in transport systems. Nat Rev Mol Cell Biol 3(11):876-881

120. O'Hara B., Johann S.V., Klinger H.P., Blair D.G., Rubinson H., Dunn K.J., Sass P., Vitek S.M., Robins T. (1990) Characterization of a human gene conferring sensitivity to infection by gibbon ape leukemia virus. Cell Growth Differ 1(3):119-127

121. Pajor A.M. (1995) Sequence and functional characterization of a renal sodium/dicarboxylate cotransporter. J Biol Chem 270(11):5779-5785

122. Pajor A.M., Hirayama B.A., Loo D.D. (1998) Sodium and lithium interactions with the Na+/Dicarboxylate cotransporter. J Biol Chem 273(30):18923-18929

123. Perez G.O., Oster J.R., Magrinat G., Vaamonde C.A. (1977) Effect of long-term lithium administration on renal phosphorus handling. Clin Pharmacol Ther 21(4):449-452

124. Petersen C.I., DeFelice L.J. (1999) Ionic interactions in the Drosophila serotonin transporter identify it as a serotonin channel. Nat Neurosci 2(7):605-610

125. Post R.L., Sen A.K., Rosenthal A.S. (1965) A phosphorylated intermediate in adenosine triphosphate-dependent sodium and potassium transport across kidney memnranes. J Biol Chem 2401437-1445

126. Radanovic T., Gisler S.M., Biber J., Murer H. (2006) Topology of the type IIa Na+/P(i) cotransporter. J Membr Biol 212(14):1-9

127. Radestock S., Forrest L.R. (2011) The Alternating-Access Mechanism of MFS Transporters Arises from Inverted-Topology Repeats. J Mol Biol ePub.

128. Rae J., Cooper K., Gates P., Watsky M. (1991) Low access resistance perforated patch recordings using amphotericin B. J Neurosci Methods 37(1):15-26

129. Ravera S., Virkki L.V., Murer H., Forster I.C. (2007) Deciphering PiT transport kinetics and substrate specificity using electrophysiology and flux measurements. Am J Physiol Cell Physiol 293(2):C606-C620

130. Ressl S., Terwisscha van Scheltinga A.C., Vonrhein C., Ott V., Ziegler C. (2009) Molecular basis of transport and regulation in the Na(+)/betaine symporter BetP. Nature 458(7234):47-52

131. Ryan R.M., Mitrovic A.D., Vandenberg R.J. (2004) The chloride permeation pathway of a glutamate transporter and its proximity to the glutamate translocation pathway. J Biol Chem 279(20):20742-20751

132. Saier M. H., Jr., Yen M. R., Noto K., Tamang D. G., Elkan C. (2009) The Transporter Classification Database: recent advances. Nucleic Acids Res 37(Database issue):D274-278

133. Sakmann B., Neher E. (2009) Single-Channel Recording. Plenum Press

134. Samarzija I., Molnar V., Frömter E. (1983) pH--dependence of phosphate absorption in rat renal proximal tubule. Proc Eur Dial Transplant Assoc 19779-783

135. Sato H., Tamba M., Ishii T., Bannai S. (1999) Cloning and expression of a plasma membrane cystine/glutamate exchange transporter composed of two distinct proteins. J Biol Chem 23(17):11455-11458

136. Schneider H.P., Bröer S., Bröer A., Deitmer J.W. (2007) Heterologous expression of the glutamine transporter SNAT3 in Xenopus oocytes is associated with four modes of uncoupled transport. J Biol Chem 282(6):3788-3798

137. Schou M. (1976) Pharmacology and toxicology of lithium. Annu Rev Pharmacol Toxicol 16231-243

138. Screpanti E., Hunte C. (2007) Discontinuous membrane helices in transport proteins and their correlation with function. J Struct Biol 159(2):261-267

139. Sen A.K., Post R.L. (1964) Stoichiometry and localization of adenosine triphosphate-dependent sodium and potassium transport in erythrocyte. J Biol Chem 239345-352

140. Shimamura T., Weyand S., Beckstein O., Rutherford N.G., Hadden J.M., Sharples D., Sansom M.S., Iwata S., Henderson P.J., Cameron A.D. (2010) Molecular basis of alternating access membrane transport by the sodium-hydantoin transporter Mhp1. Science 328(5977):470-473

141. Smith Maxwell C., Bennett E., Randles J., Kimmich G.A. (1990) Whole cell recording of sugar-induced currents in LLC-PK1 cells. Am J Physiol 258(2 Pt 1):C234-242

142. Sobczak I., Lolkema J.S. (2005) Structural and mechanistic diversity of secondary transporters. Curr Opin Microbiol 8(2):161-167

143. Soejima M., Noma A. (1984) Mode of regulation of the ACh-sensitive K-channel by the muscarinic receptor in rabbit atrial cells. Pflugers Arch 400(4):424-431

144. Sonders M.S., Zhu S.J., Zahniser N.R., Kavanaugh M.P., Amara S.G. (1997) Multiple ionic conductances of the human dopamine transporter: the actions of dopamine and psychostimulants. J Neurosci 17(3):960-974

145. Stefani E., Bezanilla F. (1998) Cut-open oocyte voltage-clamp technique. Methods Enzymol 293300-318

146. Stein W.D. (1990) Energetics and the design principles of the Na/K-ATPase. J Theor Biol 147(2):145-159

147. Su A., Mager S., Mayo S.L., Lester H.A. (1996) A multi-substrate single-file model for ion-coupled transporters. Biophys J 70(2):762-777

148. Szczepanska Konkel M., Yusufi A.N., VanScoy M., Webster S.K., Dousa T.P. (1986) Phosphonocarboxylic acids as specific inhibitors of Na+-dependent transport of phosphate across renal brush border membrane. J Biol Chem 261(14):6375-6383

149. Taglialatela M., Toro L., Stefani E. (1992) Novel voltage clamp to record small, fast currents from ion channels expressed in Xenopus oocytes. Biophys J 61(1):78-82

150. Tanford C. (1983) Translocation pathway in the catalysis of active transport. Proc Natl Acad Sci U S A 80(12):3701-3705

151. Thomsen K., Schou M. (1968) Renal lithium excretion in man. Am J Physiol 15(4):823-827

152. Tsuchiya T., Wilson T.H. (1978) Cation-sugar cotransport in the melibiose transport system of Escherichia coli. Membr Biochem 2(1):63-79

153. Turner R.J. (1985) Stoichiometry of cotransport systems. Ann N Y Acad Sci 456(10-25):

154. Ullrich K.J., Murer H. (1982) Sulfate and phosphate transport in rat kidney proximal tubule. Philos Trans R Soc Lon B Biol Sci 299549-558

155. Umbach J.A., Coady M.J., Wright E.M. (1990) Intestinal Na+/glucose cotransporter expressed in Xenopus oocytes is electrogenic. Biophys J 57(6):1217-1224

156. Villa Bellosta R., Ravera S., Sorribas V., Stange G., Levi M., Murer H., Biber J., Forster I.C. (2009) The Na+-Pi cotransporter PiT-2 (SLC20A2) is expressed in the apical membrane of rat renal proximal tubules and regulated by dietary Pi. Am J Physiol Renal Physiol 296(4):F691-F699

157. Virkki L.V., Murer H., Forster I.C. (2006) Voltage clamp fluorometric measurements on a type II Na+-coupled Pi cotransporter: shedding light on substrate binding order. J Gen Physiol 127(5):539-555

158. Virkki L.V., Murer H., Forster I.C. (2006) Mapping conformational changes of a type IIb Na+/Pi cotransporter by voltage clamp fluorometry. J Biol Chem 281(39):28837-28849

159. Virkki L.V., Biber J., Murer H., Forster I.C. (2007) Phosphate transporters: a tale of two solute carrier families. Am J Physiol Renal Physiol 293(3):F643-F654

160. Wadiche J.I., Amara S.G., Kavanaugh M.P. (1995) Ion fluxes associated with excitatory amino acid transport. Neuron 15721-728

161. Weiss J. N. (1997) The Hill equation revisited: uses and misures. FASEB J 11835-841

162. West I.C. (1997) Ligand conduction and the gated-pore mechanism of transmembrane transport. Biochim Biophys Acta 1331(3):213-234

163. Weyand S., Shimamura T., Yajima S., Suzuki S., Mirza O., Krusong K., Carpenter E.P., Rutherford N.G., Hadden J.M., O'Reilly J., Ma P., Saidijam M., Patching S.G., Hope R.J., Norbertczak H.T., Roach P.C., Iwata S., Henderson P.J., Cameron A.D. (2008) Structure and molecular mechanism of a nucleobase-cation-symport-1 family transporter. Science 322(5902):709-713

164. Widdas W.F. (1952) Inability of diffusion to account for placental glucose transfer in the sheep and considetarion of the kinetics of a possible carrier transfer. J Physiol 11823-39

165. Wright E.M., Harms V., Mircheff A.K., van Os C.H. (1981) Transport properties of intestinal basolateral membranes. Ann N Y Acad Sci 372626-636

166. Wright EM, Wright SH, Hirayama BA, I. Kippen (1982) Interactions between lithium and renal transport of Krebs cycle intermediates. Proc Natl Acad Sci U S A 79(23):7514-7517

167. Yamashita A., Singh S.K., Kawate T., Jin Y., Gouaux E. (2005) Crystal structure of a bacterial homologue of Na+/Cl--dependent neurotransmitter transporters. Nature 437(7056):215-223

168. Yao X., Pajor A.M. (2000) The transport properties of the human renal Na(+)- dicarboxylate cotransporter under voltage-clamp conditions. Am J Physiol Renal Physiol 279(1):F54-F64

169. Yernool D., Boudker O., Jin Y., Gouaux E. (2004) Structure of a glutamate transporter homologue from Pyrococcus horikoshii. Nature 431(7010):811-818

170. Young W. (2009) Review of lithium effects on brain and blood. Cell Transplant 18(9):951-975

171. Yusufi A.N., Christensen S., Dousa T.P. (1993) Effect of chronic lithium treatment upon the Na(+)-coupled cotransporters in renal brush border membranes. Kidney Int 43(5):1074-1080.

172. Zampighi G.A., Kreman M., Boorer K.J., Loo D.D., Bezanilla F., Chandy G., Hall J.E., Wright E.M. (1995) A method for determining the unitary functional capacity of cloned channels and transporters expressed in Xenopus laevis oocytes. J Membr Biol 148(1):65-78

173. Zerangue N., Kavanaugh M.P. (1996) ASCT-1 is a neutral amino acid exchanger with chloride channel activity. J Biol Chem 271(45):27991-27994

174. Zhang Z., Grewer C. (2007) The sodium-coupled neutral amino acid transporter SNAT2 mediates an anion leak conductance that is differentially inhibited by transported substrates. Biophys J 922621-2632

List of Figures

CURRICULUM VITAE

Personal information

ANDRINI Olga

Date of birth: 20.12.1982

Place of birth: Angera (Varese), Italy

Nationality: Italian

Education

2001 (July) Istituto di Istruzione secondaria superiore di Gavirate, Varese, Italy. High School Diploma (Scientific course), Mark: 80/100.

2004 (December) Department of Biotechnology and Molecular Sciences, Faculty of Science, University of Insubria (Varese), Italy. Bachelor degree in Biology. Supervisor: Dr. Stefano Giovannardi. Title: Cl^- intracellular effect on the GABA neuronal transporter transfected in tsA201 cells. Mark: 100/110.

2007 (February) Department of Biotechnology and Molecular Sciences, Faculty of Science, University of Insubria (Varese), Italy. Master degree in biological science. Supervisor: Prof. Antonio Peres. Title: Title: Electrophysiological and molecular characterization of a new potassium current expressed in Xenopus laevis photoreceptors. Mark: 110/110 cum Laude.

2007 (April) Institute of Physiology, Faculty of Science, University of Zürich, Zürich, Switzerland. PhD (in progress). Supervisor: Dr. PD. Ian C. Forster, Prof. Heini Murer group. Title: Mechanisms of leak and cotransport mode of renal phosphate transporters.

Work Experience:

November 2009. Teaching to biology students: practical course for physiology ("functions of the human body": respiration and signal transduction) University of Zürich.

April 2007 – PhD student (in progress). Institute of Physiology, University of Zürich, Zürich, Switzerland. Subject: investigation of cotransport and uncoupled leak modes of electrogenic sodiumcoupled phosphate cotransporters.

January 2006 - February 2007. As student 14 months course in Laboratory of cellular and molecular Physiology, Dept. of Structural and Functional Biology, University of Insubria, Varese – Italy.

May 2004 - December 2004. As student 8 months course in Laboratory of cellular and molecular Physiology, Dept. of Structural and Functional Biology, University of Insubria, Varese – Italy

Publications:

Andrini O., Ghezzi C., Murer H., Forster I.C. The leak mode of type II Na^+-P_i cotransporters. (2008) Channels. 2:5, 1-12.

Vigetti D.*, **Andrini O**.*, Clerici M., Negrini D., Passi A., Moriondo A. Chondroitin sulfates act as extracellular gating modifiers on voltage-dependent ion channels. (2008) Cell Physiol Biochem. 22:137-146. (*shared first authorship).

ACKNOWLEDGEMENTS

I would like to thank Heini Murer that gave me the possibility to work in his lab; my supervisor, Ian Forster for his support and his guidance during these years.

Thanks to the members of my thesis committee, Stephan Kellenberger and Jürg Biber for the interesting discussions during the meetings.

Thanks for the nice environment, lunches and table discussions to all J-floor people especially from the former Murer group. Thanks to the Verrey group, my "new" group, it was interesting to be part of the "big family".

Thanks to my office-mate from the present and past: Gerti for all your support, Alex and Soline for the sponge fights, Monica and Daniela for the interesting discussions after 18:00. A special thanks to Stine, for all your help, support and encouragement.

Thanks to the Abhi, Prajakta, Kumar and the Indian community for making the mensa-lunch more digestible.

Thanks to my friends, Hanna, Niko, Patrick, Alex and Caro, we spent memorable moments in Zurich and around Europe.

Thanks to Daniel and his family for the nice weekends with a "home" atmosphere.

Grazie ai miei amici di sempre che anche da lontanto mi hanno aiutato facendomi sentire non cosi' lontana.

Thanks to Chiara for the time spent in the lab, for working and non-working related discussions and complaining.

Thanks to my family, always there.

Thanks to Nicolas whom energy and support helped me to continue when it was difficult.

Grazie mille a tutti.